ELKIN DARIO CASTELLON CASTRILLON

DETERMINAÇÃO DA CONTRIBUIÇÃO DOS GRUPOS FUNCIONAIS PRESENTES NA ESTRUTURA QUÍMICA DOS CORANTES DE FENILMETANO NAS FORÇAS MOTRIZES DE PARTIÇÃO DOS CORANTES NOS SISTEMAS AQUOSOS BIFÁSICOS

Tese apresentada à Universidade Federal de Viçosa, como parte das exigências do Programa de Pós-Graduação em Agroquímica, para obtenção do título de *Doctor Scientiae.*

VIÇOSA
MINAS GERAIS-BRASIL
2017

Ficha catalográfica preparada pela Biblioteca Central da Universidade Federal de Viçosa - Câmpus Viçosa

T
C348d
2017

Castellon Castrillon, Elkin Dario, 1980-
Determinação da contribuição dos grupos funcionais presentes na estrutura química dos corantes de fenilmetano nas forças motrizes de partição dos corantes nos sistemas aquosos bifásicos / Elkin Dario Castellon Castrillon. – Viçosa, MG, 2017.
xxxi, 184f. : il. (algumas color.) ; 29 cm.

Orientador: Luis Henrique Mendes da Silva.
Tese (doutorado) - Universidade Federal de Viçosa.
Inclui bibliografia.

1. Sistemas aquosos bifásicos. 2. Termodinâmica. 3. Soluto - Extração. 4. Partição de fases. I. Universidade Federal de Viçosa. Departamento de Química. Programa de Pós-graduação em Agroquímica. II. Título.

CDD 22 ed. 543.55

ELKIN DARIO CASTELLON CASTRILLON

DETERMINAÇÃO DA CONTRIBUIÇÃO DOS GRUPOS FUNCIONAIS PRESENTES NA ESTRUTURA QUÍMICA DOS CORANTES DE FENILMETANO NAS FORÇAS MOTRIZES DE PARTIÇÃO DOS CORANTES NOS SISTEMAS AQUOSOS BIFÁSICOS

Tese apresentada à Universidade Federal de Viçosa, como parte das exigências do Programa de Pós-Graduação em Agroquímica, para obtenção do título de *Doctor Scientiae*.

APROVADA: 09 de agosto de 2017.

Raquel Moreira Maduro de Carvalho

Luciano de Moura Guimarães

Alexandre Gurgel

Ana Clarissa Dos Santos Pires
(Coorientadora)

Luis Henrique Mendes da Silva
(Orientador)

aprende como si fueras a vivir toda la vida y
vive como si fueras morir mañana

Charles Chaplin

AGRADECIMENTOS

Agradeço ao Deus pela concretização de mais uma etapa do longo caminho que chama felicidade.

À Universidade Federal de Viçosa e ao Programa de Pós-Graduação em Agroquímica por possibilitarem a realização deste trabalho.

Ao Conselho de Aperfeiçoamento Pessoal de Nível Superior (CAPES) pela concessão da bolsa de doutorado, ao Conselho Nacional de Desenvolvimento Científico e Tecnológico (CNPq), à Fundação de Amparo à Pesquisa do Estado de Minas Gerais (FAPEMIG) e ao Instituto Nacional de Ciências e Tecnologias Analíticas Avançadas (INCTAA), pelo auxílio financeiro.

Ao orientador Luis Henrique por todos os ensinamentos, paciência, orientação e amizade.

Às coorientadoras Maria do Carmo e Ana Clarissa pela coorientação.

Aos membros da banca que aceitaram o convite para participar desta defesa.

A Rebeca, Lorenzo, Daniela, Adriana, Kimberly, Andres, Humberto, Carlos e Jimmy, pelo apoio, carinho, amizade e por serem minha fortaleza!

A Luisa Fernada e Ramon, por serem minha família, pelo amor, apoio incondicional, aporte professional e paciência nos meus momentos de fraqueza.

Aos meus amigos Nelson, Diego, Juan, Hauster, Alan, Nain, Fred, Rafael "Batata" e Juninho, aos colegas do grupo QUIVECOM e Departamento de Química! Pelo apoio e amizade.

E a todas as pessoas que de alguma forma contribuíram no sucesso deste trabalho, o meu sincero agradecimento!

SUMÁRIO

LISTA DE SÍMBOLOS E ABREVIATURAS

SAB Sistema aquoso bifásico

PhM Fenil metano

$\Delta_{tr}\boldsymbol{G}^{\boldsymbol{\theta}}_{\boldsymbol{cor}}$ Variação de Energia livre de Gibbs padrão de transferência do corante

$\Delta_{tr}\boldsymbol{H}^{\boldsymbol{\theta}}_{\boldsymbol{cor}}$ Variação de Entalpia padrão de transferência do corante

$\Delta_{tr}\boldsymbol{S}^{\boldsymbol{\theta}}_{\boldsymbol{cor}}$ Variação de Entropia padrão de transferência do corante

$\Delta_{mix}\boldsymbol{G}$ Variação de Energia livre de Gibbs do processo de mistura

$\boldsymbol{G}_{\boldsymbol{sol}}$ Energia livre de Gibbs da solução

$\boldsymbol{G}^{*}_{\boldsymbol{i}}$ Energia livre de Gibbs do componente i puro

$\boldsymbol{\mu}_{\boldsymbol{i}}$ Potencial químicos do componente i

$\boldsymbol{\mu}^{*}_{\boldsymbol{i}}$ Potencial químico do componente i puro

$\boldsymbol{n}_{\boldsymbol{i}}$ Número de mols do componente i

CLA comprimento da linha de amarração

FS Fase superior

FI Fase inferior

$\boldsymbol{C}^{\boldsymbol{FS}}_{\boldsymbol{pol}}$ ***ou*** $\boldsymbol{C}^{\boldsymbol{FI}}_{\boldsymbol{pol}}$ concentração do polímero na fase superior ou inferior

$\boldsymbol{C}^{\boldsymbol{FS}}_{\boldsymbol{sal}}$ ***ou*** $\boldsymbol{C}^{\boldsymbol{FI}}_{\boldsymbol{sal}}$ concentração do sal na fase superior ou inferior

MV10B Violeta de metila 10B

MV6B Violeta de metila 6B

MV2B Violeta de metila 2B

PRA Pararosanilina

AUR Auramina

UV-vis Ultravioleta visível

HOMO Highest occupied molecular orbital

LUMO Lowest unoccupied molecular orbital

$\boldsymbol{K}_{\boldsymbol{soluto}}$ Coeficiente de partição do soluto

$\boldsymbol{a}^{\boldsymbol{FS}}_{\boldsymbol{i}}$ Atividade do componente i na fase superior

$\boldsymbol{a_i^{FI}}$ Atividade do componente i na fase inferior

$\boldsymbol{\gamma_i}$ Coeficiente de atividade do componente i

$\boldsymbol{x_i}$ Fração molar do componente i

$\Delta_{\boldsymbol{dil}}\boldsymbol{H_{cor}}$ Variação da entalpia de diluição do corante

$\Delta_{\boldsymbol{dil}}\boldsymbol{H_i^{\theta,\infty}}$ Variação da entalpia padrão de diluição do i em condições de diluição infinita

PEO Poli (oxido de etileno)

PPO Poli (oxido de propileno)

ATPS Aqueous two-phase system

Acet Acetato

Citr Citrato

Tart Tartrato

LISTA DE FIGURAS

Capítulo 1

Capítulo 2

LISTA DE TABELAS

Capítulo 1

Capítulo 2

Capítulo 3

RESUMO

CASTRILLON, Elkin Dario Castellón, D.Sc., Universidade Federal de Viçosa, agosto de 2017. **Determinação da contribuição dos grupos funcionais presentes na estrutura química dos corantes de fenilmetano nas forças motrizes de partição dos corantes nos sistemas aquosos bifásicos**. Orientador: Luis Henrique Mendes da Silva. Coorientadoras: Maria do Carmo Hespanhol e Ana Clarissa dos Santos Pires.

Os Sistemas Aquosos Bifásicos (SAB) são uma mistura de soluções aquosas de duas ou mais espécies diferentes que a determinadas condições de concentração, pressão e temperatura se dividem em duas fases. Esta característica torna aos SAB uma técnica de separação líquido-líquido ambientalmente segura e economicamente viável. Além disso, a diversidade de compostos utilizados para formar estes sistemas permite a regulação de diversas propriedades, como por exemplo a hidrofobicidade das fases e força iônica, potencializando a eficiência do processo de separação. No entanto, o fundamento termodinâmico do processo de transferência de solutos nestes sistemas ainda não está bem definido, já que ainda existem algumas questões por resolver como por exemplo: qual é a contribuição dos grupos funcionais do soluto nas forças motrizes que governam o processo de partição? Qual é o efeito da composição do SAB nessas contribuições? Por tanto, torna-se fundamental o desenvolvimento de um método experimental que permita a determinação da contribuição da estrutura do soluto nos diferentes parâmetros termodinâmicos de transferência em SAB diferentes. Neste trabalho foram usados seis corantes de fenilmetano com pequenas variações estruturais (Auramina, Pararosanilina, Violeta de metila B base, Violeta de metila 2B, Violeta de metila 6B e Violeta de metila 10B) como sondas moleculares para avaliar as diferentes contribuições associadas à estrutura da molécula nos fatores que governam a partição destes compostos em diferentes SAB. Nesse contexto, foram usadas misturas de duas soluções aquosas de um polímero ou copolímero com diferentes sais de sulfato ou sais orgânicas de sódio, para formar SAB com propriedades termodinâmicas diferentes. Foi possível assim

determinar os diferentes parâmetros termodinâmicos associados ao processo de transferência dos corantes no estado padrão a condições de diluição infinita, tais como a variação da energia livre de Gibbs de transferência ($\Delta_{tr}G^{o,\infty}$), a variação da entalpia de transferência ($\Delta_{tr}H^{o,\infty}$) e a variação da entropia padrão de transferência ($T\Delta_{tr}S^{o,\infty}$), e sua dependência com os grupos funcionais na estrutura do corante além do efeito da hidrofobicidade das fases do sistema e a natureza do eletrólito que forma o SAB. As contribuições do grupo CH_3 no processo de transferência, em kJ mol^{-1}, foram: $\Delta_{tr}G^{\theta,\infty}_{CH_3}$ = −0.56, $\Delta_{tr}H^{\theta,\infty}_{CH_3}$ = −4.86 e $T\Delta_{tr}S^{\theta,\infty}_{CH_3}$ = −4.53, enquanto as do grupo fenil foram: $\Delta_{tr}G^{\theta,\infty}_{PhM}$ = −13.02, $\Delta_{tr}H^{\theta,\infty}_{PhM}$ = −35.23 e $T\Delta_{tr}S^{\theta,\infty}_{PhM}$ = −28.16. A carga positiva na estrutura do corante não contribuiu nos valores de $\Delta_{tr}G^{\theta,\infty}$, embora $\Delta_{tr}H^{\theta,\infty}_{PhM}$ e $T\Delta_{tr}S^{\theta,\infty}_{PhM}$ foram ambos iguais a 11.21 kJ mol^{-1} indicando que a presença da carga na molécula do corante diminui a hidrofobicidade, melhorando o grau de liberdade na rotação das moléculas de agua e aumentando a entropia do sistema. A transferência dos grupos CH_3 diminuiu os valores de $\Delta_{tr}G^{\theta,\infty}_{PhM}$ quando o polímero é menos hidrofóbico na ordem de PEO > L64 > PPO. O efeito do cátion mostrou que a carga positiva na estrutura do corante contribui no valor negativo de $\Delta_{tr}H^{\theta,\infty}_{PhM}$ na seguinte ordem Mg^{2+} > Na^{+} > Li^{+}. Quando o SAB e formado por sais orgânicos a contribuição do grupo fenil no processo de transferência diminui a entropia do sistema dependendo do aníon que forma o SAB na seguinte ordem: Citr > Tar > Acet.

ABSTRACT

CASTRILLON, Elkin Dario Castellón, D.Sc., Universidade Federal de Viçosa, August, 2017. **Determination of the contribution of functional groups present in the chemical structure of phenylmethane dyes in the driving forces of dye partition in two-phase aqueous systems**. Advisor: Luis Henrique Mendes da Silva. Co-Advisers: Maria do Carmo Hespanhol and Ana Clarissa dos Santos Pires.

Aqueous Two-phase Systems (ATPS) are a mixture of aqueous solutions two or more different species that at certain conditions of concentration, pressure and temperature are divided into two phases. This characteristic enables the use of ATPS in liquid-liquid separation technique that are environmentally safe and economically viable. In addition, the diversity of compounds used to form these systems allows the regulation of various properties such as phase hydrophobicity and ionic strength, increasing the efficiency of the separation process. However, the thermodynamic basis of the solutes transfer process in these systems is still not well defined, since there are still some unresolved questions such as: what is the contribution of the solute functional groups in the driving forces that govern the partition process? What is the ATPS composition effect on these contributions? Therefore, it is fundamental to develop an experimental method that allows the determination of the solute structure contribution on the different thermodynamic transfer parameters in ATPS. In this work, six phenylmethane dyes with little structural variations (Auramine, Pararosaniline, methyl violet B, methyl violet 2B, methyl violet 6B and methyl violet 10B) were used as molecular probes to evaluate the different associated contributions of the molecule structure on the factors that govern the partition of these compounds in ATPS different. In this context, two aqueous solutions mixtures of a polymer or copolymer with different sulfate salts or organic sodium salts were used to form ATPSs with different thermodynamic properties, allowing to determine the different thermodynamic parameters associated with the process of transfer of the dyes in the standard state at infinite dilution conditions, such

as the variation of the Gibbs free energy of transfer ($\Delta_{tr}G^{o,\infty}$), the variation of the standard enthalpy of transfer ($\Delta_{tr}H^{o,\infty}$), and the variation of the standard entropy of transfer ($\Delta_{tr}S^{o,\infty}$), as well as their dependence on the dye structure functional groups. Besides the hydrophobicity phases effect and the effect of the electrolyte nature that forms the ATPS. The -CH_3 group contribution in the transfer process in kJ mol^{-1} was $\Delta_{tr}G^{\theta,\infty}_{CH_3} = -0.56$, $\Delta_{tr}H^{\theta,\infty}_{CH_3} = -4.86$ e $T\Delta_{tr}S^{\theta,\infty}_{CH_3} = -4.53$, while those of the phenyl group were: $\Delta_{tr}G^{\theta,\infty}_{PhM} = -13.02$, $\Delta_{tr}H^{\theta,\infty}_{PhM} = -35.23$ and $T\Delta_{tr}S^{\theta,\infty}_{PhM} = -28.16$. The positive charge in the dye structure did not contribute to the $\Delta_{tr}G^{\theta,\infty}_{PhM}$ values, although, $\Delta_{tr}H^{\theta,\infty}_{PhM}$ and $T\Delta_{tr}S^{\theta,\infty}_{PhM}$ values were both 11.21 kJ mol^{-1} indicating that the charge presence on the dye molecule decreases molecule hydrophobicity, improving the freedom degree in the water molecules increasing the entropy of the system. The CH_3 groups transfer decreases the values of $\Delta_{tr}G^{\theta,\infty}_{PhM}$ when the polymer is less hydrophobic in the order of PEO > L64 > PPO. The cation effect showed that the positive charge on the dye structure contributes in to the negative values of $\Delta_{tr}H^{\theta,\infty}_{PhM}$ in the following order Mg^{2+} > Na^{+} > Li^{+}. When the ATPS is formed by organic salts, the phenyl group contribution in the transfer process decrease the entropy depending of the anion in the following order: Citr > Tart > Acet.

CAPÍTULO 1

1.1 Introdução

Um dos desafios constantes na ciência é a extração de solutos de alto interesse a partir de fontes naturais complexas. A extração de íons metálicos[1], moléculas voláteis altamente tóxicas[2], fármacos[3], biomoléculas[4], pigmentos ou corantes orgânicos[5, 6], entre outras espécies[7], é alvo de diferentes áreas do desenvolvimento humano como a farmacêutica, confecção e tintura de têxteis, fabricação de óleos, plásticos, fotografia, alimentos, cosméticos, papelaria e na ciência medica e veterinária[8, 9]. Portanto, estas áreas necessitam de técnicas de extração que permitam purificar e/ou extrair solutos a um baixo custo e simplicidade operacional. Existem diversos métodos para separar e extrair solutos a partir de diversas matrizes, tais como adsorção[10], lixiviação seletiva[11], métodos cromatográficos[12], sistemas de extração líquido-líquido usando solventes orgânicos[2], entre outros. Estes sistemas são amplamente usados em áreas específicas por apresentar vantagens tais como eficiência e alta diversidade de compostos a serem extraídos, no entanto também possuem desvantagens como por exemplo em alguns casos alta complexidade operacional, envolvendo o uso de materiais perigosos e altos custos de operação.

Os Sistemas Aquosos Bifásicos (SABs) são misturas formadas a partir de duas ou mais soluções aquosas de diversos compostos que, a determinadas condições de concentração, pressão e temperatura, formam duas fases em equilíbrio. Estas propriedades fazem que estes sistemas sejam utilizados como uma técnica de separação líquido-líquido ambientalmente segura e economicamente viável[13]. A formação de duas fases durante o processo de mistura de soluções aquosas de um polímero e de um sal por exemplo dependerá das interações intermoleculares entre o polímero o sal e a água. Serão também estas mesmas interações as responsáveis por todas as propriedades

físicoquímicas presentes nas fases do SAB, como o coeficiente de partição de um soluto específico[14]. Portanto, para cada sistema, haberá pares de componentes que possuirão interações termodinamicamente diferentes permitindo a regulação de suas propriedades como a massa das fases, o pH, a força iônica e hidrofobicidade, podendo integrar extração e preconcentração do soluto em apenas uma etapa[15, 16]. Estas características permitem que os SAB sejam utilizados para extrair e/ou particionar inumeráveis compostos de alta importância em diversas áreas como por exemplo na biotecnológica como aminoácidos, enzimas, vírus e ácidos nucleicos [17-19]. Porém, mesmo diante desta vasta aplicabilidade, ainda existe grande expectativa de se conhecer a natureza das interações intermoleculares entre o soluto e os componentes do sistema e dessa forma compreender a relação que existe entre a estrutura molecular do soluto e as forças motrizes que governam o processo transferência nestes sistemas, avaliando o efeito da composição do SAB nas diferentes interações intermoleculares.

Neste contexto, para determinar e/ou conhecer as forças motrizes envolvidas no processo de partição é necessário analisar a termodinâmica de transferência como uma ferramenta essencial que permite compreender o processo de distribuição de solutos no SAB, no entanto, são poucos os trabalhos que fornecem informação sobre a termodinâmica do processos de partição e além disso estes trabalhos são baseados em modelos teóricos que generalizam os efeitos para todos as espécies particionadas e não em medidas experimentais que permitam determinar a variação nos parâmetros termodinâmicos de transferência causadas pelas mudanças estruturais no soluto em diferentes SABs.

Em consequência, este trabalho propõe a utilização de 6 corantes de fenilmetano (PhM) estruturalmente semelhantes para o estudo da contribuição dos grupos funcionais no processo de partição de solutos em diferentes SABs. O objetivo é propor uma

metodologia experimental para determinar os parâmetros termodinâmicos de transferência padrão ($\Delta_{tr}G^{\theta}_{cor}$, $\Delta_{tr}H^{\theta}_{cor}$ e $\Delta_{tr}S^{\theta}_{cor}$) através da relação entre estrutura molecular do soluto e coeficiente de partição e consequentemente contribuir para a otimização das aplicações da técnica.

1.2 REVISÃO DA LITERATURA

1.2.1 Sistemas Aquosos Bifásicos

Os SABs são misturas ternárias que possuem água como o componente majoritário na maior parte das vezes. Podem ser obtidos mediante a mistura de soluções aquosas de eletrólito e polímero[20], de dois polímeros quimicamente distintos[21], de dois eletrólitos[22], ou de polímeros e surfactantes não iônicos[23], que, sob determinadas condições de concentração, temperatura e pressão apresentam duas fases em equilíbrio termodinâmico.

Os primeiros estudos envolvendo esse tipo de sistemas foram atribuidos a Beijerinck e posteriormente a Ostwald e Hertel[24, 25], demostrando que em certas condições de temperatura e concentração formavam-se misturas turvas, as quais, deixadas em repouso, separavam-se em duas fases. Eles demostraram que diferenças estruturais das espécies químicas misturadas influenciam as composições das fases no equilíbrio termodinâmico, mudando as interações intermoleculares entre os componentes do sistema[26, 27].

As propriedades termodinâmicas de um SAB dependem das interações intermoleculares presentes entre os componentes em solução, que determinam por sua vez as variações nas propriedades termodinâmicas resultantes do processo de mistura. Uma forma de representar estas variações seria mediante o parâmetro termodinâmico variação energia livre de Gibbs de mistura $(\Delta_{mix}G)$, a qual faz referência à diferença

entre a energia livre de Gibbs da solução, G_{sol}, e o somatório da energia livre de Gibbs de cada componente puro, G_i^*, nas condições da solução (Equação 1).

$$\Delta_{mix}G = G_{sol} - \sum_{i=1}^{n} G_i^* = \sum_{i=1}^{n} n_i\mu_i - \sum_{i=1}^{n} n_i\,\mu_i^* = \sum_{i=1}^{n} n_i\,(\mu_i - \mu_i^*) \qquad (1)$$

Sendo μ_i e μ_i^*, são os potenciais químicos do componente i na solução e puro, respectivamente, e n_i é o número de mols do componente i.

Quando misturas de dois ou mais componentes fornecem valores de $\Delta_{mix}G < 0$, em termos termodinâmicos, um sistema homogêneo é formado. Para valores de $\Delta_{mix}G > 0$, o sistema se separa em duas ou mais fases, buscando alcançar um estado onde as interações e as configurações dos componentes levem a valores de variação de energia livre de Gibbs negativos para o sistema alcançar o equilíbrio termodinâmico[28].

Alguns trabalhos têm-se concentrado na obtenção de parâmetros termodinâmicos associados aos processos de formação dos SABs, já que a diferença nas propriedades termodinâmicas entre as fases do sistema torna-se um fator fundamental na transferência de diferentes solutos[20, 29, 30]. Por tanto, um dos requisitos para compreender a partição de espécies em SABs é conhecer as propriedades de formação e os parâmetros termodinâmicos de transferência, uma forma de realizar este estudo seria através de seu diagrama de fases.

1.2.1.1 Diagrama de fase de um SAB

Para trabalhar com SABs é fundamental conhecer os diagramas de fase. As informações que podem ser obtidas em os diagramas de fases sobre o comportamento dos SABs em diferentes condições termodinâmicas podem potencializar suas aplicações com fins diversos[31].

O conjunto das concentrações totais de todos os componentes formadores do sistema (composição global) pode ser representada em um sistema de coordenadas que permite observar de forma esquemática os dados que estão associados à formação de um sistema homogêneo ou heterogêneo em equilíbrio termodinâmico.

Um exemplo de diagrama de fases expresso em coordenadas retangulares de um sistema aquoso bifásico composto por duas soluções aquosas de polímero e sal, a uma dada pressão e temperatura é esquematizado na figura 1.

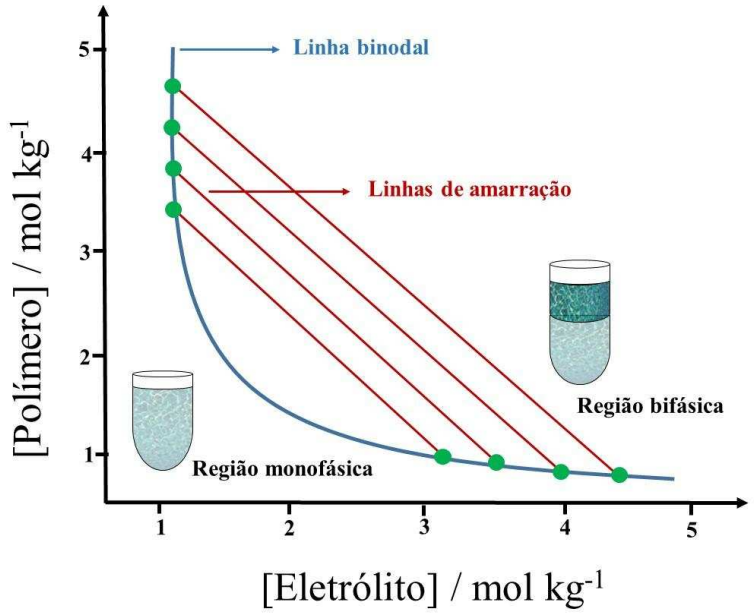

Figura 1 Diagrama de fases em coordenadas retangulares para um SAB formado por duas soluções aquosas de polímero e sal.

Os eixos da ordenada e da abscissa representam os valores de concentração de polímero e sal respectivamente em (mol kg^{-1}). A curva no diagrama que separa a região monofásica da bifásica é conhecida como curva binodal. Sua posição no diagrama depende de diversos fatores que vão desde a natureza química do sal, massa molar e

natureza do polímero, pH do sistema e temperatura do meio[32] avaliados em condições de equilíbrio termodinâmico.

O equilíbrio termodinâmico nos SABs é alcançado quando a energia livre de Gibbs do sistema é minimizada até alcançar o equilíbrio e a variação infinitesimal de G atende seu valor mínimo, então $dG = 0$, sendo o potencial químico de um dado componente formador das fases, igual na fase superior (FS) e na fase inferior (FI), incluindo a interface (IF). Isso pode ser mostrado pelas equações 2, 3, 4 e 5 para um SAB composto por polímero, sal (cátion + ânion) e água.

$$\mu_{polimero}^{FS} = \mu_{polimero}^{FI} = \mu_{polimero}^{IF} \quad (2)$$

$$\mu_{cátion}^{FS} = \mu_{cátion}^{FI} = \mu_{cation}^{IF} \quad (3)$$

$$\mu_{ânion}^{FS} = \mu_{ânion}^{FI} = \mu_{ânion}^{IF} \quad (4)$$

$$\mu_{agua}^{FS} = \mu_{agua}^{FI} = \mu_{agua}^{IF} \quad (5)$$

As linhas de amarração são as linhas retas que unem dois pontos na curva binodal, esta união representa uma possível composição de um sistema bifásico que existe em equilíbrio termodinâmico. O comprimento desta linha reta também chamado comprimento da linha de amarração (CLA) é um importante parâmetro termodinâmico que define a diferença entre as composições das fases inferior e superior, que é amplamente utilizado como variável decisiva nos processos de partição de solutos[28]. A equação 6 representa a forma como pode ser calculado o CLA.

$$CLA = [(C_{Pol}^{FS} - C_{Pol}^{FI})^2 + (C_{Sal}^{FS} - C_{Sal}^{FI})^2]^{1/2} \quad (6)$$

Onde C_{Pol}^{FS} e C_{Pol}^{FI} são as concentrações de polímero em mol kg^{-1} na fase superior e inferior respectivamente, enquanto C_{Sal}^{FS} e C_{Sal}^{FI} são as concentrações de

sal em mol kg^{-1} na fase superior e inferior respectivamente. Desta forma esclarece-se como o CLA é um parâmetro que pode expressar o quão distintas são as propriedades termodinâmicas intensivas das fases do sistema (como por exemplo, densidade, energia livre de Gibbs molar parcial, potencial químico e calor específico), das fases que coexistem em equilíbrio termodinâmico. Esta equação com sua relação de fases mostra que quanto maior o comprimento da linha de amarração, maior será a diferença entre as composições da fase superior e da fase inferior do SAB formado.

Sistemas preparados com composições de fase representadas por diferentes pontos na mesma CLA terão suas propriedades termodinâmicas intensivas iguais, porém as propriedades termodinâmicas extensivas serão diferentes, como por exemplo massa, volume e entalpia.

Na literatura são descritos diferentes métodos para a determinação do diagrama de fases de um SAB, sendo geralmente mais utilizados os métodos de titulação turbidimétrica e análise das composições das fases em equilíbrio termodinâmico[30, 33, 34].

1.2.2 Partição de corantes em SAB

Os corantes são basicamente compostos químico s que podem interagir com distintas superfícies ou tecidos para transmitir cor. Estas moléculas, são amplamente utilizados em várias indústrias, incluindo vários tipos de têxteis[35], tingimento de papel[36], plásticos, alimentos, cosméticos, impressão, entre outros, para a coloração de seus produtos relacionados[37-39]. Também são empregados no rastreamento das águas subterrâneas[40] e tratamento de água salgada[41]. Toda a ampla gama de aplicações dos corantes torna importante os processos de extração e purificação destes compostos. Os SABs vêm sendo uma excelente alternativa para particionar todo tipo de corantes. Em 1954 Albertsson investigou a partição de cloroplastos em SAB (PEO-sal)[42], em 1980

Hustedt et al[42] trabalharam com extrações de proteínas mostrando que ocorre uma forte preferência por certos materiais pigmentados intracelulares para a fase rica em PEO. Huddleston et al[43] estudaram a separação e recuperação de amaranto, ácido carmínico e quinolina amarela usados para tingir alimentos em SAB PEO e sulfato de amônia. Logo depois em 1999 Akama et al[44] propuseram a formação de um SAB usando dois surfactantes um aniônico e outro catiônico, para separar laranja de metila. Em 2009 Mageste et al[45] estudaram a separação de um pigmento natural (carmin) em SABs formados por polímero ou copolímero e diferentes sais de sulfato; dessa forma os autores conseguiram avaliar o efeito do eletrólito, hidrofobicidade das fases e pH entre outros efeitos. Em 2012 os mesmos autores (Mageste et al[46]) propuseram uma abordagem termodinâmica para o estudar e otimizam a partição de norbixim em SABs formados por polímero ou copolímero com sais orgânicos. Já em 2014 Ferreira et al[47] estudaram a partição de ácido cloranilinico, azul índigo e Sudan III a partir de fontes ambientais usando SABs formados por líquidos iônicos e sais orgânicos e inorgânicos. Um foco similar foi empregado por Alvarenga et al[6] para estudar a partição de remazol amarelo ouro a partir de fontes ambientais usando SABs formados por sais e polímeros ou líquidos iônicos.

1.2.3 Corantes de Fenilmetano

Auramina (AUR), Pararosanilina (PRA), Violeta de metila B base (MVB), Violeta de metila 2B (MV2B), Violeta de metila 6B (MV6B) e Violeta de metila 10B (MV10B) são corantes que pertencem à família dos corantes de fenilmetano (PhM)[48, 49], que apresentam um átomo de carbono central substituído por anéis de benzeno (2 ou 3) que, por sua vez, está substituído por grupos aminos (figura 2). São consideravelmente tóxicos, suspeitos de serem carcinogênicos[50] e pouco solúveis em água (na faixa de 1 a 4 g L^{-1} a 20°C[51-53]).

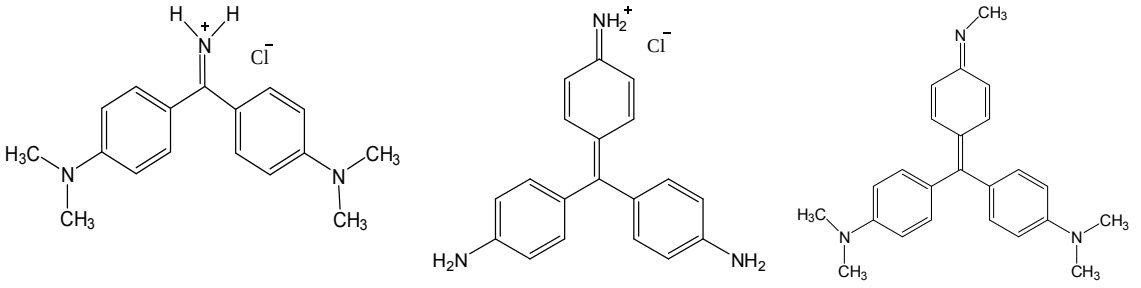

AUR PRA VMB

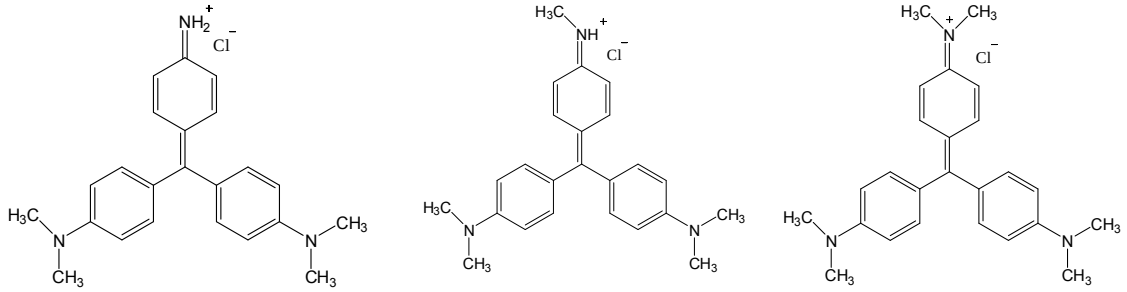

MV2B MV6B MV10B

Figura 2 Estruturas químicas dos corantes de PhM

Estes corantes são estruturalmente semelhantes, possuindo configurações compostas por um sistema de anel aromático tricíclico e bicíclico com duplas ligações conjugadas que funciona como um sistema cromóforo nestas moléculas. Possuem também três grupos amina doadores de elétrons.

Estas moléculas de PhM pertencem a uma importante classe de corantes comerciais que estão entre os primeiros pigmentos sintéticos a serem desenvolvidos[54, 55]. A família destes corantes é muito conhecida por sua alta intensidade de cor, seus brilhantes tons e sua forte resistência à luz[55], características que permitem uma ampla variedade de aplicações. A tabela 1 mostra de forma geral os potenciais usos destes corantes na atualidade.

Tabela 1 Aplicações dos corantes de PhM em diferentes áreas.

Corante	Aplicações
AUR	Lubrificante à base de tinta[56], indústria do papel, têxteis e couro[57].
PRA	Catalise enzimática[58] e multi-eletrocatálise[59], sensores em alimentos[60], impressões digitais[61].
VMB	Têxteis, tintas e vernizes[50], plásticos, papel e celulose e cosméticos[62].
MV (2- 6-10B)	Indústria têxtil em tecidos, óleos, ceras, plásticos, fotografia, alimentos, processos bacteriológicos e histopatológicos[8], tintas para pintura artística[63].

Uma vez que esta informação engloba uma variedade de campos de estudo e/ou aplicações sobre os corantes, torna-se evidente que estas espécies químicas são empregadas em uma ampla variedade de áreas científicas e industriais aproveitando suas propriedades físico-químicas únicas em solução. Estas características especificas estruturais leva a que cada área de interesse prefira uma estrutura em particular sobre outra para seus diferentes propósitos[58, 59, 64, 65].

Estes corantes exibem características espectrais interessantes, que são uma consequência direta da sua estrutura e sua interação com o ambiente circundante[66]. Estas características espectrais são muitas vezes intimamente relacionadas com o comportamento fotoquímico dos corantes e, portanto, é de grande interesse buscar uma compreensão a respeito deste fenômeno.

Os espectros de absorção UV-vis dos corantes de PhM são compostos geralmente por duas bandas de excitação π-π*, sendo uma banda α com um λ_{max} = 590 nm e uma banda β com um λ_{max} = 550 nm, correspondentes a família do violeta de metila (VMB, VM2B, VM6B e VM10B). O número de grupos metila nestas estruturas afeta pouco o espectro de absorção desses corantes. Entretanto, um efeito interessante e evidente é observado quando ocorre a substituição de todos os grupos -CH_3 na estrutura do VM10B por átomos de hidrogênio (H) dando como resultado o corante PRA. Essa mudança provoca uma variação nos λ_{max} de absorção, onde a banda α aparece com λ_{max} = 540 nm e a banda β com um λ_{max} = 480 nm. Este efeito da variação na estrutura dos corantes torna-se ainda mais evidente quando extrai-se um anel benzênico da estrutura do VM2B resultando no corante AUR. Esta mudança provoca alterações espectrais, na qual a banda α apresenta λ_{max} = 435 nm e a banda β λ_{max} = 370 nm. O espectro dos corantes é mostrado na Figura 3.

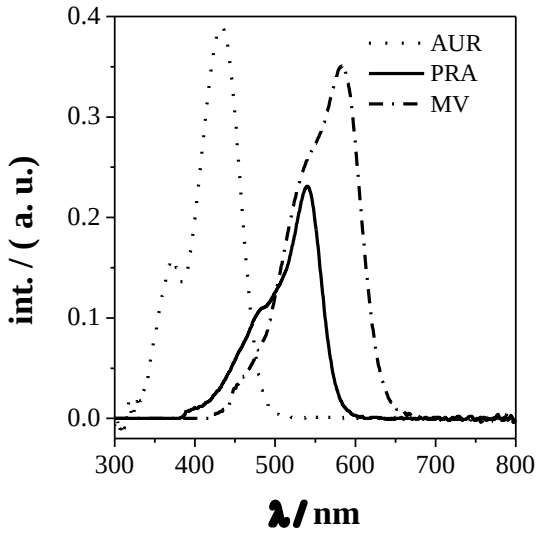

Figura 3. Espectros de absorção UV-vis de corantes PhM (•••) AUR, (—) PRA, (– • –) MV (B, 2B, 6B ou 10B).

As origens dessas bandas foram estudadas de forma alternativa dando origem a várias teorias:

a- Os perfis de excitação da maioria das bandas destes corantes substituídos foram estudados com o fim de medir os efeitos das vibrações e as uniões eletrônicas dos elétrons cromóforos do benzeno, fornecendo informações sobre a origem dos estados eletrônicos e em particular, a característica de absorção complexa de um estado eletrônico único, que apresenta uma estrutura fenil-nitrogênio. A partir deste ponto de vista concluiu-se que a resolução da estrutura que dá origem às bandas provém de um estado especifico dos elétrons pelos grupos funcionais na estrutura da molécula[67].

b- Estudos de uma possível interação de uma carga ou dipolo com um dos grupos amina pode ser responsável por quebrar a simetria da estrutura dos corantes. Assim a degeneração do estado eletrônico excitado que dá origem a absorção de luz visível e sua divisão possibilita a existência de duas conformações do estado fundamental, sendo uma simétrica e outra não simétrica. Dessa forma as bandas são produto de uma transição eletrônica para dois estados excitados[68].

Entretanto uma hipótese que em nosso caso vem sendo mais aceita é a existência de estruturas moleculares monoméricas e agregados moleculares (dímeros ou trimeros) dos corantes gerando possivelmente duas espécies em solução e que resulta na existência de duas bandas: uma banda de absorção em energias mais altas (banda β) que pode diminuir ou aumentar sua intensidade, e outra banda em energias mais baixas (banda α) que faria o oposto, quando o corante é submetido a diferentes interações [69, 70].

A deconvolução é uma técnica que serve para elucidar as diferentes bandas que compõem um espectro composto por mais de uma banda. A Figura 4 mostra o resultado

da deconvolução de um espectro de absorção UV-vis de um corante de fenilmetano diluído em dois sistemas diferentes.

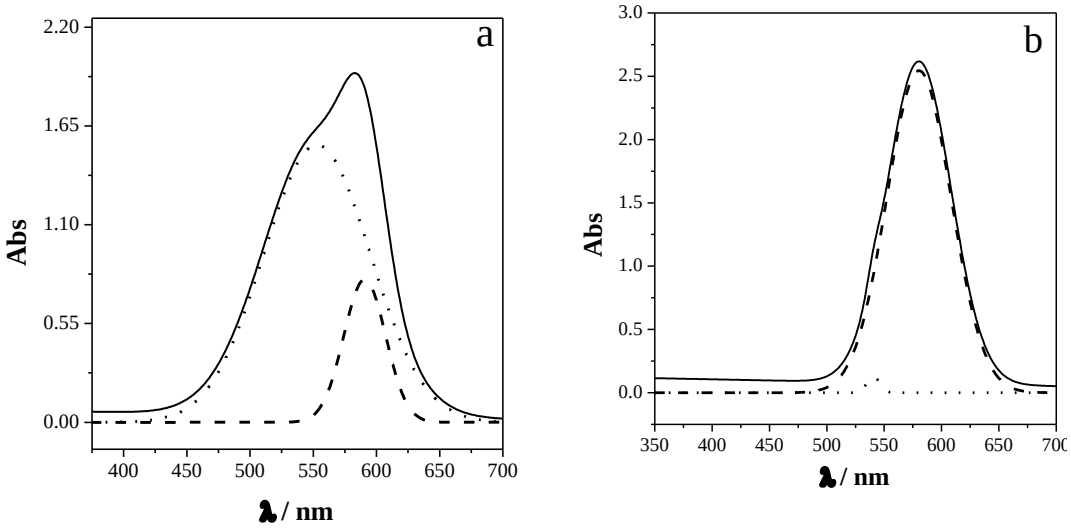

Figura 4. Espectro de absorção UV-vis de VM-6B numa concentração de $3{,}9x10^{-5}$ mol kg^{-1} (—), resultado de deconvolução da banda β (…) e banda α (---) interagindo em: (a) agua pura, e (b) fase rica em polímero de SAB (PEO1500 + $MgSO_4$ + H_2O) na primeira CLA a 25°C.

O resultado da deconvolução para (a) e (b) mostram duas bandas, uma em 550 nm (banda β) atribuída aos agregados moleculares diméricos e outra banda em 590 nm (banda α) atribuída aos monômeros, embora os espectros mostrem a existência de duas espécies em solução, nota-se a variação na intensidade das bandas quando o corante é diluído em agua pura e quando é diluído em fase de um SAB rica em polímero. Por meio da deconvolução pode-se observar como esses corantes podem auto-interagir de maneira distinta dependendo do ambiente e dessa forma, se agregar molecularmente em dímeros, tetrâmeros, octameros, etc.[71], Esses agregados, que em comparação com os monômeros devido à geometria de suas estruturas podem provocar o deslocamento de suas bandas de absorção para comprimentos de onda menores ou maiores[72, 73]. A

hidrofobicidade e as forças de van der Waals podem ser as forças motrizes para gerar as interações π-π controladas pela sobreposição direcional dos orbitais HOMO com LUMU, entre as moléculas dos corantes que provocam modificações nos estados eletrônicos fundamental e excitado[74]. Estas modificações provocam mudanças nos espectros de absorção dos corantes apresentando novas bandas.

Está claro que os corantes PhM tem atraído a atenção da comunidade científica por possuírem propriedades espectroscópicas interessantes. Segundo o trabalho de Horst B e colaboradores [52], o mecanismo depende das substituições que as estruturas podem apresentar nos estudos de agregação destes corantes. Em outros estudos realizados por Kazakova e colaboradores[79], foi verificada a formação de complexos entre Violeta de Metila (MV) e Calixareno, os quais mostraram características espectroscópicas interessantes ao interagirem com outras espécies químicas.

Estas propriedades espectroscópicas e eletrônicas dos corantes de PhM são de fundamental importância para contribuir ao estudo de partição de solutos em SAB, permitindo elucidar as forças motrizes que regem este tipo processo. Além disso, fornecem informações que determinam os diferentes comportamentos em relação às variações das interações intermoleculares, que ocorrem devido às mudanças em sua estrutura molecular com os componentes do sistema.

1.2.4 Termodinâmica de partição em SAB

Ao adicionar um soluto em um sistema líquido composto de duas fases (SAB) com diferentes propriedades termodinâmicas em equilíbrio, novas interações intermoleculares entre o soluto e os componentes das fases começam a ocorrer até que o soluto se distribuia entre as duas fases e sua concentração em cada fase atinja um valor fixo e o sistema alcance um novo estado de equilíbrio termodinâmico[80]. Portanto, a

razão da concentração do soluto entre as fases do sistema é denominada "coeficiente de partição" (K_{soluto}), e a termodinâmica pode nos auxiliar a entender o significado deste parâmetro físico-químico.

O potencial termodinâmico do processo de partição será a energia livre de Gibbs (G), como G e uma função de estado a variação dG seria expressada:

$$dG = -SdT + VdP + \sum_i \mu_i \, dn_i \tag{7}$$

Sendo $-SdT$ a variação da energia livre de Gibbs como uma função variação infinitesimal da temperatura, VdP é a variação da energia livre de Gibbs quando se apresenta variação infinitesimal na pressão do sistema e $\mu_i dn_i$ a variação da energia livre de Gibbs como uma função do número de mols de cada componente do sistema. Se considera que o sistema esteja em condições de temperatura e pressão constantes, o potencial termodinâmico do processo de partição será a energia livre de Gibbs. A variação deste potencial no sistema será a soma do produto dos potenciais químicos (μ) de cada componente multiplicado pela variação infinitesimal do número de mols para cada componente formador do SAB, mais do componente adicional "i" durante o processo de distribuição, como se mostra na equação 8.

$$dG = \mu_{pol}^{FS} \, dn_{pol}^{FS} + \mu_{sal}^{FS} \, dn_{sal}^{FS} + \mu_{agua}^{FS} \, dn_{agua}^{FS} + \mu_i^{FS} \, dn_i^{FS} + \mu_{pol}^{FI} \, dn_{pol}^{FI}$$

$$+\mu_{sal}^{FI} \, dn_{sal}^{FI} + \mu_{agua}^{FI} \, dn_{agua}^{FI} + \mu_i^{FI} \, dn_i^{FI} \tag{8}$$

Onde $\mu_{pol}^{FS} \, dn_{pol}^{FS}$; $\mu_{sal}^{FS} \, dn_{sal}^{FS}$; $\mu_{agua}^{FS} \, dn_{agua}^{FS}$; $\mu_i^{FS} \, dn_i^{FS}$ referem-se aos potenciais químicos de cada componente (polímero, sal, água e o soluto i) multiplicado pelo respectivo número de mol de cada componente na fase superior e $\mu_{pol}^{FI} \, dn_{pol}^{FI}$; $\mu_{sal}^{FI} \, dn_{sal}^{FI}$; $\mu_{agua}^{FI} \, dn_{agua}^{FI}$; $\mu_i^{FI} \, dn_i^{FI}$ referem-se aos potenciais químicos de cada

componente (polímero, sal, água e o soluto i) multiplicado pelo respectivos números de mol de cada componente na fase inferior.

Considerando que a quantidade adicionada do soluto i não mude a composição das fases, o seja a variação do número de mols do polímero, sal e agua (componentes formador do SAB) sejam desconsideradas. Deste modo, se consideramos que i foi transferido desde a fase inferior para a fase superior de um SAB (figura 6).

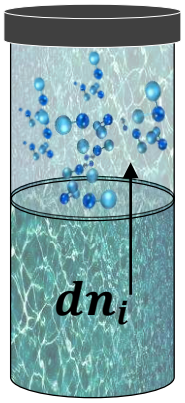

Figura 5. Transferência de *i* em um SAB

A condição de equilíbrio seria dada pela expressão 8

$$\mu_i^{FS} dn_i^{FS} + \mu_i^{FI} dn_i^{FI} = 0 \qquad (9)$$

E se cumpriria para cada variação infinitesimal no número de mols de i. Por tanto, a única maneira para que ocorra uma distribuição de i seria devido a diferencia dos potenciais químicos de i nas fases ($\mu_i^{FS} dn_i^{FS} - \mu_i^{FI} dn_i^{FI}$). Assim ocorreria uma diminuição da energia livre de Gibbs do sistema até se alcançar uma nova condição de equilíbrio termodinâmico ($dG = 0$). Por tanto como $dn_i^{FI} = -dn_i$ e $dn_i^{FS} = dn_i$ o equilíbrio atende uma nova expressão: $0 = \mu_i^{FS} dn_i - \mu_i^{FI} dn_i = (\mu_i^{FS} - \mu_i^{FI})\, dn_i$ e variação da energia livre de Gibbs do sistema neste novo equilíbrio é expressa equação 10.

$$dG = (\mu_i^{FS} - \mu_i^{FI})\, dn_i \quad (10)$$

Desta forma, após se atingir uma nova condição de equilíbrio termodinâmico no sistema, a variação da energia livre de Gibbs ficará igual a zero. Assim o potencial químico de i na fase superior (μ_i^{FS}) ficará igual ao potencial químico do componente i na fase inferior (μ_i^{FI}), como expressam as equações 11, 12 e 13.

$$dG = (\mu_i^{FS} - \mu_i^{FI})\, dn_i = 0 \quad (11)$$

$$\mu_i^{FS} - \mu_i^{FI} = 0 \quad (12)$$

$$\mu_i^{FS} = \mu_i^{FI} \quad (13)$$

Ao fazer referência ao termo de "equilíbrio de fases" para um dado sistema termodinâmico, nos referimos a qual condição de equilíbrio o potencial químico de uma espécie determinada numa dada fase deste sistema é igual ao potencial químico da mesma espécie em todas as fases nas quais ela esteja presente. Assim, o potencial químico para uma espécie (i) nas FS e FI de um SAB é expresso pelas equações 14 e 15.

$$\mu_i^{FS} = \mu_i^{\Theta}(FS) + R\ T\ lna_i^{FS} \quad (14)$$

$$\mu_i^{FI} = \mu_i^{\Theta}(FI) + R\ T\ lna_i^{FI} \quad (15)$$

Onde $\mu_i^{\Theta}(FS)$ e $\mu_i^{\Theta}(FI)$ são os potenciais químicos padrão da espécie i na FS e FI respectivamente, R é a constante universal dos gases, T é a temperatura absoluta do sistema, a_i^{FS} e a_i^{FI} é a atividade de i na FS e na FI respectivamente do SAB.

As equações (14 e 15) quando substituídas em 13 geram como resultado a equação 16 e 17.

$$\mu_i^{\Theta}(FS) + R\ T\ lna_i^{FS} = \mu_i^{\Theta}(FI) + R\ T\ lna_i^{FI} \quad (16)$$

$$\mu_i^{\Theta}(FS) - \mu_i^{\Theta}(FI) = -R\ T\ ln\frac{a_i^{FS}}{a_i^{FI}} \quad (17)$$

Onde a diferença $\mu_i^{\Theta}(FS) - \mu_i^{\Theta}(FI)$ corresponde à variação de energia livre de Gibbs de transferência do soluto i quando ele e transferido desde fase inferior do SAB no seu estado padrão nessa fase para a fase superior do mesmo SAB no seu estado padrão dessa mesma fase. O estado padrão e aquele no qual o soluto se encontra na concentração unitária (mol kg^{-1}) mas com comportamento de interação intermolecular igual do estado de diluição infinita. O termo $\frac{a_i^{FS}}{a_i^{FI}}$ é a razão das atividades de i na fase superior e na fase inferior em equilíbrio, que gera como resultado um parâmetro termodinâmico definido como **constante de partição** ($\boldsymbol{K}$). Desta forma a equação 17 tomaria a forma:

$$\Delta_{tra}G^{\theta} = -R\ T\ lnK \quad (18)$$

Como:

$$K = \frac{a_i^{FS}}{a_i^{FI}} \quad (19)$$

Nos estudos de partição é comum utilizar concentrações de soluto muito reduzidas ou no estado de diluição infinita.

1.2.5 Estado de diluição infinita.

Molecularmente falando, uma solução real (não ideal) é definida como um sistema composto por moléculas com diferente distribuição espacial e onde a magnitude das interações entre moléculas de espécies diferentes são distintas as interações de

espécies iguais. Por tanto, os potencias químicos em sistemas reais são expressados em términos de atividade e coeficiente de atividade, no entanto definimos atividade como:

$$a_i = exp^{[\mu_i - \mu_i^\theta / R\,T]} \tag{20}$$

Onde a_i é a atividade de i em qualquer solução, μ_i é o potencial quimico de i nas condições da solução e μ_i^θ o potencial químico padrão de i nas condições da solução (para uma solução rela o estado padrão seria o soluto i puro). Usando o logaritmo temos que:

$$ln a_i = (\mu_i - \mu_i^\theta)/R\,T \tag{21}$$

$$\mu_i = \mu_i^\theta + R\,T\,ln a_i \tag{22}$$

Expressando o potencial químico de i em qualquer tipo de solução.

Uma solução ideal aparece na forma onde as moléculas das diferentes espécies apresentam interações intermoleculares e distribuições espaciais semelhantes. Uma forma de solução diferente é quando a fração molar do solvente tem valores próximos a unidade, porem o soluto se encontra em concentrações muito baixas. Esta solução se denomina **solução idealmente diluída ou "estado de diluição infinita"**. Neste caso as moléculas de soluto interagem apenas com as moléculas do solvente dada as baixíssimas quantidades do soluto. Desta forma se define o potencial químico da espécie i em uma solução idealmente diluída como:

$$\mu_i = f_i(T,P) + R\,T\,ln x_i \tag{23}$$

Onde $f_i(T,P)$ é uma função da temperatura e pressão já que como as propriedades de i na solução infinitamente diluída dependem fortemente do solvente (que conforma o entorno do soluto) o potencial químico padrão do soluto i ($\mu_i^\theta(T,P)$) seria uma função

da T e P da solução (será i na concentração da solução). Por tanto, se considerando que o potencial químico de i no estado padrão seja ($\mu_i^{\theta} = f_i(T, P)$ a equação 23 se tornaria:

$$\mu_i = \mu_i^{\theta} + R\ T\ lnx_i \tag{24}$$

Isto significa que nos casos de solutos em condições de diluição infinita a fração molar de i pode ser aproximadamente proporcional a concentração molar de i. Então, partindo a equação 24 temos que:

$$\mu_i = \mu_i^{\theta} + R\ T\ lnC_i \tag{25}$$

Por tanto, a concentração de i seria:

$$C_i = exp^{[\mu_i - \mu_i^{\theta}/RT]} \tag{26}$$

Em soluções reais a concentração de i e trocada pela atividade de i (a_i) que se foi definida na equação 20. Porém, a diferença do potencial químico de uma espécie i em uma solução real (μ_i) e potencial químico de uma espécie i em uma solução idealmente diluída (μ_i^{id}) seria:

$$\mu_i - \mu_i^{id} = R\ T\ lna_i - R\ T\ lnC_i = R\ T\ ln\frac{a_i}{C_i} \tag{27}$$

Onde $\frac{a_i}{C_i}$ seria a diferença entre o comportamento real e o idealmente diluído, portanto define-se o coeficiente de atividade (γ_i) do componente i como: $\gamma_i = a_i/C_i$ de forma que $a_i = \gamma_i . C_i$ para qualquer tipo de solução real.

Portanto, em uma solução idealmente diluída o termo $a_i = C_i$, porém o coeficiente de atividade para uma solução em condições de diluição infinita seria $\gamma_i = 1$.

Dessa forma, o coeficiente de atividade no estado de diluição infinita $\boldsymbol{\gamma_{i,\infty}}$ utilizado para corrigir o valor da concentração do soluto, aproxima-se da unidade (1) e o valor da atividade pode ser conveniente aproximado ao da concentração da espécie i. Deste modo o coeficiente de partição pode ser facilmente obtido através da determinação experimental das concentrações de equilíbrio de i nas fases superior e inferior, conforme apresenta a equação 26.

$$K = \frac{C_i^{FS}}{C_i^{FI}} \tag{28}$$

Onde C_i^{FS} e C_i^{FI} são as concentrações da espécie i nas FS e FI respectivamente, expressas em mol L^{-1} ou em mol kg^{-1}. Quanto maior o valor de K maior é a quantidade do soluto que se encontra na fase superior em relação à fase inferior do SAB. Se os valores de K são maiores do que 1, o soluto concentra-se majoritariamente na FS do sistema, enquanto que os valores de K são menores do que 1, o soluto concentra-se preferencialmente na FI. Valores de K iguais à unidade significam que o soluto se distribui igualmente entre a FS e a FI do SAB.

Sendo K um parâmetro específico intrínseco, do SAB, pode ser modulado através da modificação das propriedades do sistema e seus componentes, visto que o coeficiente de partição de um soluto em um SAB é uma propriedade termodinâmica do sistema e não um parâmetro relativo apenas do soluto. Dessa forma, modular os parâmetros que caracterizam um determinado SAB pode gerar alterações significativas no comportamento de partição das espécies estudadas e consequentemente potencializando a aplicação destes sistemas em métodos de extração-separação de determinados solutos.

Os parâmetros comumente modulados num SAB depende de vários fatores como:

- **Natureza química dos componentes formadores do SAB e espécie particionada:**

  Há uma ampla gama de polímeros e sais que podem ser combinadas entre si para formar SABs com diferentes características. Por exemplo, a simples mudança do sal (ânion ou cátion) ou da diferença de hidrofobicidade e/ou massa molar do polímero formador de um SAB, pode promover mudanças significativas no comportamento de partição de uma espécie[45]. Dessa mesma forma uma pequena alteração na natureza química da espécie particionada pode ser determinante no momento de alterar os valores do coeficiente de partição[81].

- **Comprimento da linha de amarração (CLA):**

  O efeito da CLA do SAB sobre o comportamento na partição de solutos é muito frequente em trabalhos desta natureza[6]. Estudos que avaliam a alteração do coeficiente de partição de uma espécie com a mudança da CLA de determinado sistema aquoso bifásico representam uma variação nos valores de K que podem ser observados à medida que o CLA é alterado. Mesmo que não se tenha verificado uma sistemática do comportamento de K em função do CLA[45].

- **Interações que a espécie particionada tem com cada um dos componentes das fases do SAB:**

  Pelo que já foi discutido, quando um soluto entra em contato com o SAB, causa mudanças nas interações específicas entre os componentes do SAB para este alcançar novamente uma condição de equilíbrio termodinâmico. Quando se alteram os componentes formadores do sistema e/ou a natureza química do soluto em partição, modifica-se o balanço das interações entalpicas e entrópicas entre o soluto e os componentes do SAB e/ou entre os componentes deste entre si.

Estudos termodinâmicos de partição requerem que as medições desses parâmetros sejam obtidas com precisão. Por exemplo, determinar o coeficiente de partição de corantes em sistemas aquosos bifásicos pode ser desafiador quando solutos se concentram quase que majoritariamente em uma das fases, impedindo a medição exata da concentração na outra fase do sistema. Por exemplo, a figura 6 apresenta a partição do corante PRA em SAB formado por: PEO1500 + $MgSO_4$ + H_2O.

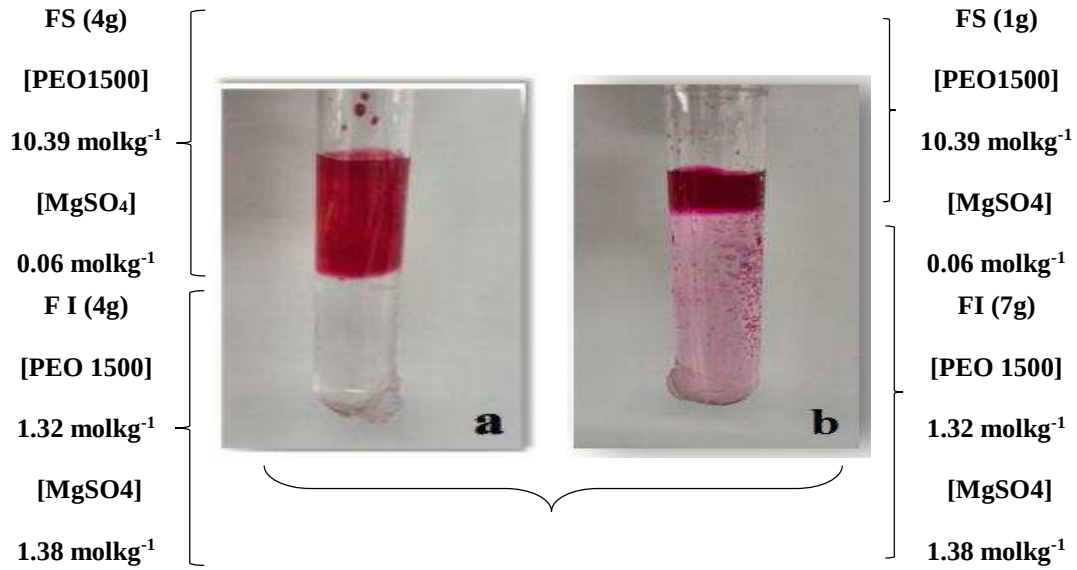

Figura 6. Partição de PRA 3,9x10^{-6} mol kg^{-1} em SAB PEO1500 + $MgSO_4$ + H_2O, na CLA 3 á 25°C. (a) Razão das fases 1:1, (b) Razão das fases 1:7.

Quando a proporção das fases é de 1:1 (a) torna-se difícil quantificar o corante na fase inferior do sistema, e quando se muda de proporção 1:7 a quantidade de corante passa ser conveniente para quantificação. Esta variação não compromete os resultados do coeficiente de partição, visto que, a mudança mostra claramente que a modulação da

proporção das fases é um dos parâmetros quem não gerar alterações significativas no comportamento de partição do corante. Sendo esta, uma forma de alterar as propriedades extensivas do sistema mantendo estável a composição das fases sem alterar o K.

Como a energia livre de Gibbs é o potencial termodinâmico do processo de transferência de um soluto da fase inferior para a fase superior de um SAB, podemos afirmar que o valor de K é resultado de um perfeito balanço de interações entalpias e entrópicas existentes entre os componentes do SAB e destes com o soluto em partição. Então, estudar estes parâmetros termodinâmicos de transferência padrão $\Delta_{tr}\boldsymbol{G^{\theta}}, \Delta_{tr}\boldsymbol{H^{\theta}}, \boldsymbol{T}\Delta_{tr}\boldsymbol{S^{\theta}}$, torna-se fundamental para conhecer as forças motrizes que dirigem o processo de transferência de solutos em SABs.

Uma das técnicas mais representativas para a abordagem destes estudos é a Calorimetria de Titulação Isotérmica, com a qual se obtêm valores de variação de $\Delta_{\boldsymbol{tr}}\boldsymbol{H^{\theta}}$ e com os valores de $\Delta_{\boldsymbol{tr}}\boldsymbol{G^{\theta}}$ (obtidos pela equação $\Delta_{tra}G^{\theta} = -RTlnK$) pode-se calcular os valores de $T\Delta_{\boldsymbol{tr}}\boldsymbol{S^{\theta}}$ usando a equação fundamental de Gibbs.

$$\Delta_{tr}G^{\theta} = \Delta_{tr}H^{\theta} - T\Delta_{tr}S^{\theta} \qquad (29)$$

1.2.6 Calorimetria de Titulação Isotérmica

A Calorimetria de Titulação Isotérmica (ITC) hoje é considerada uma das técnicas mais fortemente usadas na pesquisa para detectar mínimas variações de energia em forma de calor. Qualquer reação, interação química e/ou mudança física é acompanhada de uma mudança no valor de entalpia do sistema. Esta energia pode ser absorvida ou liberada e depende dos diferentes processos termodinâmicos gerados pela interação de duas espécies moleculares permitindo determinar diretamente valores

correspondentes a variações de entalpia de interação, em condições de temperatura e pressão constantes[82].

A primeira lei da termodinâmica expressada pela equação 30 ficaria da seguinte forma:

$$dU = dq + dw \tag{30}$$

Onde dU é a variação infinitesimal de energia interna do sistema, dq representa a quantidade infinitesimal de energia em forma de calor trocada entre sistema e vizinhança e dw é a quantidade infinitesimal do trabalho feito pelo sistema ou sobre ele. Considerando um processo que seja analisado entre um estado inicial (i) e um estado final (f), do qual esteja restrito à realização de trabalho de expansão ou compressão com pressão constante, integrando a equação 30 tem-se:

$$\int_i^f dU = \int_i^f dq - \int_i^f P_{ext} dV \tag{31}$$

Onde P_{ext} é a pressão externa no sistema e dV é a variação infinitesimal do volume do sistema. Agora resolvendo as integrais definidas na equação 31 temos que:

$$U_f - U_i = q - P_{ext}(V_f - V_i) \tag{32}$$

Reordenando em função de q :

$$(U_f + P_{ext}V_f) - (U_i + P_{ext}V_i) = q \tag{33}$$

O termo $U + P_{ext}V$ na equação recebe o nome de entalpia (H). Considerando a entalpia nos estados final e inicial, o resultado que se obtém é uma variação de entalpia como mostra a equação 34.

$$\Delta H = H_f - H_i = q \tag{34}$$

Esta equação refere-se a um processo termodinâmico em que a variação de entalpia do sistema é numericamente igual à quantidade de energia trocada na forma de calor entre sistema e vizinhança, em condições onde o sistema só pode realizar trabalho de compreensão e expansão à pressão constante.

Desta forma, poderíamos determinar as variações de energia resultantes dos processos de quebra de interações intermoleculares e formação de novas interações intermoleculares entre o soluto e os componentes das fases responsáveis pelo processo de transferência em SAB.

O instrumento no qual a técnica analítica faz as medidas calorimétricas está constituído por um par de celas, uma de amostra e outra de referência, estas celas se encontram em equilíbrio térmico com a vizinhança num ambiente de temperatura altamente controlado, como se esquematiza na Figura 8.

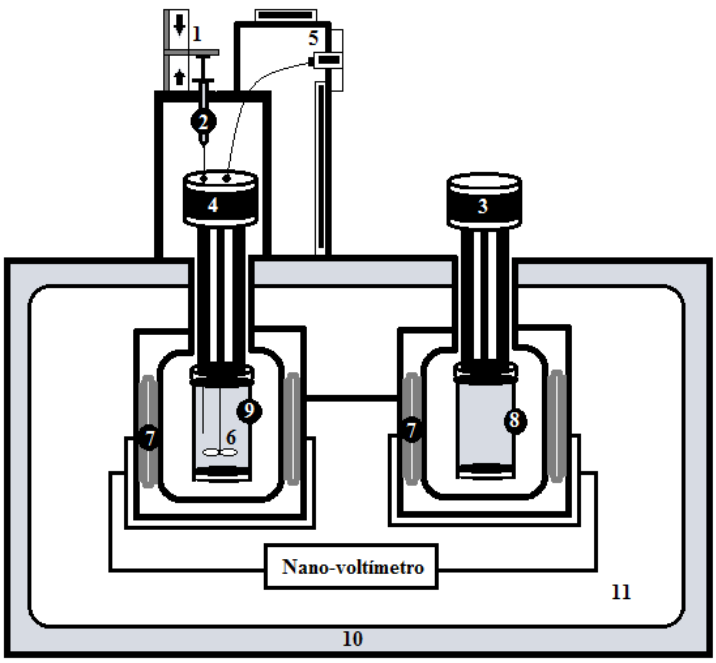

1 Motor de injeção
2 Micro seringa
3 Coluna de referência
4 Coluna de amostra
5 Motor agitador
6 Agitador
7 Termopilhas
8 Cela de referência
9 Cela de amostra
10 Banho termostático
11 Dissipador de calor

Figura 7. Descrição do Calorímetro de Titulação Isotérmica (ITC)

A cela de amostra atua como vaso de reação (9) e a outra cela como referência (8). Os efeitos térmicos que se reproduzem na cela de amostra ocorrem pela mistura de dois sistemas, onde alíquotas de volumes controlados, do sistema titulante (2) são adicionadas por meio de um injetor controlado mecanicamente (1) ao sistema titulado no interior da cela de amostra. Variações de energia na forma de calor resultantes dos processos de mistura destes sistemas, produto de rompimentos de interações já existentes e formação de novas interações intermoleculares, leva a mudanças na temperatura do sistema. Para que o equilíbrio térmico seja restabelecido, trocas de energia na forma de calor entre sistema (11) e vizinhança (10) começam a ocorrer[82]. A energia resultante, absorvida ou liberada pelo sistema, é detectada por dispositivos chamados de termo pilhas (7), as quais fazem contato com as celas calorimétricas. Essa energia gera uma diferença de potencial elétrico em seus terminais que é registrado pelo nano-voltímetro e convertido em potência por meio de uma relação que envolve a variação de energia em forma de calor ao longo do tempo, tal e como se mostra na Equação 35.

$$P = \frac{dq}{dt} \tag{35}$$

O sinal térmico obtido gera um pulso resultado dos processos de mistura entre titulante e titulado, permitindo obter um gráfico de potência, indicando o momento da adição de um volume conhecido do titulante em função do tempo. Este gráfico denominado termograma é esquematizado na figura 9.

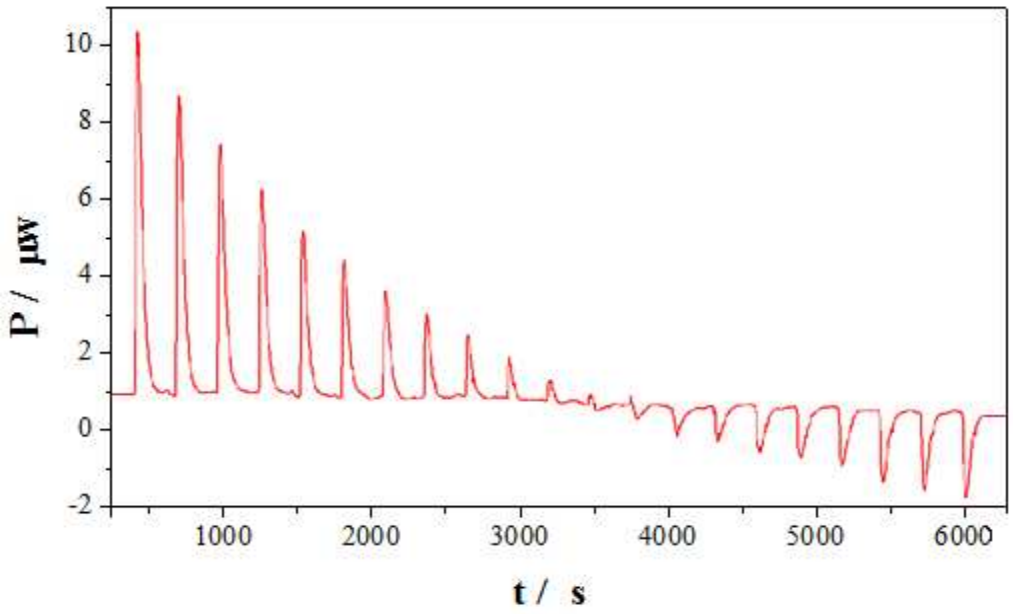

Figura 8. Termograma resultante de um experimento em um ITC

Os picos obtidos na curva de potência em função do tempo mostram se as energias correspondem a processos exotérmicos ou endotérmicos. Estes picos são integrados para determinar a quantidade de energia na forma de calor correspondente a cada injeção e consequentemente a variação de entalpia transferida no processo de mistura pode ser adquirida como se mostra na Equação 36.

$$\Delta H = q = \int_{t1}^{t2} P\, dt \tag{36}$$

Por meio do procedimento relatado, os valores de entalpia de diluição $\Delta_{dil}H$ do soluto no solvente podem ser calculados.

Os valores da variação de entalpia de diluição $\Delta_{dil}H$ são plotados em função da concentração do soluto obtendo um gráfico de $\Delta_{dil}H_i$ / kJ mol^{-1} versus $[i]$ / mol kg^{-1} para encontrar uma função matemática que permita calcular os valores de $\Delta_{dil}H_i$

quando a $[i] = 0$. Dessa forma pode-se determinar os valores de entalpia padrão de interação do soluto e o solvente em condição de diluição infinita ($\Delta_{dil}H_i^{\theta,\infty}$).

O termo variação de entalpia de transferência padrão em estado de diluição infinita ($\Delta_{tr}H^{\theta,\infty}$) faz referência as contribuições entálpicas resultantes das interações intermoleculares entre o soluto e o solvente (componentes das fases) no estado de diluição infinita, que foram determinadas a partir dos valores de ($\Delta_{dil}H_i^{\theta,\infty}$) da espécie estudada nas fases superior e inferior do SAB (equação 37). Ele fornece informação sobre em que fase estão presentes os componentes formadores do sistema com os quais a espécie particionada apresenta interações intermoleculares mais favoráveis.

$$\Delta_{tr}H^{\theta,\infty} = \Delta_{dil}H_{i-FS}^{\theta,\infty} - \Delta_{dil}H_{i-\mathrm{FI}}^{\theta,\infty} \quad (37)$$

Onde $\Delta_{dil}H_{i-FS}^{\theta,\infty}$ e $\Delta_{dil}H_{i-\mathrm{FI}}^{\theta,\infty}$ são as variações de entalpia de diluição na condição de diluição infinita, produto das interações intermoleculares envolvidas nos processos de diluição da espécie i nas fases superior e inferior respectivamente.

Determinando-se os valores de $\Delta_{tr}H^{\theta,\infty}$ e $\Delta_{tr}G^{\theta,\infty}$ pode-se calcular os valores de $T\Delta_{tr}S^{\theta,\infty}$ usando a equação 38.

$$T\Delta_{tr}S^{\theta,\infty} = \Delta_{tr}H^{\theta,\infty} - \Delta_{tr}G^{\theta,\infty} \quad (38)$$

1.3 Modelo de Johansson et al. "contribuições entálpicas e entrópicas para os valores de K"

Este modelo sugere que o processo de partição de um soluto em um SAB pode ser dirigido por contribuições entálpicas e entrópicas refletidas no coeficiente de partição K. A contribuição entrópica é dada pelo aumento ou redução do número de configurações que pode ter o soluto ao distribuir-se entre as fases superior e inferior do

SAB. A contribuição entálpica está associada aos rompimentos das interações intermoleculares e a formação de novas interações durante o processo de transferência.

O potencial químico de um soluto "i" no equilíbrio quando particionado entre as fases de um sistema aquoso bifásico é dado pela relação $\mu_i^{FS} = \mu_i^{FI}$, onde o potencial químico na fase superior é dado pela equação 39.

$$\mu_i^{FS} = \left(\frac{\partial \Delta_{mix} G^{FS}}{\partial n_i^{FS}}\right)_{T,P,n_j \neq n_i} = \mu_i^* + RT\ ln\emptyset_i^{FS} + (\mu_i^{ex})^{FS} \qquad (39)$$

Onde $\Delta_{mix} G^{FS}$ é a variação da energia livre de Gibbs provocada pela mistura da espécie i na *FS*, n_i^{FS} é o número de mols de i na *FS*, μ_i^* é o potencial químico de i puro, $(\mu_i^{ex})^{FS}$ é o excesso de potencial químico de i na fase superior e $\emptyset_i^{FS}$ é a fração de i na fase. Esta fração é definida pela equação 40:

$$\emptyset_i^{FS} = M_i \frac{n_i^{FS}}{N} \qquad (40)$$

Sendo M_i o grau de polimerização, N o número total de moléculas da espécie i na *FS*.

Como, o corante se encontra em condições de diluição infinita, pode-se assumir que sua presença não irá mudar a composição das fases. Isto significa que sob tais condições, K pode ser determinado diretamente a partir do diagrama de fase, sem contar o soluto i, segundo a equação 41.

$$ln\ K_i = ln\frac{\emptyset_i^{FS}}{\emptyset_i^{FI}} = \frac{1}{RT}[(\mu_i^{ex})^{FI} - (\mu_i^{ex})^{FS}] \qquad (41)$$

Onde $(\mu_i^{ex})^{FI}$ é o potencial químico em excesso de i na fase inferior, produto do excesso de entropia de mistura dos componentes formadores das fases, e as interações não favoráveis entre os componentes da fase inferior, por exemplo, (polímero-solvente, soluto-sal, entre outras).

1.3.1 Contribuição entrópica no *K*.

Segundo o modelo que está sendo discutido (Johansson et al[83].) a variação da energia livre de Gibbs de mistura pode ser calculada mediante a equação 42.

$$\Delta_{mix}G = \Delta_{mix}H - T\Delta S^{i} = NRT\sum_{i=1}^{m}\frac{\emptyset_i}{M_i}ln\emptyset_i + N\sum_{i=1}^{m-1}\sum_{j=i+1}^{m}\emptyset_i\,\emptyset_j w_{ij} \qquad (42)$$

Assumindo que $\Delta_{mix}H$ é zero, encontra-se a contribuição entrópica para o potencial químico do soluto i, ajustando a equação 39 em 42 de modo que:

$$\mu_i - \mu_i^{*} = T\left(\frac{\partial\Delta S^{i}}{\partial n_i}\right)_{T,P,n_j\neq n_i} = RT\left[ln\phi_i - \phi_i + 1 - M_p\sum_{i\neq j}^{m}\frac{\phi_j}{M_j}\right] \qquad (43)$$

O termo logarítmico $R\,T\,ln\phi_i$ representa a variação da entropia molar parcial ideal no processo de mistura. Os três termos restantes representam o μ_i^{ex} na fase, conforme o definido na equação 39. Sendo o coeficiente de partição do soluto definido como:

$$lnK_i = -(\,\phi_i^{FS} - \phi_i^{FI}) + M_i\left(\sum_{i\neq j}^{m}\frac{\phi_J^{FS}}{M_j} - \sum_{i\neq j}^{m}\frac{\phi_J^{FI}}{M_j}\right) = M_i\left(\sum_{i\neq j}^{m}\frac{\phi_J^{FS}}{M_j} - \sum_{i\neq j}^{m}\frac{\phi_J^{FI}}{M_j}\right) \qquad (44)$$

Onde a segunda igualdade deriva do fato de que na condição de diluição infinita, ϕ_i^{FS} e ϕ_i^{FI} devem de ter valores mínimos e semelhantes, portanto:

$$(\phi_i^{FS} - \phi_i^{FI}) = 0$$

$$(\phi_J^{FS}/M_J) = (n_J^{FS}/N^{FS}) = \left(\frac{n_J^{FS}}{\rho V^{FS}}\right) \qquad (45)$$

Onde N^{FS} é o número de sítios da rede da fase superior, $\boldsymbol{\rho}$ é o número de sítios da rede por unidade de volume, V^{FS} o volume da fase superior, e M_i é a massa molar

do soluto. Deste modo a contribuição entrópica sobre K pode ser descrita pela equação 46.

$$lnK_i = \frac{M_i}{\rho}\left(\frac{n^{FS}}{V^{FS}} - \frac{n^{FI}}{V^{FI}}\right) \quad (46)$$

Onde n^{FS} e n^{FI} representam o número total de moléculas na fase superior e inferior, respectivamente. Esta relação indica que na ausência de efeitos entálpicas, o corante se particionará entre ambas as fases devido à diferença do número de moléculas por unidade de volume (densidade numérica) entre a fase superior e a inferior do SAB. Sob tais condições, o soluto irá particionar preferencialmente para a fase com a maior densidade em número.

A entropia da mistura aumenta em proporção o número de formas distintas de distribuir as moléculas do soluto espacialmente, contribuindo na diminuição da energia livre de Gibbs de mistura no sistema. Desta forma, a fase com maior densidade numérica, dará a possibilidade de acomodar o soluto em um maior número de configurações espaciais diferentes, fazendo que a partição do soluto seja maior nesta fase. Geralmente alguns SABs tradicionais são caracterizados por apresentar uma maior densidade numérica na fase inferior, isto é causado pela diferença de moléculas de água entre as fases, então um soluto interagindo nestes sistemas se concentrará mais na fase inferior.

1.3.2 Contribuição entálpica aos valores de K.

Quando não existe uma contribuição entrópica em um SAB, por exemplo no caso em que as densidades numéricas das fases são idênticas, o processo de partição de um soluto dependera apenas da variação de entalpia molar parcial do soluto nas fases

superior e inferior, condição em que os valores de K pode ser representado da seguinte forma:

$$ln\,K = -\frac{M_i}{RT}\left[\sum_{a=1}^{3}(\Phi_a^{FS} - \Phi_a^{FI})w_{ai} - \sum_{a=1}^{2}\sum_{j=2}^{3}(\Phi_a^{FS}\Phi_a^{FS} - \Phi_a^{FI}\Phi_a^{FI})w_{aj}\right] \quad (47)$$

Onde Φ_a^{FS} e Φ_a^{FI} são as frações de volume do componente $\boldsymbol{a}$ na fase superior e inferior, respectivamente (sendo $\boldsymbol{a} =$ água, polímero ou sal), M_i é a massa molar da espécie particionada, w_{ai} e w_{aj} são as energias do par potencial a-i e a-j. Estas energias podem ser definidas pela equação 48.

$$W_{aj} = Z(\varepsilon_{aj} - \tfrac{1}{2}(\varepsilon_{aa} + \varepsilon_{jj})) \quad (48)$$

Onde Z é o número de moléculas vizinhas que interagem com o componente $\boldsymbol{a}$, enquanto a $\boldsymbol{\varepsilon_{aj}}$ representa a energia de interação envolvida na formação do par potencial e ε_{jj} e $\boldsymbol{\varepsilon_{aa}}$ representam as energias resultantes dos rompimentos das interações j- j e a-a respectivamente.

Com base na Equação 48, as interações presentes no sistema podem ser constituídas por dois somatórios, onde o primeiro seria:

$$\sum_{a=1}^{3}(\Phi_a^{FS} - \Phi_a^{FI})w_{ai}$$

Que representa a energia absorvida ou liberada no processo de interação do espécie particionada com os componentes formadores de ambas fases. O segundo somatório seria:

$$\sum_{a=1}^{2}\sum_{j=2}^{3}(\Phi_a^{FS}\Phi_a^{FS} - \Phi_a^{FI}\Phi_a^{FI})w_{aj}$$

Que representa a energia do processo de formação de uma cavidade, ou seja, o rompimento de interações intermoleculares na fase superior e o fechamento de uma cavidade fazendo referência à formação de novas interações intermoleculares na fase inferior quando o soluto é transferido da fase inferior para a fase superior. Estes somatórios fazem referência a uma energia denominada auto-energia do sistema.

As múltiplas propriedades e a grande variedade de sistemas aquosos que podem se formar em busca de impulsar o desenvolvimento da pesquisa de partição de solutos, criam a necessidade fundamental de compreender as forças motrizes fundamentais que regem o comportamento das espécies químicas formadoras das fases no momento de interagir com um soluto, e os efeitos que produzem essa interação no coeficiente de partição.

1.5 Referências

1. Nezhadali, A.; Mohammadi, R.; Akbarpour, M.; Ebrahimi, J., Selective transport of Cu(II) ions from a mixture of Mn(II), Co(II), Ni(II), Cu(II), Zn(II), and Pb(II) cations through a bulk liquid membrane using benzyl bis (thiosemicarbazone) as carrier. *Desalin. Water Treat.* **2016,** *57* (29), 13818-13828.

2. Rodrigues, G. D.; de Lemos, L. R.; Mendes da Silva, L. H.; Hespanhol da Silva, M. d. C.; Minim, L. A.; dos Reis Coimbra, J. S., A green and sensitive method to determine phenols in water and wastewater samples using an aqueous two-phase system. Talanta 2010, 80 (3), 1139-1144.

3. de Oliveira, M. H.; Ferreira, P. C. L.; Carlos, G.; Salazar, F. R.; Bergold, A. M.; Pechansky, F.; Limberger, R. P.; Frohlich, P. E., Validation and application of a liquid

chromatography-electrospray ionization mass spectrometric method for determination of mazindol in human plasma and urine. *J. Pharmacol. Toxicol. Methods* **2016,** *79*, 1-6.

4. Zaslavsky, B. Y.; Uversky, V. N.; Chait, A., Analytical applications of partitioning in aqueous two-phase systems: Exploring protein structural changes and protein-partner interactions in vitro and in vivo by solvent interaction analysis method. *BBA-Proteins Proteomics* **2016,** *1864* (5), 622-644.

5. Sheikhian, L., Adsorption behaviors of anionic and cationic dyes on ionic liquid-modified silica gel as sorbent. *Desalin. Water Treat.* **2016,** *57* (18), 8447-8453.

6. de Alvarenga, J. M.; Fideles, R. A.; da Silva, M. V.; Murari, G. F.; Taylor, J. G.; de Lemos, L. R.; Rodrigues, G. D.; Mageste, A. B., Partition study of textile dye Remazol Yellow Gold RNL in aqueous two-phase systems. *Fluid Phase Equilibria* **2015,** *391*, 1-8.

7. da Silva, N. R.; Ferreira, L. A.; Madeira, P. P.; Teixeira, J. A.; Uversky, V. N.; Zaslavsky, B. Y., Effect of sodium chloride on solute-solvent interactions in aqueous polyethylene glycol-sodium sulfate two-phase systems. *J. Chromatogr. A* **2015,** *1425*, 51-61.

8. Nakagawa, S.; Sakakibara, K.; Gotoh, H., Novel degradation mechanism for triarylmethane dyes: Acceleration of degradation speed by the attack of active oxygen to halogen groups. *Dyes and Pigments* **2016,** *124*, 130-132.

9. Takaki, K.; Wade, A. J.; Collins, C. D., Assessment and improvement of biotransfer models to cow's milk and beef used in exposure assessment tools for organic pollutants. *Chemosphere* **2015,** *138*, 390-397.

10. Han, Y.; Jin, J.; Cui, J.; Jiang, W., Effect of hydrophilicity of end-grafted polymers on protein adsorption behavior: A Monte Carlo study. *Colloids and Surfaces B: Biointerfaces* **2016,** *142*, 38-45.

11. Yang, T.; Rao, S.; Zhang, D.; Wen, J.; Liu, W.; Chen, L.; Zhang, X., Leaching of low grade zinc oxide ores in nitrilotriacetic acid solutions. *Hydrometallurgy* **2016,** *161*, 107-111.

12. Shen, Q.; Dai, Z.; Huang, Y.-W.; Cheung, H.-Y., Lipidomic profiling of dried seahorses by hydrophilic interaction chromatography coupled to mass spectrometry. *Food Chemistry* **2016,** *205*, 89-96.

13. Iqbal, M.; Tao, Y. F.; Xie, S. Y.; Zhu, Y. F.; Chen, D. M.; Wang, X.; Huang, L. L.; Peng, D. P.; Sattar, A.; Shabbir, M. A.; Hussain, H. I.; Ahmed, S.; Yuan, Z. H., Aqueous two-phase system (ATPS): an overview and advances in its applications. *Biol. Proced. Online* **2016,** *18*, 18.

14. Silva, L. H. M. d.; Loh, W., Sistemas aquosos bifásicos: fundamentos e aplicações para partição/purificação de proteínas. *Química Nova* **2006**.

15. Nezamzadeh-Ejhieh, A.; Kabiri-Samani, M., Effective removal of Ni(II) from aqueous solutions by modification of nano particles of clinoptilolite with dimethylglyoxime. *J. Hazard. Mater.* **2013,** *260*, 339-349.

16. Yoshikuni, N.; Baba, T.; Tsunoda, N.; Oguma, K., Aqueous two-phase extraction of nickel dimethylglyoximato complex and its application to spectrophotometric determination of nickel in stainless steel. *Talanta* **2005,** *66* (1), 40-44.

17. Kresheck, G. C.; Wang, Z., A new micellar aqueous two-phase partitioning system (ATPS) for the separation of proteins. *J. Chromatogr. B* **2007,** *858* (1-2), 247-253.

18. Salabat, A.; Abnosi, M. H.; Bahar, A. R., Amino acids partitioning in aqueous two-phase system of polypropylene glycol and magnesium sulfate. *J. Chromatogr. B* **2007,** *858* (1-2), 234-238.

19. de Oliveira, F. C.; Coimbra, J. S. D.; da Silva, L. H. M.; Rojas, E. E. G.; da Silva, M. D. H., Ovomucoid partitioning in aqueous two-phase systems. *Biochemical Engineering Journal* **2009,** *47* (1-3), 55-60.

20. Patricio, P. D.; Mageste, A. B.; de Lemos, L. R.; de Carvalho, R. M. M.; da Silva, L. H. M.; da Silva, M. C. H., Phase diagram and thermodynamic modeling of PEO plus organic salts + H2O and PPO + organic salts + H2O aqueous two-phase systems. *Fluid Phase Equilibria* **2011,** *305* (1), 1-8.

21. Madeira, P. P.; Teixeira, J. A.; Macedo, E. A.; Mikheeva, L. M.; Zaslavsky, B. Y., "On the Collander equation": Protein partitioning in polymer/polymer aqueous two-phase systems. *J. Chromatogr. A* **2008,** *1190* (1-2), 39-43.

22. Bridges, N. J.; Gutowski, K. E.; Rogers, R. D., Investigation of aqueous biphasic systems formed from solutions of chaotropic salts with kosmotropic salts (salt-salt ABS). *Green Chem.* **2007,** *9* (2), 177-183.

23. Liu, Y.; Wu, Z. Y.; Dai, J. H., Phase equilibrium and protein partitioning in aqueous micellar two-phase system composed of surfactant and polymer. *Fluid Phase Equilibria* **2012,** *320*, 60-64.

24. Beijerick, M. W., Parasiten und Infektionskrankenheiten. *Zentralblatt fur Bakteriologie* **1896,** *2*, 697–699.

25. Ostwald, W.; Hertel, R., Colloid chemical reactions between sols of albumin substances and polymeric carbohydrates *Kolloid ZZ Polym* **1929,** *47*, 258-268.

26. Khomutov, L. I.; Lashek, N. A.; Ptitchkina, N. M.; Morris, E. R., Temperature-composition phase diagram and gel properties of the gelatin-starch-water system. *Carbohydr. Polym.* **1995,** *28* (4), 341-345.

27. J, R.; J, A. P. A., Interfacial Tension of Dextran-Polyethylene Glycol-Water two—phase systems. *Colloid Interface Sci* **1971,** *37*, 219.

28. Silva, L. H. M. d.; Loh, W., Sistemas aquosos bifásicos: fundamentos e aplicações para partição/purificação de proteínas. *Química Nova* **2006,** *29* (6), 1345-1351.

29. Bakhshi, H.; Mobalegholeslam, P., Phase equilibria calculations of electrolyte solutions containing water- polymer- salt using a new thermodynamic model, applicable in aqueous two phase systems. *Fluid Phase Equilibria* **2017,** *434*, 222-232.

30. de Lemos, L. R.; Patricio, P. D.; Rodrigues, G. D.; de Carvalho, R. M. M.; da Silva, M. C. H.; da Silva, L. H. M., Liquid-liquid equilibrium of aqueous two-phase systems composed of poly(ethylene oxide) 1500 and different electrolytes ((NH4)(2)SO4, ZnSO4 and K2HPO4): Experimental and correlation. *Fluid Phase Equilibria* **2011,** *305* (1), 19-24.

31. Santos, I. J. B.; de Carvalho, R. M. M.; da Silva, M. C. H.; da Silva, L. H. M., Phase Diagram, Densities, and the Refractive Index of New Aqueous Two-Phase System Formed by PEO1500+Thiosulfate + H2O at Different Temperatures. *J. Chem. Eng. Data* **2012,** *57* (2), 274-279.

32. da Silva, L. H. M.; da Silva, M. D. H.; Mesquita, A. F.; do Nascimento, K. S.; Coimbra, J. S. R.; Minim, L. A., Equilibrium phase behavior of triblock copolymer plus salt plus water two-phase systems at different temperatures and pH. *J. Chem. Eng. Data* **2005,** *50* (4), 1457-1461.

33. Lemos, L. R. d.; Patrício, P. d. R.; Rodrigues, G. D.; Carvalho, R. M. M. d.; Silva, M. C. H. d.; Silva, L. H. M. d., Liquid–liquid equilibrium of aqueous two-phase systems composed of poly(ethylene oxide) 1500 and different electrolytes ((NH4)2SO4, ZnSO4 and K2HPO4): Experimental and correlation. *Fluid Phase Equilibria* **2011,** *305* (1), 19-24.

34. Baskaran, D.; Chinnappan, K.; Manivasagan, R.; Selvaraj, R., Liquid-Liquid Equilibrium of Polymer-Inorganic Salt Aqueous Two-Phase Systems: Experimental Determination and Correlation. *J. Chem. Eng. Data* **2017,** *62* (2), 738-743.

35. Sokolowska-Gajda, J.; Freeman, H. S.; Reife, A., Synthetic dyes based on environmental considerations. Part 2: Iron complexes formazan dyes. *Dyes and Pigments* **1996,** *30* (1), 1-20.

36. Ivanov, K.; Gruber, E.; Schempp, W.; Kirov, D., Possibilities of using zeolite as filler and carrier for dyestuffs in paper. *Papier* **1996,** *50* (7-8), 456-&.

37. Bensalah, N.; Alfaro, M. A. Q.; Martínez-Huitle, C. A., Electrochemical treatment of synthetic wastewaters containing Alphazurine A dye. *Chemical Engineering Journal* **2009,** *149* (1–3), 348-352.

38. Wróbel, D.; Boguta, A.; Ion, R. M., Mixtures of synthetic organic dyes in a photoelectrochemical cell. *Journal of Photochemistry and Photobiology A: Chemistry* **2001,** *138* (1), 7-22.

39. Dawood, S.; Sen, T. K.; Phan, C., Synthesis and Characterisation of Novel-Activated Carbon from Waste Biomass Pine Cone and Its Application in the Removal of Congo Red Dye from Aqueous Solution by Adsorption. *Water, Air, & Soil Pollution* **2013,** *225* (1), 1818.

40. Field, M. S.; Wilhelm, R. G.; Quinlan, J. F.; Aley, T. J., An assessment of the potential adverse properties of fluorescent tracer dyes used for groundwater tracing. *Environmental Monitoring and Assessment* **1995,** *38* (1), 75-96.

41. Hsu, T. C.; Chiang, C. S., Activated sludge treatment of dispersed dye factory wastewater. *J. Environ. Sci. Health Part A-Environ. Sci. Eng. Toxic Hazard. Subst. Control* **1997,** *32* (7), 1921-1932.

42. Walter, H., *Partitioning in aqueous two–phase system: theory, methods, uses, and applications to biotechnology*. Elsevier: 2012.

43. Huddleston, J. G.; Willauer, H. D.; Boaz, K. R.; Rogers, R. D., Separation and recovery of food coloring dyes using aqueous biphasic extraction chromatographic resins. *Journal of Chromatography B: Biomedical Sciences and Applications* **1998,** *711* (1), 237-244.

44. Akama, E.; Tong, A. J.; Ito, M.; Tanaka, S., The study of the partitioning mechanism of methyl orange in an aqueous two-phase system. *Talanta* **1999,** *48* (5), 1133-1137.

45. Mageste, A. B.; de Lemos, L. R.; Ferreira, G. M. D.; da Silva, M. D. H.; da Silva, L. H. M.; Bonomo, R. C. F.; Minim, L. A., Aqueous two-phase systems: An efficient, environmentally safe and economically viable method for purification of natural dye carmine. *J. Chromatogr. A* **2009,** *1216* (45), 7623-7629.

46. Mageste, A. B.; Senra, T. D. A.; da Silva, M. C. H.; Bonomo, R. C. F.; da Silva, L. H. M., Thermodynamics and optimization of norbixin transfer processes in aqueous biphasic systems formed by polymers and organic salts. *Sep. Purif. Technol.* **2012,** *98*, 69-77.

47. Ferreira, A. M.; Coutinho, J. A. P.; Fernandes, A. M.; Freire, M. G., Complete removal of textile dyes from aqueous media using ionic-liquid-based aqueous two-phase systems. *Sep. Purif. Technol.* **2014,** *128*, 58-66.

48. de O. Martins, A.; Canalli, V. M.; Azevedo, C. M. N.; Pires, M., Degradation of pararosaniline (C.I. Basic Red 9 monohydrochloride) dye by ozonation and sonolysis. *Dyes and Pigments* **2006,** *68* (2), 227-234.

49. Grygar, T.; Kuckova, S.; Hradil, D.; Hradilova, J., Electrochemical analysis of natural solid organic dyes and pigments. *J. Solid State Electrochem.* **2003,** *7* (10), 706-713.

50. Gupta, A. K.; Pal, A.; Sahoo, C., Photocatalytic degradation of a mixture of Crystal Violet (Basic Violet 3) and Methyl Red dye in aqueous suspensions using Ag+ doped TiO2. *Dyes and Pigments* **2006,** *69* (3), 224-232.

51. Denman, S.; Jameel, S.; Hay, J.; Sugden, J. K., Photostability of Crystal Violet (CI 42555). *Dyes and Pigments* **1996,** *30* (1), 67-72.

52. Lueck, H. B.; Rice, B. L.; McHale, J. L., Aggregation of triphenylmethane dyes in aqueous-solution - dimerization and trimerization of crystal violet and ethyl violet. *Spectroc. Acta Pt. A-Molec. Biomolec. Spectr.* **1992,** *48* (6), 819-828.

53. Poulios, I.; Avranas, A.; Rekliti, E.; Zouboulis, A., Photocatalytic oxidation of Auramine O in the presence of semiconducting oxides. *J. Chem. Technol. Biotechnol.* **2000,** *75* (3), 205-212.

54. Gordon, P. F.; Gregory, P., *Organic chemistry in colour*. 2012.

55. S, C., Rodd's Chemistry of carbon compounds: a modern comprehensive treatise. *Elsevier* **1964,** *3*.

56. Shen, G. Lubricant-based ink, useful in ball pen, includes organic solvent e.g. glycerol, coloring agent e.g. auramine, resin e.g. rosin ester, viscosity regulator e.g. polyvinyl butyral-15, thixotropic agents e.g. castor oil and additives. CN104109419-A, CN104109419-A 22 Oct 2014 C09D-011/18 201503, 2015.

57. Ozturk, A.; Malkoc, E., Adsorptive potential of cationic Basic Yellow 2 (BY2) dye onto natural untreated clay (NUC) from aqueous phase: Mass transfer analysis, kinetic and equilibrium profile. *Appl. Surf. Sci.* **2014,** *299*, 105-115.

58. Singh, R. K. L., Applicability of Positive Cooperativity Model of Enzyme Catalysis on Surfactant-Mediated Reaction of Pararosaniline Hydrochloride Carbocation with Hydroxide Ion. *J. Dispersion Sci. Technol.* **2016,** *37* (2), 239-244.

59. Fernandes, D. M.; Teixeira, A.; Freire, C., Multielectrocatalysis by Layer-by-Layer Films Based on Pararosaniline and Vanadium-Substituted Phosphomolybdate. *Langmuir* **2015,** *31* (5), 1855-1865.

60. Guo, D. Kit used for rapid detection of sulfur dioxide in food, contains standard sulfur dioxide stock solution , acid pararosaniline, formaldehyde absorbing buffer liquid, zinc lactate, formaldehyde solution, acid solution and alkali solution. CN104280515-A, CN104280515-A 14 Jan 2015 G01N-031/22 201521, 2015.

61. Sanoglan, S.; Gurbuz, S.; Ipeksac, T.; Seden, M. G.; Erol, M., Pararosaniline and crystal violet tagged montmorillonite for latent fingerprint investigation. *Appl. Clay Sci.* **2014,** *87*, 235-244.

62. Sharma, K. K.; Rao, B. S. M.; Mohan, H.; Mittal, J. P.; Oakes, J.; O'Neill, P., Free-radical-induced oxidation and reduction of 1-arylazo-2-naphthol dyes: A radiation chemical study. *J. Phys. Chem. A* **2002,** *106* (12), 2915-2923.

63. Ghelardi, E.; Degano, I.; Colombini, M. P.; Mazurek, J.; Schilling, M.; Khanjian, H.; Learner, T., A multi-analytical study on the photochemical degradation of synthetic organic pigments. *Dyes and Pigments* **2015,** *123*, 396-403.

64. De, S.; Girigoswami, A.; Mandal, S., Enhanced fluorescence of triphenylmethane dyes in aqueous surfactant solutions at supramicellar concentrations-effect of added electrolyte. *Spectroc. Acta Pt. A-Molec. Biomolec. Spectr.* **2002,** *58* (12), 2547-2555.

65. Garcia-Rio, L.; Godoy, A.; Leis, J. R., Spectroscopic characterisation of crystal violet inclusion complexes in beta-cyclodextrin. *Chem. Phys. Lett.* **2005,** *401* (1-3), 302-306.

66. Duxbury, D. F., The Photochemistry and photophyscs of triphenylmetane dyes in solid and liquid-media. *Chemical Reviews* **1993,** *93* (1), 381-433.

67. Angeloni, L.; Smulevich, G.; Marzocchi, M. P., RESONANCE RAMAN-SPECTRA OF CONJUGATED CHROMOPHORES - EVIDENCE FOR ELECTRONIC AND VIBRATIONAL COUPLINGS IN CRYSTAL VIOLET. *J. Mol. Struct.* **1980,** *61* (JAN), 331-336.

68. Lueck, H. B.; McHale, J. L.; Edwards, W. D., SYMMETRY-BREAKING SOLVENT EFFECTS ON THE ELECTRONIC-STRUCTURE AND SPECTRA OF A SERIES OF TRIPHENYLMETHANE DYES. *J. Am. Chem. Soc.* **1992,** *114* (7), 2342-2348.

69. Maruyama, Y.; Ishikawa, M.; Satozono, H., Femtosecond isomerization of crystal violet in alcohols. *J. Am. Chem. Soc.* **1996,** *118* (26), 6257-6263.

70. Maruyama, Y.; Magnin, O.; Satozono, H.; Ishikawa, M., Ground- and excited-state isomerization of triphenylmethane dyes in the femtosecond regime. *J. Phys. Chem. A* **1999,** *103* (29), 5629-5635.

71. Sheppard, S. E., On the Influence of Their State in Solution on the Absorption Spectra of Dissolved Dyes. *Proceedings of the Royal Society of London. Series A, Containing Papers of a Mathematical and Physical Character* **1909,** *82* (554), 256-270.

72. Shapiro, B. I.; Is, *Molecular ensembles of polymethine dyes*. Soc Imaging Science & Technology: Springfield, 2006; p 65-68.

73. Wuerthner, F.; Kaiser, T. E.; Saha-Moeller, C. R., J-Aggregates: From Serendipitous Discovery to Supramolecular Engineering of Functional Dye Materials. *Angewandte Chemie-International Edition* **2011,** *50* (15), 3376-3410.

74. Avakyan, V. G.; Shapiro, B. I.; Alfimov, M. V., Dimers, tetramers, and octamers of mono- and trimethyne thiacarbocyanine dyes. Structure, formation energy, and absorption band shifts. *Dyes and Pigments* **2014,** *109*, 21-33.

75. Jochum, P.; Schrott, E. L., DECONVOLUTION OF MULTICOMPONENT ULTRAVIOLET VISIBLE SPECTRA. *Anal. Chim. Acta* **1984,** *157* (2), 211-226.

76. Jochum, P.; Schrott, E. L., Deconvolution of multicomponent ultraviolet/visible spectra. *Anal. Chim. Acta* **1984,** *157*, 211-226.

77. Lagarias, J. C.; Reeds, J. A.; Wright, M. H.; Wright, P. E., Convergence properties of the Nelder-Mead simplex method in low dimensions. *SIAM J. Optim.* **1998,** *9* (1), 112-147.

78. Calabrese, I.; Merli, M.; Liveri, M. L. T., Deconvolution procedure of the UV-vis spectra. A powerful tool for the estimation of the binding of a model drug to specific solubilisation loci of bio-compatible aqueous surfactant-forming micelle. *Spectroc. Acta Pt. A-Molec. Biomolec. Spectr.* **2015,** *142*, 150-158.

79. Mironova, D. A.; Muslinkina, L. A.; Syakaev, V. V.; Morozova, J. E.; Yanilkin, V. V.; Konovalov, A. I.; Kazakova, E. K., Crystal violet dye in complexes with amphiphilic anionic calix 4 resorcinarenes: Binding by aggregates and individual molecules. *Journal of colloid and interface science* **2013,** *407*, 148-154.

80. Tongul, B.; Kavakcioglu, B.; Tarhan, L., Partitioning and purification of menadione induced NAD(P)H oxidase from Phanerochaete chrysosporium in aqueous two-phase systems. *Sep. Purif. Technol.* **2016,** *163*, 275-281.

81. da Silva, L. H. M.; da Silva, M. C. H.; de Aquino, R. A. N.; Francisco, K. R.; Cardoso, M. V. C.; Minim, L. A.; Coimbra, J. S. R., Nitroprusside-PEO enthalpic interaction as a driving force for partitioning of the Fe(CN)(5)NO (2-) anion in aqueous

two-phase systems formed by poly(ethylene oxide) and sulfate salts. *Journal of Physical Chemistry B* **2006,** *110* (46), 23540-23546.

82. Freyer, M. W.; Lewis, E. A., Isothermal titration calorimetry: Experimental design, data analysis, and probing Macromolecule/Ligand binding and kinetic interactions. In *Biophysical Tools for Biologists: Vol 1 in Vitro Techniques*, Correia, J. J.; Detrich, H. W., Eds. Elsevier Academic Press Inc: San Diego, 2008; Vol. 84, pp 79-113.

83. Johansson, H. O.; Karlstrom, G.; Tjerneld, F.; Haynes, C. A., Driving forces for phase separation and partitioning in aqueous two-phase systems. *Journal of Chromatography B* **1998,** *711* (1-2), 3-17.

CAPÍTULO 2

Chemical groups contribution to the driving forces in the partition of phenylmethane dyes in PEO1500 + $MgSO_4$ + H_2O systems

ABSTRACT

Aqueous two-phase system (ATPS) is known as an efficient and environmentally safe technique for the extraction and pre-concentration of different solutes. However, the contribution of chemical groups to the solutes-transfer driving forces is still unknown. We have examined the partition of six phenylmethane (PhM) dyes with similar chemical structure in PEO1500 + $MgSO_4$ + H_2O ATPS, enabling the calculation of chemical groups contributions to standard thermodynamic transfer parameters at infinite dilution conditions as standard Gibbs free energy change ($\Delta_{tr}G^{\theta,\infty}$), standard enthalpy change ($\Delta_{tr}H^{\theta,\infty}$) and standard entropy change ($T\Delta_{tr}S^{\theta,\infty}$). The CH_3 group average contributions, in kJ mol^{-1}, were: $\Delta_{tr}G^{\theta,\infty}_{PhM} = -0.56$, $\Delta_{tr}H^{\theta,\infty}_{PhM} = -4.86$ and $T\Delta_{tr}S^{\theta,\infty}_{PhM} = -4.53$, while those of the phenyl ring were: $\Delta_{tr}G^{\theta,\infty}_{PhM} = -13.02$, $\Delta_{tr}H^{\theta,\infty}_{PhM} = -35.23$ and $T\Delta_{tr}S^{\theta,\infty}_{PhM} = -28.16$. The positive charge in the dye molecule does not contribute to the $\Delta_{tr}G^{\theta,\infty}$ values, but $\Delta_{tr}H^{\theta,\infty}_{PhM}$ and $T\Delta_{tr}S^{\theta,\infty}_{PhM}$ increased to around 11.21 kJ mol^{-1}, indicating that the presence of charge in the dye molecule decreases its hydrophobicity, thereby enhancing the water solvation freedom rotational degree.

1. INTRODUCTION

Currently, aqueous two-phase systems (ATPSs) are used in a broad range of purposes: in drug separation[1], protein extraction[2], removal of hydrophilic ionic liquids[3], enzyme recovery[4], extraction of antimicrobial peptides[5], recovery of biomolecules[6], metal extraction and separation[7, 8], extraction of natural pigments[9-11], aminoacid partition[12],

organic compounds partition[13, 14] and dyes partition[15], among others. However, there are few thermodynamic studies answering the fundamental question: what is the relationship between the solute structure and the driving forces that determine its partitioning behavior in ATPS? If the goal is the optimization of ATPS application in the separation and purification of different kind of solutes, this important thermodynamic question should be addressed. Therefore, in order to understand what is the chemical group contribution to the ATPS solute transfer process, it is important to develop experimental methods that allow to determine all thermodynamic parameters that are responsible for the transfer of the solutes between the ATPS phases.

The main experimental approach found in the literature on the ATPS solute partitioning thermodynamics involves the determination of the temperature dependence of the partitioning coefficient, and to apply the van't Hoff approximation to calculate the transfer enthalpy change ($\Delta_{tr}H$) and the transfer entropy change ($\Delta_{tr}S$)[8, 16-20]. As is well known, this approach has some limitations: (i) since the van't Hoff $\Delta_{tr}H$ value is obtained from the ln K *versus* 1/T curve, it must have accumulative errors coming from inadequate measurements of K and T, and (ii) temperature affects the phase composition of each ATPS phase, which changes the K value due to the modifications in temperature and phase composition. In order to overcome these limitations, Mageste et al[11] proposed a new method to calculate directly $\Delta_{tr}H$ using nanocalorimetry. They added a solution of the solute (using the bottom phase as solvent) in a nanocalorimeter cell containing 0.8 mL of both ATPS phases. Since the authors have measured K values, it was possible to calculate the amount of solute transferred to the top phase, and by dividing the enthalpy measured in the calorimeter by the molar amount of solute that was transferred, it was possible to calculate $\Delta_{tr}H$. The main problem with this strategy is that the solute has a finite concentration in each ATPS phase, which makes the solute-

solute interaction a great contribution to the $\Delta_{tr}H$ values. Recently Rengifo et al[21] proposed a new approach to calculate the $\Delta_{tr}H$ from the experimental determination of the dilution enthalpy change of the solute in the ATPS components at small solute concentration by isothermal titration calorimetry (ITC). The authors considered that this low concentration could be approximated for the infinite dilution state ($\Delta_{dil}H^{\infty}$). However, even considering the small concentration state, solute-solute interactions must affect the transfer parameters.

In order to overcome this limited approach, in this paper we have investigated the partition of six phenylmethane (PhM) dyes, namely: methyl violet 10B (MV10B); methyl violet 6B (MV6B); methyl violet 2B (MV2B); pararosaniline (PRA); methyl violet B (MVB) and auramine (AUR), which are structurally very similar (figure 1) in PEO1500 + $MgSO_4$ + H_2O ATPS. This novel experimental method allows the determination of the following standard solute transfer parameters for each dye: standard transfer Gibbs free energy change ($\Delta_{tr}G^{\theta,\infty}$), standard transfer enthalpy change ($\Delta_{tr}H^{\theta,\infty}$) and standard transfer entropy change ($T\Delta_{tr}S^{\theta,\infty}$). By analyzing the dependence of each transfer parameter on the dye chemical structure, it was possible to determine the chemical group contribution for the driving forces in the PhM dyes transfer processes.

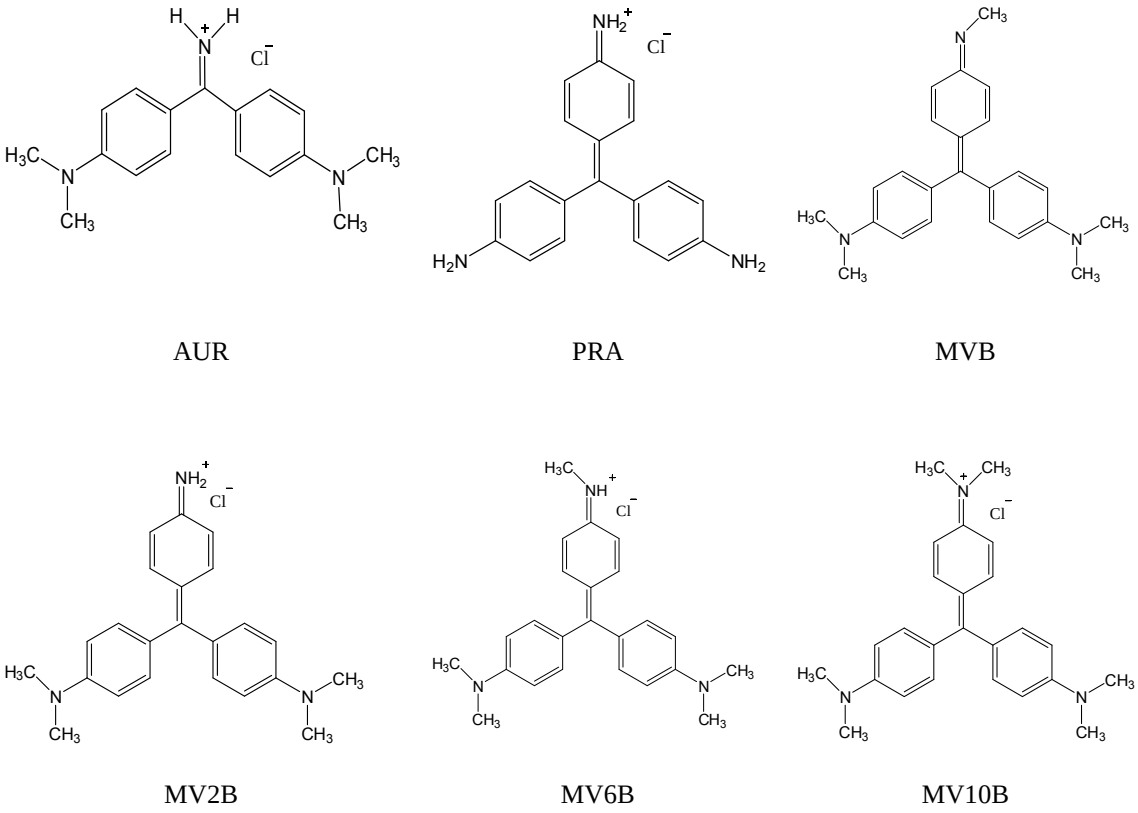

Figure 1. PhM dyes molecular structures

2.MATERIAL AND METHODS

2.1 Materials

Poly(ethylene oxide) (PEO), with a molar mass of 1500 g mol^{-1}, was purchased from Synth (Brazil). The inorganic salt magnesium sulfate heptahydrate ($MgSO_4 \bullet 7H_2O$) was purchased from Vetec (Brazil). The dyes MV10B (purity ≥ 90 %), MV6B (purity ≥ 90 %), MV2B (purity ≥ 98 %), PRA (purity ≥ 90 %), MVB (purity ≥ 87 %) and AUR (purity ≥ 85 %) were purchased from Sigma-Aldrich (USA). All chemicals used in this study were of analytical grade and used without further purification. Deionized water was used in all experiments.

2.2 Preparation of ATPS and determination of PhM dyes partition coefficients

The compositions of the ATPS ternary mixtures used in the partition experiments were chosen based on previously published phase diagrams.[22, 23] To achieve the desired composition ratio for each ATPS, appropriate amounts of PEO solutions, salt and water were taken into graduated centrifuge tubes. The tubes were shaken and left to stand at 298 K, in a thermostatic bath (Microquimica, MQBTC 99-20, 298.15 K), with an uncertainty of ± 0.1 K.

Once the system had achieved thermodynamic equilibrium, the two phases were collected separately for partition experiments. To a total of 8.0 g (divided as 1.0 g of top phase and 7.0 g of bottom phase) were added 100 μL of the PhM dye stock solution (3.1 × 10^{-3} mol kg^{-1}) in glass tubes. The final concentration of the dyes in the tubes was 3.9 × 10^{-5} mol kg^{-1}. For each tie-line length (TLL) and each ATPS, three systems were prepared: a blank without dye, a sample and a replicate. These systems were stirred manually for 3 min until the solutions became cloudy and then maintained under controlled temperature in a thermostatic bath at 298 K for a minimum of 8 h to reach thermodynamic equilibrium. Aliquots of the top and the bottom phases were collected with a syringe, and adequately diluted with deionized water for spectrophotometric analysis at 590 nm for MV2B, MV6B, MV10B and MVB, 540 nm for PRA, and 435 nm for AUR, using a Shimadzu digital double beam spectrometer (UV-2550).

The PhM dyes partition coefficients (K) between the phases were determined by the concentration ratio of the analyte in each phase of the ATPS. In agreement with the Beer-Lambert law, on specific conditions the absorbance of the analyte at a specific wavelength is directly proportional to the analyte concentration. Thus, the partition coefficient (K) can be given as described in Equation 1.

$$K = \frac{(Abs^{TP})x(fd^{TP})}{(Abs^{BP})x(fd^{BP})} \quad (1)$$

where (Abs^{TP}) and (Abs^{BP}) are the absorbance of the dyes in the diluted upper phase and the diluted bottom phase, respectively, discounting the absorbance of the corresponding blanks, and (fd^{TP}) and (fd^{BP}) are the dilution factors for the phases.

The K values were determined for different TLL values of each investigated ATPS. The TLL numerically expresses the difference in the intensive thermodynamic functions between the upper and the bottom phases, at constant pressure and temperature. It is calculated using Equation 2:

$$TLL = \sqrt{(C_{pol}^{UP} - C_{pol}^{BP})^2 + (C_{salt}^{UP} - C_{salt}^{BP})^2} \quad (2)$$

where C_p^{UP} and C_p^{BP} are the polymer concentrations in the top and bottom phases, respectively, and C_s^{UP} and C_s^{BP} are the corresponding salt concentrations in the top and bottom phases, respectively.

2.3 Thermodynamic parameters of transfer

2.3.1 Standard transfer Gibbs free energy change ($\Delta_{tr}\boldsymbol{G^{\theta}}$)

For all ATPSs, the $\Delta_{tr}\boldsymbol{G^{\theta}}$ was obtained with the thermodynamic relationship given by Equation 3:

$$\Delta_{tr}G^{\theta} = -R\,T\,ln\,K \quad (3)$$

where R is the real gas constant in (kJ mol^{-1} K^{-1}), T is the absolute temperature in K, and K is the dyes partition coefficient obtained at the infinite dilution condition, by extrapolating *K versus* [dye] curves to zero dye concentration.

2.3.2 Dyes transfer enthalpy change ($\Delta_{tr}\boldsymbol{H^{\theta}}$)

Isothermal titration calorimetry (ITC) was used to determine the dye standard dilution enthalpy change ($\Delta_{dil}\boldsymbol{H^{\theta}}$) in the ATPS bottom and the upper phases. The experiments were conducted in a CSC-4200 microcalorimeter (Science Corp. Calorimeter). The $\Delta_{tr}\boldsymbol{H^{\theta}}$ values for all PhM dyes in each TLL was obtained with the following procedure: the energy change associated with the dye dilution effects ($\Delta_{dil}H_{PhM}$) was determined by filling the reference and the sample cells with 1.80 mL of the bottom or upper phase, and titrating the sample solution with fifteen consecutive injections of 15 μL of the dyes stock solutions at a concentration of (5.8×10^{-4} mol kg^{-1}), prepared in the bottom or upper phase of the ATPS. The flow of energy registered during the whole process was recorded as a power *versus* time curve, which was integrated to obtain the enthalpy change of each dilution process. To discount the energy associated with friction effects, the same experiment was performed in the absence of dyes. A gas-tight Hamilton syringe (250 μL) controlled by an instrument was utilized for the injections, and a stirrer helix stirring at 300 rpm was used throughout the experiment. The dye standard dilution enthalpy change curve in phase α (α = bottom or upper phase) *versus* dye concentration ($\Delta_{dil}H^{\alpha}_{PhM}$ *vs* [PhM]) was plotted and the dye concentration was extrapolated to zero. Then it was possible to obtain the dye standard dilution enthalpy change in infinite dilution conditions ($\Delta_{tr}H^{\theta,\infty}_{PhM}$) for each PhM dye in both ATPS phases.

The standard enthalpy change at infinite dilution condition was determined using Equation 4:

$$\Delta_{tr}H^{\theta,\infty}_{PhM} = \Delta_{dil}H^{\infty,UP}_{PhM} - \Delta_{dil}H^{\infty,BP}_{PhM} \quad (4)$$

Where: $\Delta_{dil}H_{PhM}^{\infty,UP}$ and $\Delta_{dil}H_{PhM}^{\infty,BP}$ are the dye standard dilution enthalpy change at infinite dilution conditions in the upper and bottom phases, respectively, and $\Delta_{tr}H_{PhM}^{\theta,\infty}$ is the dye standard transfer enthalpy change at infinite dilution condition.

2.3.3. Standard transfer entropy change ($\Delta_{tr}S^{\theta}$)

The PhM dyes standard transfer entropy change at infinite dilution condition ($T\Delta_{tr}S_{PhM}^{\theta,\infty}$) was determined with the classic thermodynamic relationship given by Equation 5:

$$\Delta_{tr}G_{PhM}^{\theta,\infty} = \Delta_{tr}H_{PhM}^{\theta,\infty} - T\Delta_{tr}S_{PhM}^{\theta,\infty} \quad (5)$$

Where: $\Delta_{tr}H_{PhM}^{\theta,\infty}$ is the dye standard transfer enthalpy change at infinite dilution condition and $\Delta_{tr}G_{PhM}^{\theta,\infty}$ is the dye standard transfer Gibbs free energy change at infinite dilution condition.

3. Results and discussion

3.1 Effect of dye concentration on the partition coefficient

As is well known, depending on concentration and/or temperature, phenylmethane (PhM) molecules can self-assemble as dimers, trimers and so on, producing different chemical species with distinct partition behavior[24]. Therefore it is very important to determine the relationship between the PhM partition coefficient (K_{PhM}) and its total concentration with the ATPS studied in this work. If K_{PhM} changes with increasing dye concentration, then different chemical species are transferred between both ATPS phases. However, if K_{PhM} is independent of the colorant concentration, it can be concluded that only one chemical compound is transferred[11, 25].

Figure 2 shows the PhM partition coefficient (K_{PhM}) as a function of its total concentration, in mol kg^{-1}, in a PEO1500 +$MgSO_4$+ H_2O ATPS at 298.15 K, in the first TLL (5.27 mol kg^{-1}).

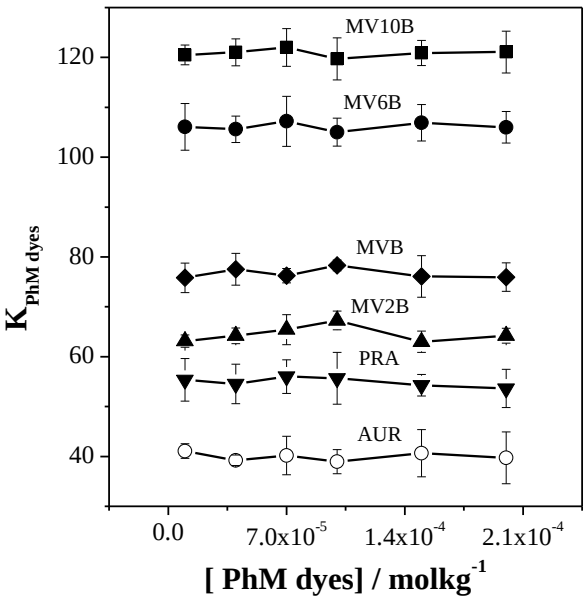

Figure 2. K values of PhM dyes as a function of the concentration measured in PEO1500 + $MgSO_4$ + H_2O ATPS at 298.15 K and TLL 1 = 5.27 mol kg^{-1}.

It can be seen that the values of K_{MV6B} and other K_{PhM} were independent of the dye concentration, suggesting that within this range of dye amount only one type of those MV6B species (monomer or dimers) is distributed between both ATPS phases. One experimental approach to determine whether MV6B monomers or dimers are partitioning in the PEO1500 + $MgSO_4$ + H_2O ATPS is to obtain dye UV-*vis* spectra for each ATPS phase and compare them with UV-*vis* spectra of dyes in pure water. In aqueous solutions, the MV6B molecules exhibit two superimposed bands: the long wavelength α-band (λ_{max} = 590 nm), which corresponds to monomer absorption, and the short wavelength β-band (λ_{max} = 550 nm), which corresponds to the dimer absorption[26-28].

The self-assembly process of MV6B can be studied by the UV-*vis* band deconvolution method, which allows to calculate the contribution of the monomer and dimer species for the UV-*vis* spectrum (Figure 3).

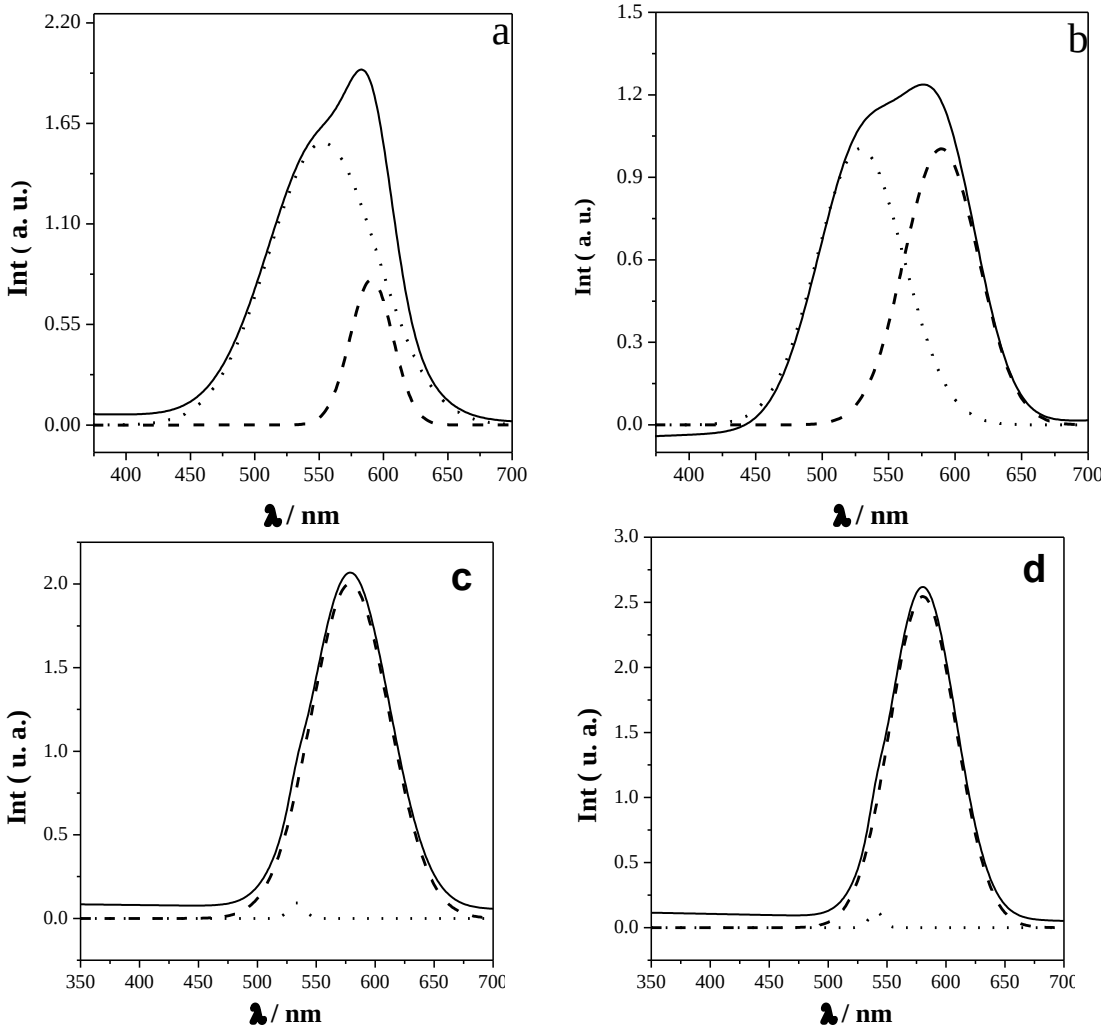

Figure 3. UV-vis absorption spectrum of MV6B at a concentration of $3.9x10^{-5}$ mol kg^{-1} (—), deconvolution result β band (…) and α band (---) obtained in: (a) pure water, (b) $MgSO_4$ aqueous solutions , (c) ATPS salt rich phase and (d) ATPS polymer concentrated phase, at 298 K at TLL = 5.27 mol kg^{-1}.

The deconvolution results show that the UV-*vis* spectrum of MV6B is the result of the sum of two bands with λ_{max} = 590 nm (α-band) and λ_{max} = 550 nm (β-band), and the relationship between its intensities (area of the band) varies according to the solvent and the dye concentration. Figure 4 shows the ratio between the areas of the α and β bands (deconvolution result for MV6B).

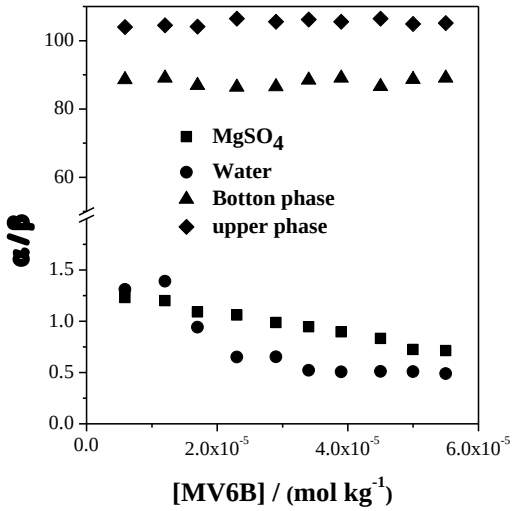

Figure 4. Ratio between α and β area band (α / β) as a function of the concentration of MV6B in pure water, in $MgSO_4$ aqueous solution and APTS bottom and upper phase of PEO1500 + $MgSO_4$ + H_2O ATPS at 298.15 K at TLL = 5.27 mol kg^{-1}.

For 3.9×10^{-5} mol kg^{-1} of MV6B in water (Figure 3a), the β band is higher than the α band (α/β = 0.50), meaning that the presence of dimers is predominant. Ghanadzadeh *et al*[29, 30] showed that methyl violet aqueous solutions at [MV6B] > 2.5×10^{-5} mol L^{-1} contain dimers in thermodynamic equilibrium with MV6B monomers, and the amount of clusters increases as the dye total concentration increases. In $MgSO_4$ aqueous solutions (Figure 3b and Figure 4), monomers and dimers have almost the same contribution (α/β= 0.89) to the UV-*vis* band, whilst in the ATPS salt rich phase, i.e, an aqueous mixture of $MgSO_4$ and PEO1500 (Figure 3c and figure 4), the concentration of monomers is predominant (α/β = 89). Since in $MgSO_4$ aqueous solutions there are almost equal concentrations of monomers and dimers, this higher monomer concentration in the $MgSO_4$-rich ATPS phase was induced by the presence of polymer in lower concentration, which enables the PEO-dye interaction to occur, disrupting any dimer present. In the polymer-concentrated ATPS phase (Figure 3d and

figure 4), an equal behavior is observed, but with less dimer formation (α/β = 105), indicating again that PEO-dye interactions impair the formation of dye dimers. These spectroscopic analyses indicate that predominantly monomeric species are transferred between both ATPS phases, giving support to the hypotheses on the existence of a specific interaction between PEO segments present in both phases of ATPS and dye monomers. The PEO-dye interaction is capable of inhibiting the MV6B-MV6B stacking π-π interaction, which is controlled by directional overlapping of HOMOs with LUMOs[31].

3.2. MV6B partition behavior

The solute distribution between the ATPS phases is determined by a delicate balance between different intermolecular interactions (van der Waals, electrostatic, hydrogen bond, hydrophobic, etc.)[32]. At [MV6B] = 3.9×10^{-5} mol kg^{-1} , the dye distribution in all ATPS studied in this work was very uneven, with high dye concentration in the polymer-rich phase. In order to understand the interactions driving PhM partition in the ATPS, we have examined the relationship between K_{PhM} or $\Delta_{tr}G^{\theta}_{PhM}$ values and ATPS phase compositions (TLL). In this case, an adaptation of Equation 2 can be made to calculate the TLL, as given by Equation 2. Figure 5 shows the K_{MV6B} and $\Delta_{tr}G^{\theta}_{MV6B}$ values as a function of the TLL of the ATPS PEO1500 + $MgSO_4$ + H_2O ATPS at 298 K.

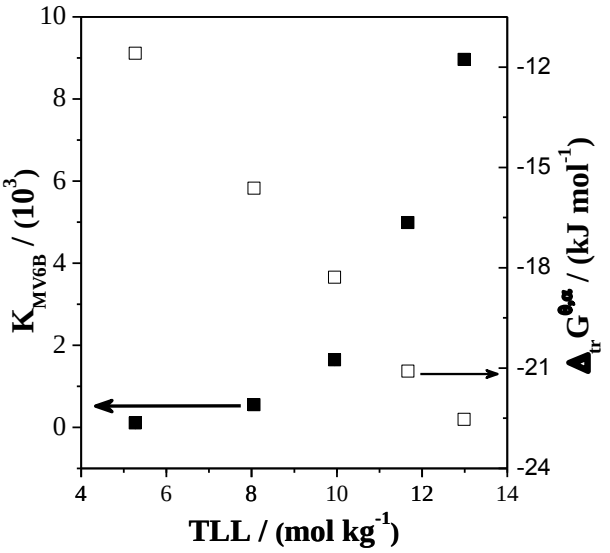

Figure 5. K_{MV6B} (■) and $\Delta_{tr}G^{\theta}_{MV6B}$ (□) as function of TLL in the PEO1500 + $MgSO_4$ + H_2O ATPS at 298.15 K.

The K_{MV6B} values ranged between (105.58 ± 4.03) and (8960.57 ± 6.25) for TLL magnitudes varying between 5.27 and 12.98 mol kg^{-1}, showing that MV6B concentrated intensely in the upper ATPS phase. Moreover, an increase in TLL caused an exponential increase [K_{MV6B} = 4.96 × exp (TLL/7.18) + 50.86] in the dye transfer process from the ATPS bottom phase to the upper phase. Therefore, the partition of MV6B decreases the Gibbs free energy of the biphasic systems, and such decrease at a standard state can be calculated by applying Equation 3 to the particular case of the MV6B dye, that is, $\Delta_{tr}G^{\theta}_{MV6B} = -R\,T \ln K_{MV6B}$.

The results of $\Delta_{tr}G^{\theta,\infty}_{MV6B}$ *versus* TLL are shown in Figure 5. The $\Delta_{tr}G^{\theta}_{MV6B}$ values for the PEO1500 + $MgSO_4$ + H_2O ATPS decreased with increasing TLL, ranging from (−11.5 ± 0.1) to (−22.5 ± 0.2) kJ mol^{-1}. The negative values of $\Delta_{tr}G^{\theta,\infty}_{MV6B}$ indicate a more favorable interaction between the dye molecules and the components of the ATPS polymer-rich phase than the interactions between the MV6B molecules and the

components of the salt-rich phase. Since the main difference between upper and bottom phase composition is the polymer and salt amounts, probably this dye partition to the upper phase is due to specific interactions between the dye molecules and the EO segments.

To the best of our knowledge, there are no studies on the partition of PhM dyes in ATPS. However, the use of ATPS formed by polymer and salt in the study of dye partition (either synthetic or natural) has been proposed as an alternative for colorant purification and extraction[11,33-36]. Shiri *et al*[33] proposed a new approach for the determination of Brilliant Blue FCF in water and food samples using different ATPS composed by PEO-(4000 or 6000 or 10000) and Na_2SO_4 or Na_2CO_3 or $(NH_4)_2SO_4$ or KH_2PO_4.They found that the best ATPS performance for the dye extraction process was effected with PEO4000 + Na_2CO_3 + H_2O at pH 5.5 and 35 °C. However the authors did not conduct any thermodynamic studies to help understanding the driving forces that are responsible for the extraction of the dye. Alvarenga *et al*[34] studied the partitioning of textile dye Remazol Yellow Gold RNL in ATPS generated by PEO with different molar masses (1500, 4000 and 6000) and inorganic [$(NH_4)_2SO_4$, Li_2SO_4, $MgSO_4.7H_2O$ and Na_2SO_4] or organic [CitrNa ($NaH_2C_6H_5O_7$) and TartNa ($Na_2C_4H_4O_6.2H_2O$)] salts, for which the highest K ($150 < K < 1200$) values were obtained with the PEO1500 + Li_2SO_4 + H_2O ATPS. The authors showed that the dye partition behavior is independent of the polymer molar mass or the anion nature, without any discussion about the thermodynamics of the transfer process. Mageste *et al*[11] studied the partition of the natural dye Norbixin in different ATPS formed by organic salts ($Na_2C_4H_4O_6.2H_2O$ and $C_4H_4O_4Na_2.6H_2O$) with hydrophilic polymers (PEO 1500 and PEO4000) or hydrophobic polymers (PPO400) or copolymers (L35). The K values did not depend on the polymer size, but were affected by the electrolyte anionic nature, following the

order: $K_{Na_2C_4H_4O_6 2\,H_2O}$. > $K_{C_4H_4O_6 6\,H_2O}$ and the polymer hydrophobicity, with K_{PEO} > K_{L35} > K_{PPO}. The authors measured the values of $\Delta_{tr}H$ (dye molar enthalpy transfer change) by microcalorimetry, ranging from −2.71 kJ mol^{-1} on the first TLL of ATPS L35 + $Na_2C_4H_4O_6.2H_2O$ + H_2O to −9.10 kJ mol^{-1}on the fifth TLL of the ATPS PPO400 + $Na_2C_4H_4O_6.2H_2O$ + H_2O. However, the use of natural dyes to investigate thermodynamic partition is restricted mainly due to the low degree of sample purity. So, as pointed out above, studies on the elucidation of the thermodynamics of colorant partition in ATPS are still incipient.

In order to better understand the MV6B transfer processes, the contributions of the standard transfer enthalpy change ($\Delta_{tr}H^{\theta}$) and the standard transfer entropy change ($\Delta_{tr}S^{\theta}$) to the standard transfer thermodynamic potential ($\Delta_{tr}G^{\theta}$) must be determined. Here we have proposed a novel approach to calculate these parameters.

3.3. Thermodynamic Transfer Parameters

Since there are no experimental thermodynamic studies describing the driving forces for PhM dyes distribution in ATPS, it is very important and strategic to evaluate the standard transfer Free Gibbs energy change ($\Delta_{tr}G^{\theta}_{PhM}$) expressed by equation 6:

$$\Delta_{tr}G^{\theta}_{PhM} = -R\,T\,lnK_{PhM} = -R\,T\,ln\frac{[PhM]^{UP}.\gamma^{UP}_{PhM}}{[PhM]^{BP}.\gamma^{BP}_{PhM}} \qquad (6)$$

Where R is the ideal gas constant, T is the system temperature, $[PhM]$ is the PhM concentration and γ_{PhM} is the PhM activity coefficient. The superscript indexes BP and UP are bottom and upper phases, respectively.

Despite the fact that Equation 6 is thermodynamically rigorous, it is of limited use, mainly because in general it is not an easy task to determine activity coefficients and their dependence on solute concentration. However, we can choose a thermodynamic state where γ_i does not affect $\Delta_{tr}G^{\theta}_{PhM}$. This condition should be such

that the solute interacts only with solvent molecules, i.e, with only ATPS components. This state is one where the solute concentration is infinitely diluted, in which case $\gamma_i = 1$. With this assumption, Equation 7 is obtained:

$$\Delta_{tr}G_{PhM}^{\theta,\infty} = -R\,T\ln\left(\lim_{[PhM]\to 0}\frac{[PhM]^{UP}}{[PhM]^{BP}}\right) = -RTlnK_{PhM}^{\infty} \quad (7)$$

Where $\Delta_{tr}G_{PhM}^{\theta,\infty}$ is the standard transfer Free Gibbs energy change at infinite dilution condition, in which case Equation 8 is satisfied:

$$\lim_{[PhM]\to 0}\gamma_{PhM}^{UP} = \lim_{[PhM]\to 0}\gamma_{PhM}^{BP} = 1 \quad (8)$$

To obtain K_{PhM}^{∞}, the K_{PhM} values were plotted against [PhM] and extrapolated to [PhM] equal to zero. Applying Equation 7, $\Delta_{tr}G_{PhM}^{\theta,\infty}$ can be estimated, which represents the system free energy change when 1 mol of PhM dyes are transferred from the bottom phase to the upper phase in infinite dilution conditions.

As is well known, in order to better understand the molecular processes occurring within the systems it is necessary to determine the components of $\Delta_{tr}G_{PhM}^{\theta,\infty}$, i.e, $\Delta_{tr}H_{PhM}^{\theta,\infty}$ and $\Delta_{tr}S_{PhM}^{\theta,\infty}$. To determine the standard enthalpy change at infinite dilution when 1 mol of PhM moves from bottom phase to upper phase in infinite dilution state ($\Delta_{tr}H_{PhM}^{\theta,\infty}$), Equation 9 can be applied. In this transfer process the dye molecule interacts only with components of the phases.

$$\Delta_{tr}H_{PhM}^{\theta,\infty} = \Delta_{dil}H_{PhM}^{\infty,UP} - \Delta_{dil}H_{PhM}^{\infty,BP} \quad (9)$$

The $\Delta_{dil}H_{PhM}^{\infty,UP}$ and $\Delta_{dil}H_{PhM}^{\infty,BP}$ values are the dye dilution (in the upper phase and in the bottom phase respectively) enthalpy changes at infinite dilutions. The $\Delta_{dil}H_{PhM}^{\infty\alpha}$ (α = UP or BP) were determined through the curve of enthalpy change of dye dilution in the α

phase *versus* dye concentration ($\Delta_{dil}H^{\alpha}_{PhM}$ *vs* [PhM]) by extrapolating the dye concentration to zero. $\Delta_{dil}H^{\alpha}_{PhM}$ expresses the following interactions: $\Delta H^{\alpha}_{PhM-PhM}$, $\Delta H^{\alpha}_{PhM-water,}$ $\Delta H^{\alpha}_{PhM-salt}$ and $\Delta H^{\alpha}_{PhM-pol}$, which could be simplified by: $\Delta_{dil}H^{\alpha}_{PhM} = \Delta H^{\alpha}_{PhM-PhM} + \Delta H^{\alpha}_{PhM-solvent}$. At infinite dilution, $\Delta_{dil}H^{\alpha}_{PhM}$ becomes equal to $\Delta H^{\alpha}_{PhM-solvent}$ only, because $\Delta H^{\alpha}_{PhM-PhM}$ is equal to zero at this thermodynamic state.

The standard transfer entropy change at infinite dilution ($\Delta_{tr}S^{\theta,\infty}_{PhM}$) can be calculated with Equation 10.

$$\Delta_{tr}S^{\theta,\infty}_{PhM} = \frac{\Delta_{tr}H^{\theta,\infty}_{PhM} - \Delta_{tr}G^{\theta,\infty}_{PhM}}{T} \quad (10)$$

Applying these theoretical approaches to the partition process of MV6B, we have obtained all thermodynamic parameters for the transfer of MV6B in the PEO1500 + $MgSO_4$ + H_2O ATPS, as a function of the TLL at 298.15 K (Table 1).

Table 1. Thermodynamic transfer parameters of MV6B as a function of the TLL values in the PEO1500 + $MgSO_4$ + H_2O ATPS at 298.15 K.

TLL	$\Delta_{tr}\boldsymbol{G}^{\boldsymbol{\theta},\infty}_{\boldsymbol{MV6B}}$	$\Delta_{tr}\boldsymbol{H}^{\boldsymbol{\theta},\infty}_{\boldsymbol{MV6B}}$	$\boldsymbol{T}\Delta_{tr}\boldsymbol{S}^{\boldsymbol{\theta},\infty}_{\boldsymbol{MV6B}}$
mol kg^{-1}	**kJ mol^{-1}**		
5.27	−11.48 ± 0.01	−25.50 ± 0.02	−13.94 ± 0.01
8.06	−15.61 ± 0.14	−39.28 ± 0.04	−23.63 ± 0.09
9.95	−18.29 ± 0.07	−55.89 ± 0.10	−37.47 ± 0.03
11.67	−21.11 ± 0.02	−76.10 ± 0.09	−55.01 ± 0.11
12.99	−22.49 ± 0.12	−99.61 ± 0.04	−77.04 ± 0.13

$\Delta_{tr}H^{\theta,\infty}_{MV6B}$ values ranged from (−25.50 ± 0.02) to (−99.61 ± 0.04) kJ mol^{-1}, showing that the transfer of VM6B from the bottom phase to the upper phase is an exothermic process which releases more energy as TLL values increase. $\Delta_{tr}H^{\theta,\infty}_{MV6B}$ could be considered as a combination of four types of interactions, as expressed by Equation 11.

$$\Delta_{tr}H^{\theta,\infty}_{PhM} = \Delta_{int}H^{\infty}_{PhM-BP} + \Delta_{int}H^{\infty}_{BP-BP} + \Delta_{int}H^{\infty}_{UP-UP} + \Delta_{int}H^{\infty}_{PhM-UP} \quad (11)$$

where $\Delta_{int}H^{\infty}_{PhM-BP}$ is the energy spent to break the interactions of PhM molecules and the bottom phase components; $\Delta_{int}H^{\infty}_{BP-BP}$ is the energy released when the bottom phase components interact with the that solvated the MV6B molecules; $\Delta_{int}H^{\infty}_{UP-UP}$ is the energy required to disrupt the interactions among the upper phase components in order to allocate MV6B molecules; and $\Delta_{int}H^{\infty}_{PhM-UP}$ is the decrease in the system energy due to the formation of the new interactions between PhM molecules and the upper phase components. Since $\Delta_{tr}H^{\theta,\infty}_{PhM}$ was negative, one can conclude that:

$$|\Delta_{int}H^{\infty}_{BP-BP} + \Delta_{int}H^{\infty}_{PhM-UP}| > |\Delta_{int}H^{\infty}_{PhM-BP} + \Delta_{int}H^{\infty}_{UP-UP}| \quad (12)$$

As TLL values increase, the number of PEO-PhM and PhM-salt interactions increases, and since $\Delta_{tr}H^{\theta,\infty}_{MV6B}$ became more negative the difference $|\Delta_{int}H^{\infty}_{BP-BP} + \Delta_{int}H^{\infty}_{PhM-UP}| - |\Delta_{int}H^{\infty}_{PhM-BP} + \Delta_{int}H^{\infty}_{UP-UP}|$ becomes higher. This enthalpic contribution to the K_{PhM} values can be described by a model developed by Johansson *et al.*[35] (Equation 13), where enthalpic effects on K_{PhM} can be represented as:

$$ln\, K_{PhM} = -\frac{M_{PhM}}{RT}\left[\sum_{a=1}^{3}(\Phi_a^{UP} - \Phi_a^{BP})w_{aPhM} + \sum_{a=1}^{2}\sum_{b=2}^{3}(\Phi_a^{UP}\Phi_b^{UP} - \Phi_a^{BP}\Phi_b^{BP})w_{ab}\right] \quad (13)$$

Where Φ_a^{UP} and Φ_a^{BP} are the volume fractions of component a in the upper and bottom phase respectively, (being a = water or polymer or salt). M_{PhM} is the PhM dye molar mass, w_{a-PhM} and w_{a-b} are the energies of effective potential pairs *a-PhM* and *a-b*. These energies can be defined by Equation 14.

$$W_{ab} = Z(\varepsilon_{ab} - \frac{1}{2}(\varepsilon_{aa} + \varepsilon_{bb})) \quad (14)$$

Where Z is the number of neighboring molecules that interact with the a component, ε_{ab} represents the interaction energy involved in the formation of the potential pair, and

ε_{aa} and ε_{bb} represent the energies resulting from the break of the *a-a* and *b-b* interactions, respectively.

Based on equation 14, the enthalpic interactions affect the partition behavior be means of two terms, the first being $\sum_{a=1}^{3}(\Phi_a^{UP} - \Phi_a^{BP})w_{aPhM}$, which represents the energy absorbed or released in the transfer of PhM dyes from the bottom phase to the upper phase due to interactions of PhM molecules with the forming components of both ATPS phases. So, a negative $\Delta_{tr}H_{PhM}^{\theta,\infty}$ refers to a specific interaction between PhM molecules and PEO segments ($w_{EO-PhM} < 0$) in order to make the term $\sum_{a=1}^{3}(\Phi_a^{UP} - \Phi_a^{BP})w_{aPhM}$ negative. The second term, $\sum_{a=1}^{2}\sum_{b=2}^{3}(\Phi_a^{UP}\Phi_a^{UP} - \Phi_a^{BP}\Phi_a^{BP})w_{ab}$, is the energetic balance caused by disruption of an existent hole on the bottom phase due to the PhM molecule movement from de bottom phase to the upper phase and the formation of a new cavity on the upper phase to accommodate the transferred dye solute. The arrangement of equation 13 results in Equation 15:

$$ln\, K_{PhM} = -\frac{M_{PhM}}{RT}[(W_{UP-PhM} - E_{UP}) - (W_{BP-PhM} - E_{BP})] \qquad (15)$$

Where W_{UP-PhM} represents the energy released because of new intermolecular interactions formed between PhM molecules and the components of the upper phase, whist E_{UP} is the energy required to break intermolecular interactions among the upper phase components to obtain cavities in this phase that accommodate PhM molecules. On the other hand, W_{BP-PhM} represents the energy required to break intermolecular interactions between PhM with the components of the bottom phase, and E_{BP} is the released energy associated with the process of formation of new intermolecular interactions between the components of the bottom phase. Then it can be concluded that PhM transfer occurs by means of a molecular process that releases and absorbs energy. The negative values of $\Delta_{tr}H_{PhM}^{\theta,\infty}$ mean that $|W_{UP-PhM} + E_{BP}| > |W_{BP-PhM} + E_{UP}|$,

i.e., the molecular processes which release energy should be more intense than that which absorbs energy.

The MV6B transfer processes occur, for all TLL values examined, with decreasing system entropy (Table 1), probably caused by the dye partition from a phase with higher configuration entropy (bottom phase) to a phase (upper phase) with a lower number of different spatial distribution. According to Johansson et al.[35], the number of configurations available for dye molecules in each phase is determined by the total number of molecules by unit volume present in these regions. The authors have emphasized that, due to the high amount of water in the ATPS, the phase molecular density is determined mainly by the amount of water molecules in the upper and bottom phases. Following the authors analyses, in the absence of enthalpic asymmetric intermolecular interactions, the entropy contribution to the partition is expressed by Equation 16.

$$ln\ K_{MV6B} = \frac{M_{MV6B}}{\rho}\left(\frac{n^{UP}}{V^{UP}} - \frac{n^{BP}}{V^{BP}}\right) \quad (16)$$

where K_{MV6B} and M_{MV6B} are the partition coefficient and the molecular weight of MV6B respectively, while $n^{UP}$and n^{BP} are the total number of molecules in the upper and bottom phases which, when divided by the V^{UP} and V^{BP}, result in the molecular density number of each phase. Finally, ρ is the total number of lattice sites per unit volume.

Equation 11 indicates that there is an entropic contribution to uneven partition if there is a density difference between the phases. For the PEO1500 + $MgSO_4$ + H_2O ATPS, a higher water content exists on the salt-rich phase than in the polymer-rich phase. Therefore, the difference in the dye configuration entropy in both phases is a

function of the difference in water content ($\Delta[H_2O]_{ATPS}$) between both ATPS phases, as indicated by Equation 17:

$$\Delta[H_2O]_{ATPS} = [H_2O]_{BP} - [H_2O]_{UP} \quad (17)$$

Where $[H_2O]_{BP}$ and $[H_2O]_{UP}$ are the concentrations of water, in mol kg^{-1}, in the bottom and upper phases respectively. For this specific ATPS, $\Delta[H_2O]_{ATPS}$ values range from 8.86 mol kg^{-1} for the first TLL to 13.82 mol kg^{-1} for the last TLL, showing that the concentration of water in the bottom phase is higher than in the upper phase. Moreover, these $\Delta[H_2O]_{ATPS}$ values are enlarged as TLL increases. As a consequence, $T\Delta_{tr}S^{\theta,\infty}_{MV6B}$ becomes negative because dye molecules move from the bottom phase (higher $\frac{n^{BP}}{V^{BP}}$) to the upper phase (lower $\frac{n^{UP}}{V^{UP}}$), thereby reducing the system entropy. Figure 6 shows $T\Delta_{tr}S^{\theta,\infty}_{MV6B}$ *versus* Δn_{water} ($\Delta n_{water} = \Delta n^{BP}_{water} - \Delta n^{UP}_{water}$), demonstrating that the system entropy decreases as the difference in the number of water molecules between both ATPS phases increases.

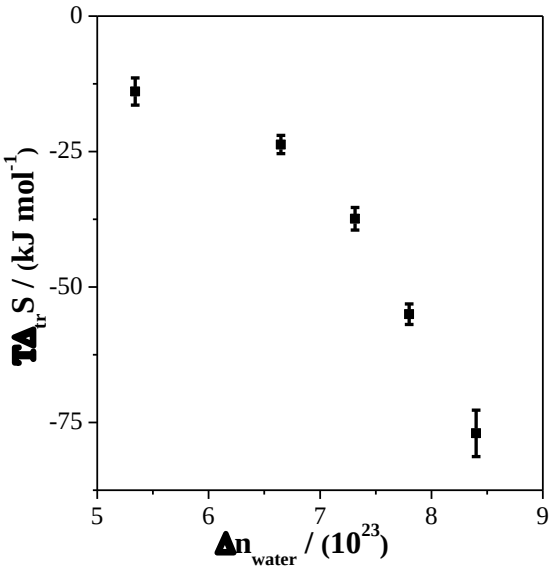

Figure 6. $T\Delta_{tr}S^{\theta,\infty}_{MV6B}$ values as a function of $[\Delta[H_2O]_{ATPS} = [H_2O]_{BP} - [H_2O]_{UP}]$ for the PEO1500 + $MgSO_4$ + H_2O ATPS at 298.15 K.

3.4. Effect of PhM chemical structure on the thermodynamic transfer

As discussed for $\Delta_{tr}G^{\theta,\infty}_{PhM}$ and $\Delta_{tr}H^{\theta,\infty}_{PhM}$ for MV6B in the PEO1500 + $MgSO_4$ + H_2O ATPS, dye partition occurs due to specific interactions between PEO and MV6B molecules. However, a question arises: what is the dye structure role in this intermolecular interaction? In order to answer this question, an investigation has been carried out on the thermodynamic of transfer of six PhM dyes with similar structures (Figure 1). The complete results of the study about enthalpy dilution change the dye structure effect on the PhM partitioning thermodynamic are showed in the Figures from 7 to 12 and the Tables from 2 to 7, the PhM dyes partition coefficient and $\Delta_{dil}H^{\infty}_{PhM}$ in both ATPS phases and the thermodynamic transfer parameters are presented for the infinite dilution condition for all six PhM dyes in the table 8.

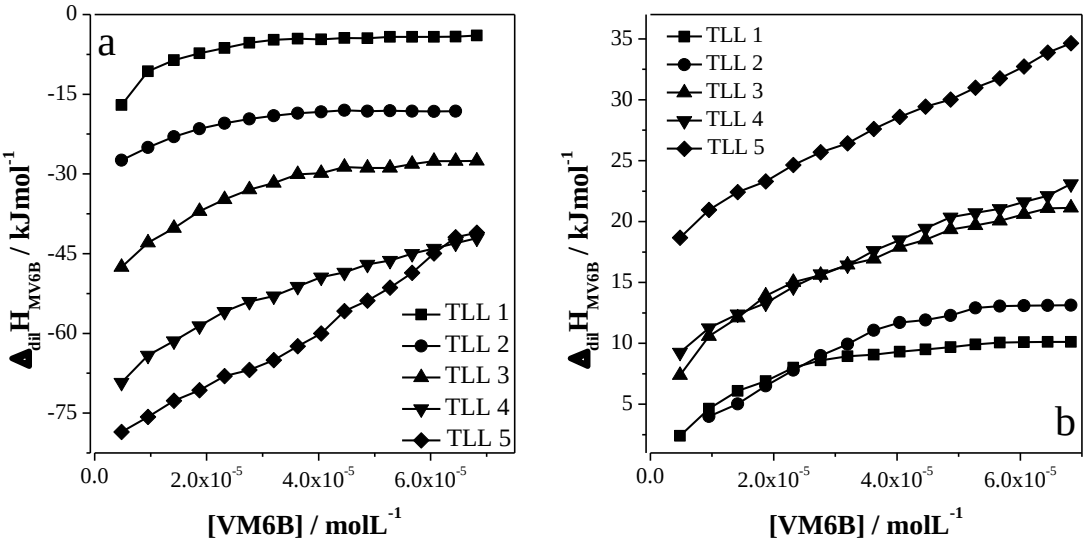

Figure 7. $\Delta_{dil}H^{UP}_{MV6B}$ (a) and $\Delta_{dil}H^{BP}_{MV6B}$ (b) as a function of dye concentration in upper and bottom phases of PEO1500+$MgSO_4$+H_2O ATPS at 298.15 K.

The result of $\Delta_{dil}H_{MV6B}$ versus [MV6B], Derives in a mathematical equation usually polynomial of 2 order (equations 18)

$$\Delta_{dil}H_{MV6B} = \text{Intercept} + b[MV6B] + a[MV6B]^2 \quad (18)$$

Thus when the dye concentrations are zero (Infinite dilution state)

$$\Delta_{dil}H^{\infty}_{MV6B} = \text{Intercept} \quad (19)$$

Table 2 K_{MV6B} values $\Delta_{dil}H_{MV6B}$ values in upper (UP) and bottom (BP) phases, for the TLL of PEO1500 + $MgSO_4$ + H_2O ATPS at 298.15 K.

TLL	K_{MV6B}	$\Delta_{dil}H^{\infty UP}_{MV6B}$	$\Delta_{dil}H^{\infty BP}_{MV6B}$
mol kg^{-1}		kJ mol^{-1}	
5.270	105.59±0.07	-25.51±0.01	-0.003±0.01
8.056	550.41±0.04	-37.57±0.09	1.77±0.05
9.949	1442.01±0.06	-49.78±0.17	6.10±0.06
11.669	3119.02±0.08	-68.09±0.03	8.01±0.04
12.987	5000.01±0.05	-82.26±0.02	17.2±0.05

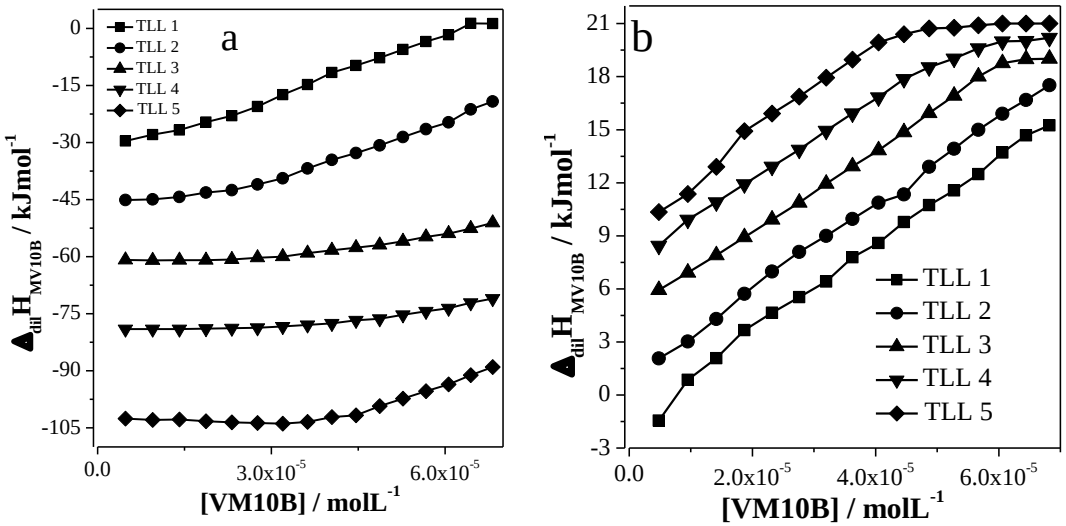

Figure 8. $\Delta_{dil}H^{UP}_{MV10B}$ (a) and $\Delta_{dil}H^{BP}_{MV10B}$ (b) as a function of dye concentration in upper and bottom phases of PEO1500+$MgSO_4$+H_2O ATPS at 298.15 K.

Table 3. K_{MV10B} values and $\Delta_{dil}H^{\infty}_{MV10B}$ values in upper (UP) and bottom (BP) phases, for the TLL of PEO1500 + $MgSO_4$ + H_2O ATPS at 298.15 K.

TLL	K_{MV10B}	$\Delta_{dil}H^{\infty UP}_{MV10B}$	$\Delta_{dil}H^{\infty BP}_{MV10B}$
mol kg^{-1}		kJ mol^{-1}	
5.270	119.93±0.02	-32.93±0.02	-2.20±0.04
8.056	1045.66±0.03	-46.21±0.07	0.79±0.03
9.949	2305.89±0.09	-60.64±0.06	4.48±0.03
11.67	4267.08±0.04	-78.42±0.04	6.81±0.07
12.99	6473.58±0.08	-101.29±0.08	7.88±0.05

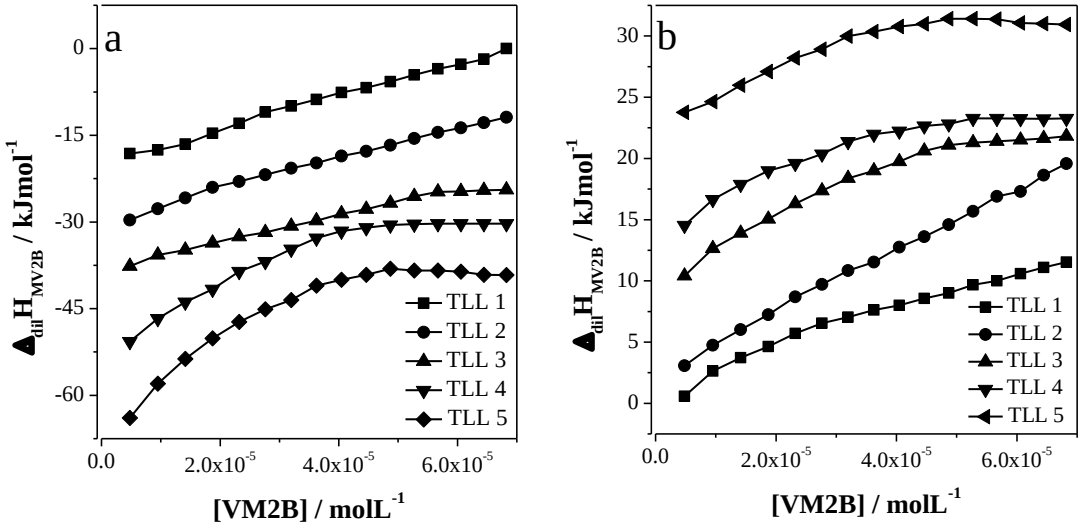

Figure 9. $\Delta_{dil}H^{UP}_{MV2B}$ (a) and $\Delta_{dil}H^{BP}_{MV2B}$ (b) as a functions of dye concentration in upper and bottom phases of PEO1500+$MgSO_4$+H_2O ATPS at 298.15 K.

Table 4. K_{MV2B} values and $\Delta_{dil}H^{\infty}_{MV2B}$ values in upper (UP) and bottom (BP) phases, for the TLL of PEO1500 + $MgSO_4$ + H_2O ATPS at 298.15 K.

TLL	K_{MV2B}	$\Delta_{dil}H^{\infty UP}_{MV2B}$	$\Delta_{dil}H^{\infty BP}_{MV2B}$
mol kg^{-1}		kJ mol^{-1}	kJ mol^{-1}
5.270	94.19±0.02	-20.37±0.03	0.08±0.01
8.056	442.89±0.08	-30.65±0.01	2.01±0.01
9.949	1194.01±0.09	-39.08±1.00	8.89±0.06
11.669	2995.04±0.07	-54.58±0.01	13.40±0.05
12.987	4097.03±0.05	-67.87±0.07	21.67±0.03

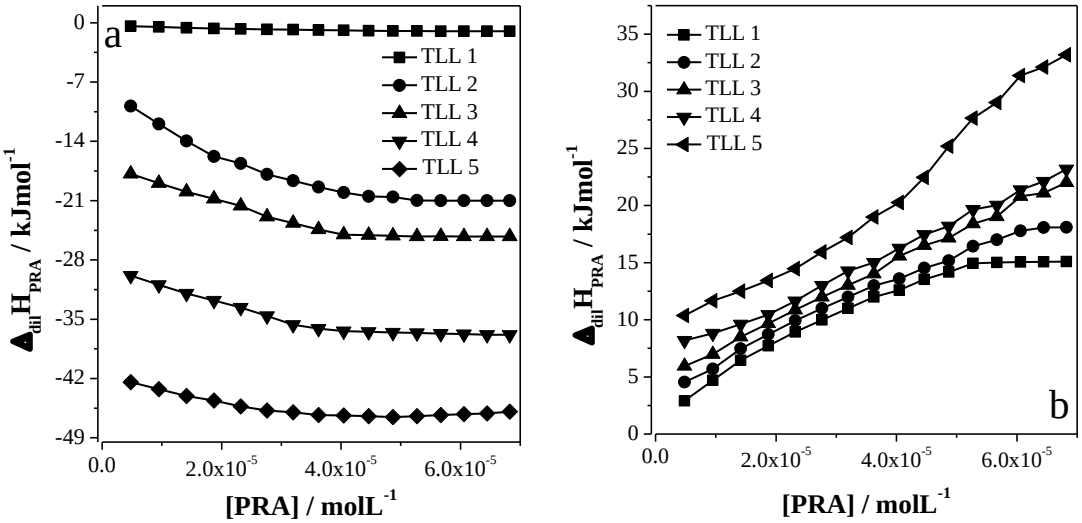

Figure 10. $\Delta_{dil}H^{UP}_{PRA}$ (a) and $\Delta_{dil}H^{BP}_{PRA}$ (b) as a function of dye concentration in upper and bottom phases of PEO1500+$MgSO_4$+H_2O ATPS at 298.15 K.

Table 5. K_{PRA} values and $\Delta_{dil}H^{\infty}_{PRA}$ values in upper (UP) and bottom (BP) phases, for the TLL of PEO1500 + $MgSO_4$ + H_2O ATPS at 298.15 K.

TLL	K_{PRA}	$\Delta_{dil}H^{\infty UP}_{PRA}$	$\Delta_{dil}H^{\infty BP}_{PRA}$
mol kg^{-1}		kJ mol^{-1}	
5.270	54.55±0.07	-0.32±0.01	1.07±0.01
8.056	265.70±0.03	-30.68±0.08	2.91±0.01
9.949	535.58±0.09	-16.01±0.04	4.60±0.04
11.669	1110.01±0.09	-28.49±0.07	6.71±0.05
12.987	1900.04±0.07	-41.50±0.03	9.36±0.07

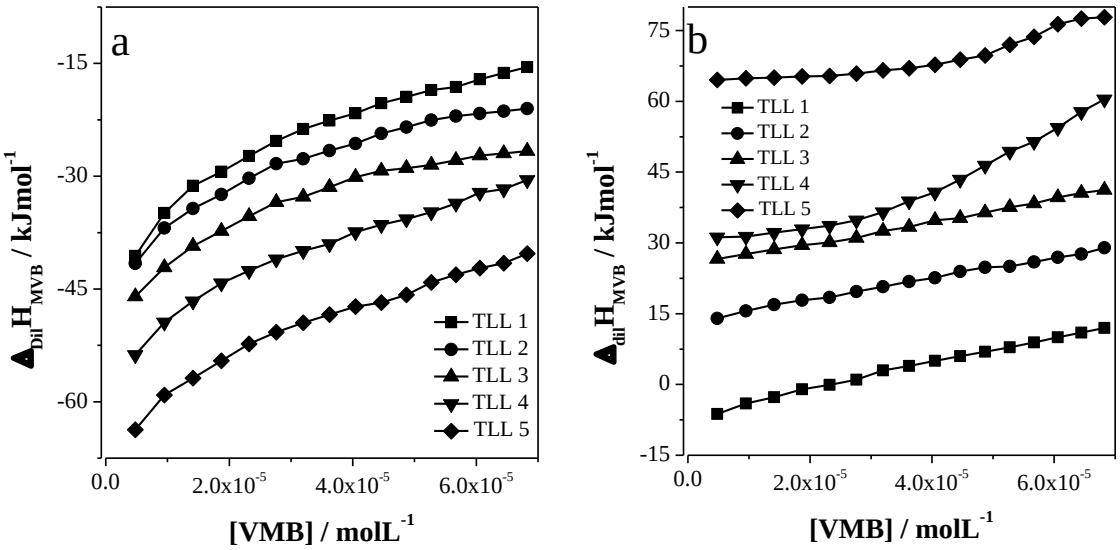

Figure 11. $\Delta_{dil}H^{UP}_{MVB}$ (a) and $\Delta_{dil}H^{BP}_{MVB}$ (b) as a function of dye concentration in upper and bottom phases of PEO1500+$MgSO_4$+H_2O ATPS at 298.15 K.

Table 6. K_{MVB} values and $\Delta_{dil}H^{\infty}_{MVB}$ values in upper (UP) and bottom (BP) phases, for the TLL of PEO1500 + $MgSO_4$ + H_2O ATPS at 298.15 K.

TLL	K_{MVB}	$\Delta_{dil}H^{\infty UP}_{MVB}$	$\Delta_{dil}H^{\infty BP}_{MVB}$
mol kg^{-1}		kJ mol^{-1}	
5.270	113.60±0.07	-41.79±0.01	-7.32±0.05
8.056	927.90±0.01	-43.23±0.04	13.11±0.07
9.949	2109.31±0.04	-47.81±0.01	25.69±0.03
11.669	3703.69±0.05	-55.58±0.06	31.10±0.01
12.987	6115.22±0.09	-64.64±0.09	65.08±0.08

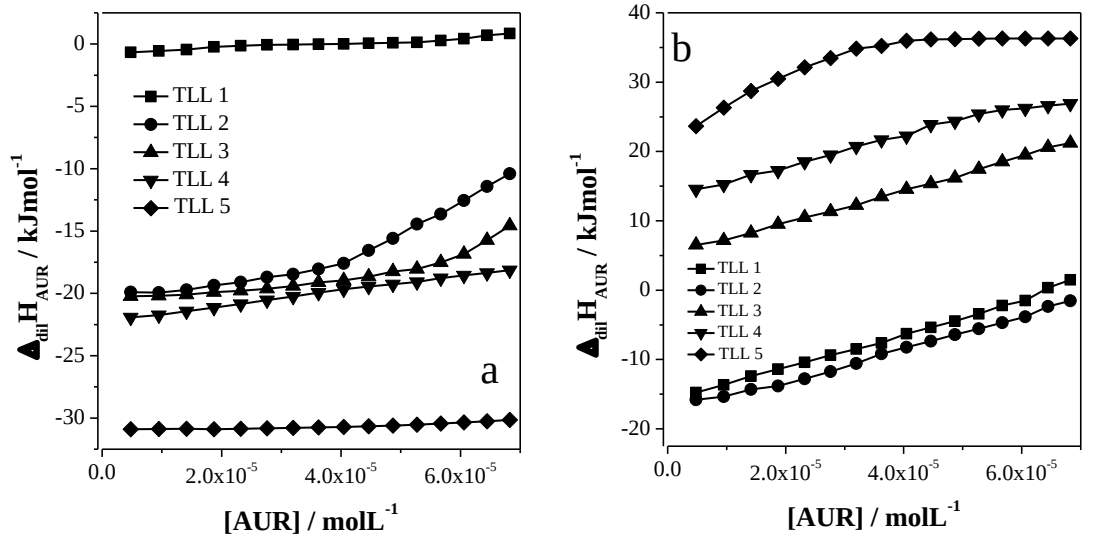

Figure 12. $\Delta_{dil}H^{UP}_{AUR}$ (a) and $\Delta_{dil}H^{BP}_{AUR}$ (b) as a function of dye concentration in upper and bottom phases of PEO1500+$MgSO_4$+H_2O ATPS at 298.15 K.

Table 7. K_{AUR} values and $\Delta_{dil}H^{\infty}_{AUR}$ values in upper (UP) and bottom (BP) phases, for the TLL of PEO1500 + $MgSO_4$ + H_2O ATPS at 298.15 K.

TLL	K_{AUR}	$\Delta_{dil}H^{\infty UP}_{AUR}$	$\Delta_{dil}H^{\infty BP}_{AUR}$
mol kg^{-1}		kJ mol^{-1}	
5.270	39.23±0.07	-1.06±0.04	-15.40±0.03
8.056	81.02±0.07	-19.75±0.07	-17.01±0.06
9.949	189.88±0.04	-20.57±0.02	5.37±0.08
11.669	387.19±0.03	-22.16±0.02	12.85±0.01
12.987	543.79±0.05	-30.81±0.01	21.39±0.04

Table 8. Thermodynamic transfer parameters of PhM dyes as a function of the TLL of PEO1500 + $MgSO_4$ + H_2O ATPS at 298.15 K.

PhM dyes	$\Delta_{tr}G^{\theta,\infty}_{PhM}$	$\Delta_{tr}H^{\theta,\infty}_{PhM}$	$T\Delta_{tr}S^{\theta,\infty}_{PhM}$
		kJ mol^{-1}	
TLL 1 / 5.27 mol kg^{-1}			
MV10B	-11.89±0.01	-30.77±0.01	-18.90±0.02
MV6B	-11.51±0.02	-25.52±0.03	-13.89±0.01
MV2B	-11.18±0.02	-20.49±0.04	-9.23±0.02
PRA	-9.90±0.04	-1.39±0.03	8.50±0.07
MVB	-11.7±0.01	-36.50±0.10	-24.76±0.09
AUR	-9.08±0.05	14.38±0.01	23.50±0.06
TLL 2 / 8.06 mol kg^{-1}			
MV10B	-17.19±0.02	-47.02±0.01	-29.65±0.03
MV6B	-15.60±0.01	-39,27±0.04	-23.77±0.03
MV2B	-15.01±0.03	-32.75±0.09	-17.74±0.06
PRA	-13.79±0.02	-10.91±0.03	2.87±0.01
MVB	-16.86±0.03	-54.26±0.05	-37.40±0.02
AUR	-10.88±0.01	-2.78±0.02	8.10±0.01
TLL 3 / 9.95 mol kg^{-1}			
MV10B	-19.08±0.04	-65.04±0.05	-45.86±0.01
MV6B	-18.01±0.02	-55.93±0.10	-37.40±0.08
MV2B	-17.46±0.01	-48.01±0.08	-30.19±0.07
PRA	-15.50±0.01	-20.67±0.04	-5.12±0.03
MVB	-18.87±0.06	-73.49±0.01	-54.45±0.07
AUR	-12.91±0.03	-16.02±0.04	-3.02±0.01
TLL 4 / 11.67 mol kg^{-1}			
MV10B	-20.71±0.06	-85.22±0.07	-64.52±0.01
MV6B	-20.04±0.03	-76.13±0.07	-56.14±0.04
MV2B	-19.76±0.05	-68.02±0.10	-48.15±0.05
PRA	-17.32±0.02	-35.18±0.08	-17.88±0.06
MVB	-20.29±0.10	-95.69±0.12	-75.39±0.02
AUR	-14.65±0.07	-35.15±0.10	-20.35±0.03

TLL 5 / 12.99 mol kg-1			
MV10B	-21.68±0.01	-109.20±0.04	-87.35±0.03
MV6B	-21.11±0.03	-99.63±0.08	-78.42±0.05
MV2B	-20.57±0.07	-89.71±0.09	-69.04±0.02
PRA	-18.60±0.09	-50.76±0.10	-32.06±0.01
MVB	-21.55±0.04	-120.84±0.03	-99.19±0.07
AUR	-15.59±0.07	-52.24±0.09	-36.57±0.02

The dependence of $\Delta_{tr}G^{\theta,\infty}_{PhM}, \Delta_{tr}H^{\theta,\infty}_{PhM}$ and $T\Delta_{tr}S^{\theta,\infty}_{PhM}$ on the dye chemical structure can be described from different contributions, as described below.

3.4.1. Contribution of the number of CH_3 groups.

The $\Delta_{tr}G^{\theta,\infty}_{PhM}$ values as a function of the number of CH_3 groups, for the partition of PhM dyes different in the PEO1500 + $MgSO_4$ + H_2O ATPS are show in the figure 13.

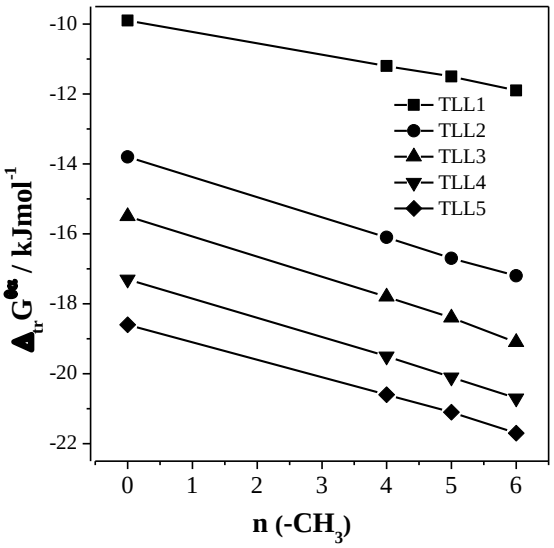

Figure 13. $\Delta_{tr}G^{\theta,\infty}_{PhM}$ values as a function of the number of CH_3 groups, for the partition of MV10B or MV6B or MV2B or PRA in the PEO1500 + $MgSO_4$ + H_2O ATPS at 298.15 K

The number of methyl groups on the dye molecules decreases in the following order: $MV10B_{(6\text{-}CH3)}$ > $MV6B_{(5\text{-}CH3)}$ > $MV2B_{(4\text{-}CH3)}$ > $PRA_{(0\text{-}CH3)}$. The change on the degree of dye methylation affects the $\Delta_{tr}G^{\theta,\infty}_{PhM}$ values becomes slightly more negative with increasing CH_3 for all TLL values. By using a simple linearization fit of the

$\Delta_{tr}G_{PhM}^{\theta,\infty}$ *versus* number of CH_3 curves, we have obtained slope values that are almost independent of TLL, which enables the calculation of an average magnitude for the term $\frac{\partial \Delta_{tr}G_{PhM}^{\theta\infty}}{\partial n_{CH_3}}$ = -0.56±0.03 kJ mol^{-1}. This result shows that the transfer of 1 mol of CH_3 groups at infinite dilution from the bottom phase to the upper phase decreases the system Gibbs free energy by 0.56 kJ. Silverio *et al.*[36] studied the partition of five dinitrophenyl aminoacids differing only in the quantity of methylene moieties in their alkyl chain, and measured the standard Gibbs free energy change in the transfer of CH_2 groups in the ATPS formed by PEO8000 or UCON (an EO-PO random copolymer) and inorganic salts [Na_2SO_4, Li_2SO_4 or $(NH_4)_2SO_4$]. The $\Delta_{tr}G_{CH_2}^{\theta}$ values were: −0.64 kJ mol^{-1} for the ATPS formed by PEO + Na_2SO_4 + H_2O; −0.69 kJ mol^{-1} for PEO + Li_2SO_4 + H_2O; −0.82 kJ mol^{-1} for PEO + $(NH)_4SO_4$ + H_2O; and for systems containing UCON the corresponding values of $\Delta_{tr}G_{CH_2}^{\theta}$ were: −0.89, −0.75 and −1.01 for Na_2SO_4, Li_2SO_4 and $(NH)_4SO_4$ respectively. The authors have attributed this $\Delta_{tr}G_{CH_2}^{\theta}$ magnitude to a more favorable hydration of CH_2 groups in the polymer-rich phase than that in the electrolyte-rich phase because the aqueous polymeric phase is more hydrophobic[39,40]. In order to confirm this hypothesis, it is necessary that the authors to determine the enthalpic and entropic components of $\Delta_{tr}G_{CH_2}^{\theta}$, and the same must apply to the present study.

Therefore, the Figure 14 shows the $\Delta_{tr}H_{PhM}^{\theta,\infty}$ and $T\Delta_{tr}S_{PhM}^{\theta,\infty}$ values as a function of the number of CH_3 groups present in the chemical structure of different PhM dyes.

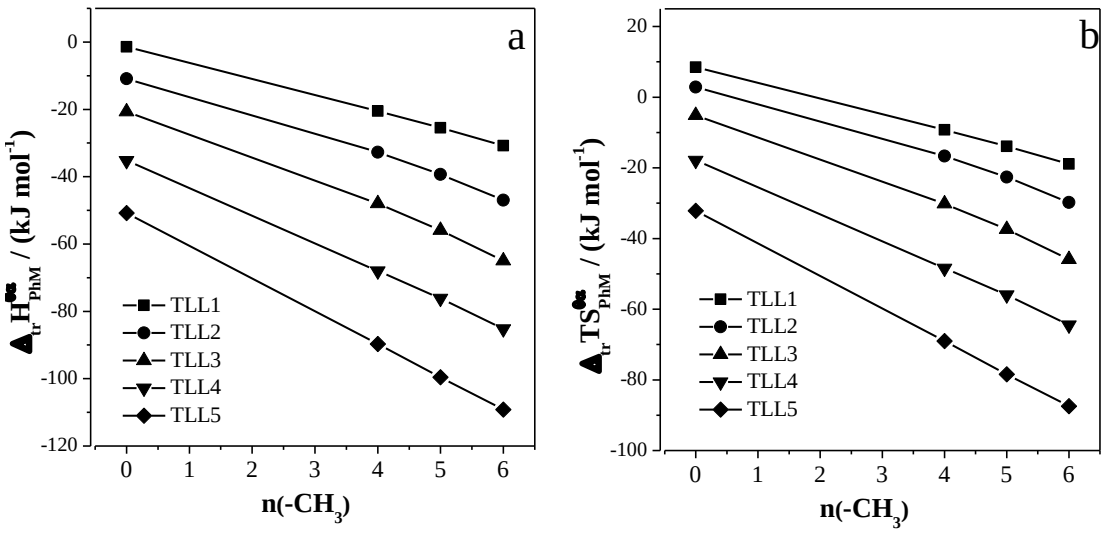

Figure 14. $\Delta_{tr}H^{\theta,\infty}_{PhM}$ (a) and $T\Delta_{tr}S^{\theta,\infty}_{PhM}$ (b) values as a function of the number of CH_3 groups, for the partition of MV10B or MV6B or MV2B or PRA in the PEO1500 + $MgSO_4$ + H_2O ATPS at 298.15 K.

Regardless of the TLL magnitude, all dye molecules are transferred from the bottom phase to the upper phase with a decrease in enthalpy ($-1.40 \pm 0.01 \leq \Delta_{tr}H^{\theta\infty}_{PhM} \leq -109.26 \pm 0.03$ kJ mol^{-1}) and entropy ($8.50 \pm 0.02 \leq \Delta_{tr}S^{\theta\infty}_{PhM} \leq -87.45 \pm 0.02$ kJ mol^{-1}), and, as the methylation degree of the PhM dye molecule increases, the $\Delta_{tr}H^{\theta\infty}_{PhM}$ and $T\Delta_{tr}S^{\theta\infty}_{PhM}$ values become more negative.

As occurred with $\Delta_{tr}G^{\theta,\infty}_{PhM}$, the values of $\Delta_{tr}H^{\theta\infty}_{PhM}$ (Figure 14a) and $T\Delta_{tr}S^{\theta\infty}_{PhM}$ (Figure 14b) decrease proportionally with increasing number of CH_3 groups. However, contrary to $R_G = \frac{\partial \Delta_{tr}G^{\theta\infty}_{PhM}}{\partial n_{CH_3}}$, the values of $R_H = \frac{\partial \Delta_{tr}H^{\theta\infty}_{PhM}}{\partial n_{CH_3}}$ and $R_S = \frac{\partial T\Delta_{tr}S^{\theta\infty}_{PhM}}{\partial n_{CH_3}}$ depend on the difference in the composition of the ATPS phases, showing that, as TLL values increase, the enthalpy release is enhanced and the entropy configuration decreases when 1 mol of CH_3 groups is transferred from the bottom to the upper phase. Figure 15 shows R_H and R_S as a function of the TLL for the PEO1500 + $MgSO_4$ + H_2O ATPS.

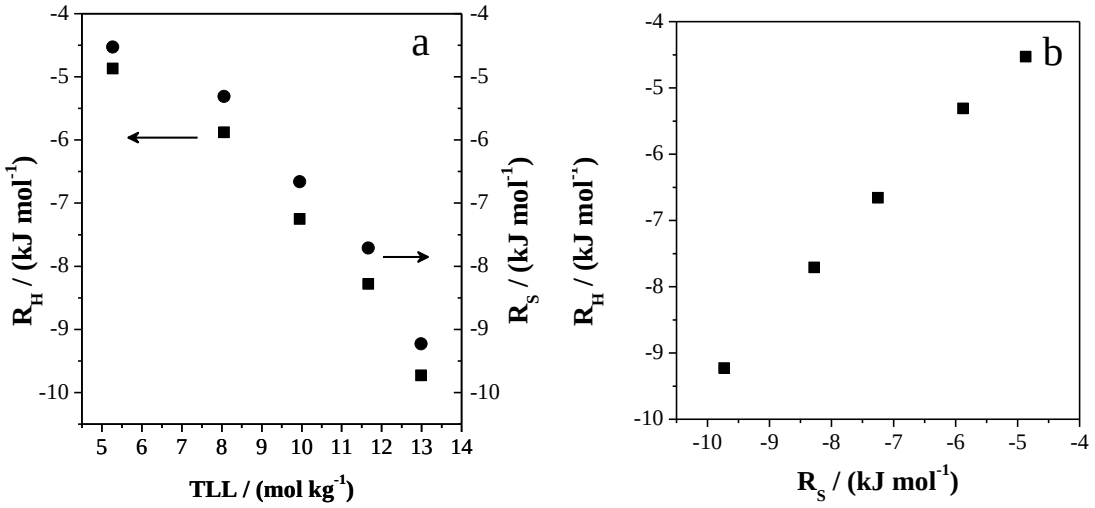

Figure 15. R_H (-■-) and R_S (-●-) values as a function of TLL for the PEO1500 + $MgSO_4$ + H_2O ATPS at 298.15 K (a) and R_H versus R_S (b).

The R_H values show that the transfer of 1 mol of CH_3 groups from the bottom phase to the upper phase at infinite dilution releases (4.86 ± 0.01) kJ in the first TLL and (9.73 ± 0.02) kJ for the last TLL of the ATPS studied. The $T\Delta_{tr}S^{\theta\infty}_{CH_3}$ values are similar to $\Delta_{tr}H^{\theta\infty}_{CH_3}$, and ranged from (−4.53 ± 0.03) to (−9.24 ± 0.01) kJ for the first and last TLL respectively. These results could be explained by considering that the methyl groups on the upper phase that are solvated by water molecules are more structured (hydrophobic effect) than those in the bottom phase. The water molecules in the upper phase are more oriented due to the presence of macromolecules that have hydrophobic segments (-CH_2-CH_2- groups), both the entropy and enthalpy decrease compensatory and proportionally (Figure 9b) resulting in small system free energy decrease, probably because both groups (-CH_3 and -CH_2-CH_2-) are very hindered.

3.4.2. Phenyl groups contribution.

While AUR is a diphenylmethane (DPhM) dye and the MV2B is a triphenylmethane (TPhM) dye, both molecules are similarly substituted. Therefore, both structures only differ by a benzene ring (Figure 1). This change in the dye chemical structure allows us to study the phenyl group effect on the driving forces of PhM dyes transfer in ATPS. Figure 16a shows the $\Delta_{tr}G^{\theta,\infty}_{PhM}$ values as a function of TLL for AUR and MV2B partitioned in the PEO1500 + $MgSO_4$ + H_2O ATPS.

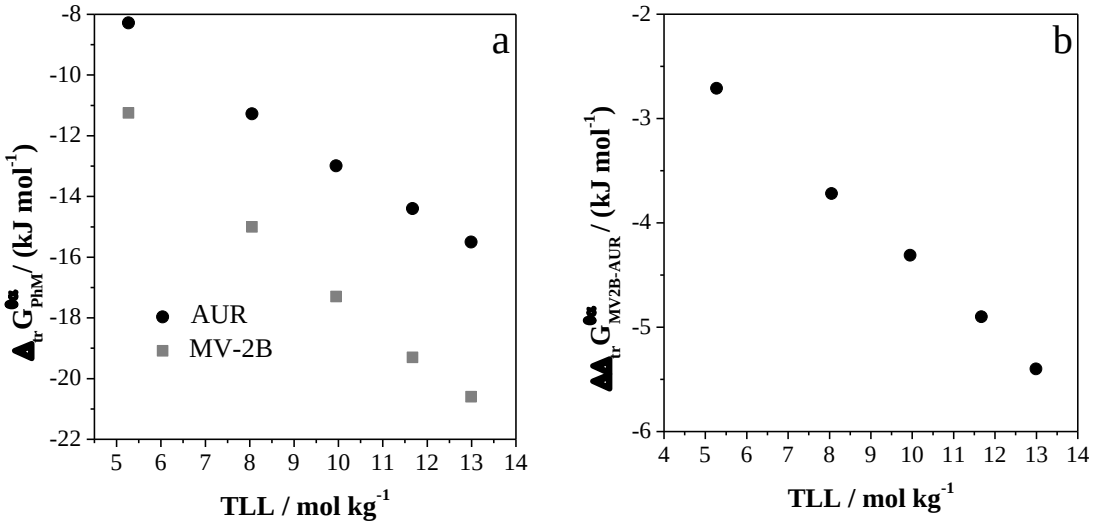

Figure 16. (a) $\Delta_{tr}G^{\theta,\infty}_{PhM}$ of AUR (-●-) and MV2B (-■-) (b) $\Delta\Delta_{tr}G^{\theta,\infty}_{MV2B-AUR}$ as a function of TLL for the PEO1500 + $MgSO_4$ + H_2O ATPS at 298.15 K.

The $\Delta_{tr}G^{\theta,\infty}_{MV2B}$ values are more negative than $\Delta_{tr}G^{\theta,\infty}_{AUR}$, indicating that hydrophobic interactions contribute to the phenilmethane dyes partition thermodynamic, and the difference $\Delta\Delta_{tr}G^{\theta,\infty}_{MV2B-AUR} = \Delta_{tr}G^{\theta,\infty}_{MV2B} - \Delta_{tr}G^{\theta,\infty}_{AUR}$ (Figure 16b) should be used as a parameter for this hydrophobic benzene ring contribution.

When the polymer concentration in the upper phase and the salt concentration in the bottom phase increase, the $\Delta\Delta_{tr}G^{\theta,\infty}_{MV2B-AUR}$ values become more negative because

the differences in the hydrophobicity of both phases is enhanced. In order to understand in detail, the origin of this difference, the $\Delta_{tr}H^{\theta,\infty}_{PhM}$ and $T\Delta_{tr}S^{\theta,\infty}_{PhM}$ parameters for both MV2B and AUR dyes were measured as a function of the TLL and the results are shown in Figure 17.

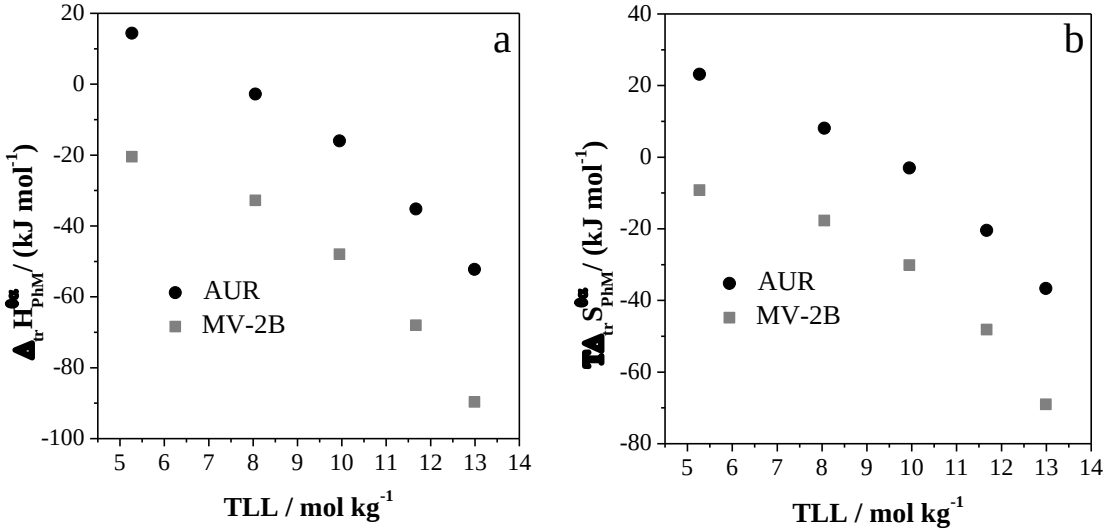

Figure 17. (a) $\Delta_{tr}H^{\theta,\infty}_{PhM}$ and (b) $T\Delta_{tr}S^{\theta,\infty}_{PhM}$ values of AUR (-●-) and MV-2B (-■-) as a function of TLL in the PEO1500 + $MgSO_4$ + H_2O ATPS at 298.15 K.

Regardless of the number of phenyl groups in the dye structure, the transfer enthalpy change decreases as the TLL increases. However, $\Delta_{tr}H^{\theta,\infty}_{AUR}(DPhM) > \Delta_{tr}H^{\theta,\infty}_{MV2B}(TPhM)$, demonstrating that less enthalpic energy is required to break dye-BP component interactions when the dye is more hydrophobic, which results in more negative transfer enthalpy. In addition, when AUR is compared with MV2B, the absence of a phenyl group in the DPhM dye structure generates a higher density of charge than in the TPhM dye. Thus, AUR can form more strong electrostatic interactions with the bottom phase components than MV2B. Therefore, the positive values of $\Delta_{tr}H^{\theta,\infty}_{AUR}$ in the first TLL are derived from the higher energy required to break

interactions between the AUR-bottom phase components than the energy released in the formation of new interactions between AUR-upper phase components. While the $T\Delta_{tr}S^{\theta,\infty}_{PhM}$ values for both dye structures decreases as TLL increases, the $T\Delta_{tr}S^{\theta,\infty}_{AUR}$ are higher than $T\Delta_{tr}S^{\theta,\infty}_{MV2B}$. Again, it can be seen that more hydrophobic dyes are able to be more effectively oriented in the dye-water solvation shell, which decreases the rotational entropy of the system.

3.4.3. Charge contribution.

Although the MV6B and MVB dyes are structurally similar (Figure 1), MV6B is an ionic species while MVB is neutral. This difference allows to determine the contribution of electrostatic interactions between the bottom phase ionic pairs (dye and the electrolyte ions) and the interactions in the upper phase (transferred dye and the pseudopolycation), on the driving force in the transfer of PhM dyes. Da Silva and Loh[37] proposed the existence of pseudopolications in upper phase of ATPS based on calorimetric studies, revealing that the interaction between sulfate salts and PEO leads to a system enthalpy increase. The positive enthalpy change is generated by endothermic processes as a result of the dehydration of the polymer chain and the electrolyte, which suggests that there is a binding between the cation and the polymer which releases water molecules in a process driven by entropy increase. This cation-polymer binding continues as more electrolyte is added, until a saturation point where there is no more entropy increase and phase separation occurs. Therefore, they concluded that the ATPS constituted by polymer and electrolyte originated from an endothermic process, resulting in the entropy increase associated with the release of water molecules that solvate the electrolyte and polymer, and giving way to the formation of the pseudopolication (cation-polymer interaction) and to the phase separation.

The Figure 18 shows the $\Delta_{tr}G_{PhM}^{\theta,\infty}$ values as a function of TLL for MV6B and MVB partitioned in the PEO1500 + $MgSO_4$ + H_2O ATPS.

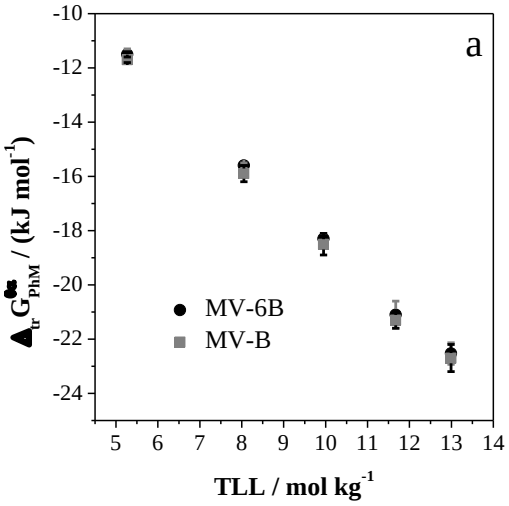

Figure 18. $\Delta_{tr}G_{PhM}^{\theta,\infty}$ as a function of the TLL for MV6B (-●-) and MVB (-■-) partitioned in the PEO1500 + $MgSO_4$ + H_2O ATPS at 298.15 K.

The $\Delta_{tr}G_{PhM}^{\theta,\infty}$ values for both ionic and neutral structures become more negative with the increment in TLL, ranging from (−11.5 ± 0.1) to (−21.0 ± 0.2), and from (−11.7 ± 0.1) to (−21.7 ± 0.2) kJ mol^{-1}), for MV6B and MVB respectively. When the dye molecule is charged, $\Delta_{tr}G_{PhM}^{\theta,\infty}$ values are a little less negative, but the difference is around the experimental error of the $\Delta_{tr}G_{PhM}^{\theta,\infty}$ measurement, so the electrostatic interaction does not contribute to the thermodynamic transfer potential. However, in order to determine if the dye charge plays an important role in the driving forces of the PhM molecules transfer process, it is necessary to determine the $\Delta_{tr}H_{PhM}^{\theta,\infty}$ and $T\Delta_{tr}S_{PhM}^{\theta,\infty}$ values for both structures. Figure 19 shows the $\Delta_{tr}H_{PhM}^{\theta,\infty}$ (18a) and

$T\Delta_{tr}S^{\theta,\infty}_{PhM}$ (18b) values for the MV6B and MVB dyes as a function of the TLL for the PEO1500 + $MgSO_4$ + H_2O ATPS at 298 K.

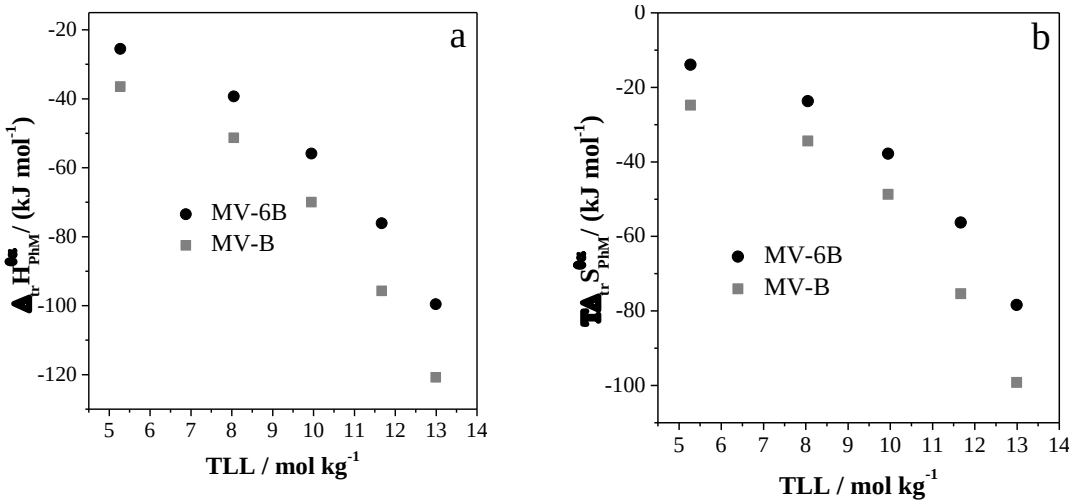

Figure 19. (a) $\Delta_{tr}H^{\theta,\infty}_{PhM}$ and (b) $T\Delta_{tr}S^{\theta,\infty}_{PhM}$ values of MV6B (-●-) and MVB (-■-) as a function of the TLL in PEO1500 + $MgSO_4$ + H_2O ATPS at 298.15 K.

For both dyes and for all TLL values, the transfer of the dye from the bottom to the upper phase decreases the system enthalpy, varying between ($-25.5 \pm 0.1 \leq \Delta_{tr}H^{\theta\infty}_{MV6B} \leq -99.6 \pm 0.3$ kJ mol^{-1}) and ($-35.5 \pm 0.4 \leq \Delta_{tr}H^{\theta\infty}_{MVB} \leq -120.8 \pm 0.7$ kJ mol^{-1}) for MV6B and MVB respectively. Similarly, the entropy change varies between ($-23.7 \pm 0.4 \leq T\Delta_{tr}S^{\theta\infty}_{MV6B} \leq -78.4 \pm 0.1$ kJ mol^{-1}) and ($-24.8 \pm 0.7 \leq T\Delta_{tr}S^{\theta\infty}_{MVB} \leq -99.2 \pm 0.7$ kJ mol^{-1}) for MV6B and MVB respectively. Clearly, the values of $\Delta_{tr}H^{\theta,\infty}_{PhM}$ and $T\Delta_{tr}S^{\theta,\infty}_{PhM}$ show significant differences for the ionic and neutral structures. The magnitude of $\Delta\Delta_{tr}H^{\theta,\infty}_{MV(B-6B)} = \Delta_{tr}H^{\theta,\infty}_{MVB} - \Delta_{tr}H^{\theta,\infty}_{MV6B}$ can be interpreted in terms of electrostatic interaction contributions for the system enthalpy change caused by the transfer of 1 mol of MV6B structure from the bottom phase to the upper phase. Analogous interpretation could be made for $\Delta[T\Delta_{tr}S^{\theta,\infty}_{MV(B-6B)}]$. The

Figure 20 presents $\Delta\Delta_{tr}H^{\theta,\infty}_{MV(B-6B)}$ and $\Delta[T\Delta_{tr}S^{\theta,\infty}_{MV(B-6B)}]$ as a function of TLL for the partition of the dye in the PEO1500 + $MgSO_4$ + H_2O ATPS at 298.15 K.

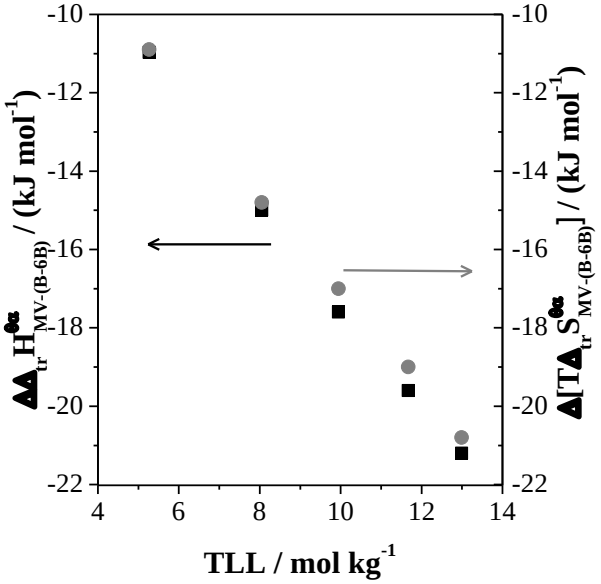

Figure 20. $\Delta\Delta_{tr}H^{\theta,\infty}_{MV(B-6B)}$ (-■-) and $\Delta[T\Delta_{tr}S^{\theta,\infty}_{MV(B-6B)}]$ (-●-) values as a function of the TLL for the dye partitioning in the PEO1500 + $MgSO_4$ + H_2O ATPS at 298.15 K.

The $\Delta\Delta_{tr}H^{\theta,\infty}_{MV(B-6B)}$ values are always negative ($\Delta_{int}H^{\infty}_{MV6B-BP} > \Delta_{int}H^{\infty}_{MVB-BP}$), indicating that the presence of the positive charge in the dye structure renders the interaction between the dye and the bottom phase components (PhM-BP) more favorable and/or renders the dye-upper phase components interaction less favorable ($\Delta_{int}H^{\infty}_{MVB-UP} > \Delta_{int}H^{\infty}_{MV6B-UP}$ in Equation 7). This means that the electrostatic interaction between the charged dye (MV6B) and the ions of the BP components are more favorable than that between neutral species and BP components. On the other hand, in the upper phase the interaction between MV6B and UP components (mainly a pseudopolication) is unfavorable because there are

electrostatic repulsions between the charged dye and the ions solvating the polymer chain. In addition, the $\Delta\Delta_{tr}H^{\theta,\infty}_{MV(B-6B)}$ values become more negative as TLL increases, indicating that the enhanced interactions between MV6B (charged dye) and such components occur because of the increase in the concentration of ionic species in the bottom phase and pseudopolycation in the upper phase. The $\Delta T\Delta_{tr}S^{\theta,\infty}_{MV(B-6B)}$ *versus* TLL curve shows similar behavior of the $\Delta\Delta_{tr}H^{\theta,\infty}_{MV(B-6B)}$ *versus* TLL curve. The $T\Delta_{tr}S^{\theta,\infty}_{MVB}$ values are more negative than $T\Delta_{tr}S^{\theta,\infty}_{MV6B}$, indicating that the presence of charge on the dye molecule decreases the dye hydrophobicity and improves the solvation water freedom rotational degree, which effectively causes the system entropy to decrease less.

4. Conclusions

A novel experimental approach made possible to accurately determine thermodynamic transfer parameters ($\Delta_{tr}G^{\theta,\infty}$, $\Delta_{tr}H^{\theta,\infty}$ and $T\Delta_{tr}S^{\theta,\infty}$) for six structurally-similar dyes, which were used as molecular probes to determine functional group contribution to the driving forces in the partition of PhM dyes in ATPS. Interestingly, the contributions of CH_3 or charge or benzene ring were very small for $\Delta_{tr}G^{\theta,\infty}$, whilst their effects on $\Delta_{tr}H^{\theta,\infty}$ and $T\Delta_{tr}S^{\theta,\infty}$ were more intense. The methyl group contribution on $\Delta_{tr}H^{\theta,\infty}$ and $T\Delta_{tr}S^{\theta,\infty}$ occurred by means of a compensatory process whereby the increase in one of the parameters was followed by a proportional increase in another. The benzene ring increase increment the hydrophobicity degree in the dye structure, thereby promoting more favorable interactions between the transferred dye and the components of the ATPS upper phase, increasing the dye partition coefficient.

5. References

1. Zafarani-Moattar, M. T.; Shekaari, H.; Jafari, P., Aqueous two-phase system based on cholinium chloride and polyethylene glycol di-methyl ether 250 and it use for acetaminophen separation. *J. Chem. Thermodyn.* **2017,** *107*, 85-94.

2. Kress, C.; Sadowski, G.; Brandenbusch, C., Solubilization of proteins in aqueous two-phase extraction through combinations of phase-formers and displacement agents. *Eur. J. Pharm. Biopharm.* **2017,** *112*, 38-44.

3. Wu, H. R.; Yao, S.; Qian, G. F.; Song, H., Development of tropine-salt aqueous two-phase systems and removal of hydrophilic ionic liquids from aqueous solution. *J. Chromatogr. A* **2016,** *1461*, 1-9.

4. Mathiazakan, P.; Shing, S. Y.; Ying, S. S.; Kek, H. K.; Tang, M. S. Y.; Show, P. L.; Ooi, C. W.; Ling, T. C., Pilot-scale aqueous two-phase floatation for direct recovery of lipase derived from Burkholderia cepacia strain ST8. *Sep. Purif. Technol.* **2016,** *171*, 206-213.

5. Sant'Anna, V.; Correa, A. P. F.; da Motta, A. D.; Brandelli, A., Liquid-liquid extraction of antimicrobial peptide P34 by aqueous two-phase and micellar systems. *Prep. Biochem. Biotechnol.* **2016,** *46* (8), 838-843.

6. Lee, S. Y.; Khoiroh, I.; Ling, T. C.; Show, P. L., Aqueous Two-Phase Flotation for the Recovery of Biomolecules. *Sep. Purif. Rev.* **2016,** *45* (1), 81-92.

7. Zhang, Y. Q.; Sun, T. C.; Lu, T. Q.; Yan, C. H., Extraction and separation of tungsten (VI) from aqueous media with Triton X-100-ammonium sulfate-water aqueous two-phase system without any extractant. *J. Chromatogr. A* **2016,** *1474*, 40-46.

8. da Silva, L. H. M.; da Silva, M. D. H.; Amin, J.; Martins, J. P.; Coimbra, J. S. D.; Minim, L. A., Hydrophobic effect on the partitioning of Fe(CN)(5)(NO) (2-) and

Fe(CN)(6) (3-) anions in aqueous two-phase systems formed by triblock copolymers and phosphate salts. *Sep. Purif. Technol.* **2008,** *60* (1), 103-112.

9. Ebrahimi, T.; Shahriari, S., Extraction of Betanin Using Aqueous Two-Phase Systems. *Bull. Chem. Soc. Jpn.* **2016,** *89* (5), 565-572.

10. Mageste, A. B.; de Lemos, L. R.; Ferreira, G. M. D.; da Silva, M. D. H.; da Silva, L. H. M.; Bonomo, R. C. F.; Minim, L. A., Aqueous two-phase systems: An efficient, environmentally safe and economically viable method for purification of natural dye carmine. *J. Chromatogr. A* **2009,** *1216* (45), 7623-7629.

11. Mageste, A. B.; Senra, T. D. A.; da Silva, M. C. H.; Bonomo, R. C. F.; da Silva, L. H. M., Thermodynamics and optimization of norbixin transfer processes in aqueous biphasic systems formed by polymers and organic salts. *Sep. Purif. Technol.* **2012,** *98*, 69-77.

12. Salabat, A.; Abnosi, M. H.; Motahari, A., Investigation of amino acid partitioning in aqueous two-phase systems containing polyethylene glycol and inorganic salts. *J. Chem. Eng. Data* **2008,** *53* (9), 2018-2021.

13. da Silva, N. R.; Ferreira, L. A.; Madeira, P. P.; Teixeira, J. A.; Uversky, V. N.; Zaslavsky, B. Y., Analysis of partitioning of organic compounds and proteins in aqueous polyethylene glycol-sodium sulfate aqueous two-phase systems in terms of solute-solvent interactions. *J. Chromatogr. A* **2015,** *1415*, 1-10.

14. Rodrigues, G. D.; de Lemos, L. R.; Mendes da Silva, L. H.; Hespanhol da Silva, M. d. C.; Minim, L. A.; dos Reis Coimbra, J. S., A green and sensitive method to determine phenols in water and wastewater samples using an aqueous two-phase system. *Talanta* **2010,** *80* (3), 1139-1144.

15. Hao, L. S.; Liu, M. N.; Xu, H. M.; Yang, N.; Nan, Y. Q.; Deng, Y. T., Partitioning of Dyes, Free Anthraquinones, and Tanshinones in Aqueous Two-Phase Systems of Cationic/Anionic Surfactants. *J. Dispersion Sci. Technol.* **2015,** *36* (7), 1047-1058.

16. Di Nucci, H.; Nerli, B.; Pico, G., Comparison between the thermodynamic features of alpha 1-antitrypsin and human albumin partitioning in aqueous two-phase systems of polyethyleneglycol-dextran. *Biophys. Chem.* **2001,** *89* (2-3), 219-229.

17. Dreyer, S.; Salim, P.; Kragl, U., Driving forces of protein partitioning in an ionic liquid-based aqueous two-phase system. *Biochemical Engineering Journal* **2009,** *46* (2), 176-185.

18. Jimenez, Y. P.; Galleguillos, H. R.; Claros, M., Liquid-liquid partition of perchlorate ion in the aqueous two-phase system formed by NaNO3 + Poly(ethylene glycol) + H2O. *Fluid Phase Equilibria* **2016,** *421*, 93-103.

19. Chen, Y. H.; Deng, Y. C.; Meng, Y. S.; Zhang, S. M., Partitioning Equilibria and Thermodynamics of Gallium, Indium, and Thallium in Aqueous Two-Phase Systems. *J. Chem. Eng. Data* **2015,** *60* (5), 1464-1468.

20. Lu, Y. M.; Lu, W. J.; Wang, W.; Guo, Q. W.; Yang, Y. Z., Thermodynamic studies of partitioning behavior of cytochrome c in ionic liquid-based aqueous two-phase system. *Talanta* **2011,** *85* (3), 1621-1626.

21. Rengifo, A. F. C.; Ferreira, G. M. D.; Ferreira, G. M. D.; da Silva, M. C. F.; Rezende, J. D.; Pires, A. C. D.; da Silva, L. H. M., Driving forces for chymosin partitioning on the macromolecule-salt aqueous two phase system. *Food Bioprod. Process.* **2016,** *100*, 361-371.

22. Martins, J. P.; Carvalho, C. d. P.; Silva, L. H. M. d.; Coimbra, J. S. d. R.; Silva, M. d. C. H. d.; Rodrigues, G. D.; Minim, L. A., Liquid–Liquid Equilibria of an Aqueous Two-Phase System Containing Poly(ethylene) Glycol 1500 and Sulfate Salts at

Different Temperatures. *Journal of Chemical & Engineering Data* **2008,** *53* (1), 238-241.

23. Huddleston, J. G.; Willauer, H. D.; Rogers, R. D., Phase Diagram Data for Several PEG + Salt Aqueous Biphasic Systems at 25 °C. *Journal of Chemical & Engineering Data* **2003,** *48* (5), 1230-1236.

24. Lueck, H. B.; Rice, B. L.; McHale, J. L., Aggregation of triphenylmethane dyes in aqueous-solution - dimerization and trimerization of crystal violet and ethyl violet. *Spectroc. Acta Pt. A-Molec. Biomolec. Spectr.* **1992,** *48* (6), 819-828.

25. Akama, E.; Tong, A. J.; Ito, M.; Tanaka, S., The study of the partitioning mechanism of methyl orange in an aqueous two-phase system. *Talanta* **1999,** *48* (5), 1133-1137.

26. Baraldi, I.; Caselli, M.; Momicchioli, F.; Ponterini, G.; Vanossi, D., Dimerization of green sensitizing cyanines in solution. A spectroscopic and theoretical study of the bonding nature. *Chemical Physics* **2002,** *275* (1-3), 149-165.

27. Mironova, D. A.; Muslinkina, L. A.; Syakaev, V. V.; Morozova, J. E.; Yanilkin, V. V.; Konovalov, A. I.; Kazakova, E. K., Crystal violet dye in complexes with amphiphilic anionic calix 4 resorcinarenes: Binding by aggregates and individual molecules. *Journal of colloid and interface science* **2013,** *407*, 148-154.

28. Dimitrijevic, N. M.; Takahashi, K.; Jonah, C. D., Visible absorption spectra of crystal violet in supercritical ethane-methanol solution. *Journal of Supercritical Fluids* **2002,** *24* (2), 153-159.

29. Ghanadzadeh, A.; Zeini, A.; Kashef, A., Environment effect on the electronic absorption spectra of crystal violet. *Journal of Molecular Liquids* **2007,** *133* (1-3), 61-67.

30. EGERTON, G. S.; MORGAN, A. G., The Photochemistry of Dyes II—Some Aspects of the Fading Process. *Department of Polymer and Fibre Science, University of Manchester Institute of Science and Technology* **1970,** *Box No. 88*.

31. Avakyan, V. G.; Shapiro, B. I.; Alfimov, M. V., Dimers, tetramers, and octamers of mono- and trimethyne thiacarbocyanine dyes. Structure, formation energy, and absorption band shifts. *Dyes and Pigments* **2014,** *109*, 21-33.

32. Rashidi-Alavijeh, M.; Javadian, S.; Gharibi, H.; Moradi, M.; Tehrani-Bagha, A. R.; Shahir, A. A., Intermolecular interactions between a dye and cationic surfactants: Effects of alkyl chain, head group, and counterion. *Colloid Surf. A-Physicochem. Eng. Asp.* **2011,** *380* (1-3), 119-127.

33. Shiri, S.; Khezeli, T.; Lotfi, S.; Shiri, S., Aqueous Two-Phase Systems: A New Approach for the Determination of Brilliant Blue FCF in Water and Food Samples. *J. Chem.* **2013**, 6.

34. de Alvarenga, J. M.; Fideles, R. A.; da Silva, M. V.; Murari, G. F.; Taylor, J. G.; de Lemos, L. R.; Rodrigues, G. D.; Mageste, A. B., Partition study of textile dye Remazol Yellow Gold RNL in aqueous two-phase systems. *Fluid Phase Equilibria* **2015,** *391*, 1-8.

35. Johansson, H. O.; Karlstrom, G.; Tjerneld, F.; Haynes, C. A., Driving forces for phase separation and partitioning in aqueous two-phase systems. *Journal of Chromatography B* **1998,** *711* (1-2), 3-17.

36. Silverio, S. C.; Madeira, P. P.; Rodriguez, O.; Teixeira, J. A.; Macedo, E. A., Delta G(CH2) in PEG-salt and Ucon-salt aqueous two-phase systems. *J. Chem. Eng. Data* **2008,** *53* (7), 1622-1625.

37. da Silva, L. H. M.; Loh, W., Calorimetric investigation of the formation of aqueous two-phase systems in ternary mixtures of water, poly(ethylene oxide) and electrolytes (or dextran). *Journal of Physical Chemistry B* **2000,** *104* (43), 10069-10073.

CAPÍTULO 3

Effect of the system chemical nature on the contribution of functional groups phenilmethane dyes on the partition driving forces in aqueous two-phase systems

ABSTRACT

Aqueous two-phase system (ATPS) is an efficient and economically viable technique to extract and purify different species. However, the solute functional group contribution on the driving forces of the partition process in ATPS is still unknown. Hence, in this paper different ATPS were used that were formed by mixing aqueous solutions of a polymer (or copolymer) with an organic salt (sodium Acetate or tartrate or citrate) or sulfate salt (lithium or sodium or magnesium) to investigate the partition of six phenylmethane (PhM) dyes with small modifications in their chemical structures and to study the chemical nature of the system components on the contribution of the functional groups of the PhM dyes in the standard transfer parameters at infinite dilution state ($\Delta_{tr}G^{\theta,\infty}$, $\Delta_{tr}H^{\theta,\infty}$ and $T\Delta_{tr}S^{\theta,\infty}$). The -$CH_3$ and phenyl groups increase hydrophobicity degree on the dye structure rendering the transfer more efficient from ATPS the bottom phase to the upper phase decreasing the $\Delta_{tr}G^{\theta,\infty}_{PhM}$ values in an entropically and enthalpically directed process favored by intermolecular interactions that depend on the polymer hydrophobicity and electrolytes that forms the ATPS. The dye structure positive charge allowed to observe that the intermolecular interactions in the bottom phase play an important role in the values of $\Delta_{tr}H^{\theta,\infty}_{PhM}$ and $T\Delta_{tr}S^{\theta,\infty}_{PhM}$ because these interactions depended nature on the anion forming the electrolyte.

1. INTRODUCTION

The great potential of the Aqueous Two-Phase System (ATPS) in the purification and extraction of different species [1-14] is based on the simplicity to modulate some the system properties, such as: relative hydrophobicity[15] and ionic strength[16], by changing the system components and/or composition. This capacity to modulate the system properties can provide the correct choice of the ATPS to extract a specific type of chemical species. However, the complex balance of intermolecular interactions taking place when certain solute is partitioned into a ATPS need to be understood and to optimize solute extraction process in ATPS. The Van't Hoff approximation was the first approach used to study thermodynamics the process of partitioning solutes, evaluating the effect chemical nature of ATPS components[9, 17-21]. The authors who used this approximation determined the partition coefficients (K) at different temperatures and with the relation ln K versus 1/T they calculated the $\Delta_{tr}H$ value. This approach has as limitation; the variation of the temperature causes changes in the composition in each phase of the ATPS causing errors in the values of K. Other authors recently used isothermal titration calorimetry to determine $\Delta_{tr}H$ values, titrating solute solutions in both phases of ATPS[15, 22]. In this approach the authors determine the enthalpy change generated by the number of moles of solute transferred between the phases, but since the solute concentration in each phase was finite, the calculation of the values of $\Delta_{tr}H$ has the solute-solute interactions contribution. With the aim to remove these limitations, we proposed a new experimental method to determine the functional group contribution in the standard solute transfer parameters at infinite dilution state: standard transfer Gibbs free energy change ($\Delta_{tr}G^{\theta,\infty}$), standard transfer enthalpy change ($\Delta_{tr}H^{\theta,\infty}$) and standard transfer entropy change ($T\Delta_{tr}S^{\theta,\infty}$) for the partition process of six PhM dyes (methyl violet 10B (MV10B); methyl violet 6B (MV6B); methyl violet 2B (MV2B);

pararosaniline (PRA); methyl violet B (MVB) and auramine (AUR), which are structurally similar (Figure 1) and the effect on these contributions of the chemical nature of the ATPS components formed by the mixture of the aqueous solutions of a polymer (PEO or PPO) or copolymer (L64) with an organic salt (sodium acetate or tartrate or citrate) or sulfate salts (lithium or sodium or magnesium).

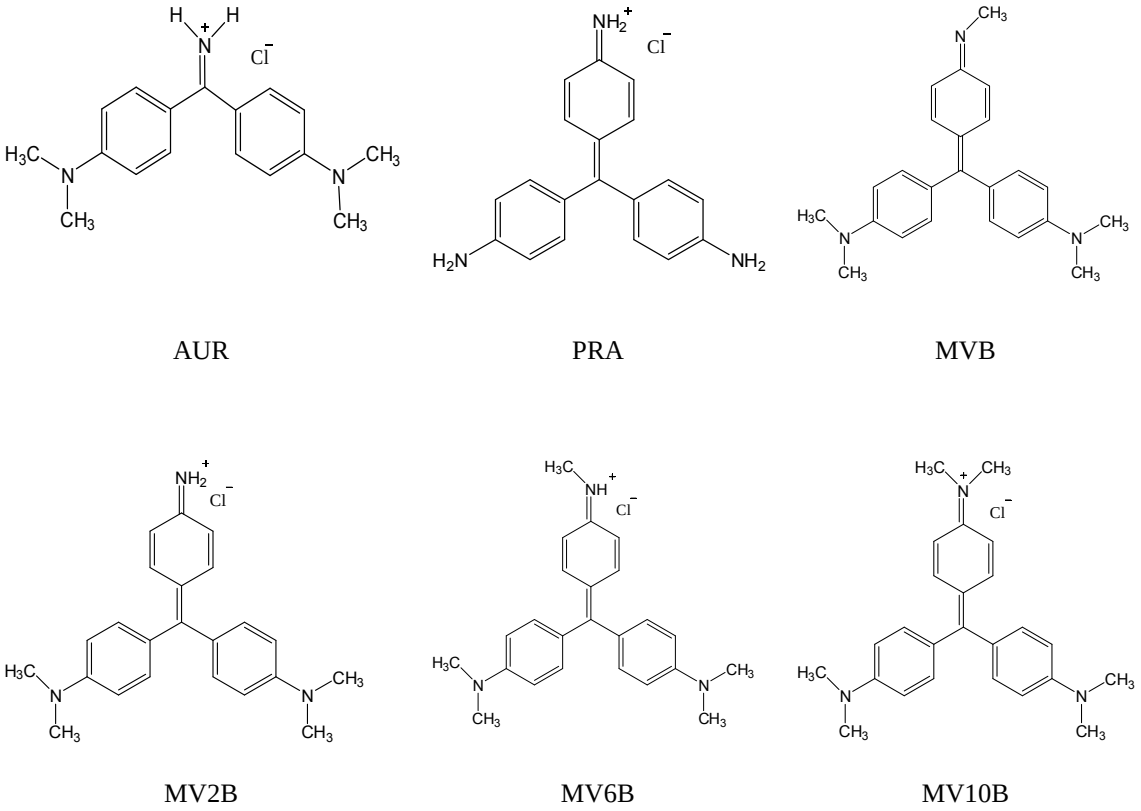

Figure 1. PhM dyes molecular structures

2. MATERIAL AND METHODS

2.1 Materials

Poly(ethylene oxide) (PEO), with a molar mass of 1500 g mol^{-1}, the triblock copolymer L64 with a molar mass equal to 2900 g mol^{-1} and poly(ethylene glycol) (PPG), with a molar mass of 425 g mol^{-1} were purchased from Synth (Brazil). The inorganic salts lithium sulfate (Li_2SO_4; 98.0%), sodium sulfate (Na_2SO_4; 99.0%), magnesium sulfate heptahydrate ($MgSO_4 \bullet 7H_2O$), the organic salts sodium Acetate (AcetNa; $NaC_2H_3O_2 \cdot 3H_2O$; 99.5%) sodium tartrate (TartNa; $Na_2C_4H_4O_6 \cdot 2H_2O$; 99.5%), and sodium citrate (CitrNa; $Na_3C_6H_5O_7 \cdot 2H_2O$; 99.0%), were all purchased from Vetec (Brazil). The PhM dyes MV10B (purity ≥ 90%), MV6B (purity ≥ 90%), MV2B (purity ≥ 98%), PRA (purity ≥ 90%), MVB (purity ≥ 87%) and AUR (purity 85%) was purchased from Sigma Aldrich (USA). All chemicals used in this study were of analytical grade and used without further purification. Distilled water was used in all experiments.

2.2 Preparation of ATPS and determination of PhM dyes thermodynamic transfer parameters.

The ternary mixtures compositions of ATPS used in the partition experiments were chosen based on the previously published phase diagrams[23-25] To achieve the desired composition ratio for each ATPS, appropriate amounts of the desired polymer and electrolytes aqueous solutions were collected in graduated centrifuge tubes. The tubes were shaken and left to stand at 298.15 K, in a thermostatic bath (Microquimica, MQBTC 99-20) at 298.15 K ± 0.1 K.

After 8 hours the system achieved thermodynamic equilibrium and the two phases were collected separately (1.0 g of upper phase and 7.0 g of bottom phase) for a

total of 8.0 g in three different glass tubes, then 100 μL of the PhM dye stock solution were added ($3.1x10^{-3}$ mol kg^{-1}) in two tubes a sample and a replicate leaving one without dye (white). The final concentration of the dyes in the tubes was $3.9x10^{-5}$ mol kg^{-1}, for each tie-line length (TLL) and each ATPS. These systems were stirred manually for 3 minutes until the solutions became cloudy and then maintained under controlled temperature in a thermostatic bath at 298.15 K for a minimum of 8 hours to reach thermodynamic equilibrium. Aliquots of the top and the bottom phases were collected with a syringe, and adequately diluted with deionized water for spectrophotometric analysis at 590 nm for MV2B, MV6B, MV10B and MVB, 540 nm for PRA, and 435 nm for AUR, using a Shimadzu digital double beam spectrometer (UV-2550).

The PhM dyes partition coefficients (K_{PhM}) between both phases was determined by the concentration ratio of the analyte in each phase of the ATPSs studied. In agreement with the Beer–Lambert law, the absorbance of the analyte at a specific wavelength is directly proportional to the analyte concentration. Thus, the K_{PhM} value can be given as described in Equation 1.

$$K_{PhM} = \frac{(Abs^{TP})x(fd^{TP})}{(Abs^{BP})x(fd^{BP})} \quad (1)$$

where $(Abs^{TP})$and (Abs^{BP}) are the absorbances the dyes of the diluted top phase and the diluted bottom phase, respectively, discounting the absorbance of the corresponding blanks, and (fd^{TP}) and (fd^{BP}) are the dilution factors of the phases.

The K_{PhM} values were studied for different TLL values of each ATPS investigated. The TLL numerically expresses the difference in the intensive thermodynamic functions between the top and the bottom phases, at constant pressure and temperature. It is calculated using Equation 2:

$$TLL = \sqrt{(C_{pol}^{UP} - C_{pol}^{BP})^2 + (C_{salt}^{UP} - C_{salt}^{BP})^2} \quad (2)$$

where C_{pol}^{UP} and C_{pol}^{BP} are the polymer concentrations in the top and bottom phases, respectively, and C_{salt}^{UP} and C_{salt}^{BP} are the corresponding salt concentrations in the upper and bottom phases, respectively.

2.3 Thermodynamic parameters of transfer

2.3.1 Standard transfer Gibbs free energy change at infinite dilution state ($\Delta_{tr}\boldsymbol{G}^{\boldsymbol{\theta},\infty}$)

For all ATPS studied, the $\Delta_{tr}\boldsymbol{G}^{\boldsymbol{\theta},\infty}$ was obtained following the thermodynamic relationship:

$$\Delta_{tr}G^{\theta,\infty} = -R\,T\,ln\,K_{PhM} \quad (3)$$

where R is the real gas constant in (kJ mol^{-1} K^{-1}), T is the absolute temperature, and K_{PhM} is the dyes partition coefficient obtained at infinite dilution state. (extrapolating of K_{PhM} versus [PhM] curves to zero dye concentration.

2.3.2 Standard transfer enthalpy change at infinite dilution state ($\Delta_{tr}\boldsymbol{H}^{\boldsymbol{\theta},\infty}$)

Isothermal titration calorimetry (ITC) was used to determine the dye standard dilution enthalpy change at infinite dilution state ($\Delta_{dil}H^{\theta,\infty}$) in the all ATPSs bottom and the upper phase. The experiments were conducted in a CSC-4200 microcalorimeter (Science Corp. Calorimeter) using the methodology proposed in the chapter 2.

The standard enthalpy change at infinite dilution state ($\Delta_{tr}H_{PhM}^{\theta,\infty}$) was determine using the following equations:

$$\Delta_{tr}H_{PhM}^{\theta,\infty} = \Delta_{dil}H_{PhM}^{\infty,UP} - \Delta_{dil}H_{PhM}^{\infty,BP} \quad (4)$$

where: $\Delta_{dil}H_{PhM}^{\infty,UP}$ and $\Delta_{dil}H_{PhM}^{\infty,BP}$ are the dye standard dilution enthalpy change in infinite dilutions state in upper phase and bottom phase respectively.

2.3.3 Standard transfer entropy change at infinite dilution state ($\Delta_{tr}S^{\theta,\infty}$)

The PhM dyes transfer entropy change at infinite dilution state ($\Delta_{tr}S^{\theta,\infty}$) was determined from the following classic thermodynamic relationship:

$$T\Delta_{tr}S^{\theta,\infty} = \Delta_{tr}H^{\theta,\infty} - \Delta_{tr}G^{\theta,\infty} \quad (5)$$

where: $\Delta_{tr}H_{PhM}^{\theta,\infty}$ is the dye standard transfer enthalpy change at infinite dilution state and $\Delta_{tr}G_{PhM}^{\theta,\infty}$ is the dye standard transfer Gibbs free energy change at infinite dilution state.

3. Results and discussion

The transference process of a solute between the both phases of a given ATPS, depends of a determined balance of the intermolecular interactions between the transferred species and the species that form both ATPS phases. Therefore, to modulate the properties of ATPS by changing the chemical nature of the species forming the system can provide a combination of components with characteristics necessary to improve factors such as the hydrophobicity degree or ionic strength in order to obtain better results in the solute transfer process in different ATPS[26].

A preliminary study showed how small variations in the molecular structure of six phenylmethane dyes caused important effect in the thermodynamic transfer parameters responsible of the dye partition process in PEO1500+$MgSO_4$+H_2O ATPS (chapter 2). The question now arises is: how the dye functional groups contribution in the thermodynamic transfer parameters is affected when the components of the system are changed?

In order to answer these question, the effect of the functional groups in the partition process of PhM dyes in different ATPS was divided in the following effects.

3.1 Effect of ATPS phases hydrophobicity.

The hydrophobic interactions probably play the major role in the partition of solutes in most ATPS and one of the more clear effects in such interactions is the phases hydrophobicity and this effect is directly related to the chemical nature of the system components as well as their concentration[27]. Hence, although both phases of the ATPS are rather hydrophilic, the top phase (usually containing polymer) is more hydrophobic considering that the degree of hydrophobicity is proportional to the carbon chain size of the polymer hydrophobic segments[28]. Therefore, three macromolecules constituted for monomeric segments with different hydrophobic degree (PEO1500 < L64 < PPO425) were used to prepare different ATPS and to partition six similar structurally PhM dyes. The figure 2 show the PhM dyes partition coefficient (K_{PhM}) values of MV10B, MV6B, MV2B, PRA, MVB and AUR as a function of the TLL of (PEO1500 or L64 or PPO425) + Na_2SO_4 + H_2O ATPS at 298.15 K.

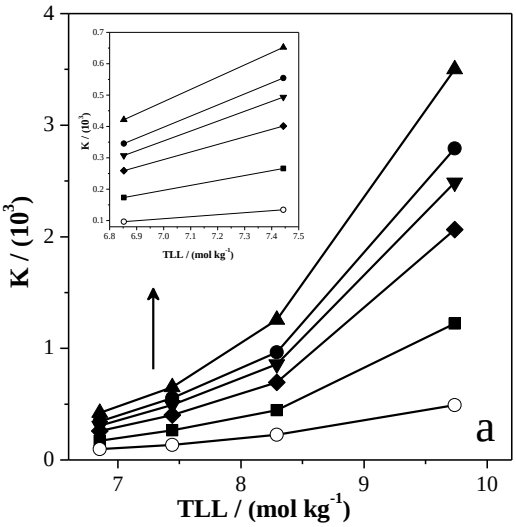

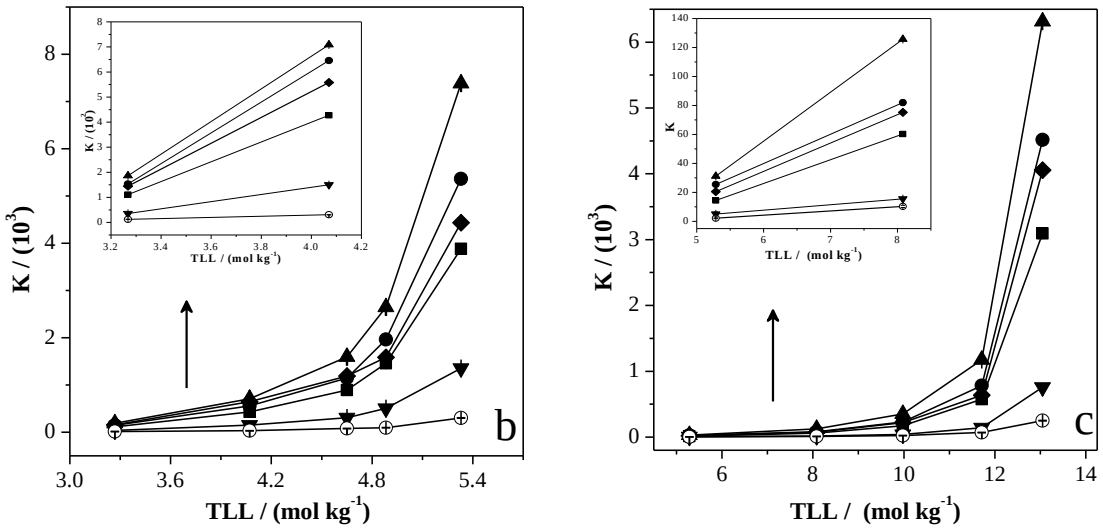

Figure 2. K_{PhM} values of MV10B (-▲-), MV6B (-●-), MV2B (-■-), PRA (-▼-) MVB (-♦-), AUR (-○-) as a function of the TLL of PEO1500+Na_2SO_4+H_2O (a), L64+Na_2SO_4+H_2O (b) and PPO425+ Na_2SO_4+H_2O (c) ATPS at 298.15 K.

Independent of the ATPS the K_{PhM} values were greater than one for all PhM dyes, meaning that the dye molecules were preferably concentrated in the polymer rich phase. For the three ATPSs studied the K_{PhM} values increase exponentially when the concentration of the ATPS components increment (TLL) and this values are greater when the number of phenyl and -CH_3 groups in the dye structure augment. Besides, this effect increases when the hydrophobicity of polymer decreased in the follow order PEO1500 > L64 > PPO425. This suggest interaction more favorable between the dye molecule and PEO than that L64 or PPO.

However, for a better understanding the relationship between the functional groups contribution and the K_{PhM} values in the different ATPSs, the standard thermodynamic transfer parameters at infinite dilution state for each dye in the different ATPS studied. The $\Delta_{tr}G^{\theta,\infty}_{PhM}$ was obtained from equation 3 using the K_{PhM} values shown in the figure 2. To determine $\Delta_{tr}H^{\theta,\infty}_{PhM}$ values the equation 4 was applied, using the relationship the dilution enthalpy variation of the dye in each phase versus the dye concentration ($\Delta_{dil}H^{\infty}_{PhM}$ versus [dye]), could be calculated the dilution enthalpy change

when the dye concentration is close to zero and the standard transfer entropy change at infinite dilution ($\Delta_{tr}S^{\theta,\infty}_{PhM}$) could be calculated with equation 5. The results are shown in the Figures from 3 to 20 and in the tables from 1 to 21.

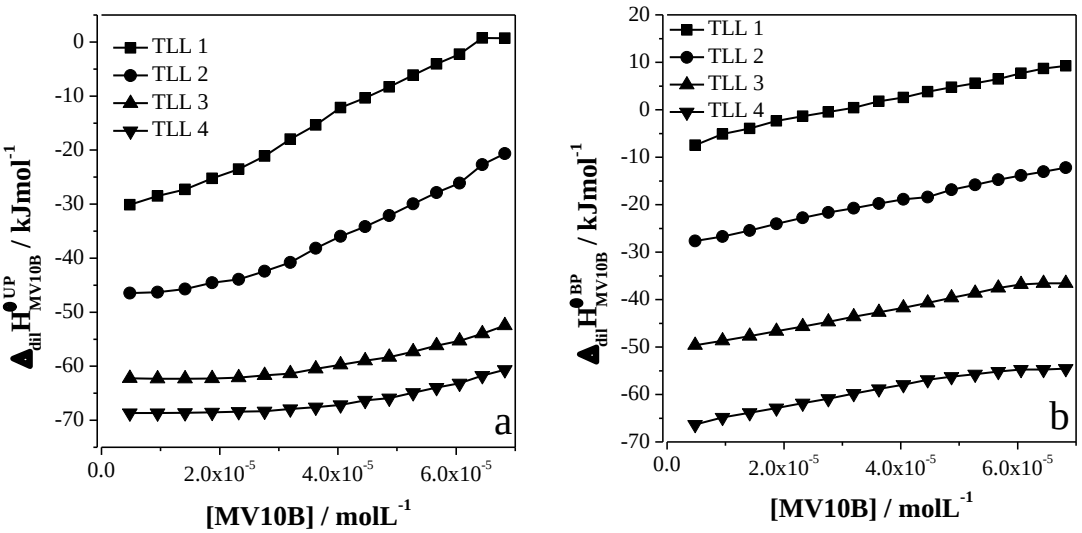

Figure 3. $\Delta_{dil}H^{UP}_{MV10B}$ (a) and $\Delta_{dil}H^{BP}_{MV10B}$ (b) as functions of dye concentration in upper and bottom phases of PEO1500+Na_2SO_4+H_2O ATPS at 298.15 K.

The result of $\Delta_{dil}H_{MV10B}$ versus [MV10B], derives in a mathematical equation usually polynomial of 2 order (equations 6)

$$\Delta_{dil}H_{MV10B} = \text{Intercept} + b[\text{MV10B}] + a[\text{MV10B}]^2 \quad (6)$$

Thus when the dye concentrations are zero (Infinite dilution state)

$$\Delta_{dil}H^{\infty}_{MV10B} = \text{Intercept} \quad (7)$$

Table 1. K_{MV10B} values and $\Delta_{dil}H^{\infty}_{MV10B}$ values in upper (UP) and bottom (BP) phases, for the TLL of PEO1500 + Na_2SO_4 + H_2O ATPS at 298 K.

TLL	K_{MV10B}	$\Delta_{dil}H^{\infty UP}_{MV10B}$	$\Delta_{dil}H^{\infty BP}_{MV10B}$
mol kg^{-1}		kJ mol^{-1}	
6.85	421.4±1.02	-33.01±0.02	-8.79±0.21
7.44	652.3±0.40	-47.05±0.08	-28.95±0.15
8.29	1256.3±0.79	-61.93±0.15	-51.10±0.34
9.74	3500.2±0.20	-69.13±0.13	-67.95±0.19

This procedure was performed with all dyes.

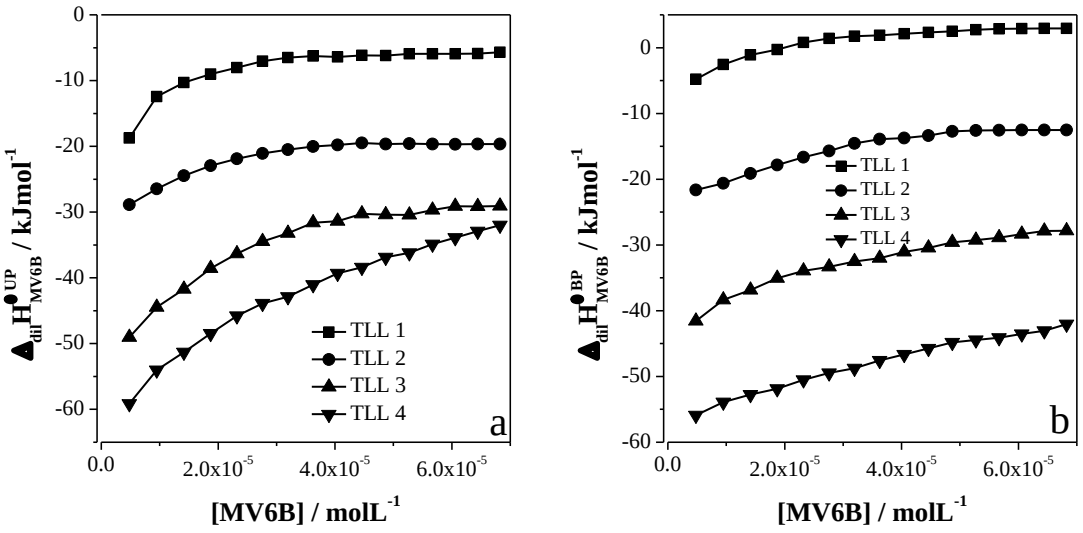

Figure 4. $\Delta_{dil}H^{UP}_{MV6B}$ (a) and $\Delta_{dil}H^{BP}_{MV6B}$ (b) as a functions of dye concentration in upper and bottom phases of PEO1500+Na_2SO_4+H_2O ATPS at 298.15 K.

Table 2. K_{MV6B} values and $\Delta_{dil}H^{\infty}_{MV6B}$ values in upper (UP) and bottom (BP) phases, for the TLL of PEO1500 + Na_2SO_4 + H_2O ATPS at 298.15 K.

TLL	K_{MV6B}	$\Delta_{dil}H^{\infty UP}_{MV6B}$	$\Delta_{dil}H^{\infty BP}_{MV6B}$
mol kg^{-1}		kJ mol^{-1}	
6.85	345.5±0.92	-27.19±0.11	-7.19±1.06
7.44	554.5±0.87	-39.01±0.09	-23.87±2.01
8.29	965.1±1.05	-51.34±1.00	-42.85±1.74
9.74	2792.0±1.00	-57.97±0.09	-57.14±1.13

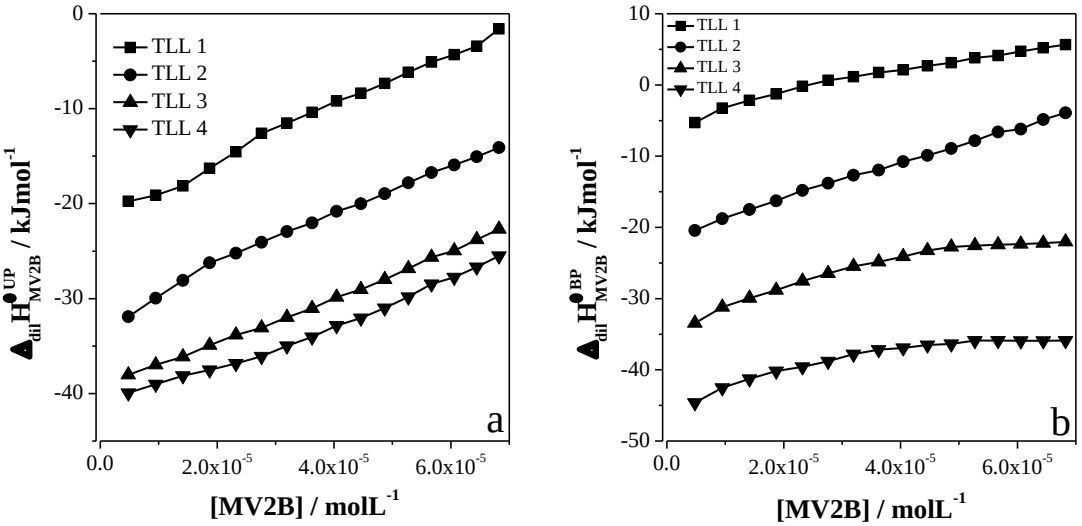

Figure 5. $\Delta_{dil}H^{UP}_{MV2B}$ (a) and $\Delta_{dil}H^{BP}_{MV2B}$ (b) as a functions of dye concentration in upper and bottom phases of PEO1500+Na_2SO_4+H_2O ATPS at 298.15 K.

Table 3. K_{MV2B} values and $\Delta_{dil}H^{\infty}_{MV2B}$ values in upper (UP) and bottom (BP)

phases, for the TLL of PEO1500 + Na_2SO_4 + H_2O ATPS at 298.15 K.

TLL	K_{MV2B}	$\Delta_{dil}H^{\infty UP}_{MV2B}$	$\Delta_{dil}H^{\infty BP}_{MV2B}$
mol kg^{-1}		kJ mol^{-1}	
6.85	258.9±0.08	-22.01±1.34	-5.81±1.10
7.44	401.2±0.09	-32.99±1.27	-21.50±1.38
8.29	695.8±0.13	-40.36±1.09	-34.96±1.05
9.74	2064.3±0.18	-43.09±0.65	-45.74±1.24

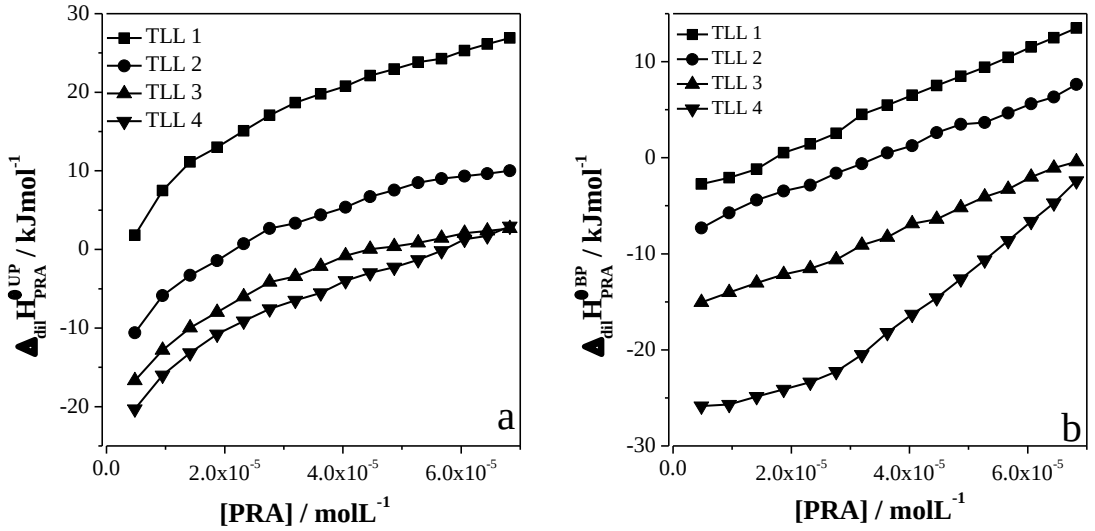

Figure 6. $\Delta_{dil}H^{UP}_{PRA}$ (a) and $\Delta_{dil}H^{BP}_{PRA}$ (b) as a functions of dye concentration in upper and bottom phases of PEO1500+Na_2SO_4+H_2O ATPS at 298.15 K.

Table 4. K_{PRA} values and $\Delta_{dil}H^{\infty}_{PRA}$ values in upper (UP) and bottom (BP) phases, for the TLL of PEO1500 + Na_2SO_4 + H_2O ATPS at 298.15 K.

TLL	K_{PRA}	$\Delta_{dil}H^{\infty UP}_{PRA}$	$\Delta_{dil}H^{\infty BP}_{PRA}$
mol kg^{-1}		kJ mol^{-1}	
6.85	173.30±1.03	-1.41±0.02	-3.92±0.12
7.44	266.06±0.10	-10.21±0.05	-8.20±0.29
8.29	445.94±0.07	-18.47±0.01	-15.97±0.55
9.74	1223.03±1.23	-21.01±0.04	-25.96±0.41

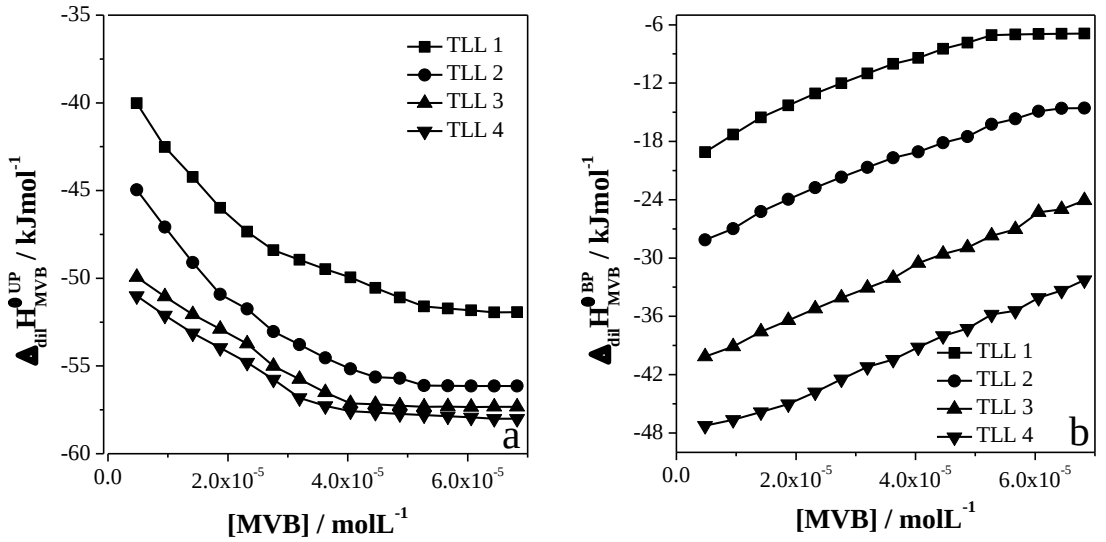

Figure 7. $\Delta_{dil}H^{UP}_{MVB}$ (a) and $\Delta_{dil}H^{BP}_{MVB}$ (b) as functions of dye concentration in upper and bottom phases of PEO1500+Na_2SO_4+H_2O ATPS at 298.15 K.

Table 5. K_{MVB} values and $\Delta_{dil}H^{\infty}_{MVB}$ values in upper (UP) and bottom (BP) phases, for the TLL of PEO1500 + Na_2SO_4 + H_2O ATPS at 298.15 K.

TLL	K_{MVB}	$\Delta_{dil}H^{\infty UP}_{MVB}$	$\Delta_{dil}H^{\infty BP}_{MVB}$
mol kg^{-1}		kJ mol^{-1}	
6.85	307.31±0.01	-39.95±0.13	-20.93±0.22
7.44	493.69±0.12	-43.17±0.25	-29.77±0.57
8.29	858.32±0.07	-48.18±0.73	-41.50±0.75
9.74	2487.11±1.04	-49.70±0.81	-48.75±0.94

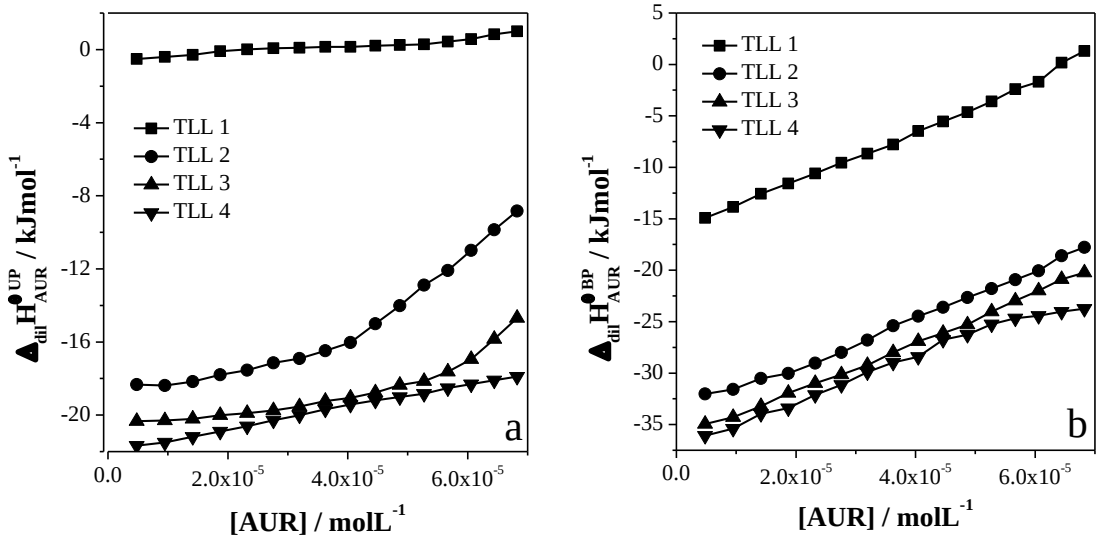

Figure 8. $\Delta_{dil}H^{UP}_{AUR}$ (a) and $\Delta_{dil}H^{BP}_{AUR}$ (b) as a functions of dye concentration in upper and bottom phases of PEO1500+Na_2SO_4+H_2O ATPS at 298.15 K.

Table 6. K_{AUR} values and $\Delta_{dil}H^{\infty}_{AUR}$ values in upper (UP) and bottom (BP) phases,

for the TLL of PEO1500 + Na_2SO_4 + H_2O ATPS at 298.15 K.

TLL	K_{AUR}	$\Delta_{dil}H_{AUR}^{\infty UP}$	$\Delta_{dil}H_{AUR}^{\infty BP}$
mol kg^{-1}		kJ mol^{-1}	
6.85	96.27±0.38	-0.91±1.48	-15.61±1.27
7.44	134.15±0.25	-18.25±1.11	-33.26±1.13
8.29	225.75±0.14	-20.75±0.99	-36.09±0.89
9.74	490.99±0.57	-21.99±2.03	-37.69±2.14

Table 7. Thermodynamic transfer parameters of PhM dyes as a function of the TLL of PEO1500 + Na_2SO_4 + H_2O ATPS at 298.15 K.

PhM dyes	$\Delta_{tr}G_{PhM}^{\theta,\infty}$	$\Delta_{tr}H_{PhM}^{\theta,\infty}$	$T\Delta_{tr}S_{PhM}^{\theta,\infty}$
		kJ mol^{-1}	
TLL 1 / 6.85 mol kg^{-1}			
MV10B	-14.96±0.03	-24.22±0.05	-9.23±0.02
MV6B	-14.47±0.01	-20.01±0.06	-5.52±0.05
MV2B	-13.76±0.05	-16.19±0.03	-2.43±0.02
PRA	-12.77±0.01	-13.39±0.07	3.36±0.06
MVB	-14.18±0.04	-19.02±0.02	-4.83±0.02
AUR	-11.31±0.02	14.73±0.01	26.01±0.01
TLL 2 / 7.44 mol kg^{-1}			
MV10B	-16.04±0.04	-18.10±0.07	-2.05±0.03
MV6B	-15.64±0.06	-15.14±0.03	0.50±0.03
MV2B	-14.84±0.09	-11.49±1.01	3.35±0.02
PRA	-13.82±0.01	-2.01±0.12	7.82±0.11
MVB	-15.35±0.10	-13.40±0.09	1.95±0.01
AUR	-12.13±0.07	15.01±0.05	27.14±0.02
TLL 3 / 8.29 mol kg^{-1}			
MV10B	-17.67±1.15	-10.83±0.07	6.84±0.08
MV6B	-17.01±1.28	-8.49±0.10	8.52±0.18
MV2B	-16.20±0.31	-5.37±0.29	10.80±2.01
PRA	-15.10±0.17	-2.49±0.87	12.60±1.29
MVB	-16.72±0.66	-6.68±0.10	10.04±1.56
AUR	-13.42±1.04	15.34±1.05	28.76±0.01
TLL 4 / 9.74 mol kg^{-1}			
MV10B	-20.20±0.15	-1.18±0.08	19.02±0.07
MV6B	-19.64±1.01	-0.83±0.10	18.81±0.09
MV2B	-18.90±0.09	2.65±0.04	21.55±0.05
PRA	-17.60±0.18	4.95±0.06	22.55±0.12
MVB	-19.36±0.23	-0.98±0.12	18.41±0.11
AUR	-15.34±0.41	15.70±0.34	31.05±0.27

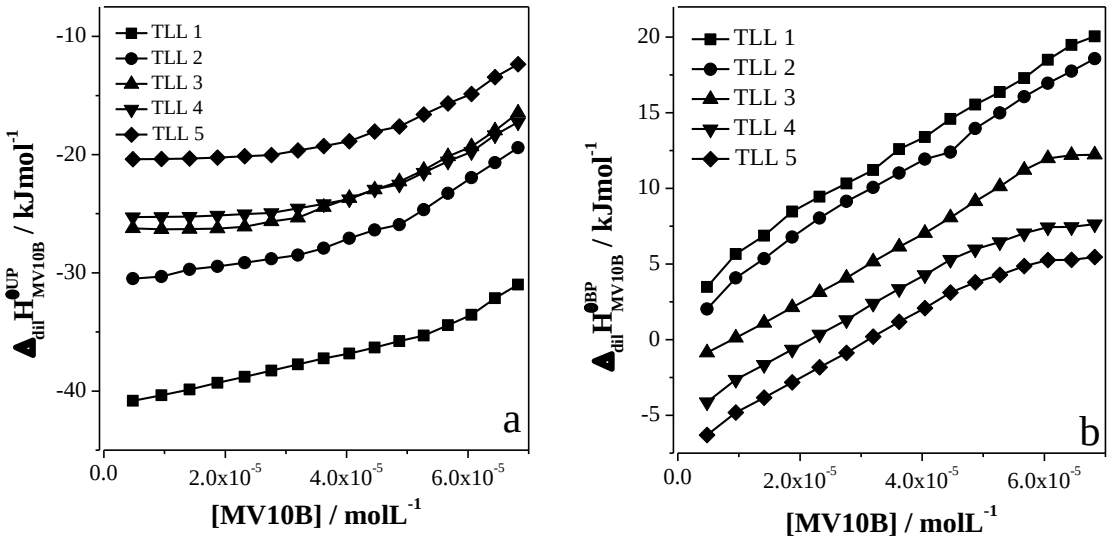

Figure 9. $\Delta_{dil}H^{UP}_{MV10B}$ (a) and $\Delta_{dil}H^{BP}_{MV10B}$ (b) as functions of dye concentration in upper and bottom phases of L64+Na_2SO_4+H_2O ATPS at 298.15 K.

Table 8. K_{MV10B} values and $\Delta_{dil}H^{\infty}_{MV10B}$ values in upper (UP) and bottom (BP) phases, for the TLL of L64 + Na_2SO_4 + H_2O ATPS at 298.15 K.

TLL	K_{MV10B}	$\Delta_{dil}H^{\infty UP}_{MV10B}$	$\Delta_{dil}H^{\infty BP}_{MV10B}$
mol kg^{-1}		kJ mol^{-1}	
3.27	140.72±0.50	-41.69±0.05	2.01±0.01
4.07	367.90±0.77	-31.05±0.02	1.85±0.08
4.65	931.31±0.32	-25.91±1.10	-2.31±1.04
4.88	1536.59±0.68	-25.75±0.07	-5.75±0.11
5.33	2618.51±0.41	-20.85±0.03	-7.93±0.06

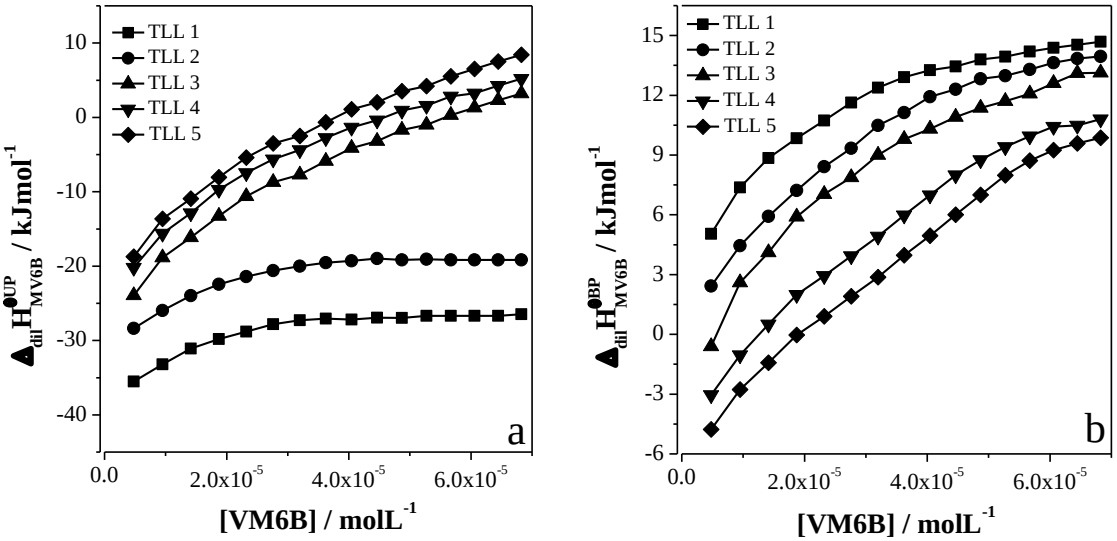

Figure 10. $\Delta_{dil}H^{UP}_{MV6B}$ (a) and $\Delta_{dil}H^{BP}_{MV6B}$ (b) as a functions of dye concentration in upper and bottom phases of L64+Na_2SO_4+H_2O ATPS at 298.15 K.

Table 9. K_{MV6B} values and $\Delta_{dil}H^{\infty}_{MV6B}$ values in upper (UP) and bottom (BP) phases, for the TLL of L64 + Na_2SO_4 + H_2O ATPS at 298.15 K.

TLL	K_{MV6B}	$\Delta_{dil}H^{\infty UP}_{MV6B}$	$\Delta_{dil}H^{\infty BP}_{MV6B}$
mol kg^{-1}		kJ mol^{-1}	
3.27	114.52±0.09	-39.46±0.09	1.74±0.03
4.07	295.82±0.28	-28.91±0.10	1.19±0.07
4.65	687.96±0.54	-23.09±0.02	-1.89±0.01
4.88	1099.01±0.31	-22.09±0.07	-4.29±0.13
5.33	1865.26±0.77	-16.88±0.11	-6.02±0.16

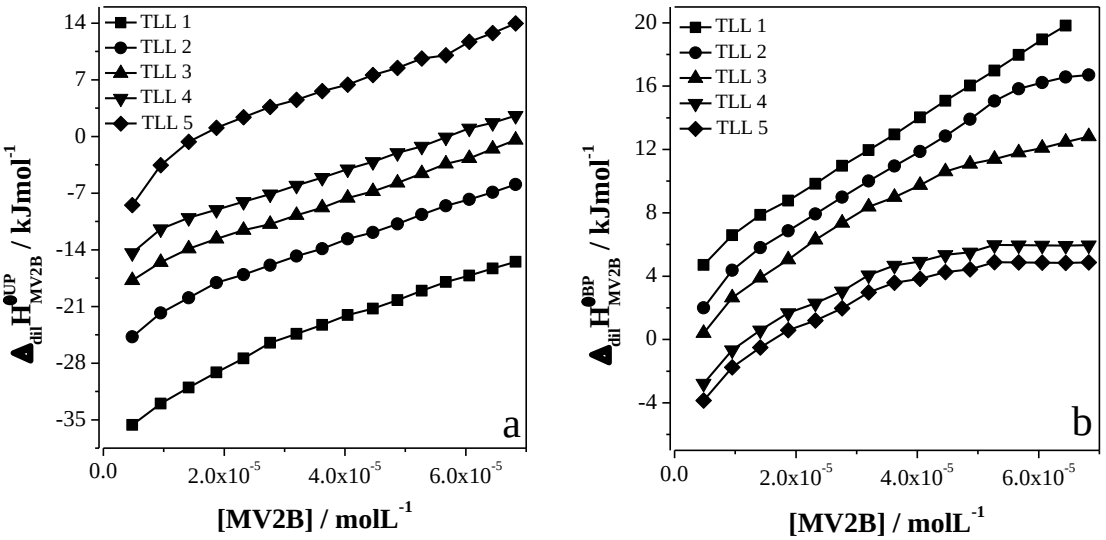

Figure 11. $\Delta_{dil}H^{UP}_{MV2B}$ (a) and $\Delta_{dil}H^{BP}_{MV2B}$ (b) as a functions of dye concentration in upper and bottom phases of L64+Na_2SO_4+H_2O ATPS at 298.15 K.

Table 10. K_{MV2B} values and $\Delta_{dil}H^{\infty}_{MV2B}$ values in upper (UP) and bottom (BP) phases, for the TLL of L64 + Na_2SO_4 + H_2O ATPS at 298.15 K.

TLL	K_{MV2B}	$\Delta_{dil}H^{\infty UP}_{MV2B}$	$\Delta_{dil}H^{\infty BP}_{MV2B}$
mol kg^{-1}		kJ mol^{-1}	
3.27	95.11±0.32	-37.49±0.05	1.21±0.01
4.07	232.17±0.19	-26.76±0.01	0.94±0.05
4.65	514.39±0.05	-20.41±0.08	-1.11±0.06
4.88	786.03±0.10	-19.38±0.02	-3.88±0.09
5.33	1339.47±0.87	-13.49±0.04	-4.97±0.07

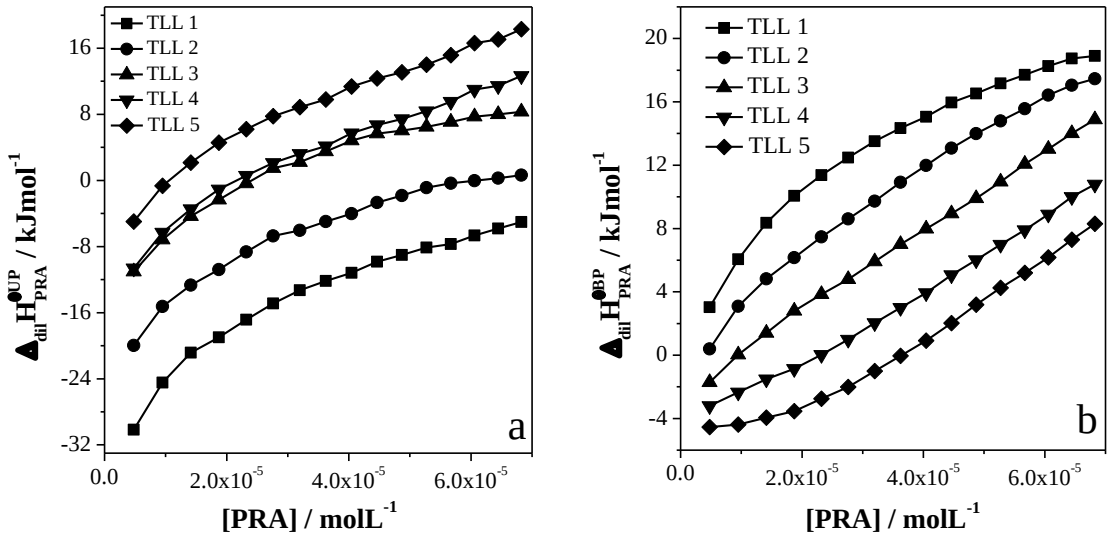

Figure 12. $\Delta_{dil}H^{UP}_{PRA}$ (a) and $\Delta_{dil}H^{BP}_{PRA}$ (b) as a functions of dye concentration in upper and bottom phases of L64+Na_2SO_4+H_2O ATPS at 298.15 K.

Table 11. K_{PRA} values and $\Delta_{dil}H^{\infty}_{PRA}$ values in upper (UP) and bottom (BP) phases, for the TLL of L64 + Na_2SO_4 + H_2O ATPS at 298.15 K.

TLL	K_{PRA}	$\Delta_{dil}H^{\infty UP}_{PRA}$	$\Delta_{dil}H^{\infty BP}_{PRA}$
mol kg^{-1}		kJ mol^{-1}	
3.27	43.28±0.91	-30.17±0.01	0.73±0.08
4.07	92.83±0.47	-19.58±0.01	-0.28±0.03
4.65	193.59±0.18	-12.83±0.02	-1.03±0.10
4.88	286.42±0.06	-11.31±0.01	-3.32±0.01
5.33	484.16±0.88	-5.68±0.01	-4.65±0.09

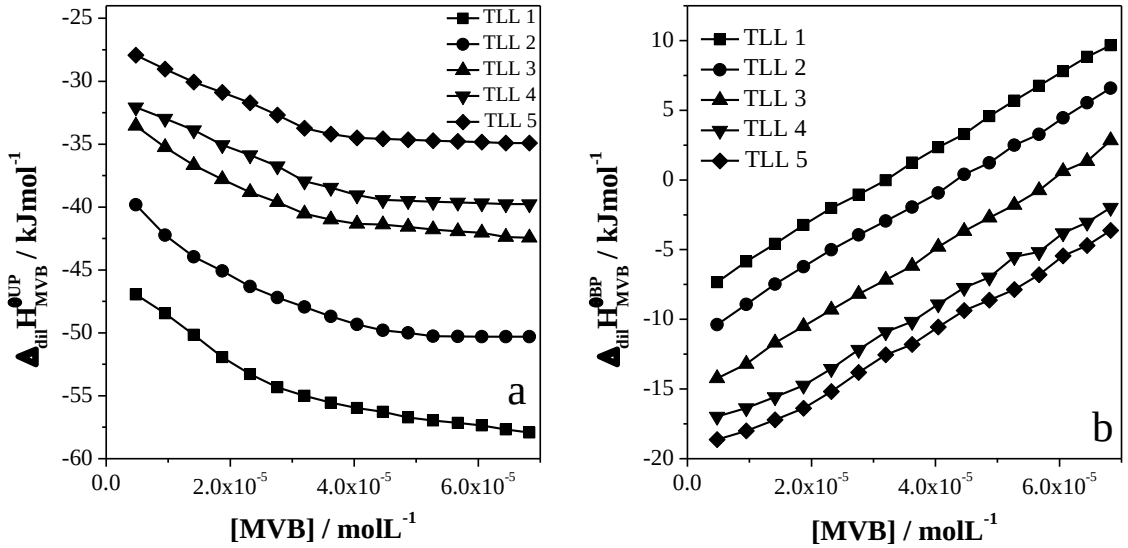

Figure 13. $\Delta_{dil}H^{UP}_{MVB}$ (a) and $\Delta_{dil}H^{BP}_{MVB}$ (b) as a functions of dye concentration in upper and bottom phases of L64+Na_2SO_4+H_2O ATPS at 298.15 K.

Table 12. K_{MVB} values and $\Delta_{dil}H^{\infty}_{MVB}$ values in upper (UP) and bottom (BP) phases, for the TLL of L64 + Na_2SO_4 + H_2O ATPS at 298.15 K.

TLL	K_{MVB}	$\Delta_{dil}H^{\infty UP}_{MVB}$	$\Delta_{dil}H^{\infty BP}_{MVB}$
mol kg^{-1}		kJ mol^{-1}	
3.27	92.46±0.02	-45.88±0.08	-9.18±0.09
4.07	268.50±0.09	-37.33±0.05	-12.03±0.07
4.65	632.03±0.08	-31.79±0.09	-15.59±0.14
4.88	855.59±0.05	-31.47±0.10	-18.47±0.05
5.33	1639.15±0.01	-26.62±0.02	-20.11±0.03

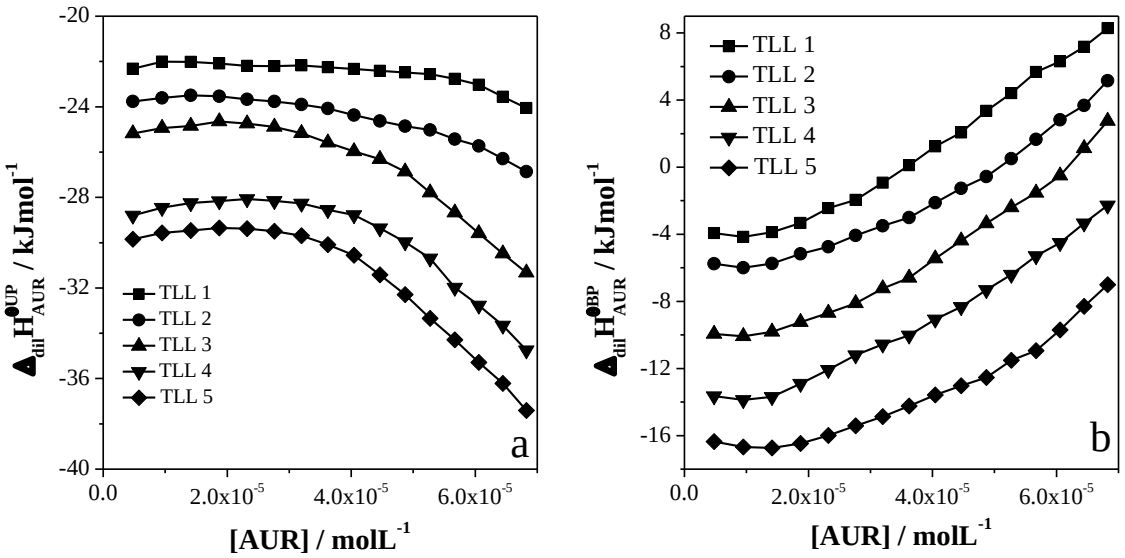

Figure 14. $\Delta_{dil}H^{UP}_{AUR}$ (a) and $\Delta_{dil}H^{BP}_{AUR}$ (b) as a functions of dye concentration in upper and bottom phases of L64+Na_2SO_4+H_2O ATPS at 298.15 K.

Table 13. K_{AUR} values and $\Delta_{dil}H^{\infty}_{AUR}$ values in upper (UP) and bottom (BP) phases, for the TLL of L64 + Na_2SO_4 + H_2O ATPS at 298.15 K.

TLL	K_{AUR}	$\Delta_{dil}H^{\infty UP}_{AUR}$	$\Delta_{dil}H^{\infty BP}_{AUR}$
mol kg^{-1}		kJ mol^{-1}	
3.27	27.64±0.10	-22.71±0.01	-3.61±0.02
4.07	52.11±0.16	-23.58±0.10	-5.98±0.09
4.65	82.91±0.02	-25.39±0.08	-9.09±0.01
4.88	102.28±0.13	-29.05±0.04	-13.25±0.10
5.33	148.89±0.09	-29.56±0.03	-14.96±0.07

Table 14. Thermodynamic transfer parameters of PhM dyes as a function of the TLL of L64 + Na_2SO_4 + H_2O ATPS at 298.15 K.

PhM dyes	$\Delta_{tr}G^{\theta,\infty}_{PhM}$	$\Delta_{tr}H^{\theta,\infty}_{PhM}$	$T\Delta_{tr}S^{\theta,\infty}_{PhM}$
		kJ mol^{-1}	
TLL 1 / 3.27 mol kg^{-1}			
MV10B	-12.31±0.09	-47.65±0.07	-31.54±0.02
MV6B	-11.69±0.03	-41.21±0.01	-29.47±0.02
MV2B	-11.27±0.01	-38.68±0.05	-27.43±0.04
PRA	-9.29±0.05	-30.87±0.08	-21.61±0.03
MVB	-11.17±0.15	-36.72±0.09	-25.46±0.06
AUR	-8.22±0.18	-19.06±0.10	-10.87±0.08
TLL 2 / 4.07 mol kg^{-1}			
MV10B	-14.57±0.14	-32.91±0.08	-18.27±0.07
MV6B	-14.11±0.21	-30,09±0.18	-16.01±0.03
MV2B	-13.48±0.03	-27.68±0.09	-14.15±0.06
PRA	-11.21±0.11	-19.34±0.03	-8.13±0.08
MVB	-13.89±0.18	-25.27±0.08	-11.48±0.09
AUR	-9.82±0.01	-17.63±0.07	-7.79±0.06
TLL 3 / 4.65 mol kg^{-1}			
MV10B	-16.93±0.09	-23.60±0.04	-6.67±0.05
MV6B	-16.18±0.04	-21.20±0.09	-5.02±0.05
MV2B	-15.46±0.15	-19.30±0.08	-3.84±0.07
PRA	-13.04±0.02	-11.80±0.05	1.24±0.03
MVB	-15.97±0.03	-16.20±0.05	-0.23±0.02
AUR	-10.94±0.02	-16.30±0.03	-5.36±0.04
TLL 4 / 4.88 mol kg^{-1}			
MV10B	-18.17±0.08	-20.01±0.03	-1.83±0.05
MV6B	-17.34±0.01	-17.80±0.04	-0.46±0.03
MV2B	-16.51±0.02	-15.50±0.01	1.01±0.01
PRA	-14.01±0.05	-7.99±0.09	6.02±0.04
MVB	-16.72±0.07	-13.02±0.08	3.72±0.01
AUR	-11.46±0.13	-15.80±0.07	-4.34±0.09
TLL 5 / 5.33 mol kg-1			
MV10B	-19.49±0.15	-12.92±0.08	6.57±0.07
MV6B	-18.65±0.20	-10.86±0.09	7.79±0.11
MV2B	-17.83±0.09	-8.52±0.07	9.31±0.02
PRA	-15.31±0.13	-1.03±0.06	14.28±0.07
MVB	-18.33±0.04	-6.51±0.01	11.82±0.03
AUR	-12.39±0.09	-14.60±0.08	-2.21±0.01

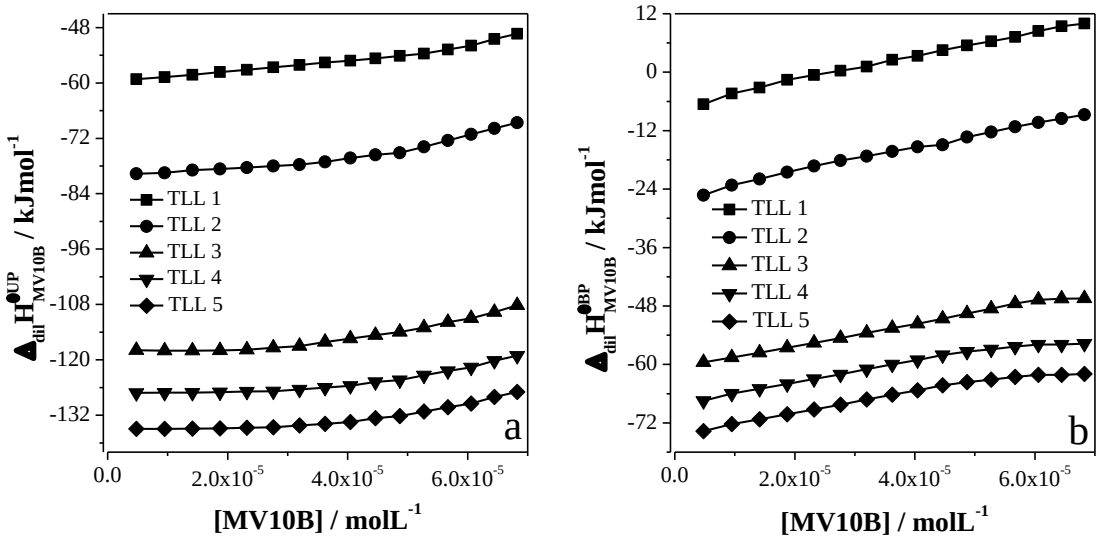

Figure 15. $\Delta_{dil}H^{UP}_{MV10B}$ (a) and $\Delta_{dil}H^{BP}_{MV10B}$ (b) as a functions of dye concentration in upper and bottom phases of PPO425+Na_2SO_4+H_2O ATPS at 298.15 K.

Table 15. K_{MV10B} values and $\Delta_{dil}H^{\infty}_{MV10B}$ values in upper (UP) and bottom (BP) phases, for the TLL of PPO425 + Na_2SO_4 + H_2O ATPS at 298.15 K.

TLL	K_{MV10B}	$\Delta_{dil}H^{\infty UP}_{MV10B}$	$\Delta_{dil}H^{\infty BP}_{MV10B}$
mol kg^{-1}		kJ mol^{-1}	
5.28	62.24±0.06	-60.04±0.10	-8.04±0.04
8.08	190.49±0.01	-80.24±0.07	-25.44±0.08
9.98	444.79±0.08	-117.61±0.15	-61.01±0.01
11.71	887.26±0.12	-127.60±0.04	-69.10±0.18
13.05	1798.68±0.22	-135.44±0.16	-75.34±0.10

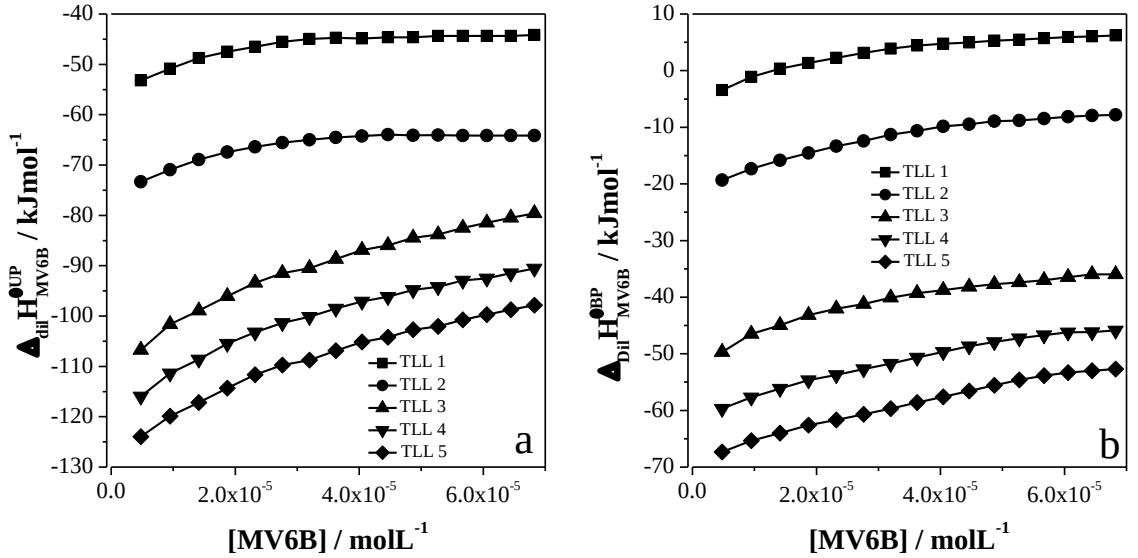

Figure 16. $\Delta_{dil}H^{UP}_{MV6B}$ (a) and $\Delta_{dil}H^{BP}_{MV6B}$ (b) as a functions of dye concentration in upper and bottom phases of PPO425+Na_2SO_4+H_2O ATPS at 298.15 K.

Table 16. K_{MV6B} values and $\Delta_{dil}H^{\infty}_{MV6B}$ values in upper (UP) and bottom (BP) phases, for the TLL of PPO425 + Na_2SO_4 + H_2O ATPS at 298.15 K.

TLL	K_{MV6B}	$\Delta_{dil}H^{\infty UP}_{MV6B}$	$\Delta_{dil}H^{\infty BP}_{MV6B}$
mol kg^{-1}		kJ mol^{-1}	
5.28	57.18±0.01	-58.14±0.02	-6.74±0.01
8.08	165.38±0.04	-73.88±0.01	-20.58±0.03
9.98	367.90±0.11	-105.87±0.10	-50.97±0.06
11.71	727.97±0.03	-117.84±0.13	-60.94±0.11
13.05	1452.13±0.16	-126.12±0.09	-68.59±0.07

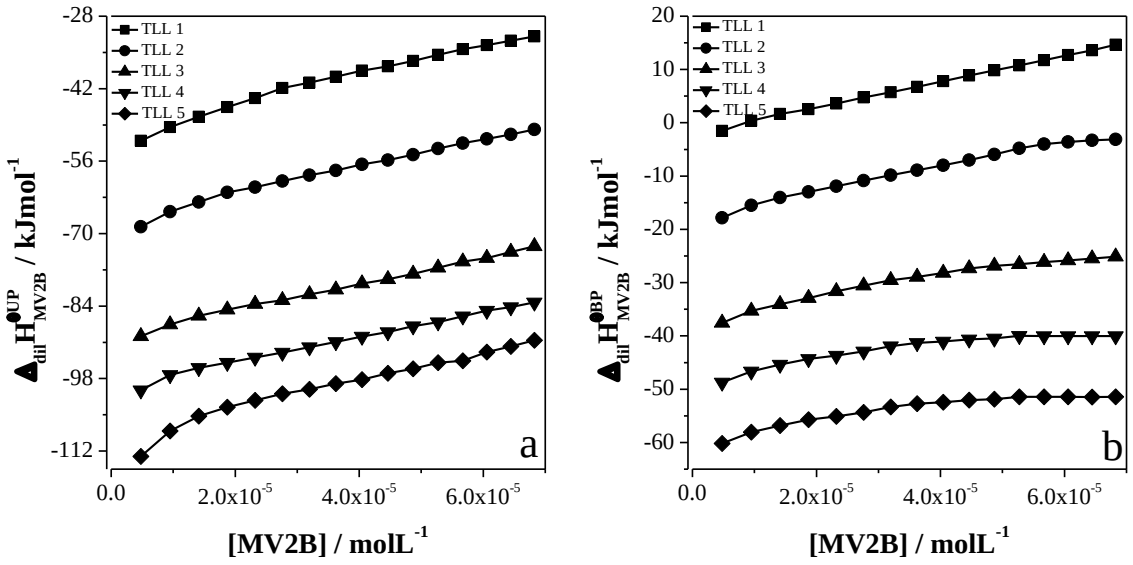

Figure 17. $\Delta_{dil}H^{UP}_{MV2B}$ (a) and $\Delta_{dil}H^{BP}_{MV2B}$ (b) as a functions of dye concentration in upper and bottom phases of PPO425+Na_2SO_4+H_2O ATPS at 298.15 K.

Table 17. K_{MV2B} values and $\Delta_{dil}H^{\infty}_{MV2B}$ values in upper (UP) and bottom (BP) phases, for the TLL of PPO425 + Na_2SO_4 + H_2O ATPS at 298.15 K.

TLL	K_{MV2B}	$\Delta_{dil}H^{\infty UP}_{MV2B}$	$\Delta_{dil}H^{\infty BP}_{MV2B}$
mol kg^{-1}		kJ mol^{-1}	
5.28	51.90±0.03	-53.91±0.01	-5.01±0.03
8.08	148.30±0.05	-70.71±0.09	-18.91±0.07
9.98	320.70±0.09	-92.44±0.01	-39.04±0.10
11.71	624.41±0.28	-105.25±0.06	-49.85±0.06
13.05	1196.26±1.01	-118.07±0.05	-61.27±0.11

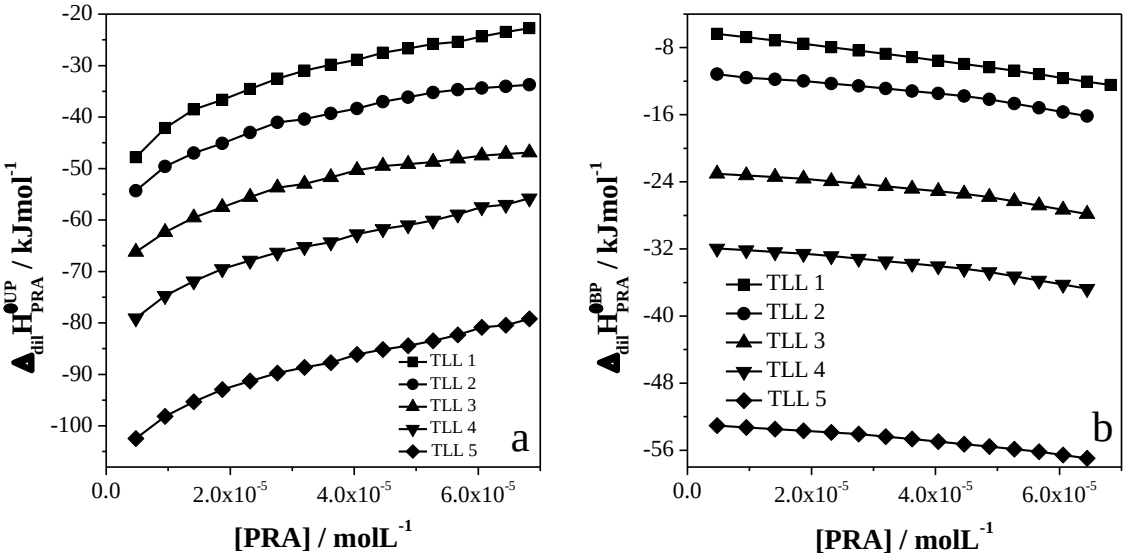

Figure 18. $\Delta_{dil}H^{UP}_{PRA}$ (a) and $\Delta_{dil}H^{BP}_{PRA}$ (b) as a functions of dye concentration in upper and bottom phases of PPO425+Na_2SO_4+H_2O ATPS at 298.15 K.

Table 18. K_{PRA} values and $\Delta_{dil}H^{\infty}_{PRA}$ values in upper (UP) and bottom (BP) phases, for the TLL of PPO425 + Na_2SO_4 + H_2O ATPS at 298.15 K.

TLL	K_{PRA}	$\Delta_{dil}H^{\infty UP}_{PRA}$	$\Delta_{dil}H^{\infty BP}_{PRA}$
mol kg^{-1}		kJ mol^{-1}	
5.28	38.03±0.07	-47.85±0.03	-4.45±0.10
8.08	94.35±0.12	-53.93±0.01	-7.73±0.05
9.98	191.26±0.04	-68.02±0.07	-20.12±0.02
11.71	353.34±0.06	-79.76±0.09	-30.06±0.08
13.05	650.15±0.22	-103.18±0.06	-52.18±0.15

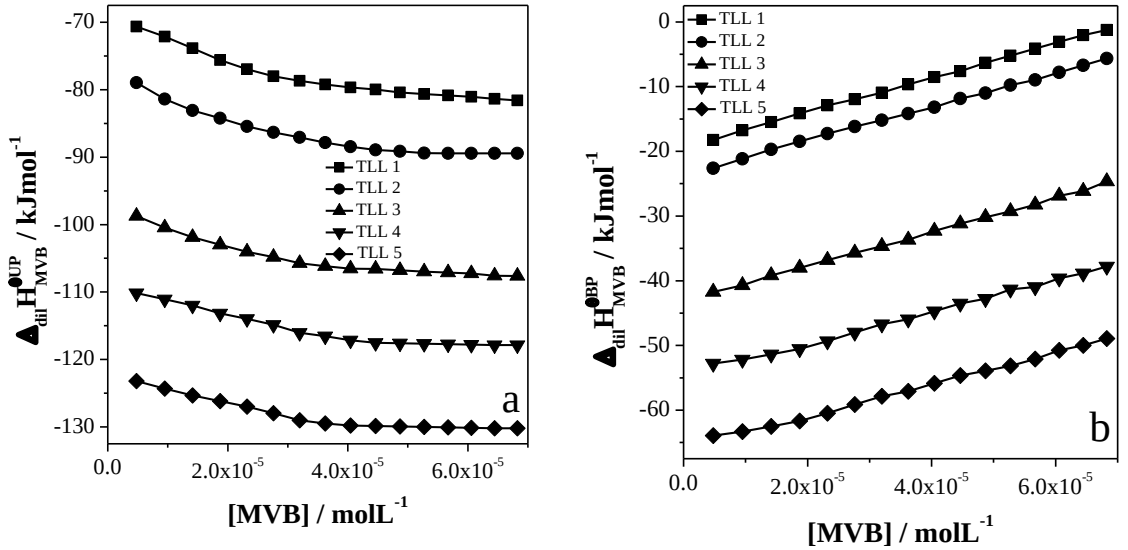

Figure 19. $\Delta_{dil}H^{UP}_{MVB}$ (a) and $\Delta_{dil}H^{BP}_{MVB}$ (b) as a functions of dye concentration in upper and bottom phases of PPO425+Na_2SO_4+H_2O ATPS at 298.15 K.

Table 19. K_{MVB} values and $\Delta_{dil}H^{\infty}_{MVB}$ values in upper (UP) and bottom (BP) phases,

for the TLL of PPO425 + Na_2SO_4 + H_2O ATPS at 298.15 K.

TLL	K_{MVB}	$\Delta_{dil}H^{\infty UP}_{MVB}$	$\Delta_{dil}H^{\infty BP}_{MVB}$
mol kg^{-1}		kJ mol^{-1}	
5.28	65.86±0.01	-69.57±0.03	-20.07±0.05
8.08	189.72±0.13	-76.47±0.19	-24.27±0.10
9.98	427.19±0.01	-96.98±0.02	-43.08±0.03
11.71	852.14±0.06	-109.57±0.04	-54.27±0.11
13.05	1645.78±0.08	-121.91±0.07	-65.41±0.01

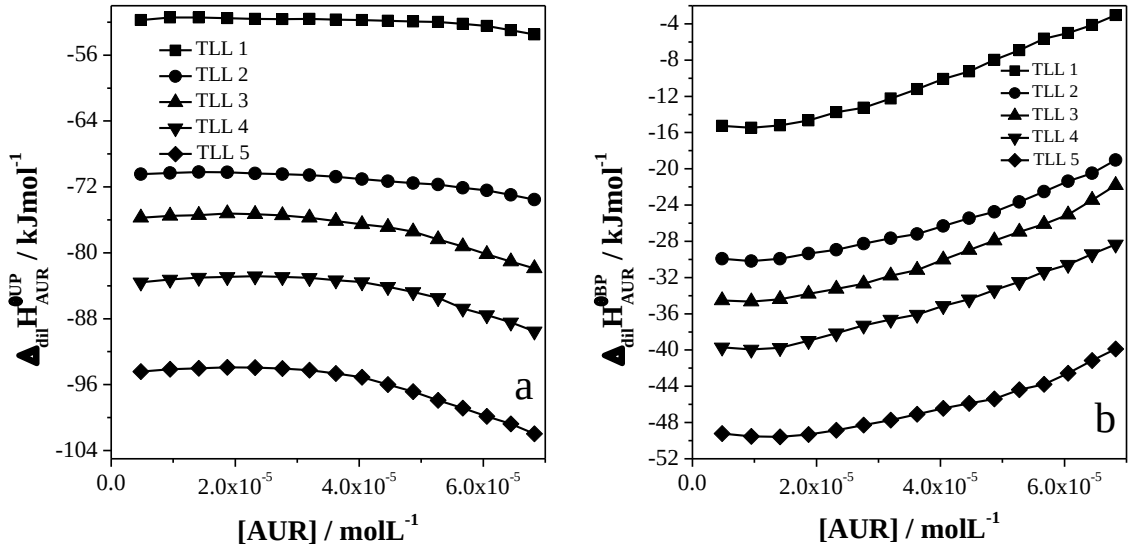

Figure 20. $\Delta_{dil}H^{UP}_{AUR}$ (a) and $\Delta_{dil}H^{BP}_{AUR}$ (b) as a functions of dye concentration in upper and bottom phases of PPO425+Na_2SO_4+H_2O ATPS at 298.15 K.

Table 20. K_{AUR} values and $\Delta_{dil}H^{\infty}_{AUR}$ values in upper (UP) and bottom (BP) phases, for the TLL of PPO425 + Na_2SO_4 + H_2O ATPS at 298.15 K.

TLL	K_{AUR}	$\Delta_{dil}H^{\infty UP}_{AUR}$	$\Delta_{dil}H^{\infty BP}_{AUR}$
mol kg^{-1}		kJ mol^{-1}	
5.28	15.52±0.01	-52.13±0.01	-14.93±0.03
8.08	31.58±0.03	-70.26±0.08	-30.16±0.01
9.98	52.96±0.01	-75.96±0.03	-33.66±0.06
11.71	84.60±0.02	-83.82±0.05	-39.32±0.09
13.05	127.72±0.05	-94.12±0.02	-47.82±0.04

Table 21. Thermodynamic transfer parameters of PhM dyes as a function of the TLL of PPO425 + Na_2SO_4 + H_2O ATPS at 298.15 K.

PhM dyes	$\Delta_{tr}G^{\theta,\infty}_{PhM}$	$\Delta_{tr}H^{\theta,\infty}_{PhM}$	$T\Delta_{tr}S^{\theta,\infty}_{PhM}$
		kJ mol^{-1}	
TLL 1 / 5.28 mol kg^{-1}			
MV10B	-10.23±0.03	-52.00±0.10	-41.77±0.07
MV6B	-10.02±0.05	-50.40±0.03	-40.38±0.08
MV2B	-9.78±0.12	-48.90±0.06	-39.12±0.06
PRA	-9.01±0.07	-43.40±0.01	-34.39±0.08
MVB	-10.37±0.08	-49.50±0.02	-39.13±0.06
AUR	-6.79±0.19	-37.20±0.11	-30.41±0.08
TLL 2 / 8.08 mol kg^{-1}			
MV10B	-13.01±0.08	-54.80±0.01	-41.80±0.09
MV6B	-12.65±0.07	-53.30±0.10	-40.65±0.03
MV2B	-12.38±0.11	-51.80±0.03	-39.42±0.08
PRA	-11.26±0.03	-46.20±0.12	-34.94±0.09
MVB	-12.99±0.04	-52.20±0.01	-39.21±0.05
AUR	-8.55±0.15	-40.10±0.08	-31.55±0.07
TLL 3 / 9.98 mol kg^{-1}			
MV10B	-15.10±0.15	-56.60±0.10	-41.50±0.05
MV6B	-14.63±0.03	-54.88±0.05	-40.27±0.02
MV2B	-14.29±0.01	-53.40±0.03	-39.11±0.04
PRA	-13.01±0.10	-47.91±0.07	34.89±0.17
MVB	-15.00±0.07	-53.86±0.01	-38.90±0.08
AUR	-9.83±0.09	-42.31±0.02	-32.47±0.11
TLL 4 / 11.71 mol kg^{-1}			
MV10B	-16.81±0.01	-58.53±0.04	-41.69±0.03
MV6B	-16.32±0.12	-56.90±0.14	-40.58±0.02
MV2B	-15.94±0.09	-55.41±0.10	-39.46±0.01
PRA	-14.53±0.03	-39.46±0.07	-35.17±0.04
MVB	-16.41±0.08	-35.17±0.18	-38.59±0.10
AUR	-10.99±0.11	-33.51±0.01	-33.51±0.12
TLL 5 / 13.05 mol kg-1			
MV10B	-18.56±0.04	-60.11±0.09	-41.54±0.05
MV6B	-18.03±0.10	-58.53±0.11	-40.50±0.01
MV2B	-17.55±0.03	-56.79±0.05	-39.25±0.02
PRA	-16.04±0.07	-51.01±0.10	-34.96±0.03
MVB	-18.34±0.20	-56.48±0.15	-38.16±0.05
AUR	-12.01±0.19	-46.26±0.09	-34.29±0.10

For a better analysis, the results can be discussed in the following sections, which establish appropriated contributions for each parameter.

3.1.1 Contribution of the methyl groups

If we assume that the solute thermodynamic transfer potential is the sum of the independent contributions of each functional group[29]. Then by investigating four PhM

dyes with different methylation degree ($MV10B_{(6\text{-}CH3)}$, $MV6B_{(5\text{-}CH3)}$, $MV2B_{(4\text{-}CH3)}$ and $PRA_{(0\text{-}CH3)}$), one can determine the -CH_3 groups contribution in the thermodynamics transfer potential at infinite dilution state ($\Delta_{tr}G^{\theta,\infty}_{PhM}$) of PhM dyes in ATPSs hydrophobically different. Figure 21 show the $\Delta_{tr}G^{\theta,\infty}_{PhM}$ values as a function of number of -CH_3 groups in ATPS formed by (PEO1500 or L64 or PPO425) + Na_2SO_4 + H_2O at 298.15 K.

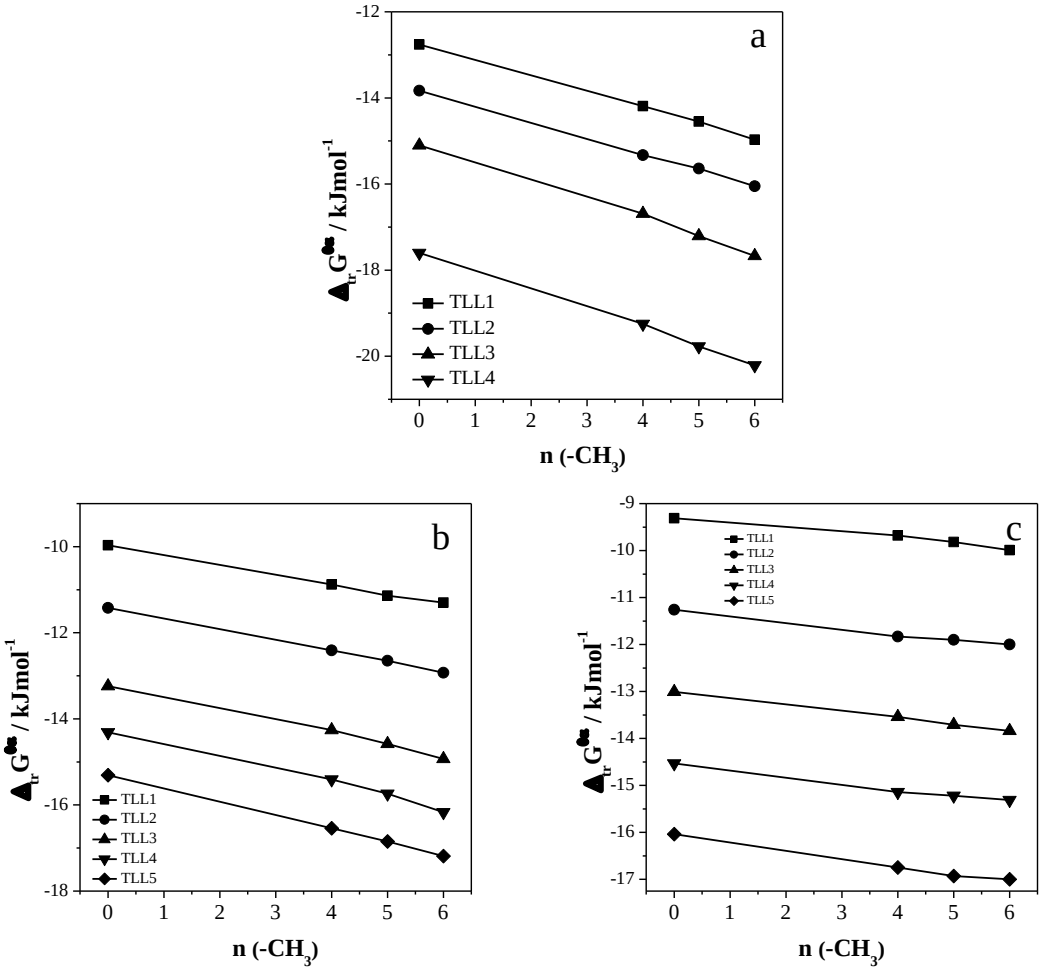

Figure 21. $\Delta_{tr}G^{\theta,\infty}_{CH_3}$ as a function of the number of -CH_3 groups, of $MV10B_{(6\text{-}CH3)}$, $MV6B_{(5\text{-}CH3)}$, $MV2B_{(4\text{-}CH3)}$ and $PRA_{(0\text{-}CH3)}$ partitioning in (a) PEO1500 + Na_2SO_4 + H_2O (b) L64 + Na_2SO_4 + H_2O and (c) PPO425 + Na_2SO_4 + H_2O ATPS at 298.15 K.

Independent of the ATPS, the PhM dye transfer is carried out with decrease in $\Delta_{tr}G^{\theta,\infty}_{PhM}$. Besides, this values become more negatives as the polymer hydrophobicity decreases in the order PEO1500 < L64 < PPO425. Since in each ATPS studied the $\Delta_{tr}G^{\theta,\infty}_{PhM}$ values decrease linearly with the increment in the TLL and the number of -CH_3 groups in the dye structure, one can calculate the average slope of the liner relationship $\Delta_{tr}G^{\theta,\infty}_{CH_3}$ versus number of -CH_3 groups, allowing to comparate the methyl groups contribution in each ATPS studied. Therefore, the slope of the linear relationship was $\frac{\partial \Delta_{tr}G^{\theta\infty}_{CH_3}}{\partial n_{\mathrm{CH_3}}}$ = -0.39±0.03; -0.27±0.03 and -0.13±0.02 kJ mol^{-1} for the ATPS formed by PEO1500; L64 and PPO425 respectively, revealing that the -CH_3 groups contribute more favorably for $\Delta_{tr}G^{\theta,\infty}_{PhM}$ in ATPS formed by PEO1500 than L64 or PPO425. This suggest that the intermolecular dye-EO segment interactions are more favorable than between dye-EO+PO segment or dye-PO segments. Besides, these results prove that the transfer of hydrophobic groups does not depend proportionally of the phase relative hydrophobicity, but of the specific interactions between the solute and upper phase components.

These results contradict that reported by Silverio et al[30] when studied the -CH_2 groups contributions in the partition process of five dinitrophenylated amino-acids in ATPSs with different hydrophobicity degree. The authors measured the Gibbs free energy of transfer of -CH_2 groups, in ATPS formed by PEO or UCON and salts (Na_2SO_4 or Li_2SO_4 or $(NH_4)_2SO_4$). The $\Delta_{tr}G^{\theta}_{CH_2}$ values found were: -0.64, -0.69, -0.82

kJ mol^{-1} for PEO + Na_2SO_4, Li_2SO_4 and $(NH_4)_2SO_4$respectively. For the ATPS composed by UCON and Na_2SO_4, Li_2SO_4 and $(NH_4)_2SO_4$the values were -0.89, -0.75 and -1.01 respectively. The results show that the $\Delta_{tr}G_{CH_2}$ values are more negative in the ATPS with greater relative hydrophobicity of the phases (UCON). The UCON is a copolymer of ethylene oxide and propylene oxide and the alkyl chain of the propylene oxide units stands for a higher hydrophobicity that when is compared with PEO that is an ethylene oxide homopolymer. Therefore, they concluded that the hydrophobic -CH_2 groups are preferably transferred for a more hydrophobic phase. Similarly, Maia et al[31] studied the free energy of transfer of methylene group in ATPS formed by ionic liquid (IL) with different hydrophobic degree. The authors evaluated the relative hydrophobicity of the phases by means of the free energy of transfer of -CH_2, and the results of $\Delta_{tr}G_{CH2}$ were -2.14; -2.27 and -2.45 kJ mol^{-1}, concluding that the $\Delta_{tr}G_{CH2}$ values are more negatives when the ATPS is formed by IL with longer alkyl chains i.e. a more hydrophobic IL.

According to the Gibbs fundamental equation, the thermodynamic transfer potential variation depends on two fundamental parameters linked to the intermolecular interactions that occur in the system. These parameters are the standard transfer enthalpy change and standard transfer entropy change ($\Delta_{tr}H_{PhM}^{\theta,\infty}$ and $T\Delta_{tr}S_{PhM}^{\theta,\infty}$). Therefore, the determining of the methyl group contribution of in these two parameters becomes fundamental in the understanding of the dyes partition process. The Figure 22 shows the $\Delta_{tr}H_{PhM}^{\theta,\infty}$ values as a function of the number -CH_3 groups in ATPS formed by (PEO1500 or L64 or PPO425) + Na_2SO_4 + H_2O at 298 K.

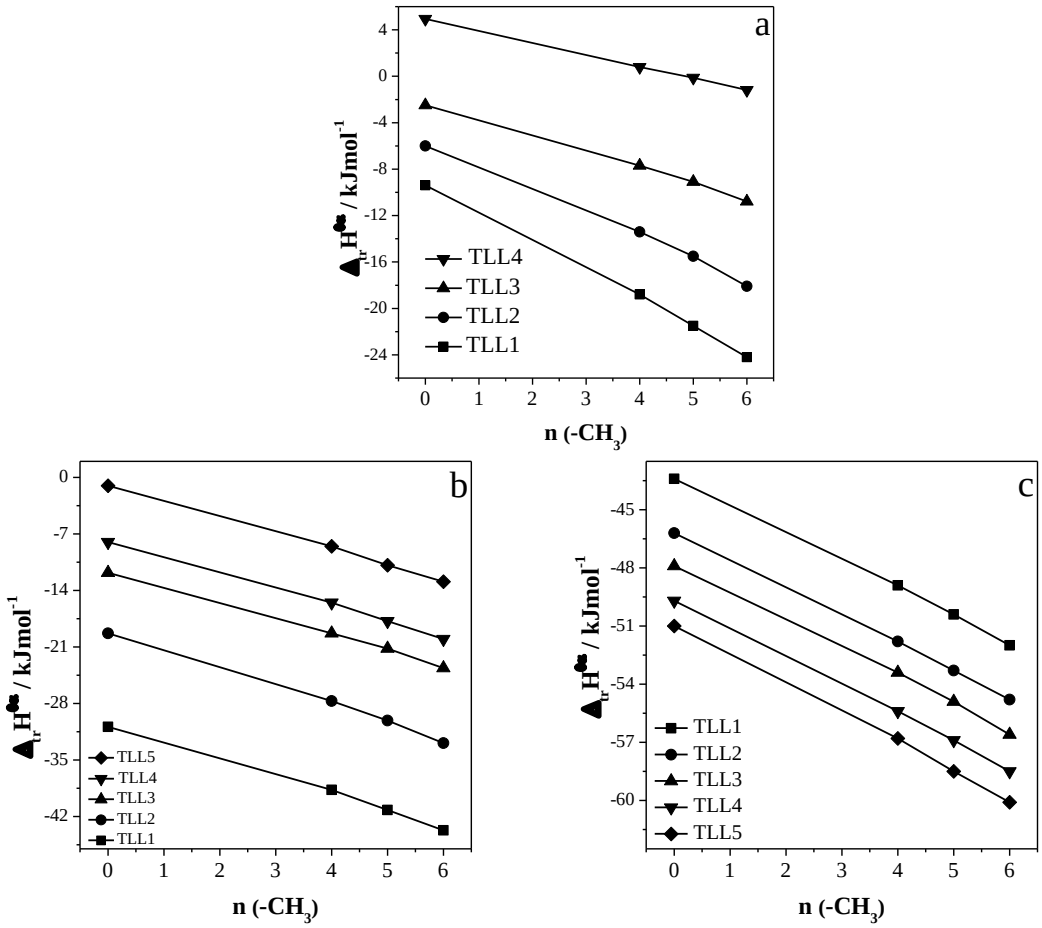

Figure 22. $\Delta_{tr}H^{\theta,\infty}_{PhM}$ values as a function of the number of -CH_3 groups, for $MV10B_{(6\text{-}CH3)}$, $MV6B_{(5\text{-}CH3)}$, $MV2B_{(4\text{-}CH3)}$ and $PRA_{(0\text{-}CH3)}$ partitioning in (a) PEO1500 + Na_2SO_4 + H_2O, (b) L64 + Na_2SO_4 + H_2O and (c) PPO425 + Na_2SO_4 + H_2O ATPS at 298.15 K.

For the ATPS formed by PEO1500, the $\Delta_{tr}H^{\theta,\infty}_{PhM}$ values became less negative when the TLL increased, $PRA_{(0\text{-}CH3)}$ even reached a positive value in the fourth TLL. In addition, when the methylations degree in the dye structure increment the $\Delta_{tr}H^{\theta,\infty}_{PhM}$ values decrease in a range of 4.95±0.05 to -24.2±0.03 kJ mol^{-1} for $PRA_{(0\text{-}CH3)}$ to $MV10B_{(6\text{-}CH3)}$ respectively.

Similarly, in the ATPS formed by L64 the $\Delta_{tr}H^{\theta,\infty}_{PhM}$ values decrease in a range of -1.03±0.07 to -43.7±0.1 kJ mol^{-1} for $PRA_{(0\text{-}CH3)}$ to $MV10B_{(6\text{-}CH3)}$ respectively. In contrast, the $\Delta_{tr}H^{\theta,\infty}_{PhM}$ values in ATPS formed by PPO425 become more negative when

the TLL and the dye molecule methylations degree increase in a range of -43.41±0.08 to -60.13±0.02 kJ mol^{-1} for $PRA_{(0\text{-}CH3)}$ to $MV10B_{(6\text{-}CH3)}$ respectively.

The methyl group contribution to the $\Delta_{tr}H_{PhM}^{\theta,\infty}$ values can be determinates calculating the average slope of the linear relationship $\frac{\partial \Delta_{tr}H_{CH_3}^{\theta\infty}}{\partial n_{CH_3}}$ = -2.44±0.05 kJ mol^{-1} in PEO1500; -1.97±0.06 kJ mol^{-1} in L64 and -1.50±0.03 kJ mol^{-1} in PPO425. These values indicate that the -CH_3 groups contribution in the $\Delta_{tr}H_{PhM}^{\theta,\infty}$ values were more favorable when the transference process is carried out in ATPS formed by PEO1500 > L64 > PPO. Moreover, if we consider that $\Delta_{tr}H_{PhM}^{\theta,\infty}$ as a parameter composed of four processes that involve absorption and/or release of energy, as expressed by equation 8:

$$\Delta_{tr}H_{PhM}^{\theta,\infty} = \Delta_{int}H_{BP-BP}^{\infty} + \Delta_{int}H_{PhM-UP}^{\infty} + \Delta_{int}H_{PhM-BP}^{\infty} + \Delta_{int}H_{UP-UP}^{\infty} \quad (8)$$

Where $\Delta_{int}H_{BP-BP}^{\infty}$ is the energy released in the formation of new interactions between the bottom phase components, $\Delta_{int}H_{PhM-UP}^{\infty}$ is the energy released due to the formation of the new interactions between dye molecules and the upper phase components, $\Delta_{int}H_{PhM-BP}^{\infty}$ is the energy absorbed to break the interactions of dye molecules and the bottom phase components and $\Delta_{int}H_{UP-UP}^{\infty}$ is the energy absorbed to disrupt the interactions between the upper phase components. Therefore, in order for the $\Delta_{tr}H_{PhM}^{\theta,\infty}$ values to be negative it is necessary that the processes that release energy have magnitudes greater than the processes that absorb energy, i.e., $|\Delta_{int}H_{BP-BP}^{\infty} + \Delta_{int}H_{PhM-UP}^{\infty}| > |\Delta_{int}H_{PhM-BP}^{\infty} + \Delta_{int}H_{UP-UP}^{\infty}|$. In consequence, as the interaction between the dye and bottom phases component are similar for all ATPS studied, the $\Delta_{tr}H_{PhM}^{\theta,\infty}$ values is more negative in PEO1500 than that with L64 or PPO, because the energy absorption is less in the breakdown of interactions between the EO-EO segments

($\Delta_{int}H^{\infty}_{UP-UP}$) and releases more energy to form the new interactions between the PhM dye and upper phase components ($\Delta_{int}H^{\infty}_{PhM-UP}$).

The Figure 23 shows the $T\Delta_{tr}S^{\theta,\infty}_{PhM}$ values as function of the number -CH_3 groups in ATPS formed by (PEO1500 or L64 or PPO425) + Na_2SO_4 + H_2O at 298 K.

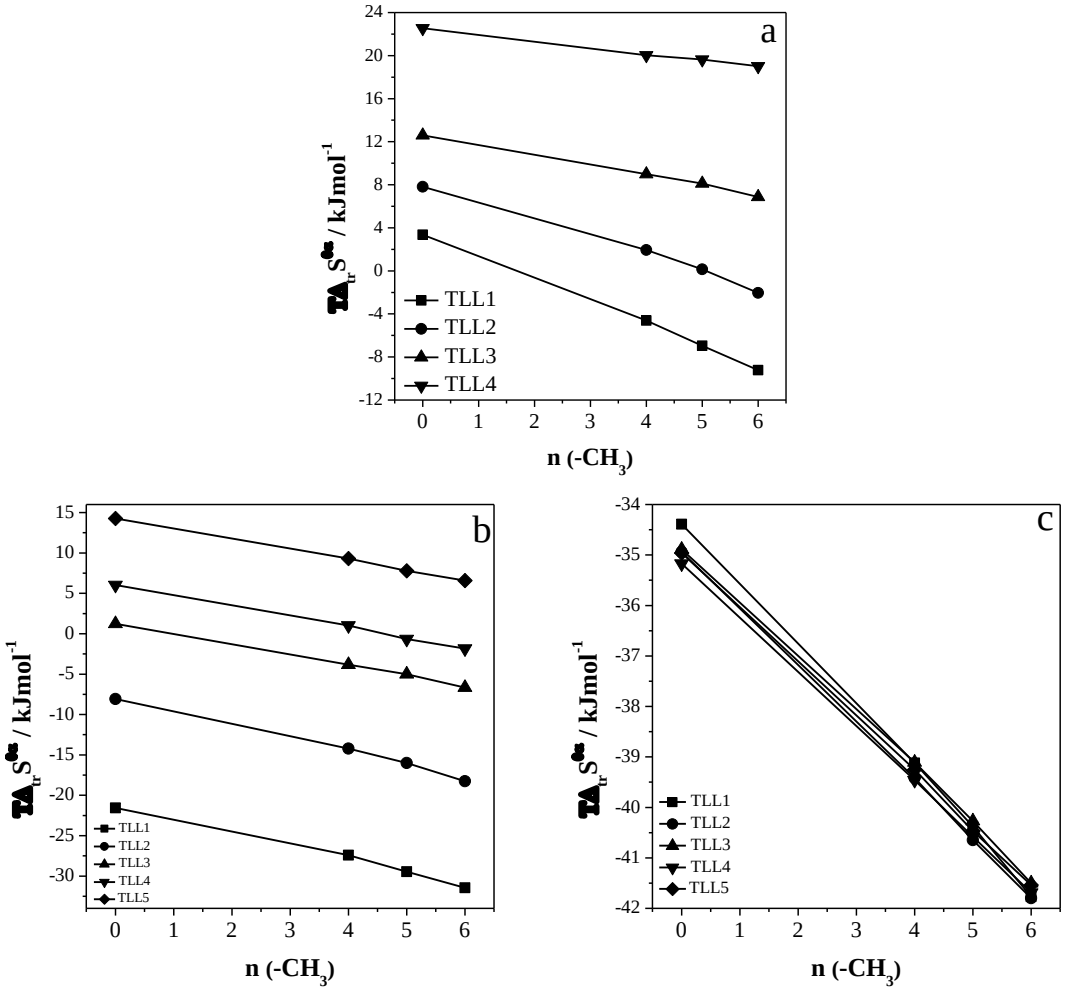

Figure 23. $T\Delta_{tr}S_{PhM}^{\theta,\infty}$ values as a function of the number of -CH_3 groups, for $MV10B_{(6\text{-}CH3)}$, $MV6B_{(5\text{-}CH3)}$, $MV2B_{(4\text{-}CH3)}$ and $PRA_{(0\text{-}CH3)}$ partition in (a) PEO1500 + Na_2SO_4 + H_2O (b) L64 + Na_2SO_4 + H_2O and (c) PPO425 + Na_2SO_4 + H_2O ATPS at 298.15 K.

For the ATPS formed by PEO or L64, the transfer process is carried out with an increase in entropy and the $T\Delta_{tr}S_{PhM}^{\theta,\infty}$ values are more positives when the TLL increases. However, when the methylation degree on the dye structure increases, the transfer entropy decreases to negative values in the first TLL of the ATPS with PEO and in the first two of the ATPS with L64. On the other hand, in the presence of PPO the transfer process was carried out with negative $T\Delta_{tr}S_{PhM}^{\theta,\infty}$ values and became more negative when the degree of methylation in the dye structure increased. This mean that, when the dye molecule is transferred from bottom phase to phase rich in PEO the system gains more entropy than in L64 and PPO, indicating that the increment of hydrophobic groups in the polymeric alkyl chain (L64 and/or PPO) increase the hydrophobicity dye-polymer interaction and decrease the freedom rotational degree solvation water, which effectively causes the system entropy to decrease.

The methyl group contribution to the $T\Delta_{tr}S_{PhM}^{\theta,\infty}$ values was determinate calculating the average slope of the linear relationship $\frac{\partial[T\Delta_{tr}S_{CH_3}^{\theta\infty}]}{\partial n_{CH_3}}$ for each ATPS studied and the results were -0.58±0.02; -1.61±0.04 and -1.21±0.01 kJ mol^{-1} to PEO; L64 and PPO respectively. The transfers of 1 mole of methyl group from the ATPS bottom phase to the upper phase decreases the system entropy. This decrease in the $T\Delta_{tr}S_{PhM}^{\theta,\infty}$ values is proportional to the hydrophobicity degree of the system forming polymer. Demonstrating that the interaction dye-EO segment (less hydrophobic segment) requires a smaller number of water molecules to solvate. The dye-PO segment

interaction is more hydrophobic due to the methyl group presence in the polymer alkyl chain causing a greater organization in the water molecules that solvate this interaction decreasing the system entropy.

3.1.2 Contribution of the phenyl groups

MV2B is a triphenylmethane (TPhM) dye substituted for two tertiary amines and one primary, while AUR is a diphenylmethane (DPhM) dye similarly substituted (figure 1). Therefore, both structures only differ in a phenyl group that can be used to study its contribution in the thermodynamic transference parameter. The figure 24a shows the $\Delta_{tr}G^{\theta,\infty}_{PhM}$ values of AUR and MV2B as functions of the TLL of ATPS formed by (PEO1500 or L64 or PPO425) + Na_2SO_4 + H_2O ATPS.

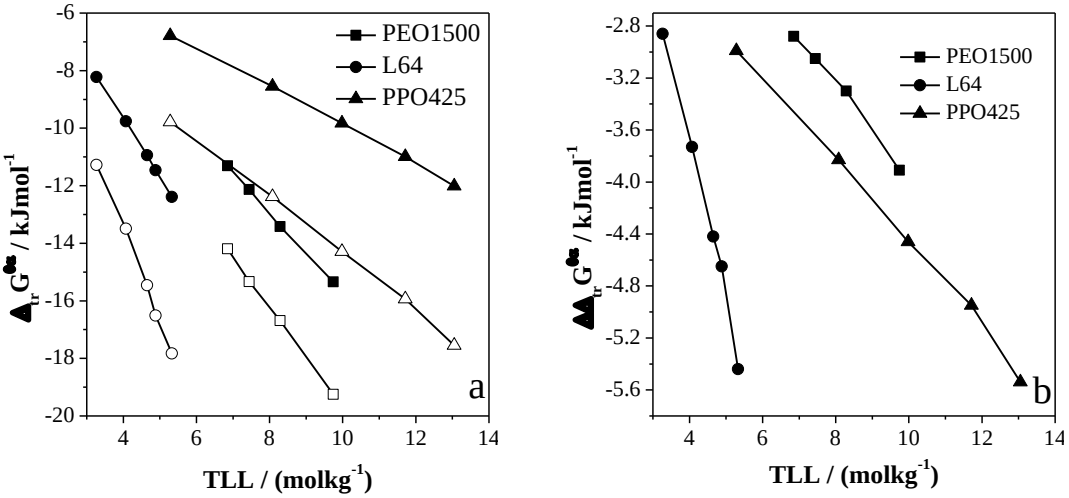

Figure 24. (a) $\Delta_{tr}G^{\theta,\infty}_{PhM}$ values of AUR (closed symbols) and MV2B (open symbols) and (b) $\Delta\Delta_{tr}G^{\theta,\infty}_{PhM}$ as a function of the TLL of ATPS formed by (square symbol) PEO1500 + Na_2SO_4 + H_2O, (round symbol) L64 + Na_2SO_4 + H_2O and (triangular symbol) PPO425 + Na_2SO_4 + H_2O ATPS at 298.15 K.

Independent of the ATPS, the AUR and MV2B transference occur with a decrease of Gibbs energy. However, the $\Delta_{tr}G^{\theta,\infty}_{VM2B}$ values are more negative than $\Delta_{tr}G^{\theta,\infty}_{AUR}$ in all the ATPS studied, indicating that the benzene ring plays a fundamental

role in the hydrophobic interaction dye-UP components responsible for the dye molecules migration from the bottom phase to the upper phase in all the ATPSs studied. Therefore, for better understand the effect of the phase hydrophobicity in phenyl groups contribution, was calculated the difference between the $\Delta_{tr}G^{\theta,\infty}_{PhM}$ values of each dye ($\Delta\Delta_{tr}G^{\theta,\infty}_{MV2B-AUR} = \Delta_{tr}G^{\theta,\infty}_{MV2B} - \Delta_{tr}G^{\theta,\infty}_{AUR}$). The figure 4b show the $\Delta\Delta_{tr}G^{\theta,\infty}_{MV2B-AUR}$ values as a function of the TLL of each ATPS studied.

The results of the $\Delta\Delta_{tr}G^{\theta,\infty}_{MV2B-AUR}$ for each ATPS as a function of the TLL, shows that $\Delta\Delta_{tr}G^{\theta,\infty-PEO}_{MV2B-AUR}$ were from -2.88 to -3.91; $\Delta\Delta_{tr}G^{\theta,\infty-L64}_{MV2B-AUR}$ were from -2.86 to -4.65 and $\Delta\Delta_{tr}G^{\theta,\infty-PPO}_{MV2B-AUR}$ from -2.99 to -4.95. This suggest that the dye transfer is favored by the phenyl ring presence and this effect is more favorable when the system is more hydrophobic.

In order to understand in detail, the origin of this effect, were determined the standard transfer enthalpy change of the diphenylmethane (DPhM) dye AUR ($\Delta_{tr}H^{\theta,\infty}_{DPhM}$) and triphenylmethane (TPhM) dye MV2B ($\Delta_{tr}H^{\theta,\infty}_{TPhM}$) as a function of the TLL of (PEO1500 or L64 or PPO425) + Na_2SO_4 + H_2O ATPS. The results are shown in the figure 25.

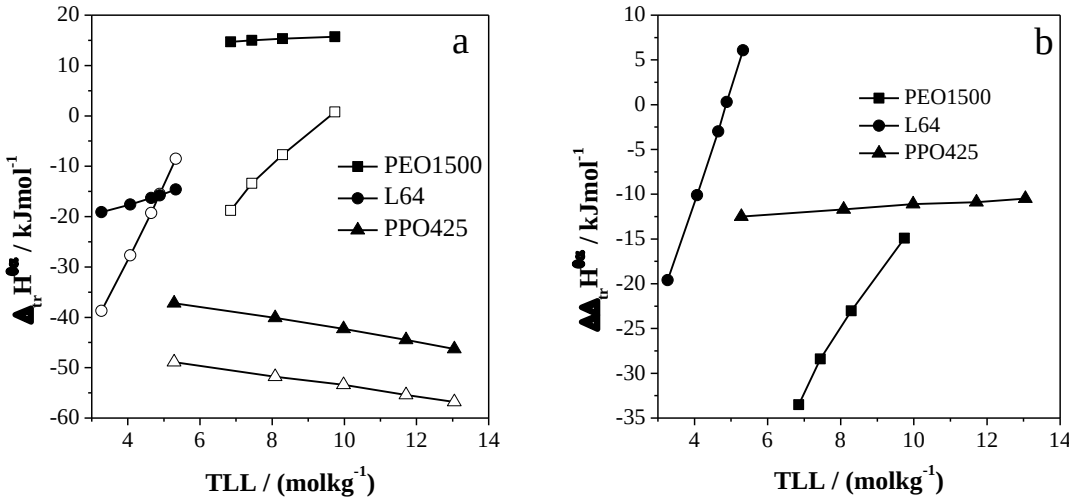

Figure 25. (a) $\Delta_{tr}H^{\theta,\infty}_{DPhM}$ values of AUR (closed symbols) and $\Delta_{tr}H^{\theta,\infty}_{TPhM}$ MV2B (open symbols) and (b) $\Delta\Delta_{tr}H^{\theta,\infty}_{MV2B-AUR}$ as a function of the TLL of ATPS formed by (square symbol) PEO1500 + Na_2SO_4 + H_2O, (round symbol) L64 + Na_2SO_4 + H_2O and (triangular symbol) PPO425 + Na_2SO_4 + H_2O ATPS at 298.15 K.

When PEO was the polymer that formed the ATPS, the transference process of DPhM dye was endothermic and the variation in the $\Delta_{tr}H^{\theta,\infty}_{DPhM}$ values was from 14.70±0.03 to 15.76±0.02 kJ mol^{-1} with the TLL increment. In contrast, the $\Delta_{tr}H^{\theta,\infty}_{TPhM}$ values were from -18.83±0.01 to 0.79±0.01 kJ mol^{-1}, this mean that the TPhM dye transference process became exothermic in the three first TLL and endothermic in the last, showing that the effect of the TLL was more intense in the TPhM dye. In the ATPS formed by L64, the transfer process for both molecules was exothermic. However, the effect of the TLL was similar to the previous, being smaller for DPhM dye than that TPhM dye (-19.10±0.04 ≤ $\Delta_{tr}H^{\theta,\infty-L64}_{DPhM}$ ≤ -14.62±0.03 kJ mol^{-1} and -38.69±0.05 ≤ $\Delta_{tr}H^{\theta,\infty-L64}_{TPhM}$ ≤ -8.52±0.02 kJ mol^{-1}) respectively. On the other hand, in the ATPS formed by PPO the transfer process was exothermic and unlike previous ATPSs and the $\Delta_{tr}H^{\theta,\infty-PPO}_{PhM}$ values became more negatives with the TLL increment for both molecules. Nevertheless, the $\Delta_{tr}H^{\theta,\infty}_{DPhM}$ values varied between -37.21±0.06 and -

46.29±0.03 kJ mol^{-1} and were less negative than the $\Delta_{tr}H^{\theta,\infty}_{TPhM}$ values that varied from -49.68±0.04 to -56.79±0.06 kJ mol^{-1} when the TLL increase.

For a better analysis of the phenyl group contribution in the standard enthalpy transfer change in each ATPS studied, was calculate the difference $\Delta\Delta_{tr}H^{\theta,\infty}_{MV2B-AUR} = \Delta_{tr}H^{\theta,\infty}_{MV2B} - \Delta_{tr}H^{\theta,\infty}_{AUR}$. The results were show in the figure 25b.

The $\Delta\Delta_{tr}H^{\theta,\infty}_{MV2B-AUR}$ values show that the phenyl groups contribution in the ATPS formed by PEO varied from -33.5±0.02 to -14.91±0.01 kJ mol^{-1}; when is formed by L64 varied from -19.59±0.02 to 6.08±0.01 kJ mol^{-1} and in presence de PPO the values varied from -12.51±0.02 to -10.51±0.03 kJ mol^{-1}. This shows that the phenyl group contributes favorably to the values of $\Delta_{tr}H^{\theta,\infty}_{PhM}$ in the three ATPS studied, but this contribution is more favorable when the ATPS hydrophobicity decreases. This can be explained following way; the phenyl group absence into dye structure causes an increase the charge density, generating a interaction dye-BP component more intense and to break this interaction is needs to absorb a greater energy amount. On the other hand, the phenyl group increases the dye molecule degree hydrophobicity, becoming more favorable the hydrophobic interaction between the dye and the polymer segments releasing more energy in the following order PEO > PPO > L64.

The figure 26 shows the $T\Delta_{tr}S^{\theta,\infty}_{DPhM}$ and $T\Delta_{tr}S^{\theta,\infty}_{TPhM}$ as a function of the TLL of (PEO1500 or L64 or PPO425) + Na_2SO_4 + H_2O ATPS.

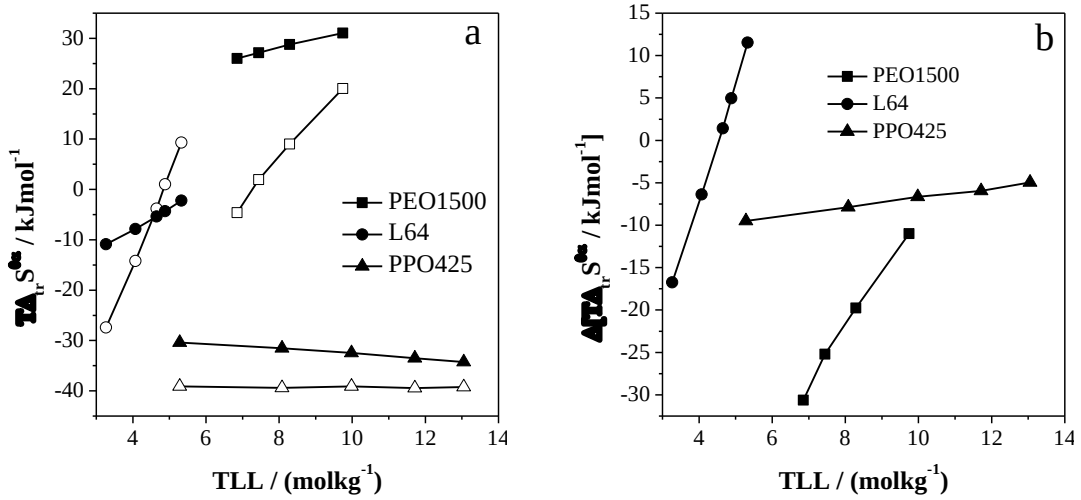

Figure 26. (a) $T\Delta_{tr}S^{\theta,\infty}_{DPhM}$ values of AUR (closed symbols) and $T\Delta_{tr}S^{\theta,\infty}_{TPhM}$ values of MV2B (open symbols) and (b) $\Delta T\Delta_{tr}S^{\theta,\infty}_{MV2B-AUR}$ as a function of the TLL of ATPS formed by (square symbol) PEO1500 + Na_2SO_4 + H_2O, (round symbol) L64 + Na_2SO_4 + H_2O and (Triangular symbol) PPO425 + Na_2SO_4 + H_2O ATPS at 298.15 K.

In ATPS formed by PEO, the transference process of both dye molecules was carried out with entropy increment, becoming more positive with the TLL increase. However, the phenyl group increase in the dye structure causes a decrease in the $T\Delta_{tr}S^{\theta,\infty}_{PhM}$ values. Suggesting that the phenyl ring addition to the dye structure causes an increase in the molecule hydrophobicity and consequently the water molecules that cover the interaction between TPhM and EO segment, loss rotational freedom degrees, causing a entropy decrease. On the other hand, when the ATPS hydrophobicity degree increases, the transfer process generates $T\Delta_{tr}S^{\theta,\infty}_{PhM}$ values negative in both molecules, but more negatives in TPhM dyes, this effect is observed when the ATPS is formed by L64 or PPO. Nevertheless, for a better understanding of the hydrophobicity effect on the phenyl group contribution in the variation of standard transfer entropy is necessary to calculate the difference $\Delta[T\Delta_{tr}S^{\theta,\infty}_{MV2B-AUR}] = T\Delta_{tr}S^{\theta,\infty}_{MV2B} - T\Delta_{tr}S^{\theta,\infty}_{AUR}$ for each ATPS studied. The results are shown in the figure 26b.

The $\Delta[T\Delta_{tr}S^{\theta,\infty}_{MV2B-AUR}]$ values show that only in ATPS formed by L64, the phenyl groups contribution was positive in the three last TLL exhibiting values from -16.74 to 11.52. It is due to the increase in the concentration of L64 (TLL), incrementing the formation of micellar aggregates, inducing to the most hydrophobic molecule (TPhM) to the nucleus of the micelle. This process releases a greater number of water molecules for the bulk causing an increase in the system configurational entropy.

When we compared the $\Delta[T\Delta_{tr}S^{\theta,\infty}_{MV2B-AUR}]$ values obtained in the ATPSs formed by PEO versus PPO we observed that; The phenyl group contributes to a greater decrease of the entropy in PEO than in PPO. This suggest that in the PEO presence a greater number of dye molecules transferred to upper phase, incrementing the hydration degree of the hydrophobic interactions. this cause that a greater number of the water molecules loss freedom degree and consequently decrease the system entropy.

3.1.3 Contribution of the charge on the dye molecule

The PhM dyes MV6B and MVB (figure 1) are structurally similar, but, MV6B is a cationic specie and MVB is a neutral specie. This difference was used to determine the charge contribution in the PhM dye thermodynamics transference parameters in different ATPS. The Figure 27 shows the $\Delta_{tr}G^{\theta,\infty}_{PhM}$ (a), $\Delta_{tr}H^{\theta,\infty}_{PhM}$ (b) and $T\Delta_{tr}S^{\theta,\infty}_{PhM}$ (c) values of MV6B and MVB as a function of the TLL of three ATPSs formed by (PEO1500 or L64 or PPO425) + Na_2SO_4 + H_2O at 298.15 K.

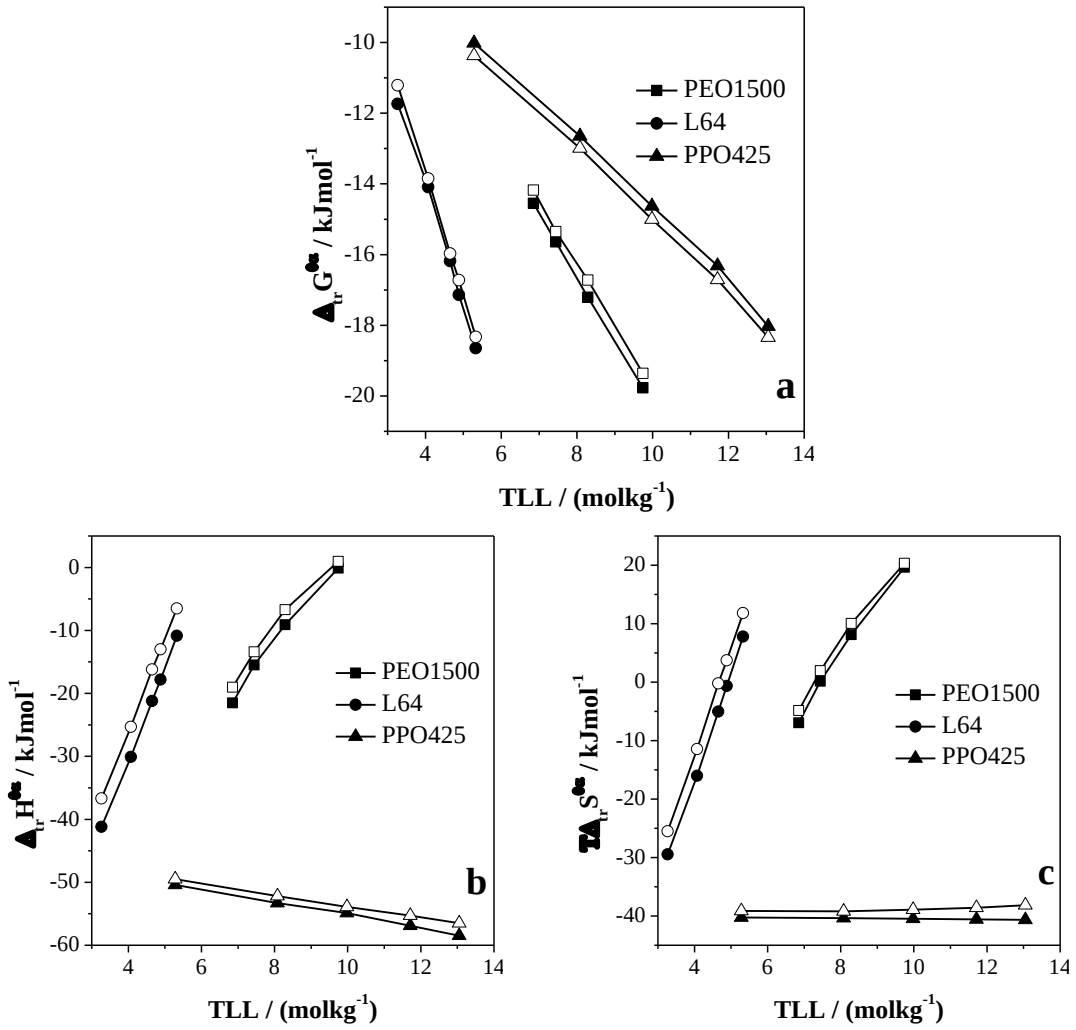

Figure 27. (a) $\Delta_{tr}G^{\theta,\infty}_{PhM}$ (b) $\Delta_{tr}H^{\theta,\infty}_{PhM}$ (c) $T\Delta_{tr}S^{\theta,\infty}_{PhM}$ values of MV6B (closed symbols) and MVB (open symbols) as a function of the TLL of ATPS formed by (square symbol) PEO1500 + Na_2SO_4 + H_2O, (round symbol) L64 + Na_2SO_4 + H_2O and (triangular symbol) PPO425 + Na_2SO_4 + H_2O ATPS at 298.15 K.

The results show that independent of the polymer hydrophobicity that form the ATPS, the positive charge in the dye structure does not contribute in the thermodynamics transference parameters. Since, the small difference in the $\Delta_{tr}G^{\theta,\infty}_{PhM}$, $\Delta_{tr}H^{\theta,\infty}_{PhM}$, $T\Delta_{tr}S^{\theta,\infty}_{PhM}$ values are around of experimental error of measurement.

3.2 Effect of the electrolyte nature

The chemical nature of the ATPS components has a strong impact on the thermodynamics properties of this systems influencing the partition process of the solutes[32]. The electrolytes are ionic species commonly used in the formation of different ATPSs, a wide range of electrolytes can be used to form ATPS with different characteristics, so that, an anion or cation simple change, can promote significant changes in the species partition behavior[33]. Therefore, the study of this component in the phenylmethane dyes partitioning process into ATPS was divided into the following effects:

3.2.1 Cation effect in the PhM dyes partition process.

The cation effect on the PhM dye partitioning process will be studied considering the pseudopolycation existence in upper phase of ATPS proposed by da Silva et al[34]. These authors using isothermal titration calorimetry to study the separation between aqueous solutions of PEO and sulfate salts, determining that these interactions as a result of endothermic processes caused by the dehydration of the polymer chain and electrolyte. Therefore, the binding between the cation of the salt and the polymer polar segment releasing the water molecules in a process entropically driven. This cation-polymer binding continues until a saturation point where there is no more entropy increase and phase separation becomes more favorable. Therefore, the interaction between polymer and electrolyte originate a process endothermic, resulting in the entropy increase associated with the release of water molecules giving way to pseudopolication formation of the (cation-polymer interaction) and to the phases separation. Concluding that lithium has a higher capacity to generate positive charge density on the PEO molecular chain than sodium.

In order to study the cation effect in the partition process of different PhM dyes in ATPS, were measured the K_{PhM} values of six PhM dyes in different ATPSs formed by ($MgSO_4$ or Na_2SO_4 or Li_2SO_4) + PEO1500 + H_2O at 298.15 K. The results are show in the Figure 28.

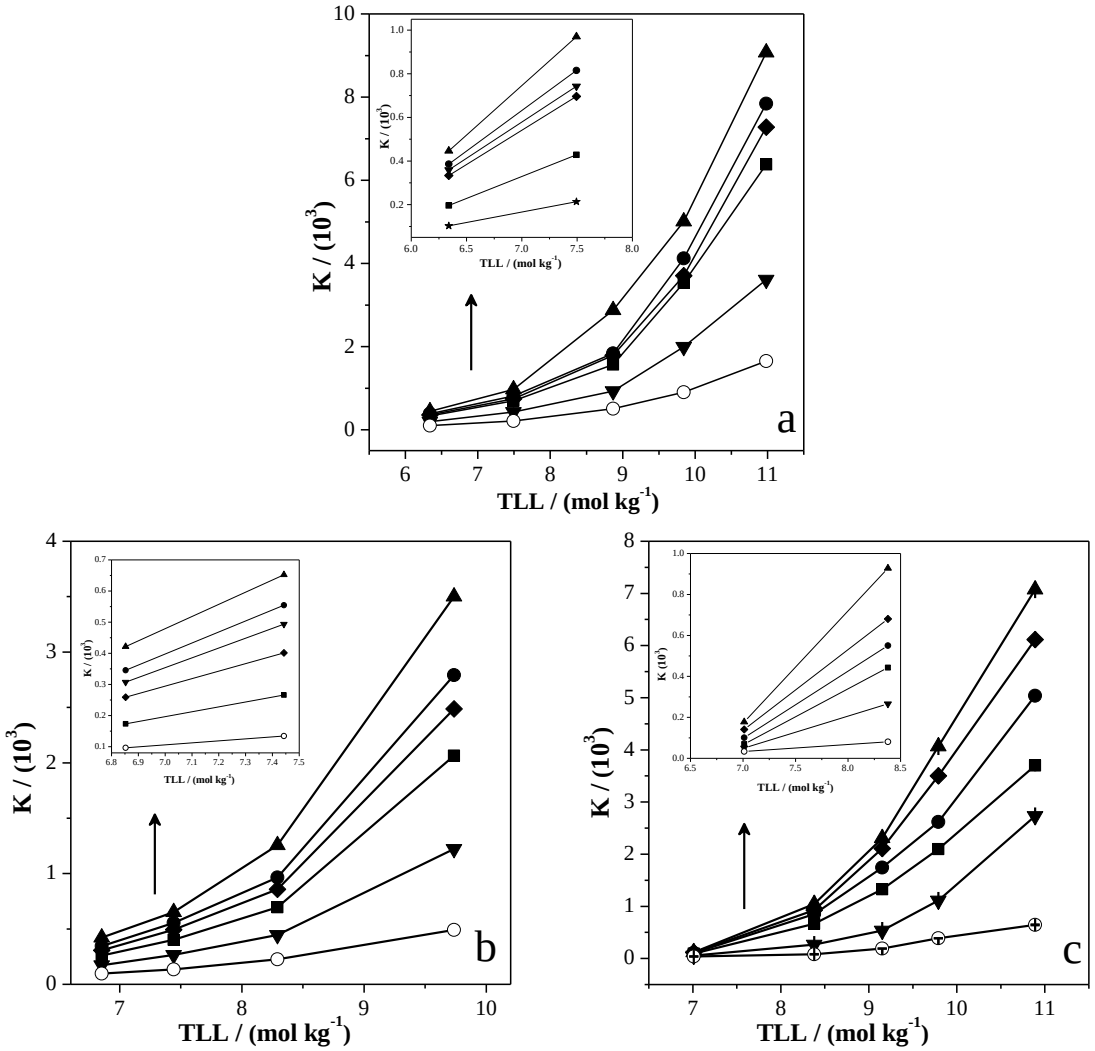

Figure 28. K_{PhM} of MV10B (-▲-), MV6B (-●-), MV2B (-■-), PRA (-▼-) MVB (-♦-), AUR (-○-) as function of the TLL of PEO1500+Li_2SO_4+H_2O (a), PEO1500+Na_2SO_4+H_2O (b) and PEO1500+$MgSO_4$+H_2O (c) ATPS at 298.15 K.

The K_{PhM} values showed that all PhM dyes were concentrated preferably in the ATPS upper phase. Besides, the K_{PhM} values in each dye increase with the cation change in the following order: Li^+ > Na^+ > Mg^{2+}. This suggest that, the

pseudopolycation formed by the Li^+-EO segment has a greater capacity to promote the transfer of PhM dyes from bottom phase to upper phase of the ATPS.

These results are similar to those reported by Alvarenga et al[10]. The authors determined the Remazol Yellow partition coefficient in ATPS formed by different sulfate salts (Li^+, Na^+ and NH_4^+) + PEO1500 + H_2O. Finding that the K values were higher in the Li + presence caused by a better electrostatic interaction between the pseudopolication and the dye molecules. However, the driving forces responsible for this interaction and the dye structure influence on the K values were not elucidated.

In this approach it is observed that, the K_{PhM} values varied with the different modifications in the dye molecular structure. However, for a better discussion of the cation effect on the contribution of the dye structure in the partition process, were the thermodynamic transfer parameters determined. Figures 29 to 40 and Tables 22 to 36 show the corresponding results.

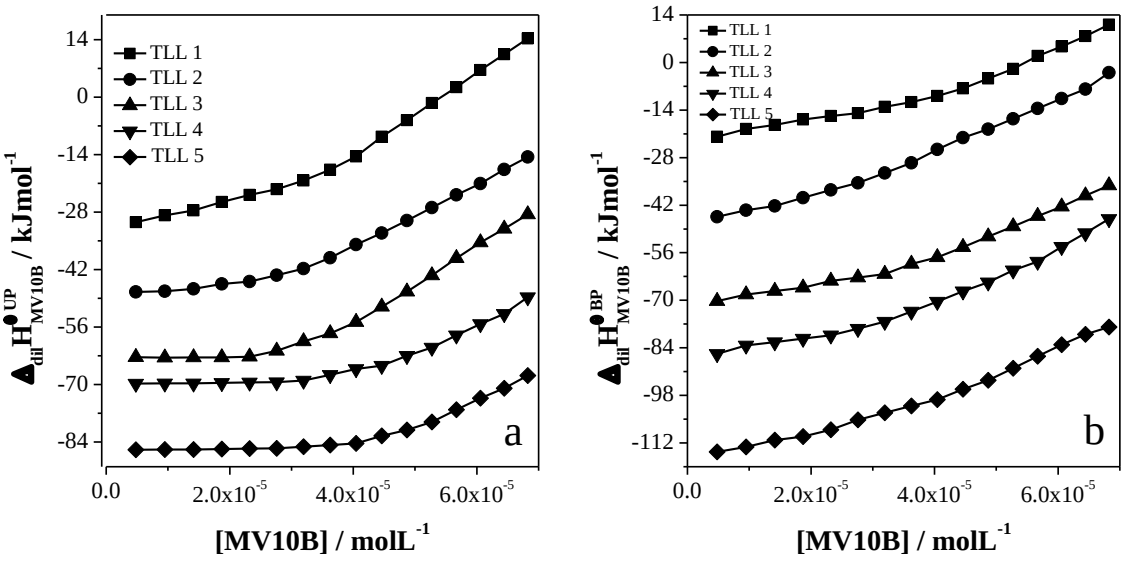

Figure 29. $\Delta_{dil}H^{UP}_{MV10B}$ (a) and $\Delta_{dil}H^{BP}_{MV10B}$ (b) as a functions of dye concentration in upper and bottom phases of PEO1500+Li_2SO_4+H_2O ATPS at 298.15 K.

Table 22. K_{MV10B} values and $\Delta_{dil}H^{\infty}_{MV10B}$ values in upper (UP) and bottom (BP) phases, for the TLL of PEO1500 + Li_2SO_4 + H_2O ATPS at 298.15 K.

TLL	K_{MV10B}	$\Delta_{dil}H^{\infty UP}_{MV10B}$	$\Delta_{dil}H^{\infty BP}_{MV10B}$
mol kg^{-1}		kJ mol^{-1}	
6.34	446.29±0.05	-33.34±0.05	-23.22±0.08
7.49	969.87±0.08	-48.01±0.01	-46.71±0.10
8.87	2877.71±0.11	-63.02±0.01	-71.72±0.04
9.84	5007.23±0.03	-70.20±0.08	-87.41±0.01
10.98	9072.08±0.04	-86.31±0.10	-115.25±0.03

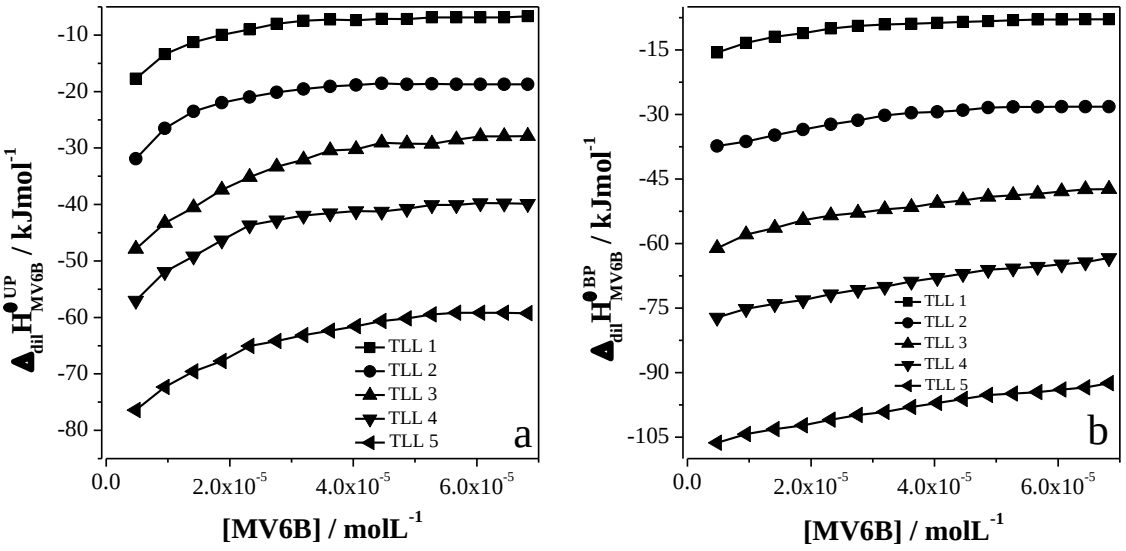

Figure 30. $\Delta_{dil}H^{UP}_{MV6B}$ (a) and $\Delta_{dil}H^{BP}_{MV6B}$ (b) as functions of dye concentration in upper and bottom phases of PEO1500 + Li_2SO_4 + H_2O ATPS at 298.15 K.

Table 23. K_{MV6B} values and $\Delta_{dil}H^{\infty}_{MV6B}$ values in upper (UP) and bottom (BP) phases, for the TLL of PEO1500 + Li_2SO_4 + H_2O ATPS at 298.15 K.

TLL	K_{MV6B}	$\Delta_{dil}H^{\infty UP}_{MV6B}$	$\Delta_{dil}H^{\infty BP}_{MV6B}$
mol kg^{-1}		kJ mol^{-1}	
6.34	385.82±0.09	-26.23±0.09	-18.03±0.07
7.49	815.11±0.10	-39.96±0.02	-39.56±0.03
8.87	1837.15±0.12	-52.51±0.03	-62.41±0.01
9.84	4123.98±0.08	-60.09±0.11	-78.44±0.06
10.98	7843.29±0.13	-77.25±0.07	-107.58±0.05

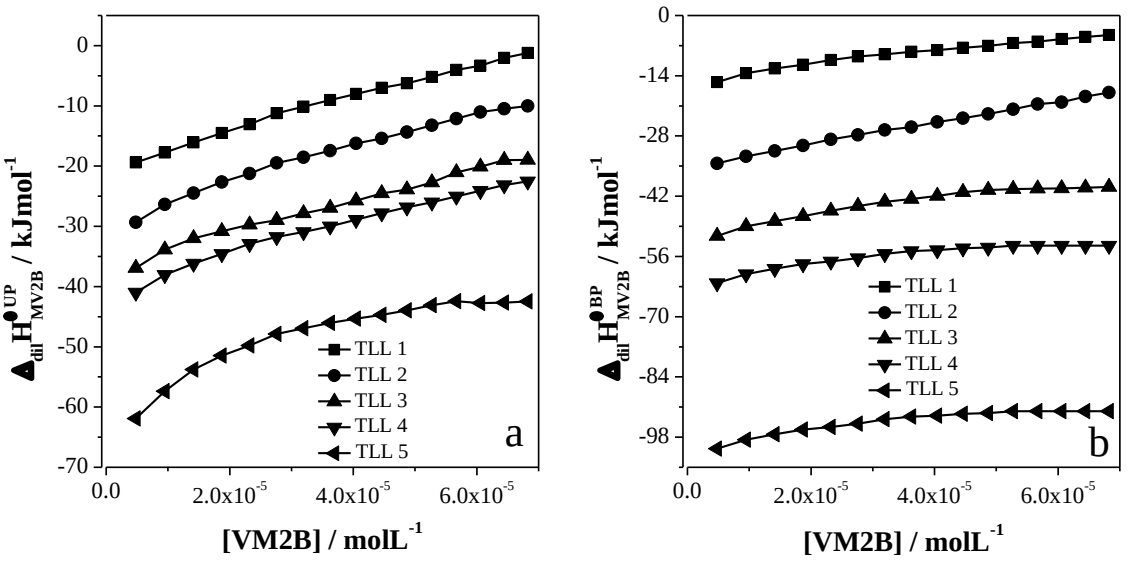

Figure 31. $\Delta_{dil}H^{UP}_{MV2B}$ (a) and $\Delta_{dil}H^{BP}_{MV2B}$ (b) as a functions of dye concentration in upper and bottom phases of PEO1500 + Li_2SO_4 + H_2O ATPS at 298.15 K.

Table 24. K_{MV2B} values and $\Delta_{dil}H^{\infty}_{MV2B}$ values in upper (UP) and bottom (BP) phases, for the TLL of PEO1500 + Li_2SO_4 + H_2O ATPS at 298.15 K.

TLL	K_{MV2B}	$\Delta_{dil}H^{\infty UP}_{MV2B}$	$\Delta_{dil}H^{\infty BP}_{MV2B}$
mol kg^{-1}		kJ mol^{-1}	
6.34	333.56±0.15	-22.38±0.01	-15.98±0.03
7.49	696.21±0.04	-33.58±0.05	-35.46±0.01
8.87	1569.15±0.03	-41.47±0.06	-52.77±0.08
9.84	3536.66±0.16	-44.12±0.02	-63.32±0.04
10.98	6381.89±0.20	-69.06±0.07	-101.80±0.01

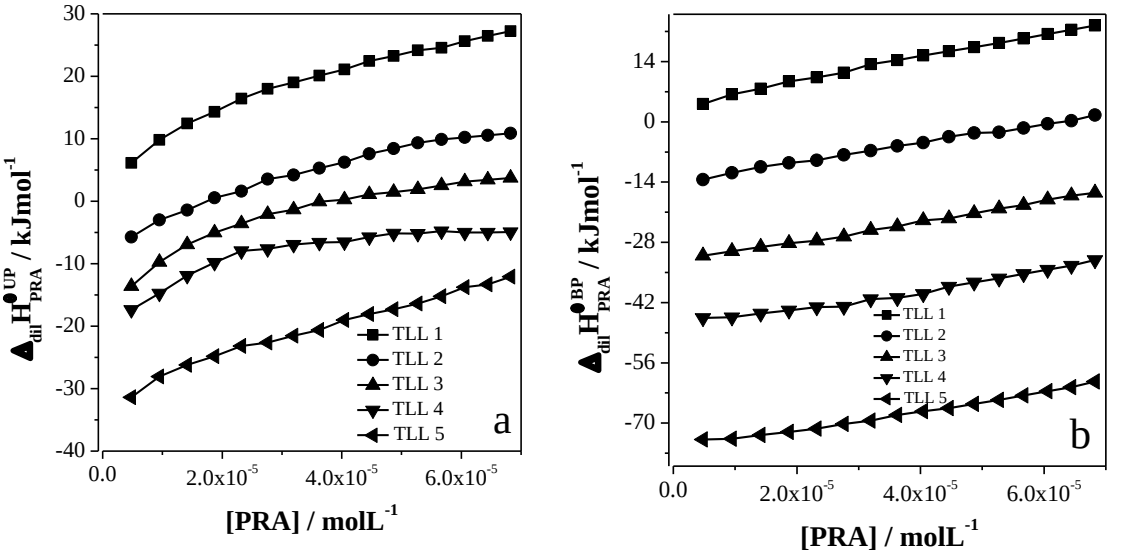

Figure 32. $\Delta_{dil}H^{UP}_{PRA}$ (a) and $\Delta_{dil}H^{BP}_{PRA}$ (b) as a functions of dye concentration in upper and bottom phases of PEO1500 + Li_2SO_4 + H_2O ATPS at 298.15 K.

Table 25. K_{PRA} values and $\Delta_{dil}H^{\infty}_{PRA}$ values in upper (UP) and bottom (BP) phases, for the TLL of PEO1500 + Li_2SO_4 + H_2O ATPS at 298.15 K.

TLL	K_{PRA}	$\Delta_{dil}H^{\infty UP}_{PRA}$	$\Delta_{dil}H^{\infty BP}_{PRA}$
mol kg^{-1}		kJ mol^{-1}	
6.34	196.41±0.03	-1.73±0.08	3.07±0.07
7.49	428.58±0.02	-11.09±0.01	-14.29±0.05
8.87	927.69±0.11	-19.53±0.10	-32.03±0.18
9.84	2996.42±0.13	-21.96±0.03	-45.66±0.02
10.98	3608.88±0.16	-36.07±0.04	-73.90±0.07

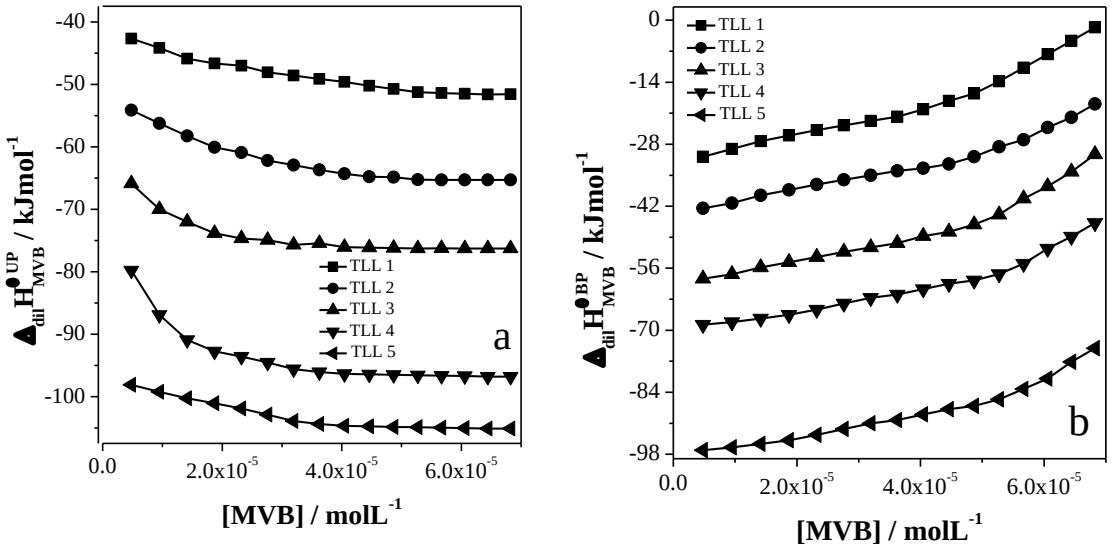

Figure 33. $\Delta_{dil}H^{UP}_{MVB}$ (a) and $\Delta_{dil}H^{BP}_{MVB}$ (b) as functions of dye concentration in upper and bottom phases of PEO1500 + Li_2SO_4 + H_2O ATPS at 298.15 K.

Table 26. K_{MVB} values and $\Delta_{dil}H^{\infty}_{MVB}$ values in upper (UP) and bottom (BP) phases, for the TLL of PEO1500 + Li_2SO_4 + H_2O ATPS at 298.15 K.

TLL	K_{MVB}	$\Delta_{dil}H^{\infty UP}_{MVB}$	$\Delta_{dil}H^{\infty BP}_{MVB}$
mol kg^{-1}		kJ mol^{-1}	
6.34	319.41±0.03	-40.28±0.02	-32.68±0.01
7.49	742.82±0.02	-44.00±0.12	-44.10±0.05
8.87	1887.99±0.11	-49.23±0.06	-59.73±0.01
9.84	3705.75±0.13	-50.91±0.07	-70.25±0.03
10.98	8276.97±0.16	-96.82±0.14	-128.57±0.08

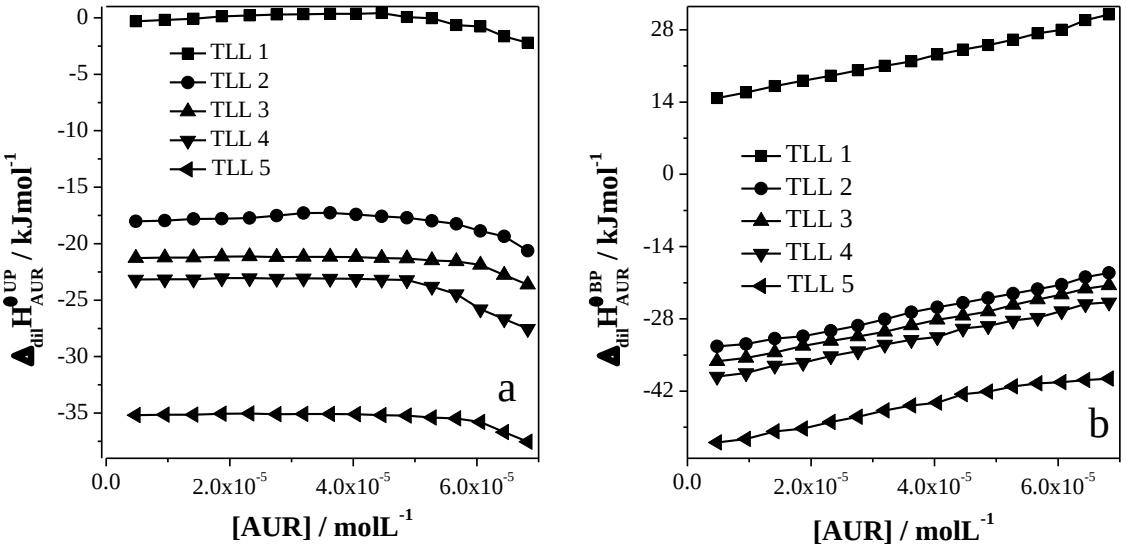

Figure 34. $\Delta_{dil}H^{UP}_{AUR}$ (a) and $\Delta_{dil}H^{BP}_{AUR}$ (b) as functions of dye concentration in upper and bottom phases of PEO1500 + Li_2SO_4 + H_2O ATPS at 298.15 K.

Table 27. K_{AUR} values and $\Delta_{dil}H^{\infty}_{AUR}$ values in upper (UP) and bottom (BP) phases, for the TLL of PEO1500 + Li_2SO_4 + H_2O ATPS at 298.15 K.

TLL	K_{AUR}	$\Delta_{dil}H^{\infty UP}_{AUR}$	$\Delta_{dil}H^{\infty BP}_{AUR}$
mol kg^{-1}		kJ mol^{-1}	
6.34	102.69±0.12	-1.12±0.05	14.07±0.03
7.49	213.29±0.09	-18.87±0.03	-34.57±0.01
8.87	508.20±0.15	-21.82±0.01	-38.12±0.08
9.84	901.70±0.11	-22.89±0.04	-39.79±0.09
10.98	1652.44±0.21	-36.13±0.06	-53.53±0.09

Table 28. Thermodynamic transfer parameters of PhM dyes as a function of the TLL of PEO1500 + Li_2SO_4 + H_2O ATPS at 298.15 K.

PhM dyes	$\Delta_{tr}G^{\theta,\infty}_{PhM}$	$\Delta_{tr}H^{\theta,\infty}_{PhM}$	$T\Delta_{tr}S^{\theta,\infty}_{PhM}$
	kJ mol^{-1}		
TLL 1 / 6.34 mol kg^{-1}			
MV10B	-15.11±0.04	-10.12±0.06	4.99±0.02
MV6B	-14.75±0.10	-8.20±0.01	6.55±0.05
MV2B	-14.39±0.11	-6.40±0.04	7.99±0.01
PRA	-13.08±0.05	-4.80±0.03	8.28±0.06
MVB	-14.28±0.01	-7.60±0.05	6.68±0.03
AUR	-11.47±0.07	-15.19±0.03	-3.72±0.09
TLL 2 / 7.49 mol kg^{-1}			
MV10B	-17.03±0.02	-1.30±0.01	15.73±0.03
MV6B	-16.60±0.05	-0.40±0.04	16.20±0.01
MV2B	-16.21±0.09	1.88±0.01	18.09±0.10
PRA	-15.01±0.06	3.20±0.03	18.21±0.03
MVB	-16.37±0.09	0.11±0.05	16.47±0.04
AUR	-13.28±0.07	15.70±0.06	28.98±0.01

TLL 3 / 8.87 mol kg^{-1}			
MV10B	-19.72±0.04	8.70±0.09	28.42±0.05
MV6B	-18.61±0.01	9.90±0.07	28.51±0.06
MV2B	-18.22±0.03	11.30±0.02	29.52±0.05
PRA	-16.92±0.01	12.50±0.05	29.42±0.04
MVB	-18.68±0.05	10.50±0.06	29.18±0.01
AUR	-15.30±0.05	16.30±0.07	31.73±0.02
TLL 4 / 9.84 mol kg^{-1}			
MV10B	-21.10±0.05	17.21±0.01	38.31±0.04
MV6B	-20.61±0.03	18.35±0.06	38.96±0.03
MV2B	-20.23±0.01	19.20±0.05	39.43±0.04
PRA	-19.82±0.03	23.70±0.06	43.52±0.03
MVB	-20.35±0.02	19.34±0.07	39.69±0.05
AUR	-16.85±0.06	16.90±0.10	33.75±0.04
TLL 5 / 10.98 mol kg^{-1}			
MV10B	-22.57±0.01	28.94±0.03	51.51±0.02
MV6B	-22.21±0.09	30.33±0.01	52.54±0.10
MV2B	-21.70±0.02	32.74±0.09	54.44±0.07
PRA	-20.28±0.05	37.83±0.02	58.11±0.07
MVB	-22.34±0.10	31.75±0.11	54.09±0.01
AUR	-18.35±0.04	17.40±0.08	35.75±0.04

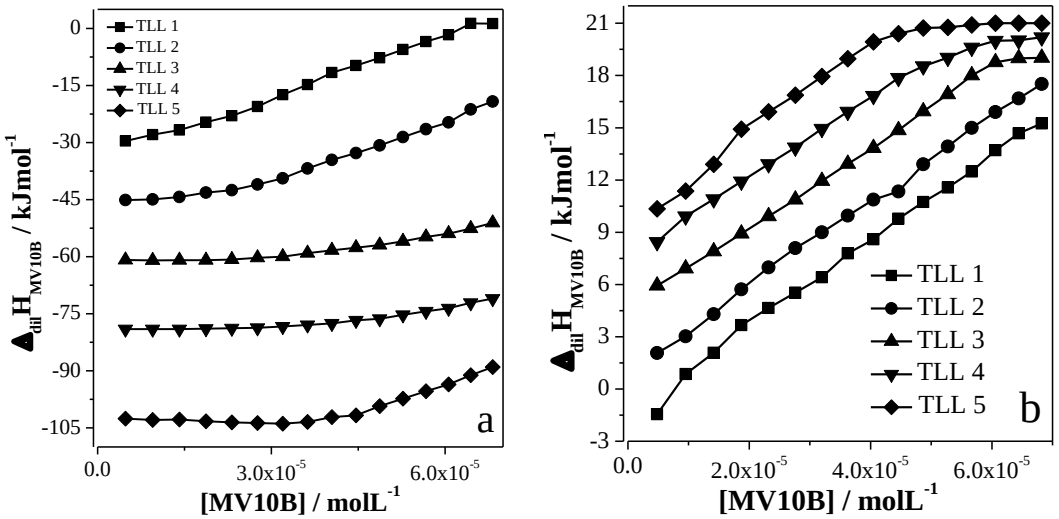

Figure 35. $\Delta_{dil}H^{UP}_{MV10B}$ (a) and $\Delta_{dil}H^{BP}_{MV10B}$ (b) as a functions of dye concentration in upper and bottom phases of PEO1500+$MgSO_4$+H_2O ATPS at 298.15 K.

Table 29. K_{MV10B} values and $\Delta_{dil}H^{\infty}_{MV10B}$ values in upper (UP) and bottom (BP) phases, for the TLL of PEO1500 + $MgSO_4$ + H_2O ATPS at 298.15 K.

TLL	K_{MV10B}	$\Delta_{dil}H^{\infty UP}_{MV10B}$	$\Delta_{dil}H^{\infty BP}_{MV10B}$
mol kg^{-1}		kJ mol^{-1}	
5.270	119.93±0.02	-32.90±0.02	-2.19±0.03
8.056	1045.71±0.02	-46.18±0.07	0.79±0.02
9.949	2305.89±0.09	-60.60±0.15	4.48±0.13
11.67	4267.08±0.07	-78.41±0.13	6.81±0.17
12.99	6473.59±0.18	-101.28±0.17	7.88±0.15

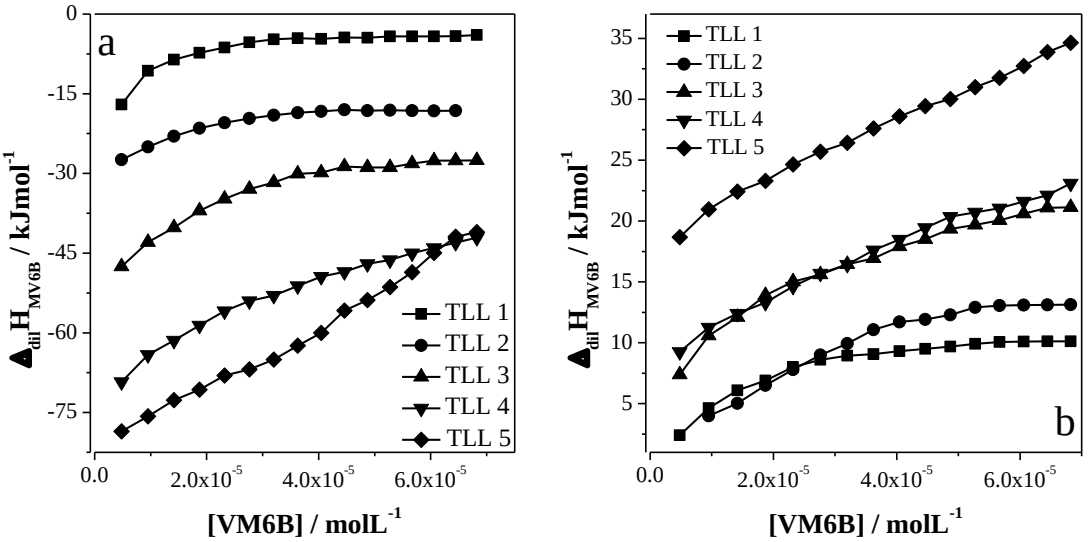

Figure 36. $\Delta_{dil}H^{UP}_{MV6B}$ (a) and $\Delta_{dil}H^{BP}_{MV6B}$ (b) as a functions of dye concentration in upper and bottom phases of PEO1500+$MgSO_4$+H_2O ATPS at 298.15 K.

Table 30 K_{MV6B} values $\Delta_{dil}H_{MV6B}$ values in upper (UP) and bottom (BP) phases, for the TLL of PEO1500 + $MgSO_4$ + H_2O ATPS at 298.15 K.

TLL	K_{MV6B}	$\Delta_{dil}H^{\infty UP}_{MV6B}$	$\Delta_{dil}H^{\infty BP}_{MV6B}$
mol kg^{-1}		kJ mol^{-1}	
5.270	105.61±0.07	-25.50±0.01	-0.003±0.01
8.056	550.39±0.14	-37.60±0.09	1.77±0.05
9.949	1442.01±0.16	-49.80±0.27	6.10±0.06
11.669	3119.05±0.18	-68.10±0.03	8.01±0.04
12.987	5000.02±0.05	-82.30±2.00	17.2±0.05

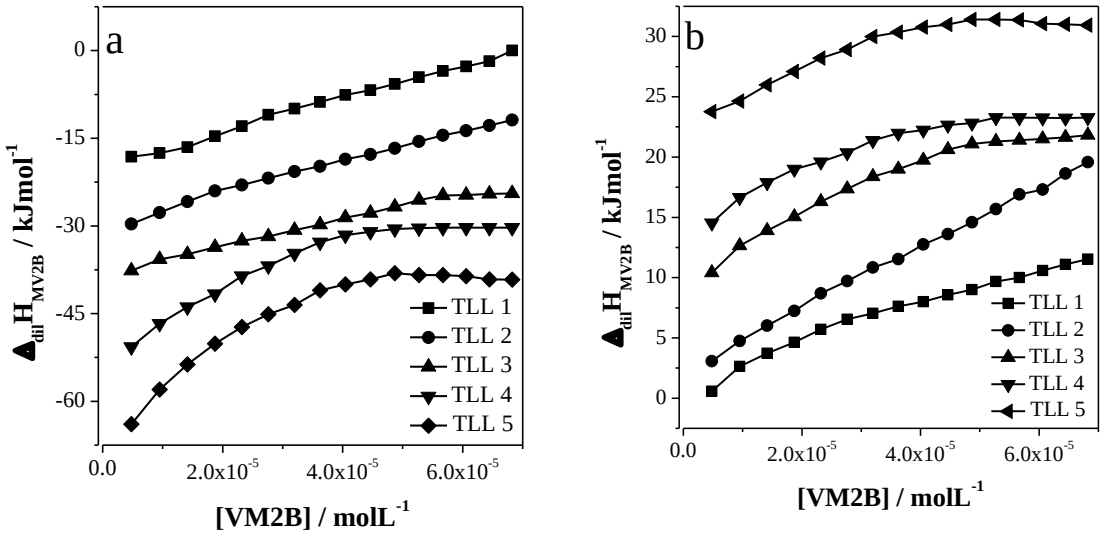

Figure 37. $\Delta_{dil}H^{UP}_{MV2B}$ (a) and $\Delta_{dil}H^{BP}_{MV2B}$ (b) as a functions of dye concentration in upper and bottom phases of PEO1500+$MgSO_4$+H_2O ATPS at 298.15 K.

Table 31 K_{MV2B} values and $\Delta_{dil}H^{\infty}_{MV2B}$ values in upper (UP) and bottom (BP) phases, for the TLL of PEO1500 + $MgSO_4$ + H_2O ATPS at 298.15 K.

TLL	K_{MV2B}	$\Delta_{dil}H^{\infty UP}_{MV2B}$	$\Delta_{dil}H^{\infty BP}_{MV2B}$
mol kg^{-1}		kJ mol^{-1}	kJ mol^{-1}
5.270	94.21±0.02	-20.39±0.13	0.08±0.11
8.056	442.93±0.08	-30.71±0.10	2.01±0.12
9.949	1194.01±1.09	-39.08±0.02	8.89±0.06
11.669	2995.08±1.07	-54.56±0.12	13.4±0.15
12.987	4097.04±0.10	-67.87±0.27	21.7±0.13

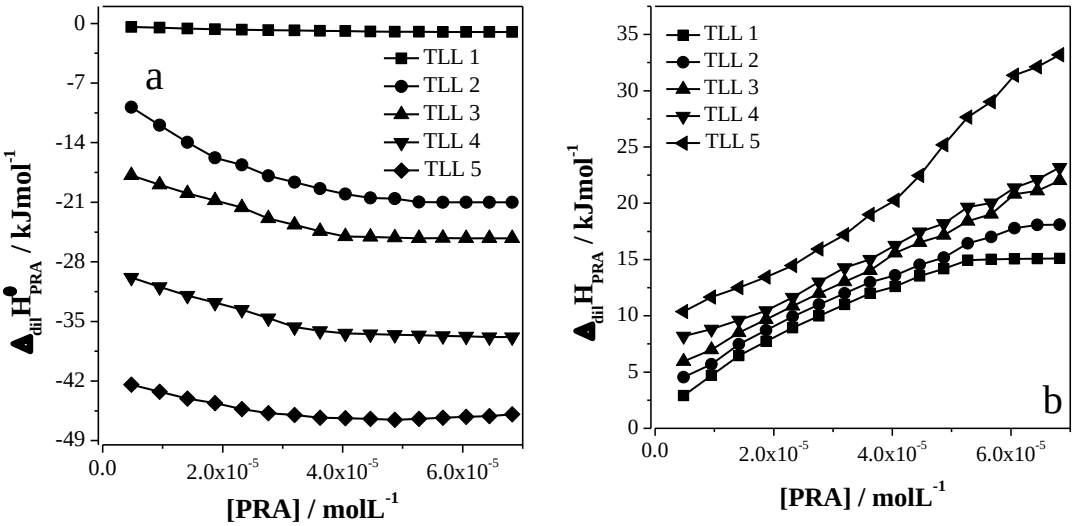

Figure 38. $\Delta_{dil}H^{UP}_{PRA}$ (a) and $\Delta_{dil}H^{BP}_{PRA}$ (b) as a functions of dye concentration in upper and bottom phases of PEO1500+$MgSO_4$+H_2O ATPS at 298.15 K.

Table 33. K_{PRA} values and $\Delta_{dil}H^{\infty}_{PRA}$ values in upper (UP) and bottom (BP) phases, for the TLL of PEO1500 + $MgSO_4$ + H_2O ATPS at 298.15 K.

TLL	K_{PRA}	$\Delta_{dil}H^{\infty UP}_{PRA}$	$\Delta_{dil}H^{\infty BP}_{PRA}$
mol kg^{-1}		kJ mol^{-1}	
5.270	54.55±1.01	-0.32±0.01	1.07±0.01
8.056	265.70±0.03	-30.67±0.08	2.91±0.01
9.949	535.64±0.16	-16.01±0.04	4.60±0.04
11.669	1110.02±0.09	-28.53±0.07	6.71±0.05
12.987	1900.04±0.13	-41.45±0.03	9.36±0.07

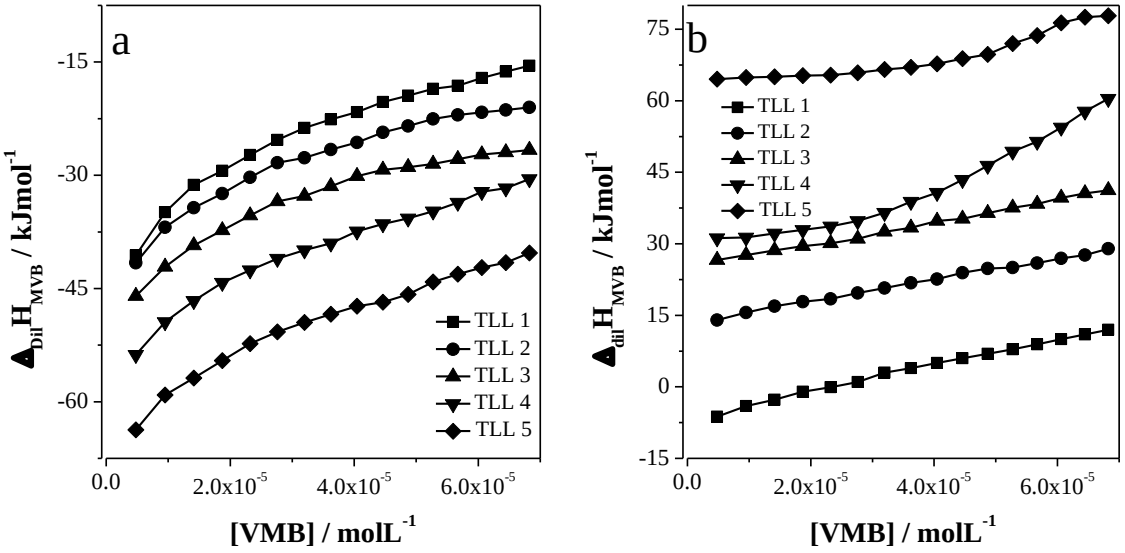

Figure 39. $\Delta_{dil}H^{UP}_{MVB}$ (a) and $\Delta_{dil}H^{BP}_{MVB}$ (b) as a functions of dye concentration in upper and bottom phases of PEO1500+$MgSO_4$+H_2O ATPS at 298.15 K.

Table 34. K_{MVB} values and $\Delta_{dil}H^{\infty}_{MVB}$ values in upper (UP) and bottom (BP) phases, for the TLL of PEO1500 + $MgSO_4$ + H_2O ATPS at 298.15 K.

TLL	K_{MVB}	$\Delta_{dil}H^{\infty UP}_{MVB}$	$\Delta_{dil}H^{\infty BP}_{MVB}$
mol kg^{-1}		kJ mol^{-1}	
5.270	113.61±0.07	-41.76±0.01	-7.31±0.05
8.056	927.91±1.01	-43.19±0.04	13.02±0.07
9.949	2109.29±0.04	-47.82±0.01	25.69±0.03
11.669	3703.68±0.05	-55.59±0.06	31.11±0.01
12.987	6115.22±0.19	-64.63±0.09	65.08±0.08

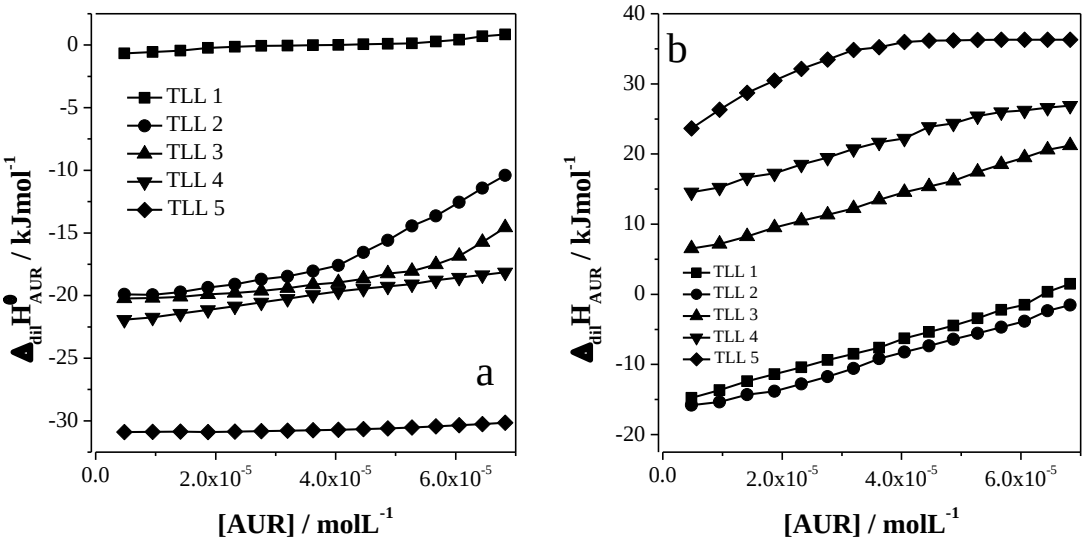

Figure 40. $\Delta_{dil}H^{UP}_{AUR}$ (a) and $\Delta_{dil}H^{BP}_{AUR}$ (b) as a functions of dye concentration in upper and bottom phases of PEO1500+$MgSO_4$+H_2O ATPS at 298.15 K.

Table 35. K_{AUR} values and $\Delta_{dil}H^{\infty}_{AUR}$ values in upper (UP) and bottom (BP) phases, for the TLL of PEO1500 + $MgSO_4$ + H_2O ATPS at 298.15 K.

TLL	K_{AUR}	$\Delta_{dil}H^{\infty UP}_{AUR}$	$\Delta_{dil}H^{\infty BP}_{AUR}$
mol kg^{-1}		kJ mol^{-1}	
5.270	39.23±0.16	-1.06±0.04	-15.40±0.03
8.056	81.01±0.07	-19.81±0.07	-17.01±0.06
9.949	189.89±0.04	-20.59±0.02	5.35±0.08
11.669	387.21±0.13	-22.17±0.02	12.89±0.01
12.987	543.92±0.11	-30.75±0.01	21.37±0.04

Table 36. Thermodynamic transfer parameters of PhM dyes as a function of the TLL of PEO1500 + $MgSO_4$ + H_2O ATPS at 298.15 K.

TLL 1 / 5.27 mol kg^{-1}			
PhM dyes	$\Delta_{tr}G^{\theta,\infty}_{PhM}$	$\Delta_{tr}H^{\theta,\infty}_{PhM}$	$T\Delta_{tr}S^{\theta,\infty}_{PhM}$
	kJ mol^{-1}		
MV10B	-11.89±0.01	-30.77±0.01	-18.90±0.02
MV6B	-11.51±0.02	-25.52±0.03	-13.89±0.01
MV2B	-11.18±0.02	-20.49±0.04	-9.23±0.02
PRA	-9.90±0.04	-1.39±0.03	8.50±0.07
MVB	-11.7±0.01	-36.50±0.10	-24.76±0.09
AUR	-9.08±0.05	14.38±0.01	23.50±0.06

TLL 2 / 8.06 mol kg^{-1}			
MV10B	-17.19±0.02	-47.02±0.01	-29.65±0.03
MV6B	-15.60±0.01	-39,27±0.04	-23.77±0.03
MV2B	-15.01±0.03	-32.75±0.09	-17.74±0.06
PRA	-13.79±0.02	-10.91±0.03	2.87±0.01
MVB	-16.86±0.03	-54.26±0.05	-37.40±0.02
AUR	-10.88±0.01	-2.78±0.02	8.10±0.01
TLL 3 / 9.95 mol kg^{-1}			
MV10B	-19.08±0.04	-65.04±0.05	-45.86±0.01
MV6B	-18.01±0.02	-55.93±0.10	-37.40±0.08
MV2B	-17.46±0.01	-48.01±0.08	-30.19±0.07
PRA	-15.50±0.01	-20.67±0.04	-5.12±0.03
MVB	-18.87±0.06	-73.49±0.01	-54.45±0.07
AUR	-12.91±0.03	-16.02±0.04	-3.02±0.01
TLL 4 / 11.67 mol kg^{-1}			
MV10B	-20.71±0.06	-85.22±0.07	-64.52±0.01
MV6B	-20.04±0.03	-76.13±0.07	-56.14±0.04
MV2B	-19.76±0.05	-68.02±0.10	-48.15±0.05
PRA	-17.32±0.02	-35.18±0.08	-17.88±0.06
MVB	-20.29±0.10	-95.69±0.12	-75.39±0.02
AUR	-14.65±0.07	-35.15±0.10	-20.35±0.03
TLL 5 / 12.99 mol kg-1			
MV10B	-21.68±0.01	-109.20±0.04	-87.35±0.03
MV6B	-21.11±0.03	-99.63±0.08	-78.42±0.05
MV2B	-20.57±0.07	-89.71±0.09	-69.04±0.02
PRA	-18.60±0.09	-50.76±0.10	-32.06±0.01
MVB	-21.55±0.04	-120.84±0.03	-99.19±0.07
AUR	-15.59±0.07	-52.24±0.09	-36.57±0.02

The results of the different parameters ($\Delta_{tr}G^{\theta,\infty}_{PhM}$, $\Delta_{tr}H^{\theta,\infty}_{PhM}$ and $T\Delta_{tr}S^{\theta,\infty}_{PhM}$) are discussed considering the following contributions:

3.2.1.1. Contribution of the -CH_3 group

The cation effect on the -CH_3 groups contribution will be discussed for each thermodynamic parameter similarly to Section 3.1.1. Therefore, the calculation of the $\Delta_{tr}G^{\theta,\infty}_{PhM}$ values as a function of the CH_3 groups in the dyes $MV10B_{(6\text{-}CH_3)}$, $MV6B_{(5\text{-}CH_3)}$, $MV2B_{(4\text{-}CH_3)}$, and $PRA_{(0\text{-}CH_3)}$ for ATPS formed by (Li_2SO_4 or Na_2SO_4 or $MgSO_4$) + PEO1500 + H_2O at 298.15 K are shown in Figure 41.

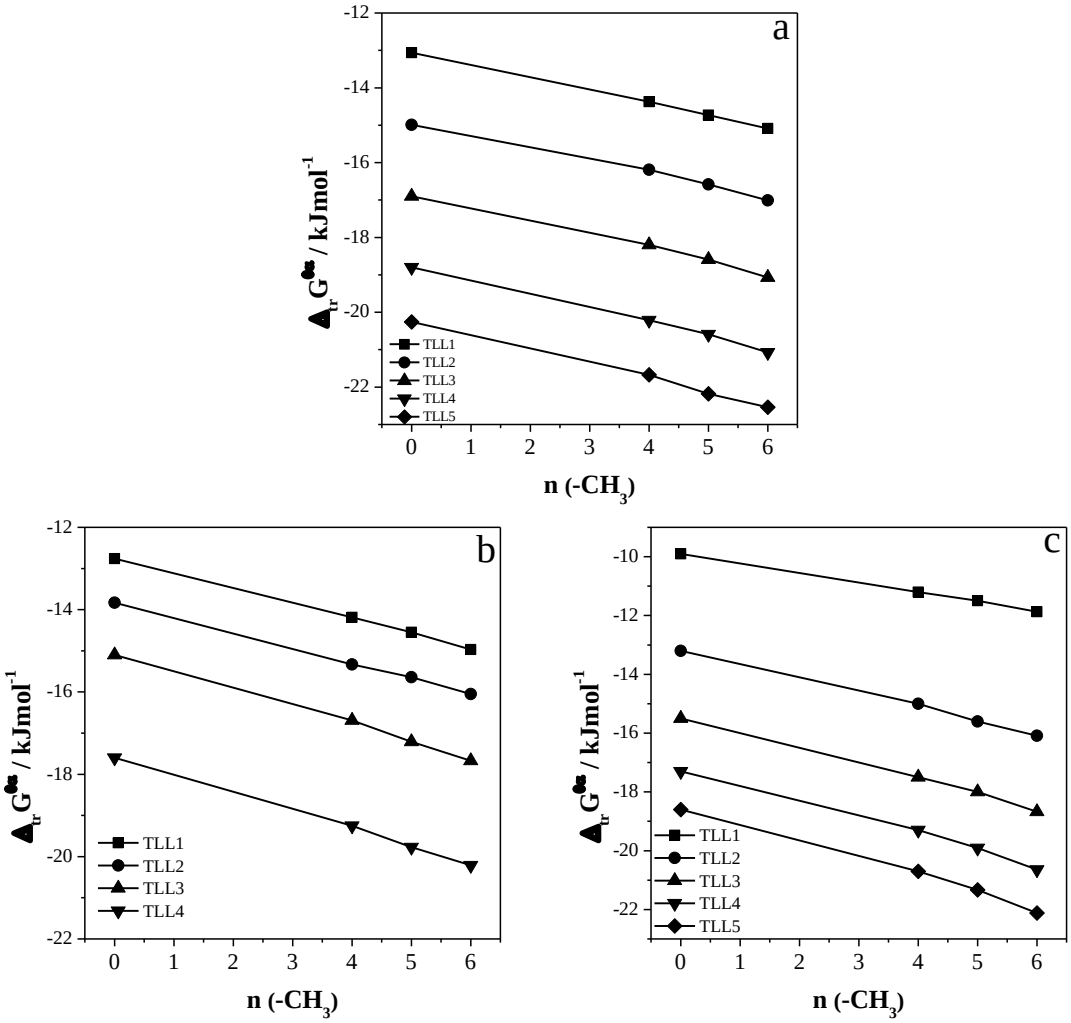

Figure 41. $\Delta_{tr}G^{\theta,\infty}_{CH_3}$ as a function of -CH_3 groups for $MV10B_{(6\text{-}CH3)}$, $MV6B_{(5\text{-}CH3)}$, $MV2B_{(4\text{-}CH3)}$ and $PRA_{(0\text{-}CH3)}$ partitioning in (a) PEO1500 + Li_2SO_4 + H_2O, (b) PEO1500 + Na_2SO_4 + H_2O and (c) PEO1500 + $MgSO_4$ + H_2O ATPS at 298.15 K.

Independent of the ATPS, the PhM dyes transference process from bottom phase to upper phase occurs with a decrease in the $\Delta_{tr}G^{\theta,\infty}_{PhM}$ values. These values become more negatives with the methylation degree increase, indicating that the -CH_3 groups promote the dye transference from bottom phase to upper phase. Besides, the $\Delta_{tr}G^{\theta,\infty}_{PhM}$ values are more negatives when the cation forming the ATPS is changed in the follow order: $Li^+ > Na^+ > Mg^{2+}$. However, to determine the methyl group contribution in the thermodynamic transfer potential for each ATPS, we calculated the average of the slope

linear relationship $\Delta_{tr}G_{PhM}^{\theta,\infty}$ versus n_{CH_3} and the results were: $\frac{\partial \Delta_{tr}G_{CH_3}^{\theta\infty}}{\partial n_{CH_3}}$ = -0.33±0.01, -0.40±0.01 and -0.56±0.03 kJ mol^{-1} for the ATPS formed by Li^+, Na^+ and Mg^{2+} respectively.

Despite, the $\Delta_{tr}G_{PhM}^{\theta,\infty}$ values are more negative in ATPS formed by Li^+, the -CH_3 groups contribution in the standard transference Gibbs free energy change is more favorable in the order Mg^{2+} > Na^+ > Li^+. To elucidate the origin of these results were determinate the methyl groups contribution in the standard transference enthalpy and entropy change at infinite dilution state ($\Delta_{tr}H_{PhM}^{\theta,\infty}$ and $T\Delta_{tr}S_{PhM}^{\theta,\infty}$). The Figures 42 and 43 shows the $\Delta_{tr}H_{PhM;}^{\theta,\infty}$ and $T\Delta_{tr}S_{PhM}^{\theta,\infty}$ values as a function of the CH_3 groups in the dyes $MV10B_{(6\text{-}CH3)}$, $MV6B_{(5\text{-}CH3)}$, $MV2B_{(4\text{-}CH3)}$, and $PRA_{(0\text{-}CH3)}$ for ATPS formed by (Li_2SO_4 or Na_2SO_4 or $MgSO_4$) + PEO1500 + H_2O at 298.15 K.

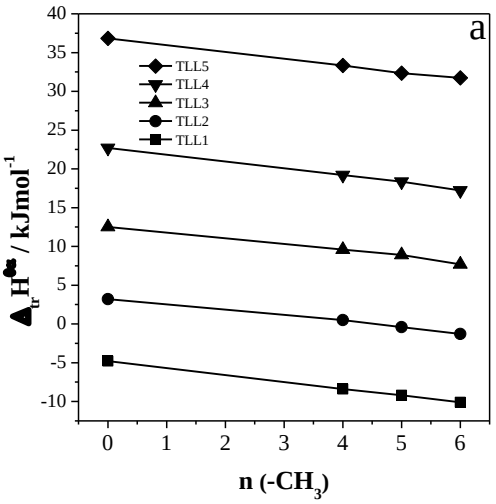

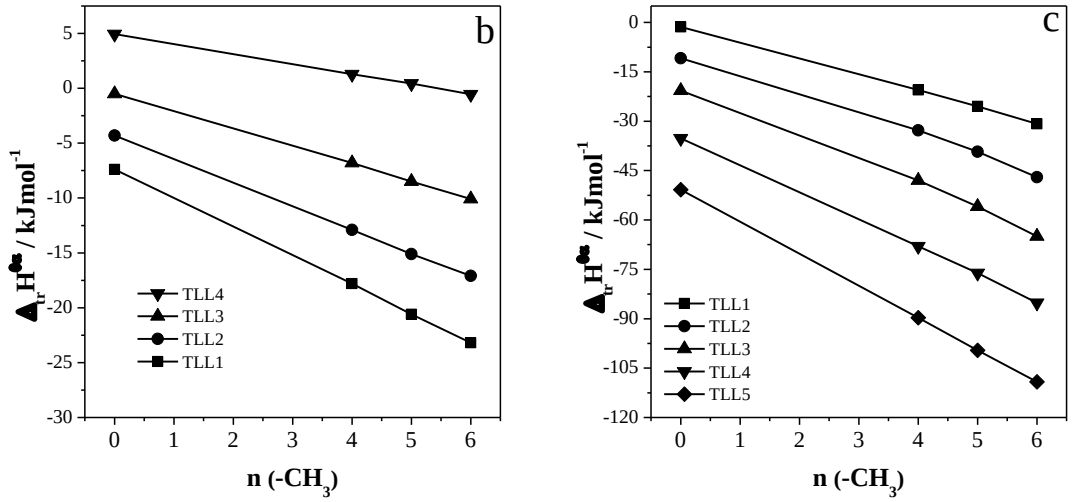

Figure 42. $\Delta_{tr}H^{\theta,\infty}_{CH_3}$ as a function of -CH_3 groups for $MV10B_{(6\text{-}CH3)}$, $MV6B_{(5\text{-}CH3)}$, $MV2B_{(4\text{-}CH3)}$ and $PRA_{(0\text{-}CH3)}$ partitioning in (a) PEO1500 + Li_2SO_4 + H_2O, (b) PEO1500 + Na_2SO_4 + H_2O and (c) PEO1500 + $MgSO_4$ + H_2O ATPS at 298.15 K.

When Li^+ is the cation that forms the ATPS, the PhM dyes transfer from bottom phase to upper phase is carried out with the $\Delta_{tr}H^{\theta,\infty}_{PhM}$ values negative only in the first TLL, become more negatives with the increment of dye methylation degree. Nevertheless, when the TLL increase the $\Delta_{tr}H^{\theta,\infty}_{PhM}$ values are positive and increases proportionally with the TLL increment, but the process is less endothermic when the number -CH_3 group increases. This behavior in the $\Delta_{tr}H^{\theta,\infty}_{PhM}$ values is reduced in the ATPS composed by Na^+, where only the last TLL has positive values. In contrast, in the presence of Mg^{2+} where the dye transfer process is exothermic and the $\Delta_{tr}H^{\theta,\infty}_{PhM}$ values becoming more negative with the TLL increment and the methyl number in the dye structure increasing.

Based on equation 8 and considering that the pseudopolycation corresponds to the UP components this results shows that the $\Delta_{int}H^{\infty}_{PhM-UP}$ interaction occur whit the release of less energy in the order $Li^+ < Na^+ < Mg^{2+}$. This means that a higher charge

density in the Li^+-EO segments pseudopolycation causes a greater electrostatic repulsion to interact with the cationic dye, releasing less energy, making the $\Delta_{tr}H^{\theta,\infty}_{CH_3}$ values positives because of the relationship $|\Delta_{int}H^{\infty}_{BP-BP} + \Delta_{int}H^{\infty}_{PhM-UP}| < |\Delta_{int}H^{\infty}_{PhM-BP} + \Delta_{int}H^{\infty}_{UP-UP}|$. Therefore, this energy increases when the pseudopolycation charge density decrease, investing the previous relationship to obtain $\Delta_{tr}H^{\theta,\infty}_{CH_3}$ values.

To evaluate the -CH_3 group contribution in the $\Delta_{tr}H^{\theta,\infty}_{PhM}$ in each ATPS the relationship slope $\frac{\partial \Delta_{tr}H^{\theta\infty}_{PhM}}{\partial n_{CH_3}}$ was determined. The results were, -0.87±0.01, -1.77±0.01, -2.44±0.06 kJ mol^{-1}, for ATPS formed by Li^+, Na^+ and Mg^{2+} respectively, suggesting that the -CH_3 group contribute more favorable to the $\Delta_{tr}H^{\theta,\infty}_{PhM}$ values in the following order $Mg^{2+} > Na^+ > Li^+$. Indicating that the -CH_3 transfer process is enthalpically driven in the ATPS formed by Mg^{2+} or Na^+.

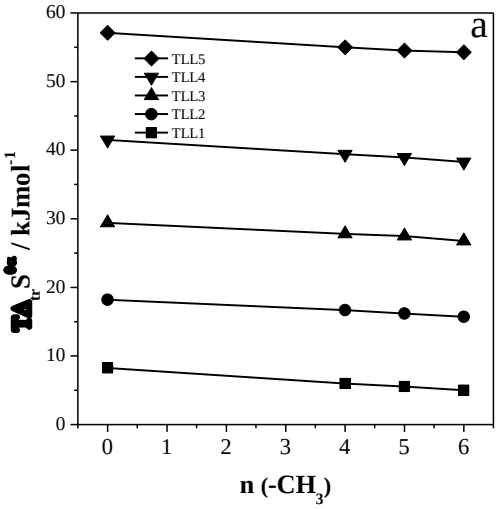

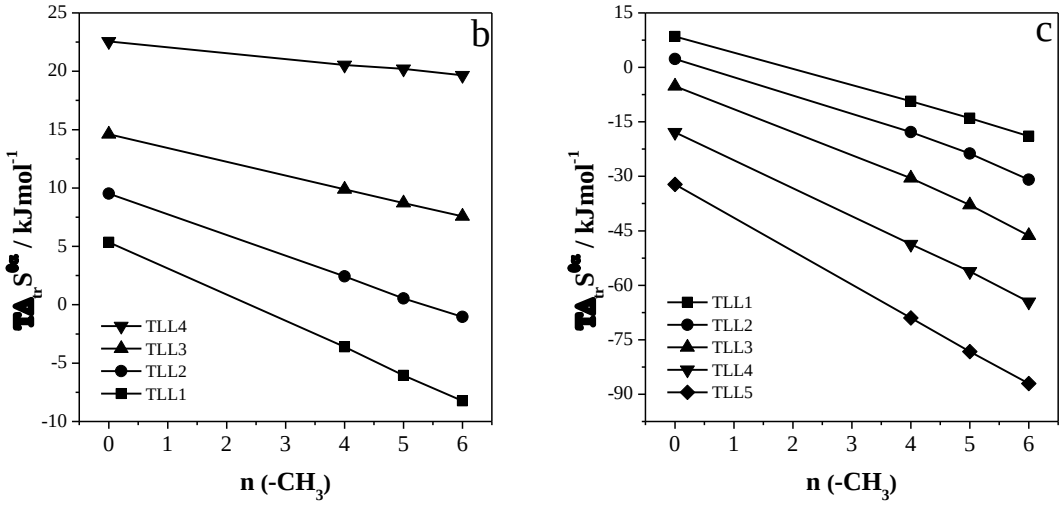

Figure 43. $T\Delta_{tr}S^{\theta,\infty}_{CH_3}$ as a function of -CH_3 groups for $MV10B_{(6\text{-}CH_3)}$, $MV6B_{(5\text{-}CH_3)}$, $MV2B_{(4\text{-}CH_3)}$ and $PRA_{(0\text{-}CH_3)}$ partitioning in (a) PEO1500 + Li_2SO_4 + H_2O, (b) PEO1500 + Na_2SO_4 + H_2O and (c) PEO1500 + $MgSO_4$ + H_2O ATPS at 298.15 K.

In the presence of Li^+ the PhM dyes transfer process occurs with an entropy increment, besides when the TLL increase the $T\Delta_{tr}S^{\theta,\infty}_{PhM}$ values are more positive. However, these values show a small decrease when the methylation degree in the dye structure increase. Similarly, for Na^+ cation presence the $T\Delta_{tr}S^{\theta,\infty}_{PhM}$ values are positive when there are no methyl groups in the dye molecule. When the TLL increase these values are more positive, but, with the methyl groups increment in the dye structure the $T\Delta_{tr}S^{\theta,\infty}_{PhM}$ values decrease becoming are negative in the first TLL.

In ATPS formed by Mg^{2+} and absence of -CH_3 groups the transference process is carried out with $T\Delta_{tr}S^{\theta,\infty}_{PhM}$ values going from positive to negative with the TLL increase. Besides, when the dye structure methylation degree increments, the $T\Delta_{tr}S^{\theta,\infty}_{PhM}$ values become more negative. This results reveals that, the smaller Li^+ ion size allows for less steric hindrance in the pseudopolication-dye interaction. Therefore, more dye molecules take part in this interaction and consequently increase the degree of

configurational freedom of the water molecules that solvated the dye molecules incrementing the system entropy. So that as the size of the cation increases this effect decreases.

The average of the slope linear relationship $T\Delta_{tr}S^{\theta,\infty}_{PhM}$ versus n_{CH_3} allows us to determine the contribution of the methyl group in this parameter. The values of $\frac{\partial[T\Delta_{tr}S^{\theta\infty}_{CH_3}]}{\partial n_{\mathrm{CH_3}}}$ = -0.48±0.03, -1.18±0.01, -8.73±0.07 kJ mol^{-1}, for ATPS formed by Li^+, Na^+ and Mg^{2+} respectively, demonstrating that, the -CH_3 group contribute unfavorably in the $T\Delta_{tr}S^{\theta,\infty}_{CH_3}$ values in the order $Li^+ > Na^+ > Mg^{2+}$.

3.2.1.2 Contribution of the phenyl group

In order to study the contribution of the benzene ring in the dye structure in the motriz forces that govern the partition process and the dependence of this contribution with the cation that forming the ATPS. The Figure 44 show the parameters $\Delta_{tr}G^{\theta,\infty}_{PhM}$, $\Delta_{tr}H^{\theta,\infty}_{PhM}$ and $T\Delta_{tr}S^{\theta,\infty}_{PhM}$ of AUR (DPhM) and MV2B (TPhM) in PEO1500 + Li_2SO_4 + H_2O; PEO1500 + Na_2SO_4 + H_2O and PEO1500 + $MgSO_4$ + H_2O ATPS at 298.15 K.

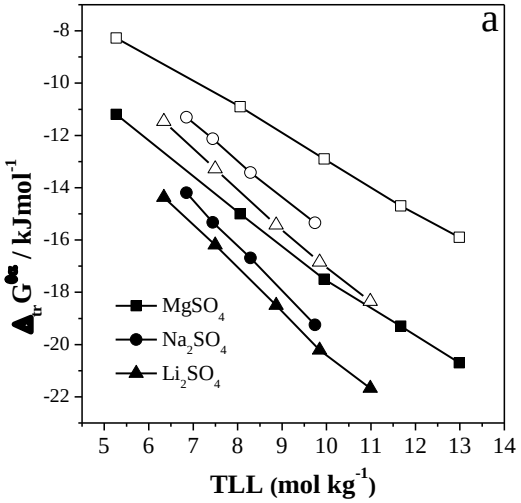

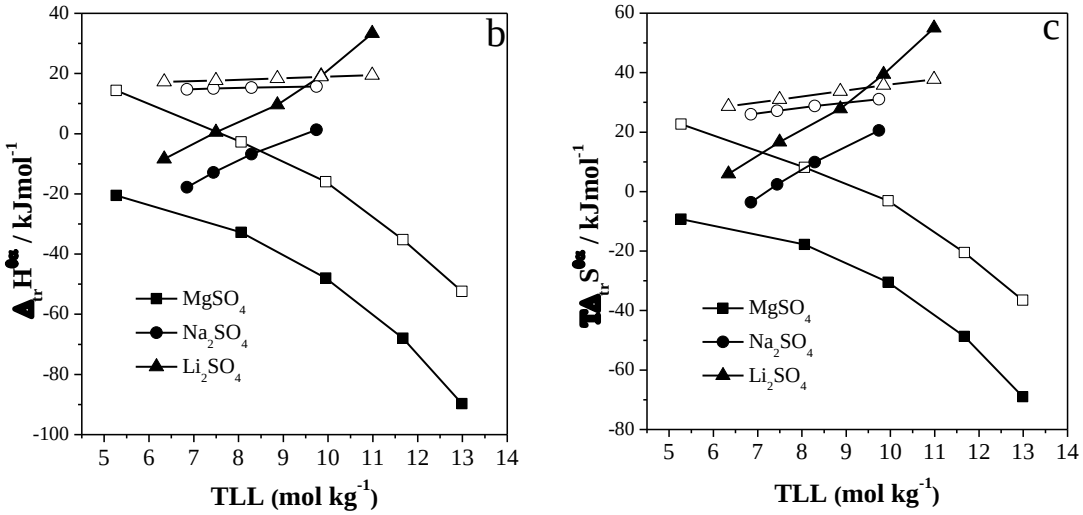

Figure 44. (a) $\Delta_{tr}G^{\theta,\infty}_{PhM}$ (b) $\Delta_{tr}H^{\theta,\infty}_{PhM}$ and (c) $T\Delta_{tr}S^{\theta,\infty}_{PhM}$ values of MV2B (closed symbols) and AUR (open symbols) as a function of the TLL of PEO1500 + $MgSO_4$ + H_2O (square symbol), PEO1500 + Na_2SO_4 + H_2O (round symbol) and PEO1500 + Li_2SO_4 + H_2O (Triangular symbol) ATPS at 298.15 K.

Independent of the ATPS the both molecules transfer process is generated with a decrease in the Gibbs free energy. The $\Delta_{tr}G^{\theta,\infty}_{PhM}$ values become more negative depending on the cation in the following order $Li^+ > Na^+ > Mg^{2+}$. This show that Independent of the dye molecular structure, Li^+ cation promotes greater dye transfer for the system upper phase. On the other hand, the $\Delta_{tr}G^{\theta,\infty}_{PhM}$ of TPhM dye was more negative than that DPhM dye in all ATPS studied, becoming more negative with the TLL increase.

Nevertheless, to better understand this difference caused by the phenyl group in the dye structure, we calculate the difference in the values of $\Delta\Delta_{tr}G^{\theta,\infty}_{MV2B-AUR} = \Delta_{tr}G^{\theta,\infty}_{MV2B} - \Delta_{tr}G^{\theta,\infty}_{AUR}$. The Figure 45a shows the results of the $\Delta\Delta_{tr}G^{\theta,\infty}_{MV2B-AUR}$ values as a function of the TLL of the studied ATPS.

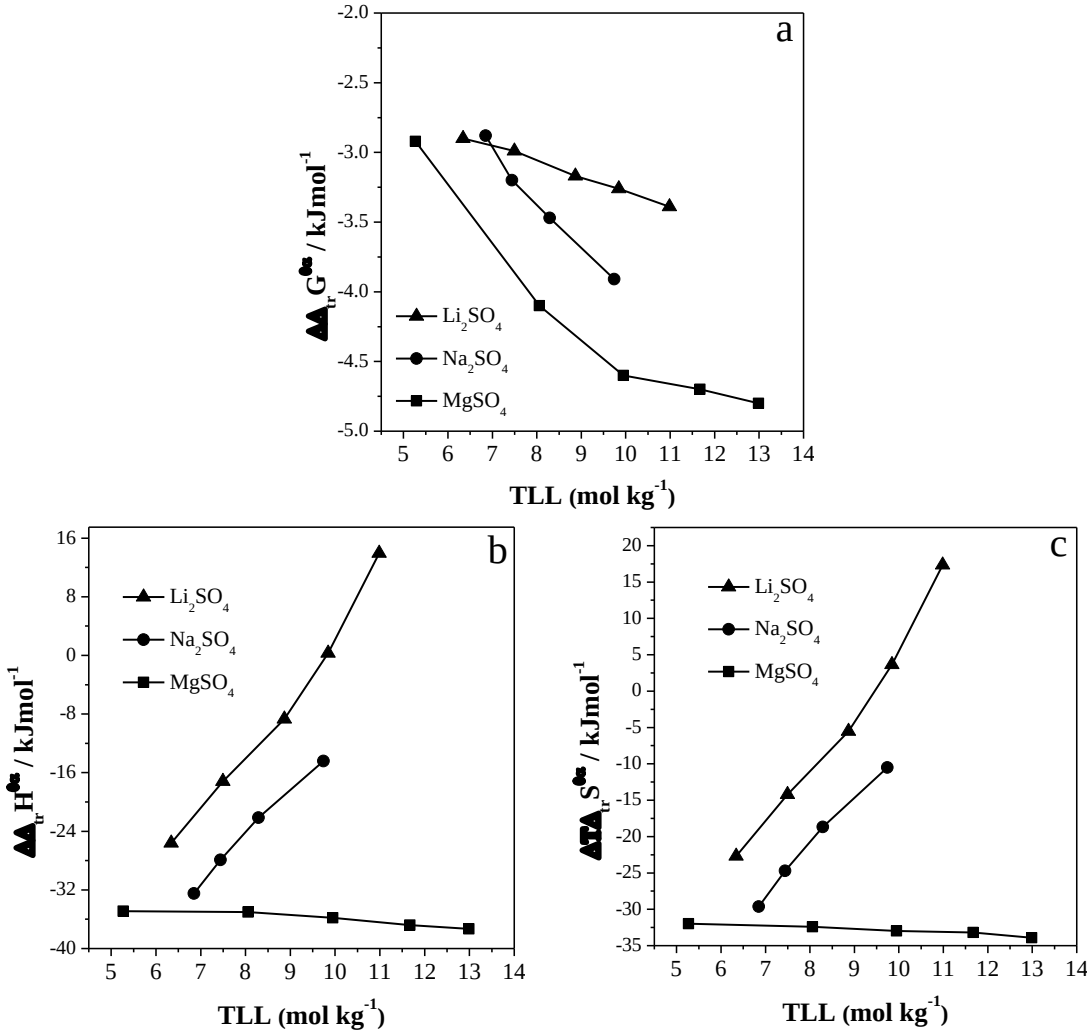

Figure 45. (a) $\Delta\Delta_{tr}G^{\theta,\infty}_{PhM}$ (b) $\Delta\Delta_{tr}H^{\theta,\infty}_{PhM}$ and (c) $\Delta T\Delta_{tr}S^{\theta,\infty}_{PhM}$ values as function of the TLL of PEO1500 + $MgSO_4$ + H_2O (square symbol), PEO1500 + Na_2SO_4 + H_2O (round symbol) and PEO1500 + Li_2SO_4 + H_2O (Triangular symbol) ATPSs at 298.15

The $\Delta\Delta_{tr}G^{\theta,\infty}_{MV2B-AUR}$ values are more negatives for the ATPS formed by Mg^{2+} then by Na^+ and last Li^+, indicating that the phenyl group has a more favorable contribution in the standard transfer Gibbs free energy change in the ATPS formed by $Mg^{2+} > Na^+ > Li^+$. To understand the origin of this contribution were studied the values of $\Delta_{tr}H^{\theta,\infty}_{PhM}$ and $T\Delta_{tr}S^{\theta,\infty}_{PhM}$ and the results are shows in the Figure 44b and 44c respectively.

For DPhM dye the $\Delta_{tr}H^{\theta,\infty}_{PhM}$ values show that the transfer process is endothermic in the ATPS formed by $Li^+ > Na^+$. But when this process is in presence of Mg^{2+} become exothermic. However, the transfer process of the TPhM dye occur with the $\Delta_{tr}H^{\theta,\infty}_{PhM}$ values negatives in the first TLL but become positive in the next TLLs when Li^+ is the cation that form the ATPS. In ATPS formed by Mg^{2+}, the transference is exothermic and the $\Delta_{tr}H^{\theta,\infty}_{PhM}$ values are more negatives when the TLL increase. Nevertheless, a better propose to analyze the phenyl group contribution to the standard enthalpy of transference change is by the difference $\Delta\Delta_{tr}H^{\theta,\infty}_{MV2B-AUR}$. The Figure 45b shows the values of $\Delta\Delta_{tr}H^{\theta,\infty}_{MV2B-AUR}$ as a function of the TLL of the ATPS studied.

The results of the $\Delta\Delta_{tr}H^{\theta,\infty}_{MV2B-AUR}$ values reveal that the phenyl group has a greater contribution in the ATPS formed by Mg^{2+}, but this contribution has a small variation with the TLL increase. On the other hand, this phenyl groups contribution decreases when the TLL increase in the ATPS formed by Na^+ and becomes lower until reaching positive values when Li^+ is the cation that form the ATPS, suggesting that the DPhM dye has a higher charge density than that TPhM, absorbing more energy to break the DPhM-BP component interactions and releasing less energy because of greater electrostatic repulsion in the DPhM-pseudopolication interaction. But this difference becomes smaller as the cation increases the charge density of the pseudopolication, causing the same effect for both molecules or greater in the last TLL system with Li^+.

Thereupon the $\Delta[T\Delta_{tr}S^{\theta,\infty}_{MV2B-AUR}]$ values show an entropic compensatory effect, where the phenyl group transfer contributes to the entropy decrease of the system formed by Mg^{2+}. Moreover, in the ATPSs formed by Na^+ or Li^+ the phenyl group contribution on the dye transfer process generates negative $\Delta[T\Delta_{tr}S^{\theta,\infty}_{MV2B-AUR}]$ values

that become less negative with the TLL increase, even reaching positive values in the last TLL of the Li^+ system.

These results evidenced the degree of hydrophobicity increase in the dye molecule caused by the phenyl group addition, inducing the loss in the freedom degree of the water molecules that solvate this functional group, decreasing the system entropy. This effect decreases proportionally to the steric impediment caused by the cation size that forms the pseudopolycation, therefore the cation Li^+ smaller size generates a greater number of hydrophobic interaction with the TPhM releasing the water molecules that solvating the dye increasing the system entropy.

3.2.1.3 Contribution of the positive charge on the dye structure

The partition process of two species with similar structure but one neutral and one charged, allows us to determine the electrostatic impediment effect caused by the dye molecule positive charge and the pseudopolication positive charge.

The figure 46 shows the $\Delta_{tr}G^{\theta,\infty}_{PhM}$, $\Delta_{tr}H^{\theta,\infty}_{PhM}$ and $T\Delta_{tr}S^{\theta,\infty}_{PhM}$ values of MV6B (charged specie) and MVB (neutral specie) as a function of the TLL of ($MgSO_4$ or Na_2SO_4 or Li_2SO_4) + PEO1500 + H_2O, ATPS at 298.15 K.

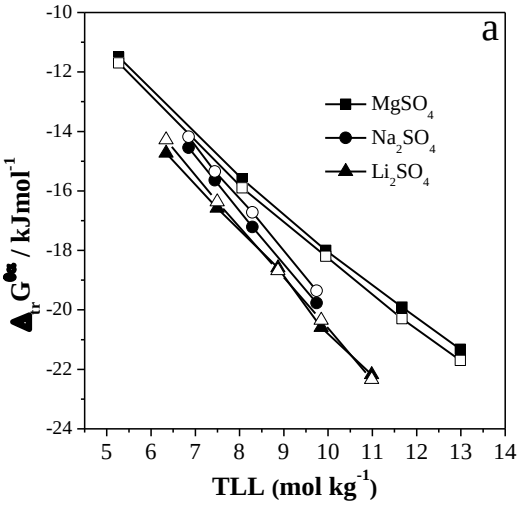

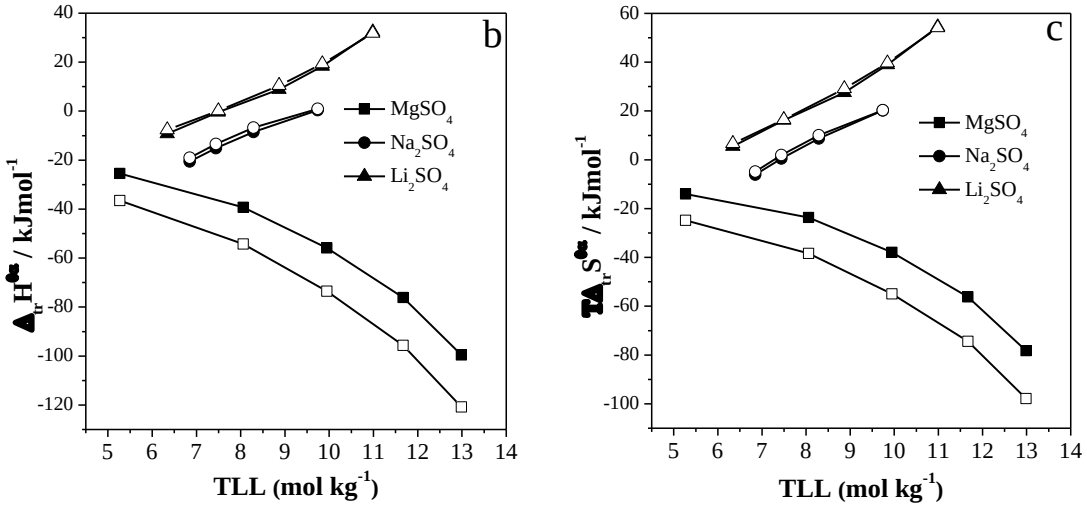

Figure 46. (a) $\Delta_{tr}G^{\theta,\infty}_{PhM}$ (b) $\Delta_{tr}H^{\theta,\infty}_{PhM}$ and (c) $T\Delta_{tr}S^{\theta,\infty}_{PhM}$ values of MV6B (closed symbols) and MVB (open symbols) as a function of the TLL of ATPS formed by (square symbol) PEO1500 + $MgSO_4$ + H_2O, (round symbol) PEO1500 + Na_2SO_4 + H_2O and (Triangular symbol) PEO1500 + Li_2SO_4 + H_2O ATPS at 298.15 K.

In all ATPS studied, the charge in the dye molecular structure does not contribute in the $\Delta_{tr}G^{\theta,\infty}_{PhM}$ values. However, the transfer process of both structures occurs with decrease of $\Delta_{tr}G^{\theta,\infty}_{PhM}$ values and these are more negative when the TLL increase in the following order $Li^+ < Na^+ < Mg^{2+}$.

The $\Delta_{tr}H^{\theta,\infty}_{PhM}$ values show that in presence of Li^+ cation the dye transference process is exothermic for both molecules in the first TLL, but become endothermic when the TLL increase. Besides, the charge in the dye structure does not contribute in the $\Delta_{tr}H^{\theta,\infty}_{PhM}$ values. When the cation that form the ATPS is Na^+, the $\Delta_{tr}H^{\theta,\infty}_{PhM}$ values are negative for both molecules in the three first TLL. However, these values are less negative with the TLL increase, even the $\Delta_{tr}H^{\theta,\infty}_{PhM}$ values for both molecules are positive in the last TLL. Similar to previous ATPS the charge in the dye structure does not contribute in the standard enthalpy transference change.

On the other hand, when the ATPS is formed by Mg^{2+} cation the dye transference process is carried out with enthalpy decrease, this enthalpy change is less when the TLL increase. The $\Delta_{tr}H^{\theta,\infty}_{MV6B}$ values in the cationic specie are less negative than the $\Delta_{tr}H^{\theta,\infty}_{MVB}$ values of the neutral specie. Suggesting that the charged on the dye molecule generates more intense interactions between the PhM dye and the BP components, absorbing more energy to break this interaction resulting in values of $\Delta_{tr}H^{\theta,\infty}_{MV6B}$ less negative than that $\Delta_{tr}H^{\theta,\infty}_{MVB}$.

The $T\Delta_{tr}S^{\theta\infty}_{PhM}$ values shows that, the charge in the dye structure does not contribute in the standard entropy transference change, when the ATPS is formed by Li^+ or Na^+. Nevertheless, the dye transference process occurs with the $T\Delta_{tr}S^{\theta\infty}_{PhM}$ values positive that become more positive with TLL increase in the order $Li^+ > Na^+$. In the ATPS formed by Mg^{2+} the transference process is carried out with $T\Delta_{tr}S^{\theta\infty}_{PhM}$ values negative and with the TLL increment these values are more negative. The charge lack in the dye molecule increases the PhM dye hydrophobicity, this results in a greater rotational freedom loss the water molecules that solvate this molecule decreasing the system entropy.

3.2.2 Anion effect in the PhM dyes partition process.

As was previously observed, the cation plays a fundamental role in the functional groups contribution on the PhM dyes thermodynamic transference parameters. Therefore, determine the anion effect in the partition process become important and fundamental. The figure 47 shows the K_{PhM} values of six PhM dyes measure in ATPS formed by ($NaC_2H_3O_2$ (AcetNa) + PPO425 + H_2O; $Na_3C_6H_5O_7$ (CitrNa) + PPO425 + H_2O and $Na_2C_4H_4O_6$ (TartNa) + PPO425 + H_2O at 298.15 K.

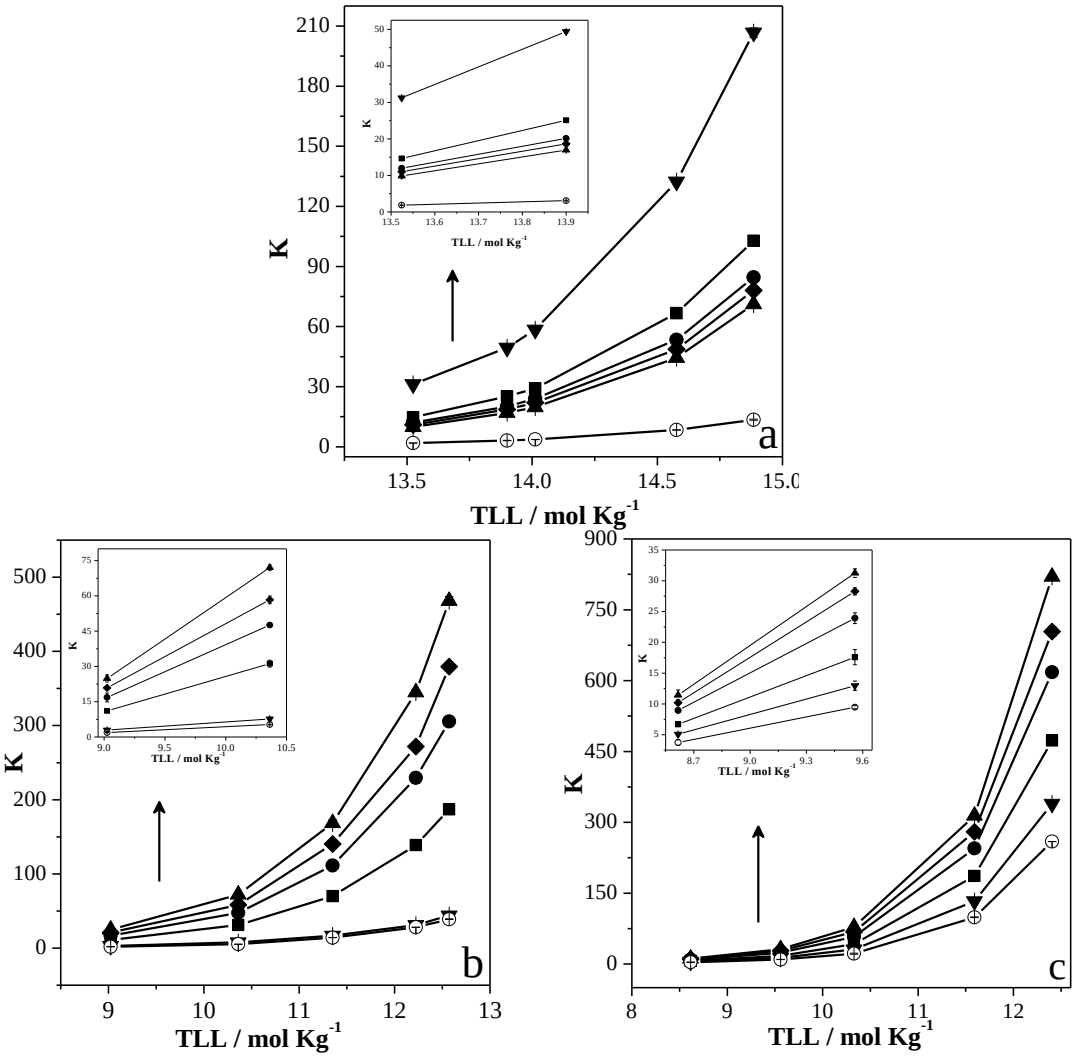

Figure 47. Partition Coefficient of MV10B (-▲-), MV6B (-●-), MV2B (-■-), PRA (-▼-) MVB (-♦-), AUR (-○-) as function of the TLL of PPO425+AcetNa+H_2O (a), PPO425+CitrNa+H_2O (b) and PPO425+TartNa+H_2O (c) ATPS at 298.15 K.

Although the K_{PhM} values show that all the partitioned dyes were concentrated preferentially in the ATPS upper phase studied, is important to consider that the anion nature strongly influences the PhM dyes transference process, mainly when the is inorganic anion (SO_4^{2-}), presenting values of K_{PhM} > 1000 and for organic anion the K_{PhM} values are less than 900. These results show a similar behavior to that found by de Oliveira et al[11], where the authors studied the anion effect on the Ovomucoid partition in ATPS formed by (sodium sulfate, sodium carbonate or sodium citrate) + PEO1500 + H_2O, finding that the K values are lower when in anion is of organic

character. They argue that this effect is caused by an increase in the hydrophobicity of the protein caused by the dehydration induced by the interactions between protein-salt in the order inorganic > organic.

This suggest that the nature of the interactions in the ATPS bottom phase are also of fundamental importance in the solutes partition in this system. But as the PhM dyes thermodynamic transfer parameters to Na_2SO_4+ PPO425 + H_2O ATPS were studied in the 3.1 section, in this section we will concentrate on the PhM thermodynamic transfer parameters (Figures from 48 to 65 and table from 36 to 57) in systems formed by sodium organic salts + PPO425 + H_2O.

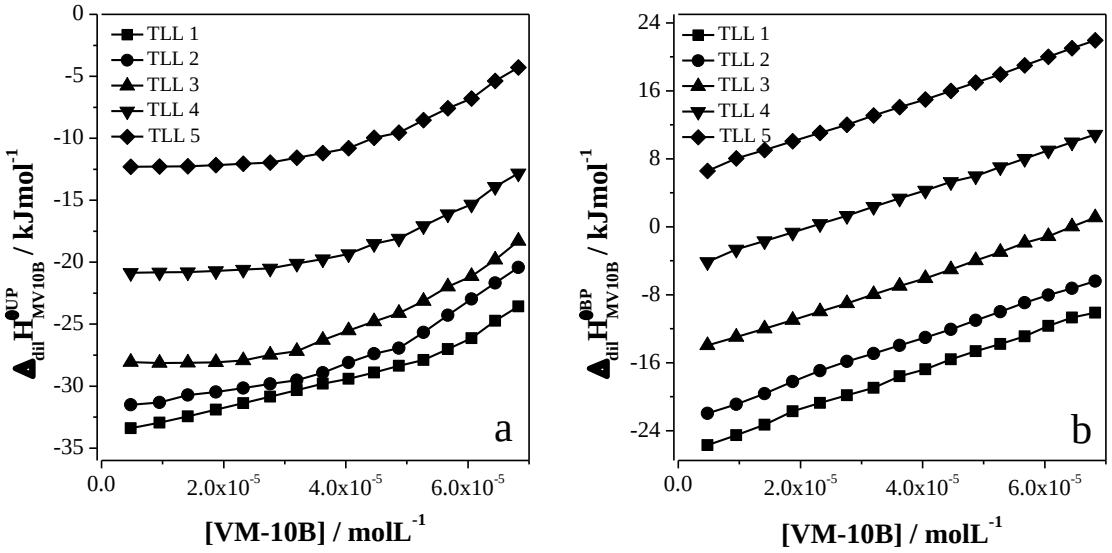

Figure 48. $\Delta_{dil}H^{UP}_{MV10B}$ (a) and $\Delta_{dil}H^{BP}_{MV10B}$ (b) as a functions of dye concentration in upper and bottom phases of PPO425+AcetNa+H_2O ATPS at 298.15 K.

Table 37. K_{MV10B} values and $\Delta_{dil}H^{\infty}_{MV10B}$ values in upper (UP) and bottom (BP) phases, for the TLL of PPO425+AcetNa+H_2O ATPS at 298.15 K.

TLL	K_{MV10B}	$\Delta_{dil}H^{\infty UP}_{MV10B}$	$\Delta_{dil}H^{\infty BP}_{MV10B}$
mol kg^{-1}		kJ mol^{-1}	
13.52	9.86±0.08	-34.27±0.05	-28.16±0.02
13.90	16.94±0.03	-32.06±0.02	-23.13±0.07
14.01	19.70±0.06	-27.74±0.01	-15.42±0.01
14.58	44.37±0.03	-21.31±0.07	-5.76±0.09
14.88	71.19±0.02	-12.77±0.09	4.95±0.07

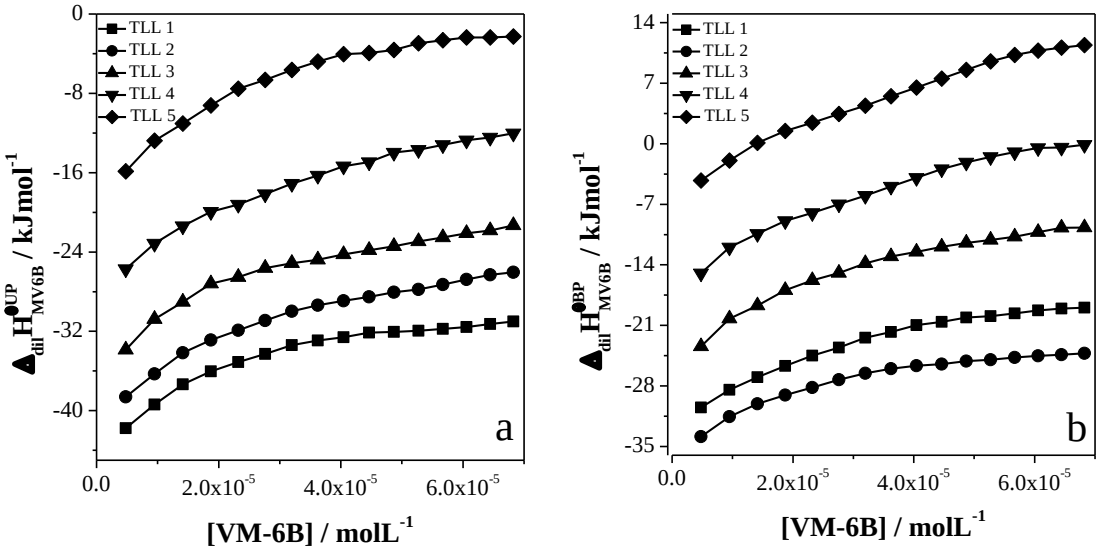

Figure 49. $\Delta_{dil}H^{UP}_{MV6B}$ (a) and $\Delta_{dil}H^{BP}_{MV6B}$ (b) as a functions of dye concentration in upper and bottom phases of PPO425+AcetNa+H_2O ATPS at 298.15 K.

Table 38. K_{MV6B} values and $\Delta_{dil}H^{\infty}_{MV6B}$ values in upper (UP) and bottom (BP) phases, for the TLL of PPO425+AcetNa+H_2O ATPS at 298.15 K.

TLL	K_{MV6B}	$\Delta_{dil}H^{\infty UP}_{MV6B}$	$\Delta_{dil}H^{\infty BP}_{MV6B}$
mol kg^{-1}		kJ mol^{-1}	
13.52	11.98±0.07	-47.55±0.01	-39.54±0.05
13.90	20.14±0.05	-45.31±0.09	-34.32±0.02
14.01	24.01±0.01	-41.01±0.04	-26.89±0.03
14.58	53.35±0.07	-34.62±0.07	-17.52±0.09
14.88	84.56±0.09	-26.02±0.02	-6.50±0.01

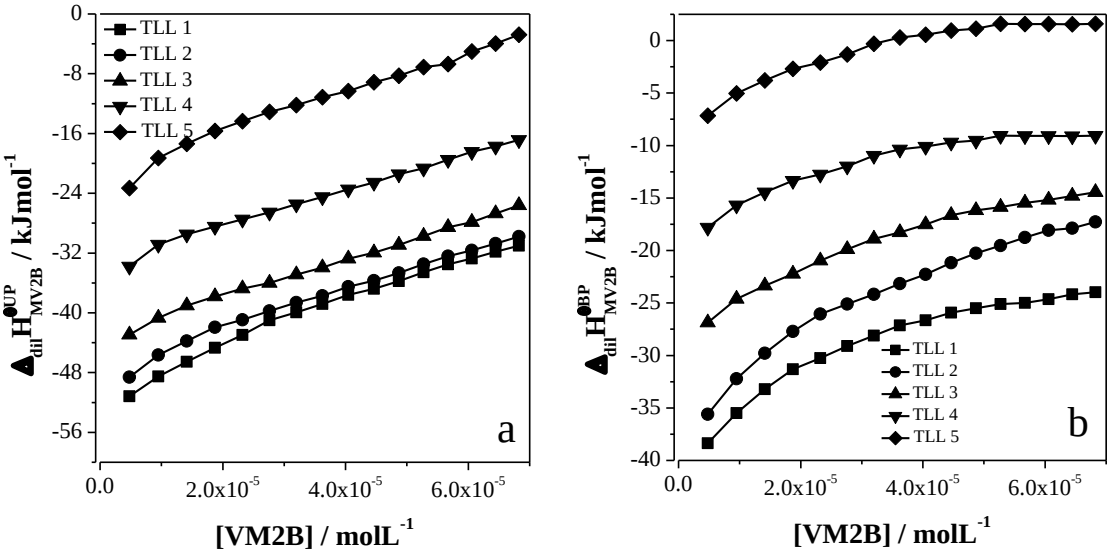

Figure 50. $\Delta_{dil}H^{UP}_{MV2B}$ (a) and $\Delta_{dil}H^{BP}_{MV2B}$ (b) as a functions of dye concentration in upper and bottom phases of PPO425+AcetNa+H_2O ATPS at 298.15 K.

Table 39. K_{MV2B} values and $\Delta_{dil}H^{\infty}_{MV2B}$ values in upper (UP) and bottom (BP) phases, for the TLL of PPO425+AcetNa+H_2O ATPS at 298.15 K.

TLL	K_{MV2B}	$\Delta_{dil}H^{\infty UP}_{MV2B}$	$\Delta_{dil}H^{\infty BP}_{MV2B}$
mol kg^{-1}		kJ mol^{-1}	
13.52	14.64±0.02	-56.03±0.05	-45.99±0.02
13.90	25.10±0.01	-53.80±0.03	-40.77±0.07
14.01	29.12±0.09	-49.44±0.02	-33.49±0.04
14.58	66.62±0.04	-42.97±0.08	-24.03±0.10
14.88	102.78±0.10	-34.45±0.11	-13.38±0.10

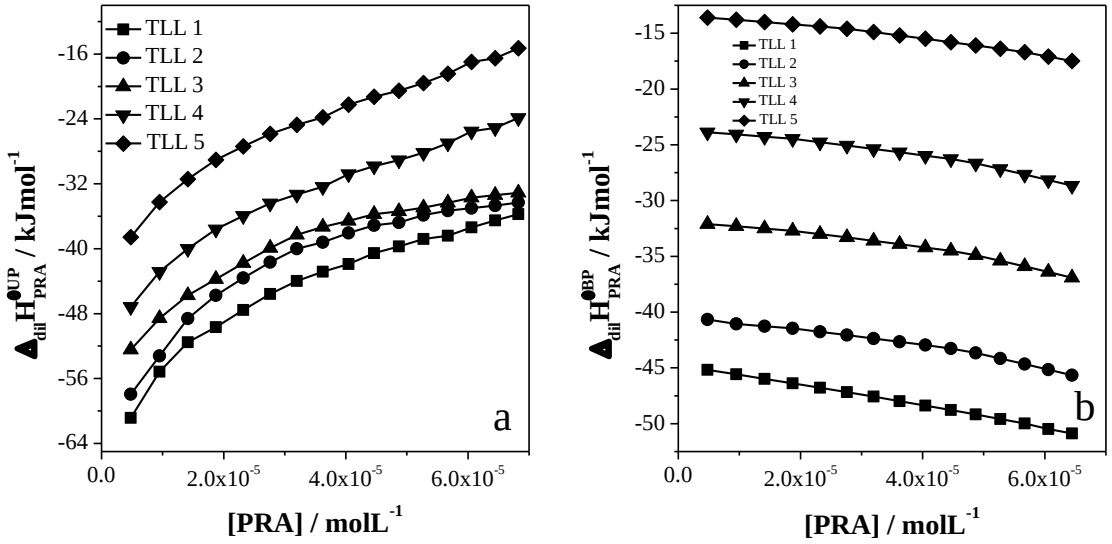

Figure 51. $\Delta_{dil}H^{UP}_{PRA}$ (a) and $\Delta_{dil}H^{BP}_{PRA}$ (b) as a functions of dye concentration in upper and bottom phases of PPO425+AcetNa+H_2O ATPS at 298.15 K.

Table 40. K_{PRA} values and $\Delta_{dil}H^{\infty}_{PRA}$ values in upper (UP) and bottom (BP) phases, for the TLL of PPO425+AcetNa+H_2O ATPS at 298.15 K.

TLL	K_{PRA}	$\Delta_{dil}H^{\infty UP}_{PRA}$	$\Delta_{dil}H^{\infty BP}_{PRA}$
mol kg^{-1}		kJ mol^{-1}	
13.52	31.24±0.08	-62.59±0.10	-45.07±0.02
13.90	49.40±0.05	-60.30±0.05	-40.01±0.07
14.01	58.50±0.10	-55.97±0.06	-32.99±0.04
14.58	132.41±0.03	-49.55±0.09	-23.97±0.10
14.88	206.73±0.04	-41.01±0.07	-13.50±0.10

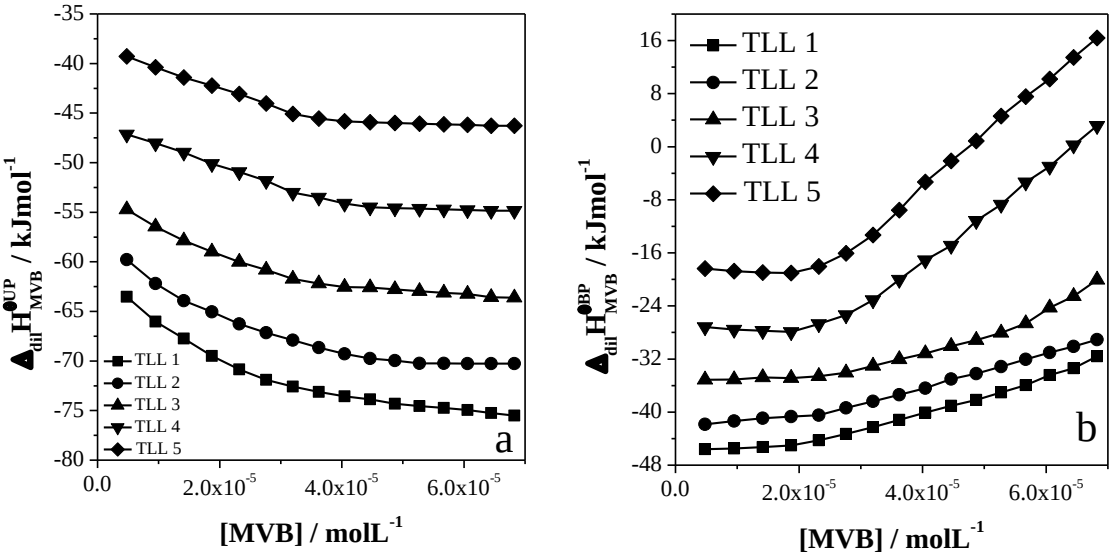

Figure 52. $\Delta_{dil}H^{UP}_{MVB}$ (a) and $\Delta_{dil}H^{BP}_{MVB}$ (b) as a functions of dye concentration in upper and bottom phases of PPO425+AcetNa+H_2O ATPS at 298.15 K.

Table 41. K_{MVB} values and $\Delta_{dil}H^{\infty}_{MVB}$ values in upper (UP) and bottom (BP) phases, for the TLL of PPO425+AcetNa+H_2O ATPS at 298.15 K.

TLL	K_{MVB}	$\Delta_{dil}H^{\infty UP}_{MVB}$	$\Delta_{dil}H^{\infty BP}_{MVB}$
mol kg^{-1}		kJ mol^{-1}	
13.52	11.02±0.01	-59.49±0.10	-46.41±0.04
13.90	18.66±0.04	-57.29±0.05	-41.47±0.03
14.01	22.00±0.02	-52.98±0.06	-35.47±0.01
14.58	48.62±0.05	-46.54±0.09	-27.65±0.05
14.88	78.02±0.01	-37.97±0.07	-17.87±0.02

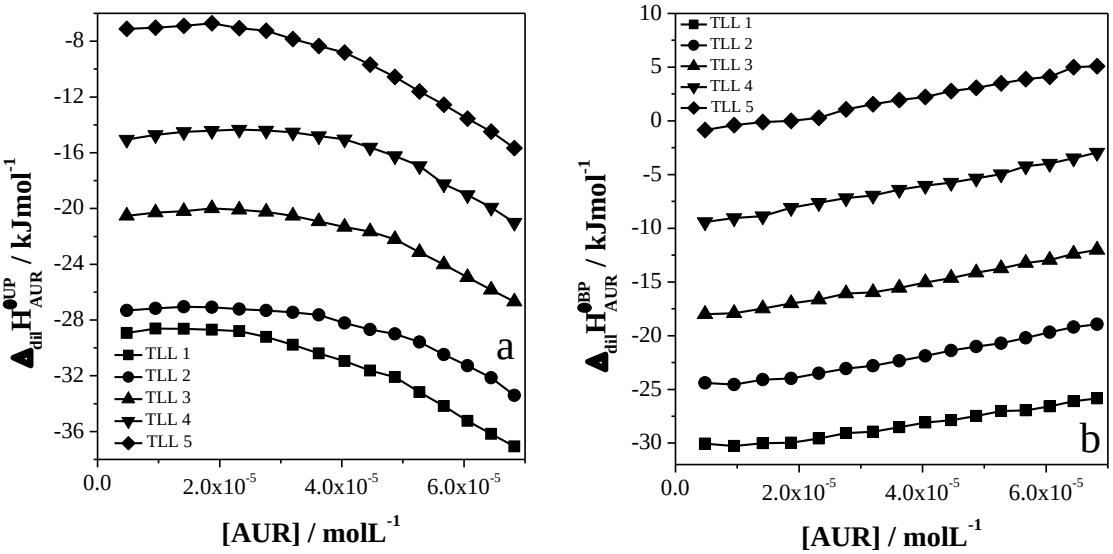

Figure 53. $\Delta_{dil}H^{UP}_{AUR}$ (a) and $\Delta_{dil}H^{BP}_{AUR}$ (b) as a functions of dye concentration in upper and bottom phases of PPO425+AcetNa+H_2O ATPS at 298.15 K.

Table 42. K_{AUR} values and $\Delta_{dil}H^{\infty}_{AUR}$ values in upper (UP) and bottom (BP) phases, for the TLL of PPO425+AcetNa+H_2O ATPS at 298.15 K.

TLL	K_{AUR}	$\Delta_{dil}H^{\infty UP}_{AUR}$	$\Delta_{dil}H^{\infty BP}_{AUR}$
mol kg^{-1}		kJ mol^{-1}	
13.52	1.86±0.03	-29.32±0.04	-29.74±0.01
13.90	3.09±0.05	-27.13±0.03	-24.63±0.07
14.01	3.64±0.01	-22.74±0.09	-18.05±0.05
14.58	8.41±0.01	-16.31±0.01	-9.43±0.09
14.88	13.46±0.08	-7.82±0.06	0.85±0.06

Table 43. Thermodynamic transfer parameters of PhM dyes as a function of the TLL of PPO425 + AcetNa + H2O ATPS at 298.15 K.

PhM dyes	$\Delta_{tr}G^{\theta,\infty}_{PhM}$	$\Delta_{tr}H^{\theta,\infty}_{PhM}$	$T\Delta_{tr}S^{\theta,\infty}_{PhM}$
		kJ mol^{-1}	
TLL 1 / 13.52 mol kg^{-1}			
MV10B	-5.67±0.05	-6.11±0.05	-0.44±0.01
MV6B	-6.15±0.01	-8.012±0.10	-1.86±0.07
MV2B	-6.65±0.04	-10.04±0.07	-3.39±0.08
PRA	-8.52±0.01	-17.52±0.01	-9.00±0.02
MVB	-5.94±0.03	-13.08±0.09	-7.14±0.03
AUR	-1.54±0.02	0.42±0.06	1.96±0.09
TLL 2 / 13.90 mol kg^{-1}			
MV10B	-7.01±0.03	-8.93±0.05	-1.92±0.01
MV6B	-7.44±0.06	-10.99±0.07	-3.55±0.07
MV2B	-7.98±0.02	-13.03±0.01	-5.05±0.02
PRA	-9.66±0.01	-20.29±0.04	-10.63±0.09
MVB	-7.25±0.07	-15.82±0.06	-8.57±0.03
AUR	-2.80±0.01	-2.50±0.01	0.30±0.01
TLL 3 / 14.01 mol kg^{-1}			
MV10B	-7.38±0.01	-12.32±0.01	-4.94±0.03
MV6B	-7.87±0.05	-14.12±0.09	-6.25±0.06
MV2B	-8.35±0.02	-15.95±0.01	-7.60±0.02
PRA	-10.10±0.08	-22.98±0.07	-12.90±0.11
MVB	-7.65±0.06	-17.51±0.05	-9.86±0.05
AUR	-3.20±0.01	-4.69±0.01	-1.49±0.01
TLL 4 / 14.58 mol kg^{-1}			
MV10B	-9.39±0.01	-15.55±0.02	-6.16±0.05
MV6B	-9.85±0.05	-17.10±0.06	-7.25±0.02
MV2B	-10.40±0.10	-18.94±0.03	-8.54±0.03
PRA	-12.10±0.09	-25.60±0.04	-13.50±0.08
MVB	-9.62±0.02	-18.89±0.08	-9.27±0.02
AUR	-5.27±0.02	-6.88±0.03	-1.61±0.01
TLL 5 / 14.88 mol kg^{-1}			

MV10B	-10.56±0.03	-17.72±0.02	-7.16±0.04
MV6B	-10.99±0.05	-19.52±0.01	-8.53±0.07
MV2B	-11.47±0.01	-21.07±0.05	-9.60±0.01
PRA	-13.20±0.10	-27.51±0.03	-14.31±0.08
MVB	-10.79±0.06	-20.10±0.01	-9.31±0.02
AUR	-6.40±0.01	-8.67±0.02	-2.23±0.03

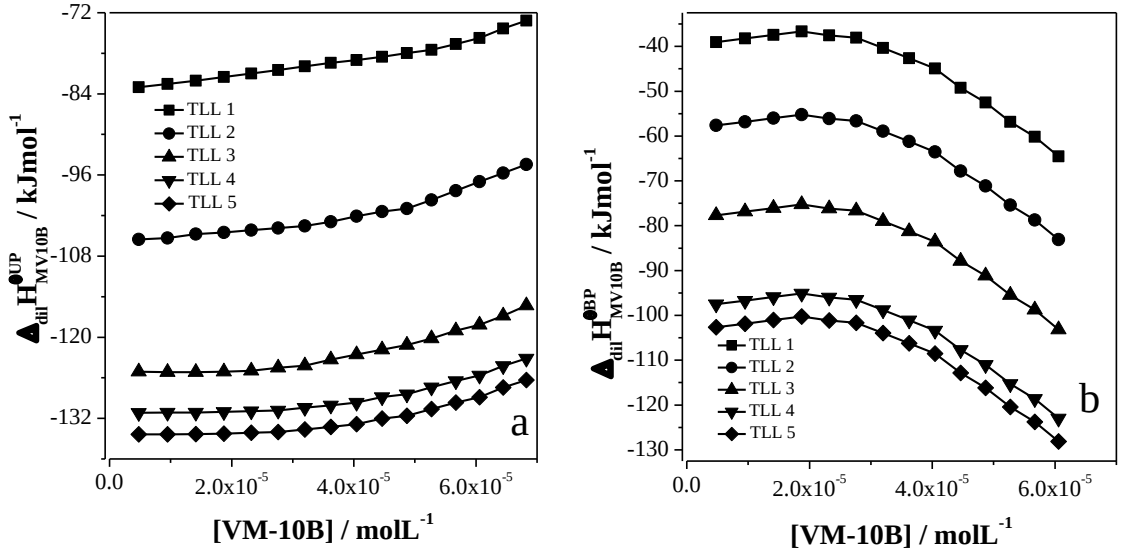

Figure 54. $\Delta_{dil}H^{UP}_{MV10B}$ (a) and $\Delta_{dil}H^{BP}_{MV10B}$ (b) as a functions of dye concentration in upper and bottom phases of PPO425 + CitrNa + H_2O ATPS at 298.15 K.

Table 44. K_{MV10B} values and $\Delta_{dil}H^{\infty}_{MV10B}$ values in upper (UP) and bottom (BP) phases, for the TLL of PPO425 + CitrNa + H_2O ATPS at 298.15 K.

TLL	K_{MV10B}	$\Delta_{dil}H^{\infty UP}_{MV10B}$	$\Delta_{dil}H^{\infty BP}_{MV10B}$
mol kg^{-1}		kJ mol^{-1}	
13.52	24.90±0.10	-83.88±0.06	-40.59±0.03
13.90	72.01±0.08	-106.08±0.07	-58.16±0.01
14.01	168.48±0.06	-124.77±0.10	-78.41±0.12
14.58	344.69±0.07	-131.64±0.03	-98.04±0.04
14.88	468.03±0.08	-134.84±0.09	-103.19±0.10

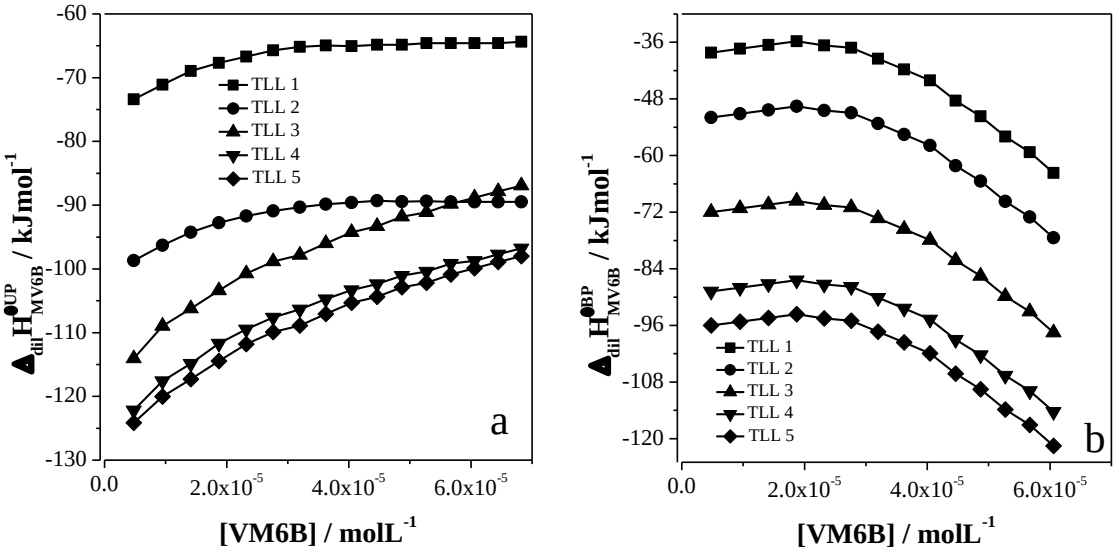

Figure 55. $\Delta_{dil}H^{UP}_{MV6B}$ (a) and $\Delta_{dil}H^{BP}_{MV6B}$ (b) as a functions of dye concentration in upper and bottom phases of PPO425 + CitrNa + H_2O ATPS at 298.15 K.

Table 45. K_{MV6B} values and $\Delta_{dil}H^{\infty}_{MV6B}$ values in upper (UP) and bottom (BP) phases, for the TLL of PPO425 + CitrNa + H_2O ATPS at 298.15 K.

TLL	K_{MV6B}	$\Delta_{dil}H^{\infty UP}_{MV6B}$	$\Delta_{dil}H^{\infty BP}_{MV6B}$
mol kg^{-1}		kJ mol^{-1}	
13.52	16.82±0.07	-77.35±0.01	-39.18±0.05
13.90	47.56±0.02	-99.22±0.07	-52.93±0.03
14.01	111.17±0.09	-115.08±0.10	-73.05±0.11
14.58	229.47±0.12	-124.08±0.05	-89.75±0.09
14.88	305.38±0.15	-127.28±0.03	-97.00±0.08

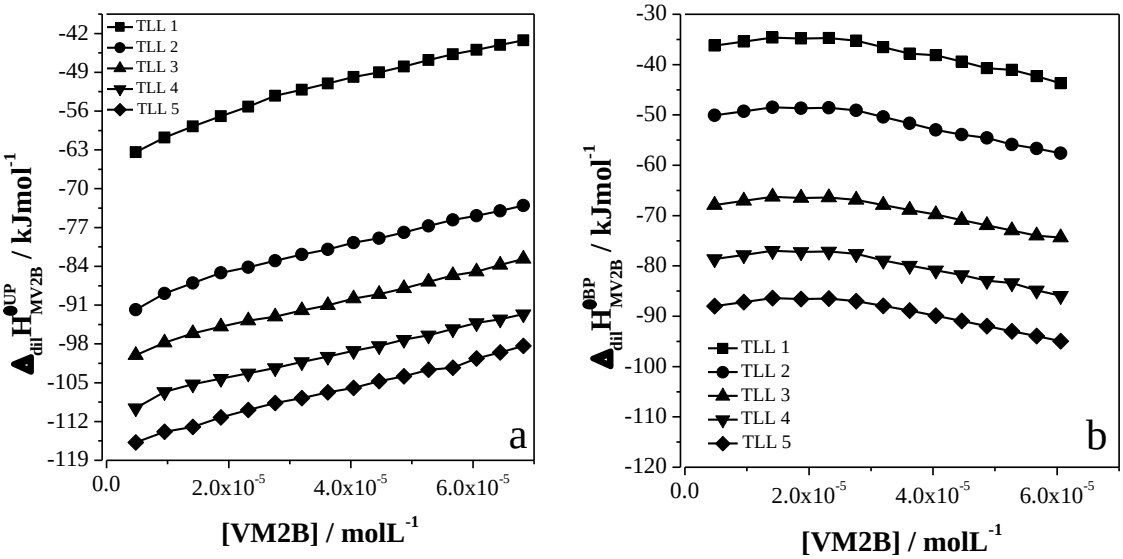

Figure 56. $\Delta_{dil}H^{UP}_{MV2B}$ (a) and $\Delta_{dil}H^{BP}_{MV2B}$ (b) as a functions of dye concentration in upper and bottom phases of PPO425 + CitrNa + H_2O ATPS at 298.15 K.

Table 46. K_{MV2B} values and $\Delta_{dil}H^{\infty}_{MV2B}$ values in upper (UP) and bottom (BP) phases, for the TLL of PPO425 + CitrNa + H_2O ATPS at 298.15 K.

TLL	K_{MV2B}	$\Delta_{dil}H^{\infty UP}_{MV2B}$	$\Delta_{dil}H^{\infty BP}_{MV2B}$
mol kg^{-1}		kJ mol^{-1}	
13.52	11.12±0.05	-65.25±0.03	-37.34±0.01
13.90	31.20±0.01	-93.85±0.06	-51.13±0.05
14.01	69.98±0.07	-102.64±0.01	-68.98±0.01
14.58	138.94±0.09	-114.60±0.07	-78.61±0.03
14.88	186.99±0.10	-117.80±0.08	-89.05±0.09

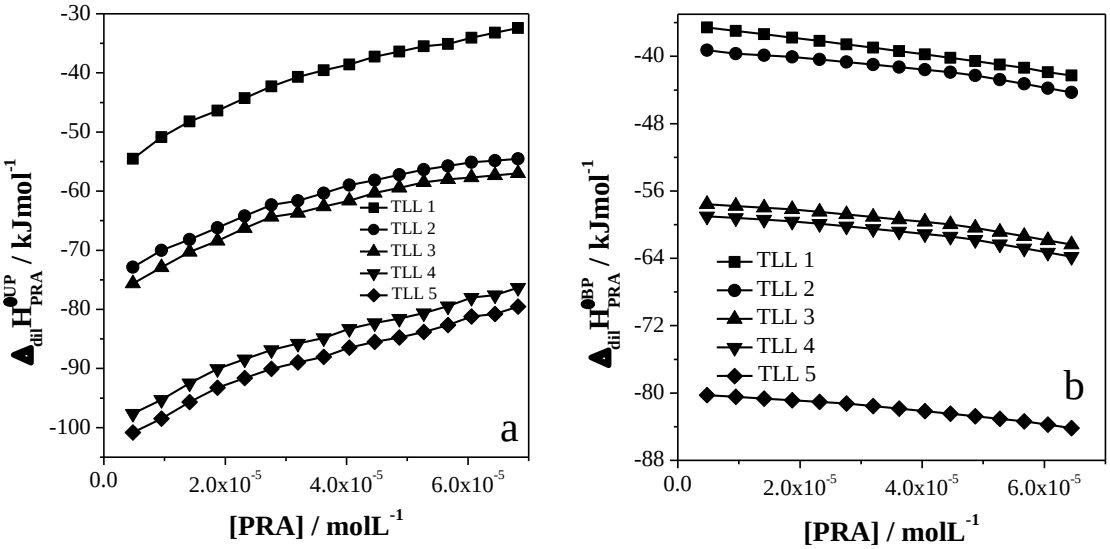

Figure 57. $\Delta_{dil}H^{UP}_{PRA}$ (a) and $\Delta_{dil}H^{BP}_{PRA}$ (b) as a functions of dye concentration in upper and bottom phases of PPO425 + CitrNa + H_2O ATPS at 298.15 K.

Table 47. K_{PRA} values and $\Delta_{dil}H^{\infty}_{PRA}$ values in upper (UP) and bottom (BP) phases, for the TLL of PPO425 + CitrNa + H_2O ATPS at 298.15 K.

TLL	K_{PRA}	$\Delta_{dil}H^{\infty UP}_{PRA}$	$\Delta_{dil}H^{\infty BP}_{PRA}$
mol kg^{-1}		kJ mol^{-1}	
13.52	2.68±0.09	-57.56±0.01	-36.68±0.03
13.90	7.67±0.03	-77.22±0.04	-39.84±0.07
14.01	16.67±0.08	-77.66±0.01	-58.09±0.10
14.58	30.97±0.05	-100.32±0.03	-58.69±0.07
14.88	44.10±0.06	-103.52±0.09	-80.37±0.10

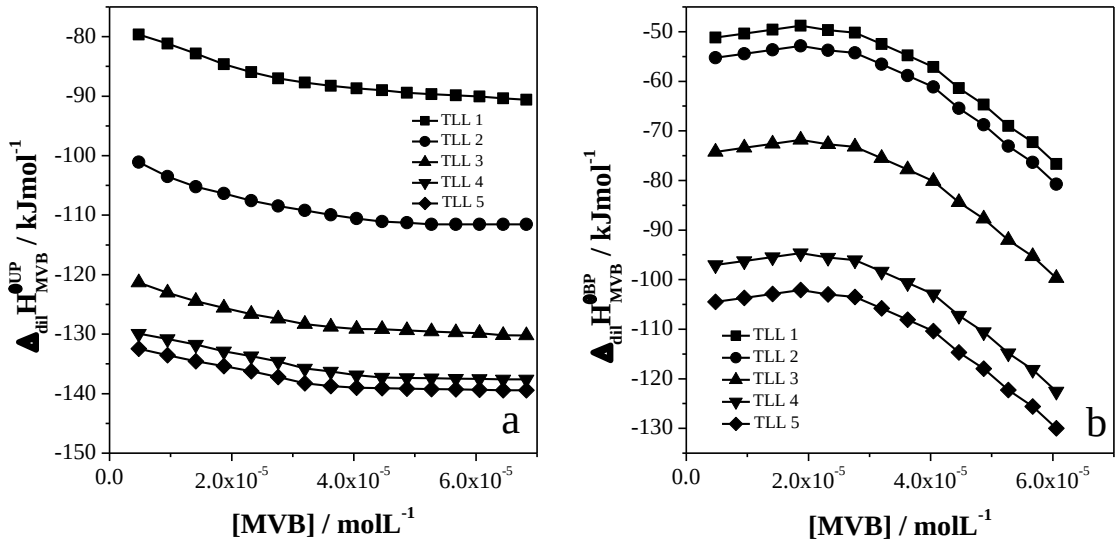

Figure 58. $\Delta_{dil}H^{UP}_{MVB}$ (a) and $\Delta_{dil}H^{BP}_{MVB}$ (b) as a functions of dye concentration in upper and bottom phases of PPO425 + CitrNa + H_2O ATPS at 298.15 K.

Table 48. K_{MVB} values and $\Delta_{dil}H^{\infty}_{MVB}$ values in upper (UP) and bottom (BP) phases, for the TLL of PPO425 + CitrNa + H_2O ATPS at 298.15 K.

TLL	K_{MVB}	$\Delta_{dil}H^{\infty UP}_{MVB}$	$\Delta_{dil}H^{\infty BP}_{MVB}$
mol kg^{-1}		kJ mol^{-1}	
13.52	20.88±0.03	-79.88±0.08	-51.80±0.05
13.90	58.30±0.04	-100.80±0.02	-55.86±0.11
14.01	140.20±0.01	-121.70±0.06	-74.93±0.09
14.58	271.59±0.01	-130.54±0.01	-97.27±0.02
14.88	379.53±0.15	-133.74±0.01	-104.79±0.03

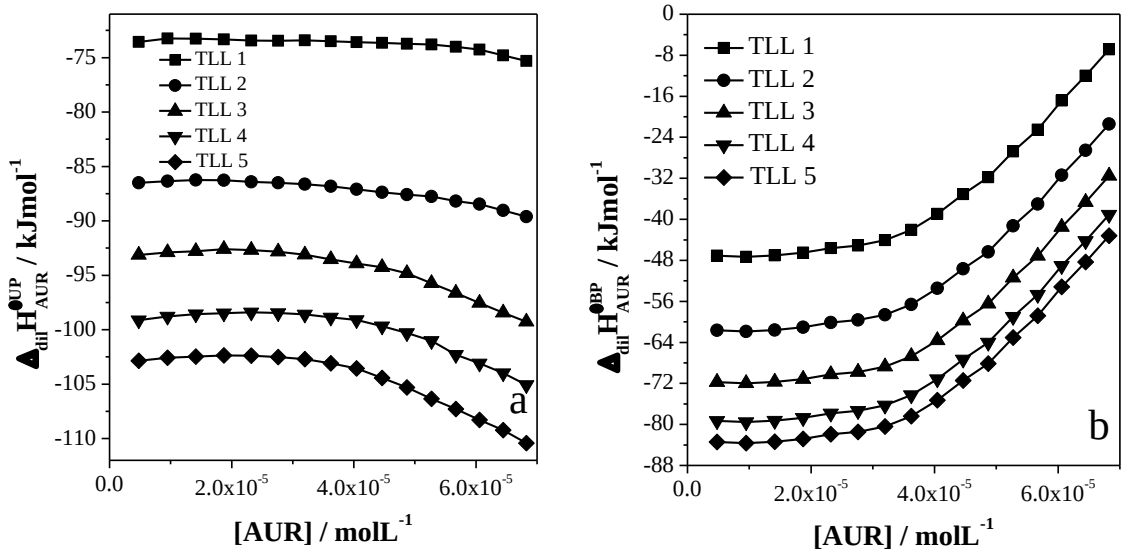

Figure 59. $\Delta_{dil}H^{UP}_{AUR}$ (a) and $\Delta_{dil}H^{BP}_{AUR}$ (b) as a functions of dye concentration in upper and bottom phases of PPO425 + CitrNa + H_2O ATPS at 298.15 K.

Table 49. K_{AUR} values and $\Delta_{dil}H^{\infty}_{AUR}$ values in upper (UP) and bottom (BP) phases, for the TLL of PPO425 + CitrNa + H_2O ATPS at 298.15 K.

TLL	K_{AUR}	$\Delta_{dil}H^{\infty UP}_{AUR}$	$\Delta_{dil}H^{\infty BP}_{AUR}$
mol kg^{-1}		kJ mol^{-1}	
13.52	1.90±0.01	-73.95±0.01	-46.78±0.03
13.90	5.29±0.01	-86.32±0.05	-61.63±0.08
14.01	14.17±0.03	-93.34±0.07	-71.65±0.09
14.58	28.14±0.01	-99.37±0.09	-79.31±0.10
14.88	39.01±0.06	-102.57±0.12	-83.42±0.07

Table 50. Thermodynamic transfer parameters of PhM dyes as a function of the TLL of PPO425 + CitrNa + H2O ATPS at 298.15 K.

PhM dyes	$\Delta_{tr}G^{\theta,\infty}_{PhM}$	$\Delta_{tr}H^{\theta,\infty}_{PhM}$	$T\Delta_{tr}S^{\theta,\infty}_{PhM}$
		kJ mol^{-1}	
TLL 1 / 9.02 mol kg^{-1}			
MV10B	-7.96±0.09	-43.29±0.03	-35.33±0.05
MV6B	-6.99±0.08	-38.17±0.01	-31.18±0.01
MV2B	-5.97±0.09	-27.91±0.04	-21.94±0.03
PRA	-2.45±0.06	-20.88±0.02	-18.43±0.03
MVB	-7.42±0.07	-28.08±0.07	-20.56±0.04
AUR	-1.59±0.09	-27.17±0.01	-25.58±0.02
TLL 2 / 10.36 mol kg^{-1}			
MV10B	-10.59±0.06	-47.92±0.01	-37.33±0.07
MV6B	-9.56±0.08	-46.29±0.05	-36.73±0.06
MV2B	-8.52±0.09	-42.72±0.03	-34.20±0.03
PRA	-5.04±0.09	-37.82±0.01	-32.78±0.09
MVB	-10.07±0.05	-44.94±0.05	-34.87±0.08
AUR	-4.13±0.07	-24.69±0.05	-20.56±0.06
TLL 3 / 11.35 mol kg^{-1}			
MV10B	-12.70±0.06	-46.36±0.04	-33.66±0.05
MV6B	-11.67±0.08	-42.03±0.03	-30.37±0.07
MV2B	-10.52±0.07	-33.66±0.04	-23.14±0.07
PRA	-6.97±0.05	-19.13±0.06	-12.16±0.09
MVB	-12.24±0.09	-46.77±0.09	-34.53±0.10
AUR	-6.57±0.01	-21.69±0.02	-15.12±0.05
TLL 4 / 12.22 mol kg^{-1}			
MV10B	-14.47±0.07	-33.60±0.03	-19.13±0.06
MV6B	-13.46±0.07	-34.33±0.05	-20.87±0.08
MV2B	-12.22±0.05	-35.99±0.07	-23.77±0.09
PRA	-8.50±0.01	-41.63±0.08	-33.13±0.10
MVB	-13.88±0.06	-33.27±0.06	-19.39±0.07
AUR	-8.26±0.01	-20.06±0.02	-11.80±0.05

TLL 5 / 12.57 mol kg^{-1}			
MV10B	-15.23±0.07	-31.65±0.03	-16.42±0.05
MV6B	-14.17±0.09	-30.28±0.05	-16.11±0.09
MV2B	-12.95±0.03	-28.75±0.02	-15.80±0.04
PRA	-9.38±0.01	-23.15±0.04	-13.77±0.08
MVB	-14.71±0.08	-28.95±0.01	-14.24±0.03
AUR	-9.07±0.02	-19.15±0.03	-10.08±0.06

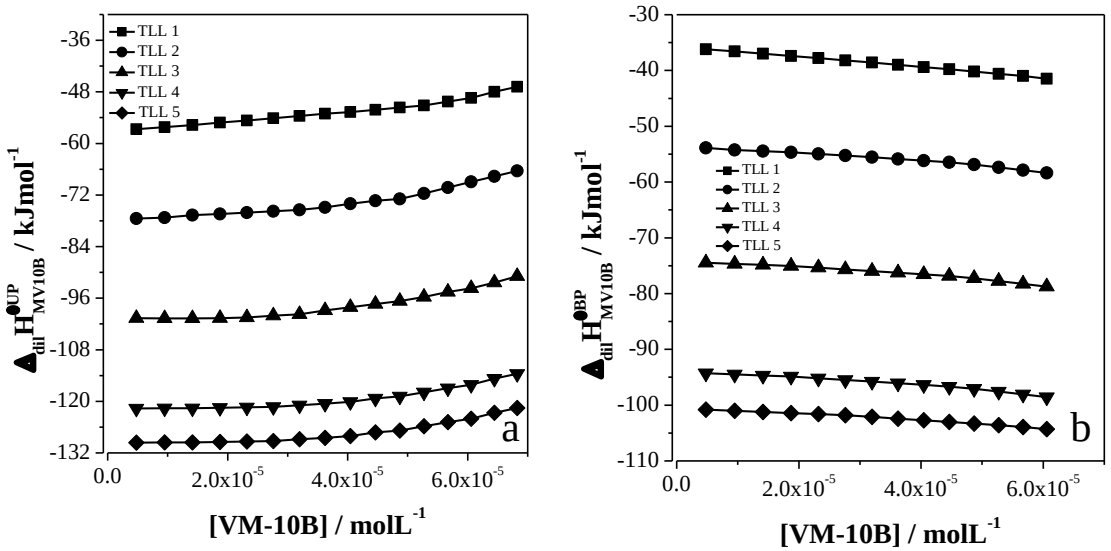

Figure 60. $\Delta_{dil}H^{UP}_{MV10B}$ (a) and $\Delta_{dil}H^{BP}_{MV10B}$ (b) as a functions of dye concentration in upper and bottom phases of PPO425 + TartNa + H_2O ATPS at 298.15 K.

Table 51. K_{MV10B} values and $\Delta_{dil}H^{\infty}_{MV10B}$ values in upper (UP) and bottom (BP) phases, for the TLL of PPO425 + TartNa + H_2O ATPS at 298.15 K.

TLL	K_{MV10B}	$\Delta_{dil}H^{\infty UP}_{MV10B}$	$\Delta_{dil}H^{\infty BP}_{MB10B}$
mol kg^{-1}		kJ mol^{-1}	
13.52	11.44±0.03	-57.54±0.03	-36.09±0.05
13.90	31.25±0.07	-78.01±0.08	-53.76±0.09
14.01	78.21±0.06	-100.31±0.03	-74.26±0.07
14.58	314.01±0.12	-122.10±0.01	-94.15±0.11
14.88	820.03±0.10	-130.05±0.05	-100.50±0.02

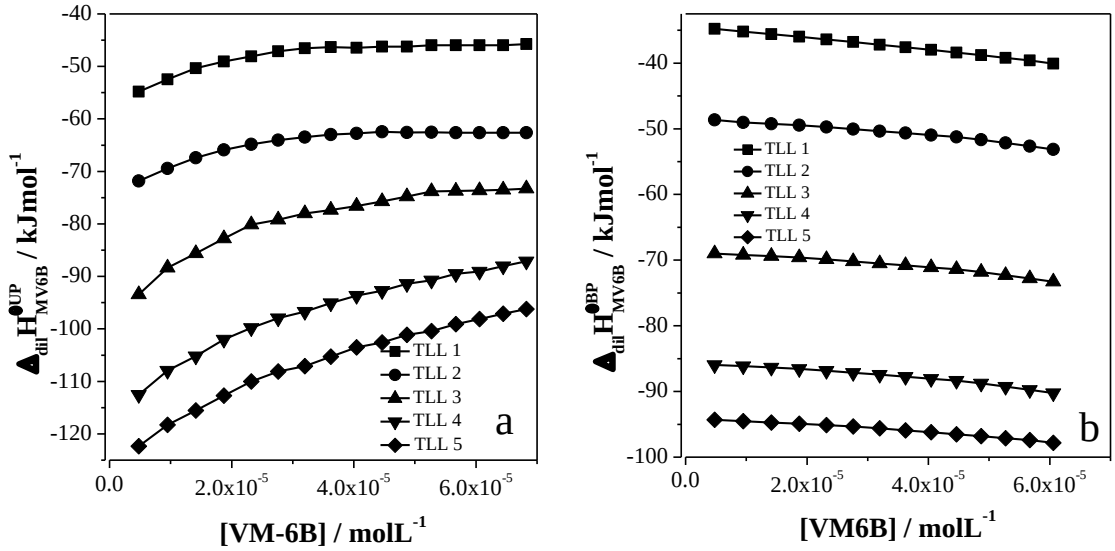

Figure 61. $\Delta_{dil}H^{UP}_{MV6B}$ (a) and $\Delta_{dil}H^{BP}_{MV6B}$ (b) as a functions of dye concentration in upper and bottom phases of PPO425 + TartNa + H_2O ATPS at 298.15 K.

Table 52. K_{MV6B} values and $\Delta_{dil}H^{\infty}_{MV6B}$ values in upper (UP) and bottom (BP) phases, for the TLL of PPO425 + TartNa + H_2O ATPS at 298 K.

TLL	K_{MV6B}	$\Delta_{dil}H^{\infty UP}_{MV6B}$	$\Delta_{dil}H^{\infty BP}_{MB6B}$
mol kg^{-1}		kJ mol^{-1}	
13.52	8.94±0.01	-54.74±0.04	-34.69±0.01
13.90	23.93±0.04	-71.49±0.09	-48.54±0.01
14.01	57.56±0.02	-93.46±0.07	-68.91±0.03
14.58	244.79±0.08	-112.42±0.14	-85.87±0.17
14.88	617.82±0.09	-122.50±0.08	-94.32±0.01

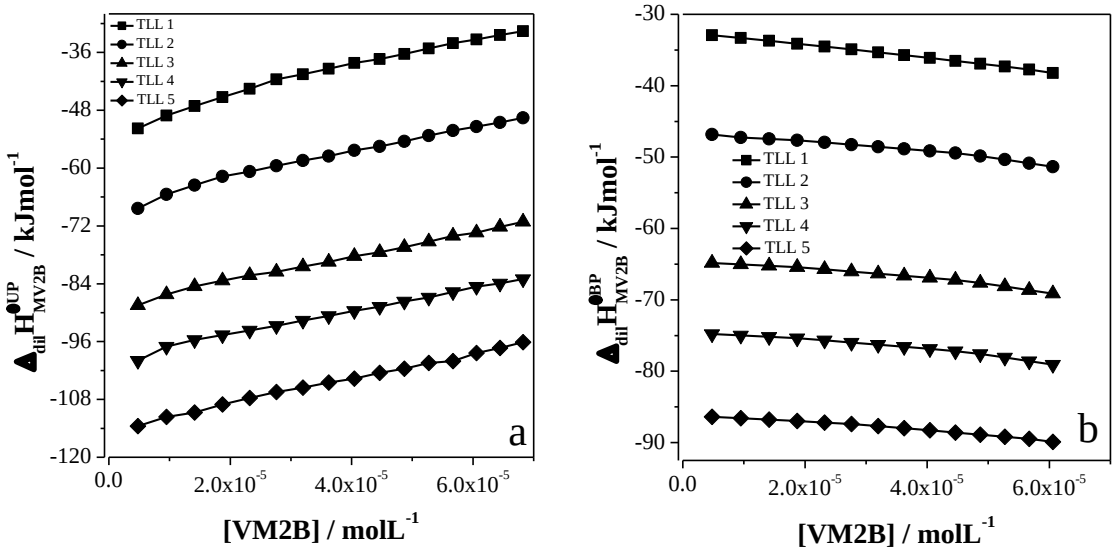

Figure 62. $\Delta_{dil}H^{UP}_{MV2B}$ (a) and $\Delta_{dil}H^{BP}_{MV2B}$ (b) as a functions of dye concentration in upper and bottom phases of PPO425 + TartNa + H_2O ATPS at 298.15 K.

Table 53. K_{MV2B} values and $\Delta_{dil}H^{\infty}_{MV2B}$ values in upper (UP) and bottom (BP) phases, for the TLL of PPO425 + TartNa + H_2O ATPS at 298 K.

TLL	K_{MV2B}	$\Delta_{dil}H^{\infty UP}_{MV2B}$	$\Delta_{dil}H^{\infty BP}_{MB2B}$
mol kg^{-1}		kJ mol^{-1}	
13.52	6.68±0.07	-51.61±0.03	-32.86±0.07
13.90	17.60±0.02	-68.40±0.07	-46.75±0.09
14.01	42.10±0.09	-88.10±0.02	-64.85±0.05
14.58	186.55±0.13	-99.99±0.05	-74.74±0.08
14.88	473.31±0.19	-113.03±0.02	-86.38±0.10

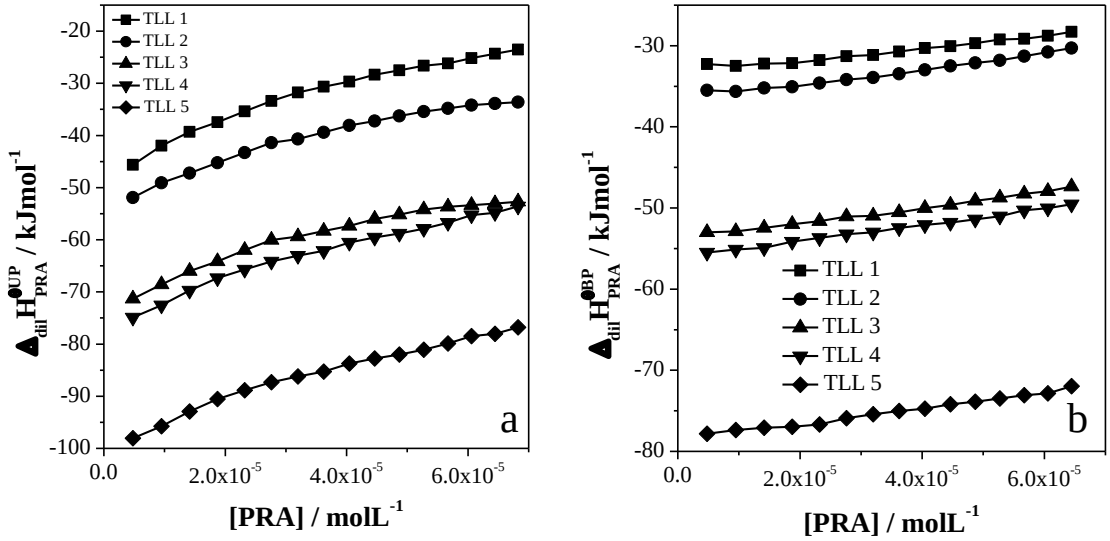

Figure 63. $\Delta_{dil}H^{UP}_{PRA}$ (a) and $\Delta_{dil}H^{BP}_{PRA}$ (b) as a functions of dye concentration in upper and bottom phases of PPO425 + TartNa + H_2O ATPS at 298.15 K.

Table 54. K_{PRA} values and $\Delta_{dil}H^{\infty}_{PRA}$ values in upper (UP) and bottom (BP) phases, for the TLL of PPO425 + TartNa + H_2O ATPS at 298.15 K.

TLL	K_{PRA}	$\Delta_{dil}H^{\infty UP}_{PRA}$	$\Delta_{dil}H^{\infty BP}_{PRA}$
mol kg^{-1}		kJ mol^{-1}	
13.52	5.08±0.01	-45.66±0.05	-32.21±0.08
13.90	12.96±0.05	-51.72±0.09	-35.47±0.12
14.01	30.73±0.06	-71.92±0.01	-53.97±0.03
14.58	132.80±0.02	-74.58±0.03	-54.83±0.10
14.88	339.50±0.07	-98.76±0.06	-77.71±0.07

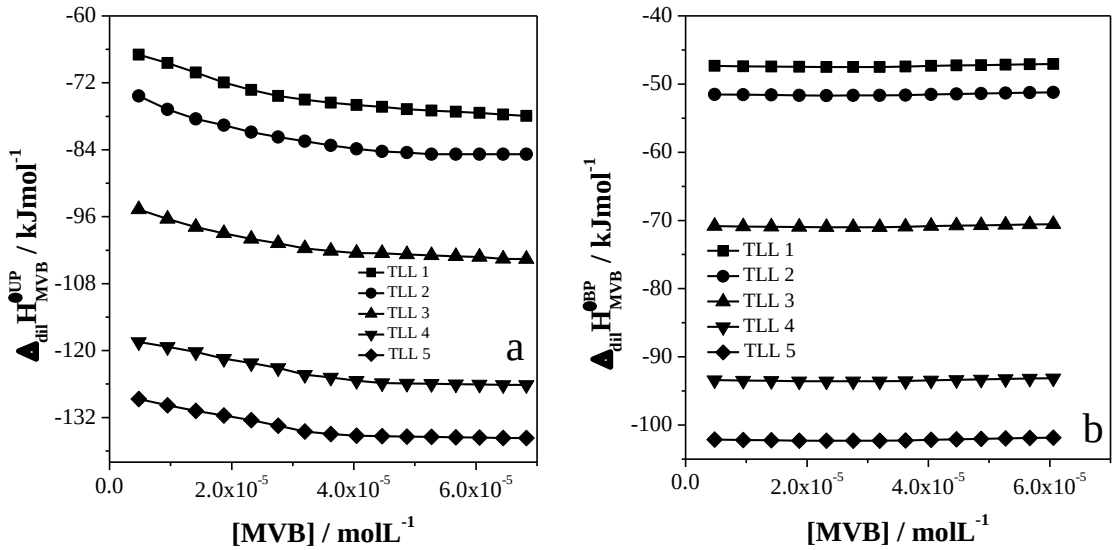

Figure 64. $\Delta_{dil}H^{UP}_{MVB}$ (a) and $\Delta_{dil}H^{BP}_{MVB}$ (b) as a functions of dye concentration in upper and bottom phases of PPO425 + TartNa + H_2O ATPS at 298.15 K.

Table 55. K_{MVB} values and $\Delta_{dil}H^{\infty}_{MVB}$ values in upper (UP) and bottom (BP) phases, for the TLL of PPO425 + TartNa + H_2O ATPS at 298.15 K.

TLL	K_{MVB}	$\Delta_{dil}H^{\infty UP}_{MVB}$	$\Delta_{dil}H^{\infty BP}_{MVB}$
mol kg^{-1}		kJ mol^{-1}	
13.52	10.20±0.03	-67.19±0.03	-47.34±0.05
13.90	28.28±0.07	-74.05±0.02	-51.50±0.07
14.01	67.77±0.01	-95.07±0.05	-70.82±0.09
14.58	279.75±0.07	-119.07±0.04	-93.42±0.03
14.88	703.76±0.09	-128.99±0.01	-102.14±0.05

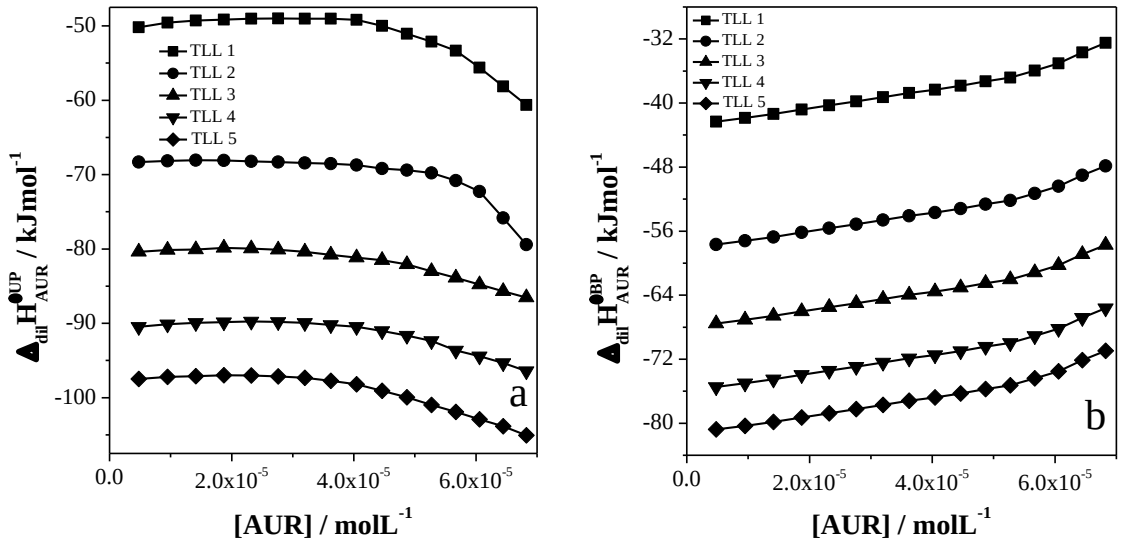

Figure 65. $\Delta_{dil}H^{UP}_{AUR}$ (a) and $\Delta_{dil}H^{BP}_{AUR}$ (b) as a functions of dye concentration in upper and bottom phases of PPO425 + TartNa + H_2O ATPS at 298.15 K.

Table 56. K_{AUR} values and $\Delta_{dil}H^{\infty}_{AUR}$ values in upper (UP) and bottom (BP) phases, for the TLL of PPO425 + TartNa + H_2O ATPS at 298.15 K.

TLL	K_{AUR}	$\Delta_{dil}H^{\infty UP}_{AUR}$	$\Delta_{dil}H^{\infty BP}_{AUR}$
mol kg^{-1}		kJ mol^{-1}	
13.52	3.74±0.01	-50.28±0.02	-42.33±0.03
13.90	9.46±0.01	-68.13±0.05	-57.28±0.09
14.01	25.92±0.03	-80.60±0.09	-67.55±0.10
14.58	98.95±0.01	-90.72±0.01	-75.47±0.06
14.88	259.28±0.07	-97.83±0.13	-80.78±0.15

Table 57. Thermodynamic transfer parameters of PhM dyes as a function of the TLL of PPO425 + TartNa + H2O ATPS at 298.15 K.

PhM dyes	$\Delta_{tr}G^{\theta,\infty}_{PhM}$	$\Delta_{tr}H^{\theta,\infty}_{PhM}$	$T\Delta_{tr}S^{\theta,\infty}_{PhM}$
		kJ mol^{-1}	
TLL 1 / 8.62 mol kg^{-1}			
MV10B	-6.04±0.10	-21.45±0.08	-15.41±0.18
MV6B	-5.43±0.07	-20.03±0.05	-14.62±0.12
MV2B	-4.70±0.01	-18.76±0.05	-14.05±0.04
PRA	-4.03±0.02	-13.44±0.06	-9.42±0.04
MVB	-5.75±0.08	-19.85±0.02	-14.10±0.11
AUR	-3.27±0.01	-7.96±0.03	-4.68±0.02
TLL 2 / 9.56 mol kg^{-1}			
MV10B	-8.52±0.03	-24.25±0.07	-15.73±0.04
MV6B	-7.86±0.01	-22.94±0.08	-15.09±0.07
MV2B	-7.10±0.11	-21.63±0.01	-14.55±0.12
PRA	-6.34±0.06	-16.26±0.05	-9.91±0.11
MVB	-8.26±0.09	-22.57±0.01	-14.27±0.10
AUR	-5.57±0.05	-10.85±0.10	-5.28±0.05
TLL 3 / 10.33 mol kg^{-1}			
MV10B	-10.80±0.02	-26.06±0.08	-15.25±0.06
MV6B	-10.04±0.04	-24.55±0.01	-14.51±0.05
MV2B	-9.26±0.09	-23.24±0.05	-13.99±0.14
PRA	-8.48±0.01	-17.93±0.07	-9.47±0.08
MVB	-10.44±0.01	-24.26±0.09	-13.81±0.10
AUR	-8.06±0.01	-13.04±0.01	-4.99±0.02
TLL 4 / 11.59 mol kg^{-1}			
MV10B	-14.24±0.03	-27.94±0.05	-13.71±0.02
MV6B	-13.62±0.09	-26.53±0.01	-12.93±0.10
MV2B	-12.95±0.04	-25.26±0.10	-12.30±0.06
PRA	-12.11±0.02	-19.75±0.09	-7.64±0.07
MVB	-13.95±0.07	-25.64±0.09	-11.70±0.02
AUR	-11.38±0.10	-15.25±0.11	-3.87±0.01

TLL 5 / 12.41 mol kg^{-1}			
MV10B	-16.61±0.09	-29.53±0.10	-12.94±0.01
MV6B	-15.91±0.08	-28.17±0.09	-12.27±0.01
MV2B	-15.25±0.02	-26.64±0.07	-11.40±0.05
PRA	-14.43±0.01	-21.06±0.05	-6.62±0.04
MVB	-16.24±0.07	-26.86±0.01	-10.61±0.08
AUR	-13.76±0.01	-17.05±0.04	-3.29±0.03

For a better analysis of the anion effect the thermodynamic transfer parameters were analyzed from the following contributions:

3.2.2.1 Contribution of the -CH_3 groups

The effect of the anion forming the electrolyte on the -CH_3 groups contribution will be studied in each thermodynamic transfer parameter applying the proposal of the section 3.1.1. Consequently, the calculation of the $\Delta_{tr}G^{\theta,\infty}_{PhM}$ values as a function of the -CH_3 groups for ATPS formed by ($NaC_2H_3O_2$ (AcetNa) or $Na_2C_4H_4O_6$ (TartNa) or $Na_3C_6H_5O_7$ (CitrNa)) + PPO425 + H_2O at 298.15 K are shown in the Figures 66.

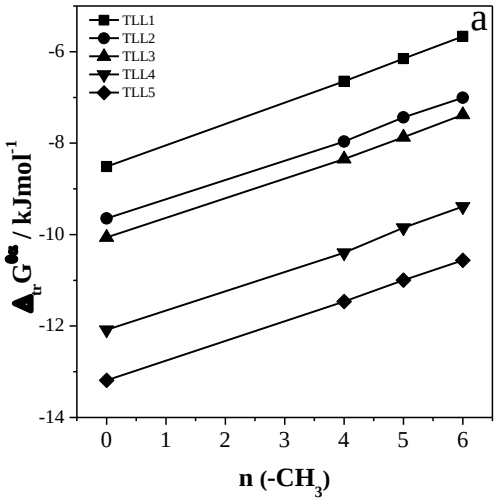

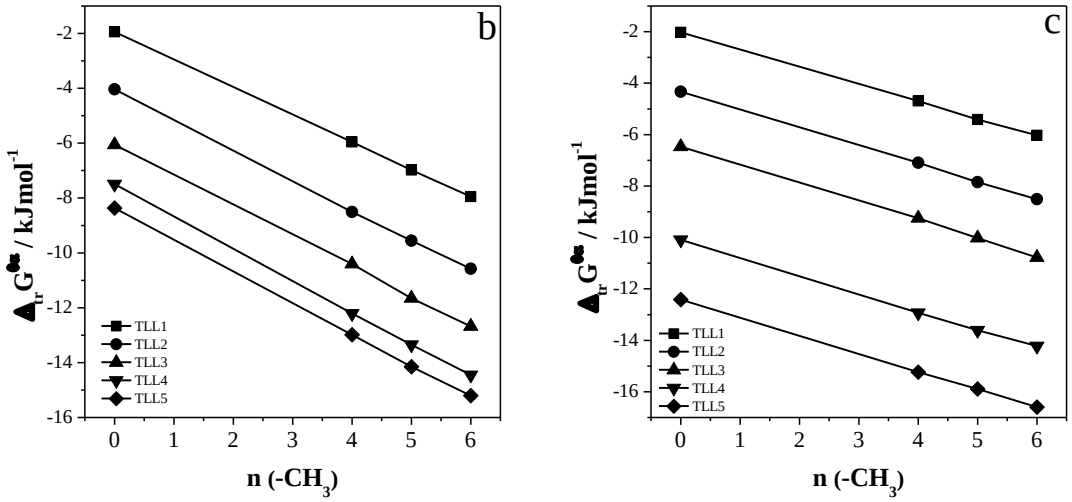

Figure 66. $\Delta_{tr}G_{PhM}^{\theta,\infty}$ as a function of -CH_3 groups $MV10B_{(6\text{-}CH3)}$, $MV6B_{(5\text{-}CH3)}$, $MV2B_{(4\text{-}CH3)}$ and $PRA_{(0\text{-}CH3)}$ partitioning in (a) AcetNa + PPO425 + H_2O (b) CitrNa + PPO425 + H_2O and (c) TartNa + PPO425 + H_2O ATPS at 298.15 K.

The $\Delta_{tr}G_{PhM}^{\theta,\infty}$ values show that independent of the ATPS the transference process occur with the decrease of Gibbs free energy. Moreover, when the ATPS is formed by Acetate (Acet) anion, the $\Delta_{tr}G_{PhM}^{\theta,\infty}$ values are negative for all PhM dyes and become more negative with the TLL increment. Nevertheless, these values are less negative when the -CH_3 groups number in the dye structure increase. Indicating that the dye molecules number transferred from the bottom phase to the upper phase of the ATPS decreases with the methyl groups increase in the dye molecular structure. However, in the ATPSs formed by Citrate (Citr) or Tartrate (Trat) anions, the $\Delta_{tr}G_{PhM}^{\theta,\infty}$ values are negative for all dyes and are more negative when the TLL and the -CH_3 groups number increase. Suggesting that the methyl group contributes favorably in the dye transfer process depending on the ATPS forming anion in the following order Tart > Citr.

To better understand the methyl group contribution to the PhM dyes thermodynamic transfer potential, was calculated the slope average of the linear relationship $\Delta_{tr}G_{PhM}^{\theta,\infty}$ versus -CH_3 groups for each ATPS. The results were $\frac{\partial \Delta_{tr}G_{CH_3}^{\theta\infty}}{\partial n_{\mathrm{CH_3}}}$ = 0.44±0.01, -0.69±0.05 and -1.09±0.01 kJ mol^{-1} for the ATPS formed by Acet, Tart and Citr respectively, demonstrating that the -CH_3 groups contributes unfavorably to the transfer process in the presence of the Acet anion and favorably in the presence of the anions Citr > Tart. However, the $\Delta_{tr}H_{PhM}^{\theta,\infty}$ and $T\Delta_{tr}S_{PhM}^{\theta,\infty}$ values can contribute to a better understanding of the methyl groups contribution on the partition proces in the studied ATPSs. The results are show in the Figures 67 and 68 respectively.

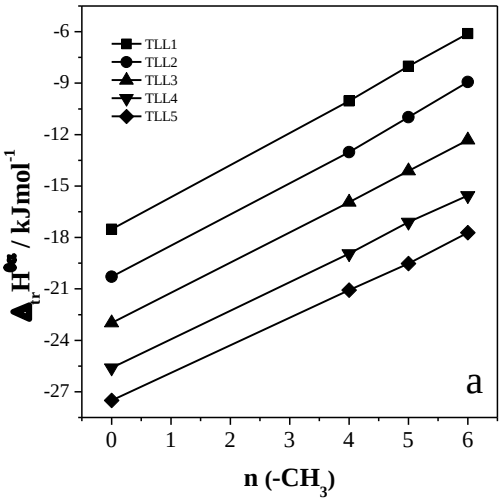

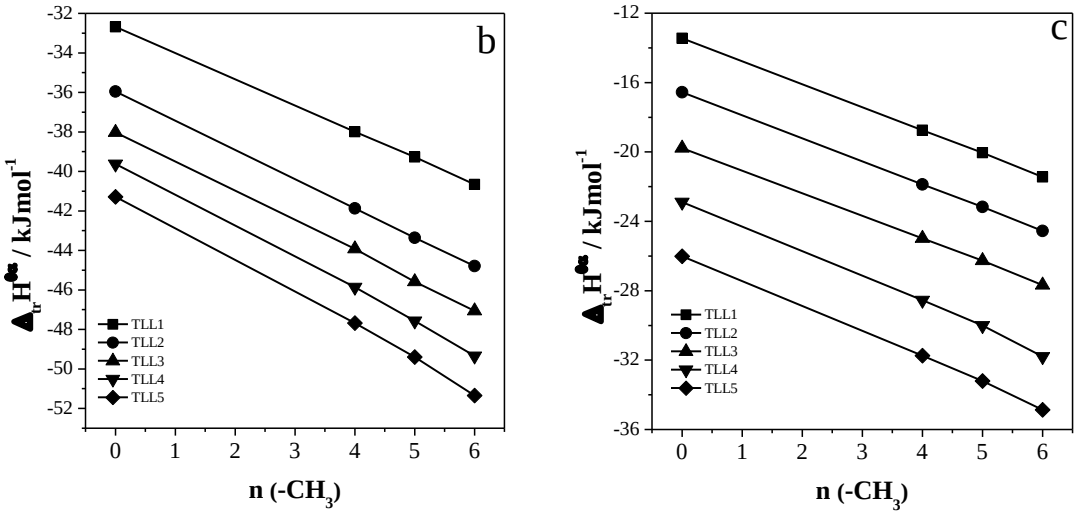

Figure 67. $\Delta_{tr}H^{\theta,\infty}_{CH_3}$ as a function of -CH_3 groups $MV10B_{(6\text{-}CH3)}$, $MV6B_{(5\text{-}CH3)}$, $MV2B_{(4\text{-}CH3)}$ and $PRA_{(0\text{-}CH3)}$ partitioning in (a) AcetNa + PPO425 + H_2O (b) CitrNa + PPO425 + H_2O and (c) TartNa + PPO425 + H_2O ATPS at 298.15 K.

When the PhM dye are transfer from the bottom phase to the upper phase, the standard enthalpy transference change decrease depending of the anion that form ATPS in the following order: Acet < Tart < Citr. Considering that the interactions dye-UP components ($|\Delta_{int}H^{\infty}_{PhM-UP}+\Delta_{int}H^{\infty}_{UP-UP}|$) are the same for the three ATPS, then the interactions that promote the difference in the $\Delta_{tr}H^{\theta,\infty}_{CH_3}$ values are in the bottom phase ($|\Delta_{int}H^{\infty}_{PhM-BP}+\Delta_{int}H^{\infty}_{BP-BP}|$). Hence, the news interactions formation between the bottom phase components releases energy depending on the anion that forming electrolyte in the following order: Citr > Trat > Acet. Consequently, the break of the interactions between the PhM dye and the BP components absorb energy in the order: Acet > Tart > Citr, resulting in the $\Delta_{tr}H^{\theta,\infty}_{CH_3}$ values less negatives for Acet and more negatives for Tart and Citr respectively.

On the other hand, in the ATPS formed by Citr or Tart the $\Delta_{tr}H^{\theta,\infty}_{CH_3}$ values become more negatives when the methylation degree on the dye structure increment,

unlike the system with Acet that the $\Delta_{tr}H_{CH_3}^{\theta,\infty}$ values are less negatives when the methylation degree increment. This can be observed in the calculation of $\frac{\partial \Delta_{tr}H_{CH_3}^{\theta\infty}}{\partial n_{\mathrm{CH_3}}}$ = 1.80±0.03, -1.32±0.07 and -1.46±0.03 kJ mol^{-1} for the ATPS formed by Acet, Tart and Citr respectively. Showed that the phenyl group contribute unfavorably in the PhM dyes transfer in ATPS formed by Acet and favorably in presence of Citr > Tart.

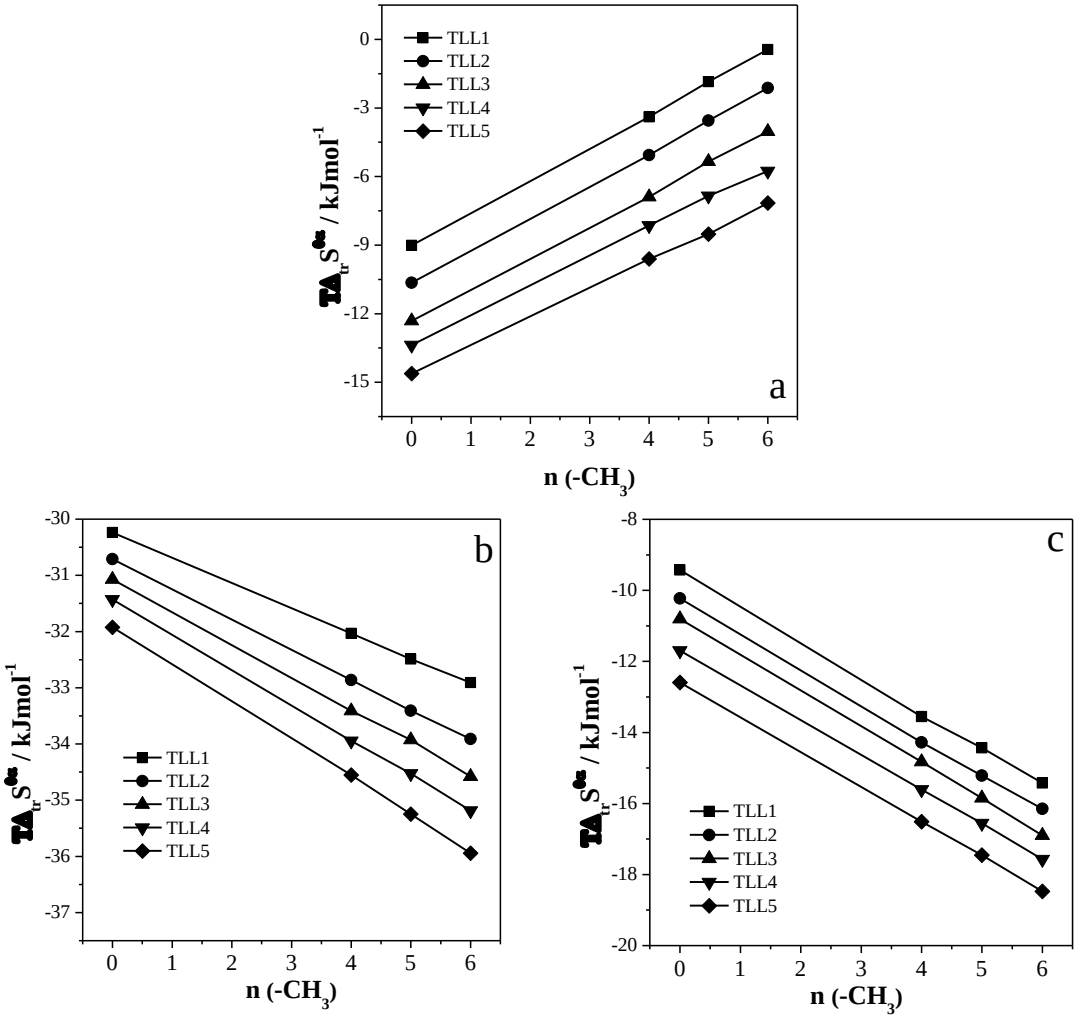

Figure 68. $T\Delta_{tr}S_{PhM}^{\theta,\infty}$ as function of -CH_3 groups for MV10B(6-CH_3), MV6B(5-CH_3), MV2B(4-CH_3) and PRA(0-CH_3) partitioning in (a) AcetNa + PPO425 + H_2O (b) CitrNa + PPO425 + H_2O and (c) TartNa + PPO425 + H_2O ATPS at 298.15 K.

The $T\Delta_{tr}S^{\theta\infty}_{CH_3}$ values show that the dye transference process occurs with an entropy decrease and this values become more negatives when the TLL increment in all ATPS studied. However, in the ATPS formed by Acet the $T\Delta_{tr}S^{\theta\infty}_{CH_3}$ values are less negative when the methyl groups number increase. Unlike, the ATPSs formed by Citr or Tart that the $T\Delta_{tr}S^{\theta\infty}_{CH_3}$ values become more negative with methylation degree increase. This means that, as the interaction between the dye and the anion acetate is more intense, less dye molecules are transferred from a region with a greater number of configurations (BP) for a region with a smaller number of configurations (UP) this results in a lower loss of the system entropy and this effect is less intense depending of the anion in the order: Tart < Citr. The methyl group contribution show values of $\frac{\partial T\Delta_{tr}S^{\theta\infty}_{CH_3}}{\partial n_{\mathrm{CH_3}}}$ = 1.41±0.01, -0.59±0.02 and -1.01±0.02 kJ mol^{-1} for the ATPS formed by Acet, Tart and Citr respectively. Indicating that the CH_3 groups transference contribute favorably on the standard transfer entropy change in the ATPS formed by Acet, unlike in presence of Tart or Citr contribute unfavorably.

3.2.2.2 Contribution of phenyl groups

The figure 69 shows the $\Delta_{tr}G^{\theta,\infty}_{PhM}$, $\Delta_{tr}H^{\theta,\infty}_{PhM}$ and $T\Delta_{tr}S^{\theta,\infty}_{PhM}$ values of AUR (DPhM) and MV2B (TPhM) as functions of the TLL in PPO425 + H_2O + sodium organics salts ATPSs.

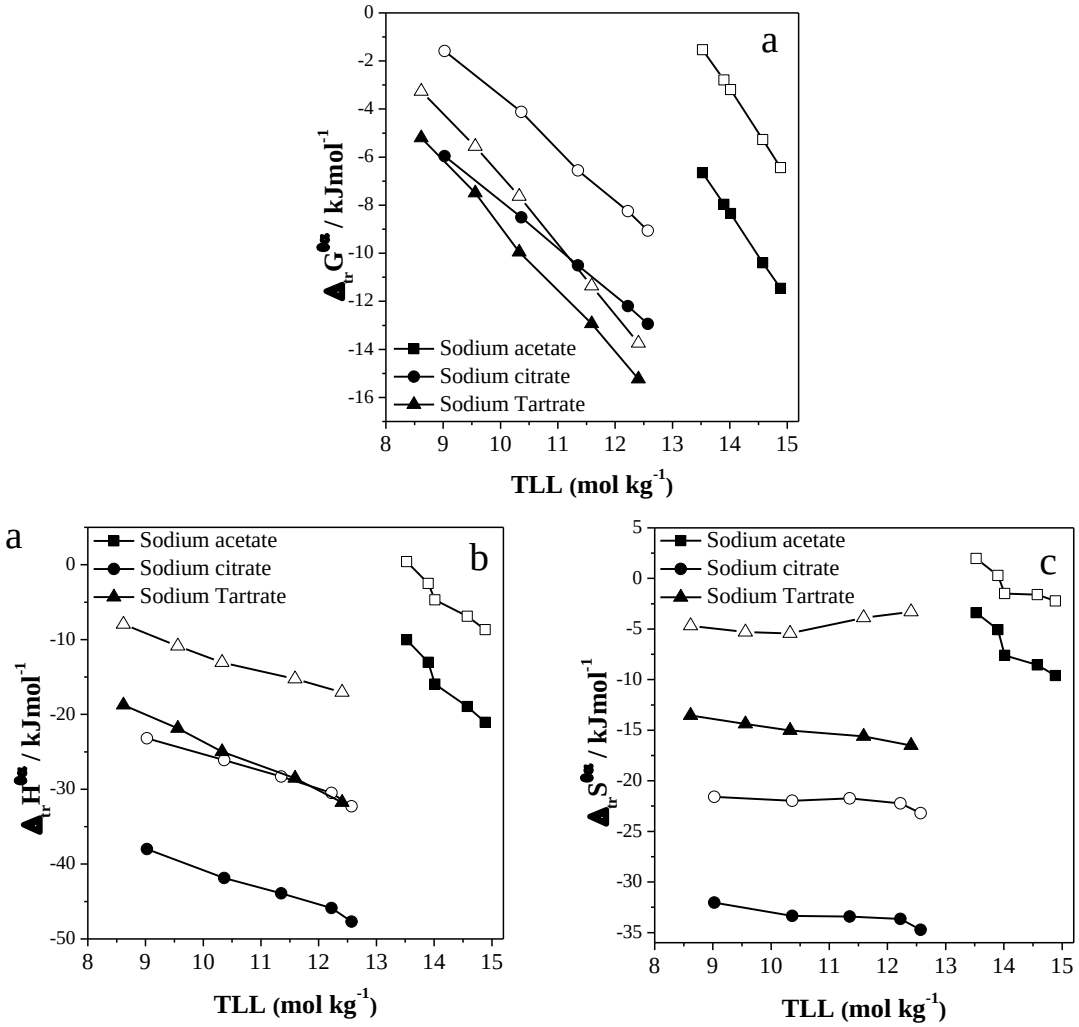

Figure 69. (a) $\Delta_{tr}G^{\theta,\infty}_{PhM}$ (b) $\Delta_{tr}H^{\theta,\infty}_{PhM}$ and (c) $T\Delta_{tr}S^{\theta,\infty}_{PhM}$ values of MV2B (closed symbols) and AUR (open symbols) as a function of the TLL of AcetNa + PPO425 + H_2O (square symbol), CitrNa + PPO425 + H_2O (round symbol) and TartNa + PPO425 + H_2O (Triangular symbol) ATPS at 298.15 K.

The $\Delta_{tr}G^{\theta,\infty}_{TPhM}$ values are more negative than $\Delta_{tr}G^{\theta,\infty}_{DPhM}$, in all ATPS studied, indicating that the transference process from bottom phase to upper phase is more efficient when the dye structure has three phenyl groups. This efficiency is greater depending of the anion that form the ATPS in following order Tart > Citr > Acet. Besides, the $\Delta_{tr}G^{\theta,\infty}_{PhM}$ values for both structures decrease when the TLL increase in all ATPSs studied. Indicating that the phenyl group makes dye molecules transfer from the

bottom phase to upper phase more efficient. However, this efficiency decreases when the ATPS is formed by Acet anions, probably due to the formation of intermolecular interactions dye-Acet more intense.

The $\Delta_{tr}H^{\theta,\infty}_{PhM}$ and $T\Delta_{tr}S^{\theta,\infty}_{PhM}$ values are more negative for the TPhM that for DPhM molecules. Besides, this difference between both molecules depends of the forming anion of the ATPS in the following order: Tart < Citr < Acet. Nevertheless, to understand better the phenyl group contribution on this parameters, were calculate the difference $\Delta\Delta_{tr}H^{\theta,\infty}_{MV2B-AUR}$ and $\Delta[T\Delta_{tr}S^{\theta,\infty}_{MV2B-AUR}]$. The results are shown in the Figure 70.

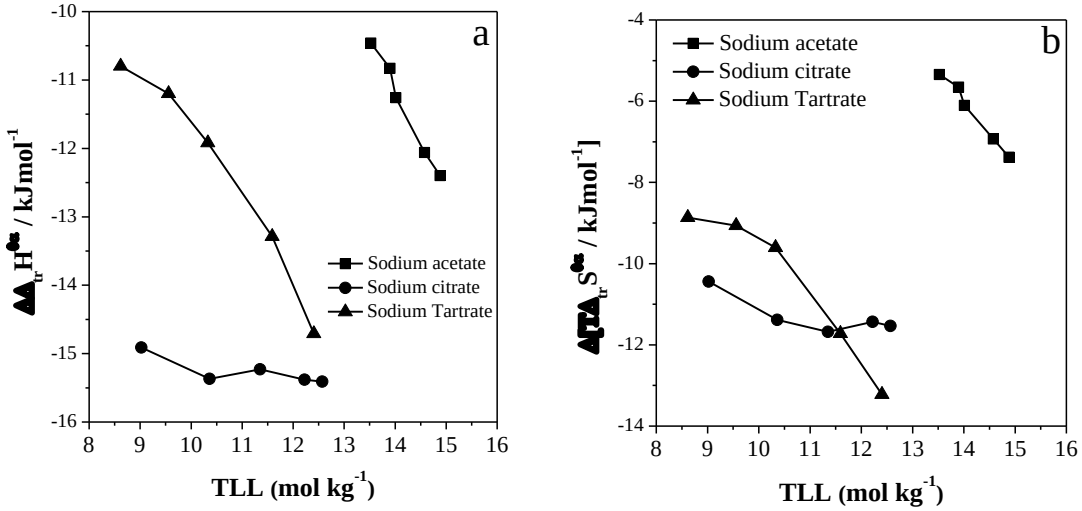

Figure 70. (a) $\Delta\Delta_{tr}H^{\theta,\infty}_{MV2B-AUR}$ and (b) $\Delta[T\Delta_{tr}S^{\theta,\infty}_{MV2B-AUR}]$ as function of the TLL of AcetNa + PPO425 + H_2O (square symbol), CitrNa + PPO425 + H_2O (round symbol) and TartNa + PPO425 + H_2O (Triangular symbol) ATPS at 298.15 K.

The $\Delta\Delta_{tr}H^{\theta,\infty}_{MV2B-AUR}$ values show that; the phenyl group addition decreases the charge density on the dye structure causing the ion pairs formation with the bottom phase anions ($\Delta_{int}H^{\infty}_{TPhM-BP}$) weaker. Therefore, the needed energy to break these

interactions is less, and how the energy released for form the new interaction $\Delta_{int}H^{\infty}_{BP-BP}$ is similar for both molecules, the result in the $\Delta_{tr}H^{\theta,\infty}_{TPhM}$ values is more negative.

On the other hand, if we consider the interactions magnitude in the upper phase of the similar system in the three ATPS and how the energy absorbed to break the ion pairs is greater in the following order: $\Delta_{int}H^{\infty}_{TPhM-Acet} > \Delta_{int}H^{\infty}_{TPhM-Tart} > \Delta_{int}H^{\infty}_{TPhM-Citr}$ and the energy released for form the new interaction is greater in the next order: $\Delta_{int}H^{\infty}_{Citr-Citr} > \Delta_{int}H^{\infty}_{Tart-Tart} > \Delta_{int}H^{\infty}_{Acet-Acet}$. The result in the $\Delta\Delta_{tr}H^{\theta,\infty}_{MV2B-AUR}$ values more negatives in the order: Citr > Tart > Acet.

When the ATPS is formed by Acet anion the $\Delta[T\Delta_{tr}S^{\theta,\infty}_{MV2B-AUR}]$ values are more negatives, suggesting that the interaction between the TPhM dye and the Acet anion increases the dye structure hydrophobicity. Hence, causing the increase the number of water molecules needed to solvate this interaction decreasing the system entropy. In consequence this effect is less intense for the Tart and Citr anions respectively.

3.2.2.3 Contribution of the positive charge on the dye molecule

In order to determine how the charge on the dye structure affects the thermodynamic transfer parameters and the dependence of the anion in this effect. The Figure 71 show the $\Delta_{tr}G^{\theta,\infty}_{PhM}$, $\Delta_{tr}H^{\theta,\infty}_{PhM}$ and $T\Delta_{tr}S^{\theta,\infty}_{PhM}$ of MV6B (charge specie) and MVB (neutral specie) as a function of the TLL of ATPSs formed by PPO425 + H2O + sodium organic salts at 298.15 K.

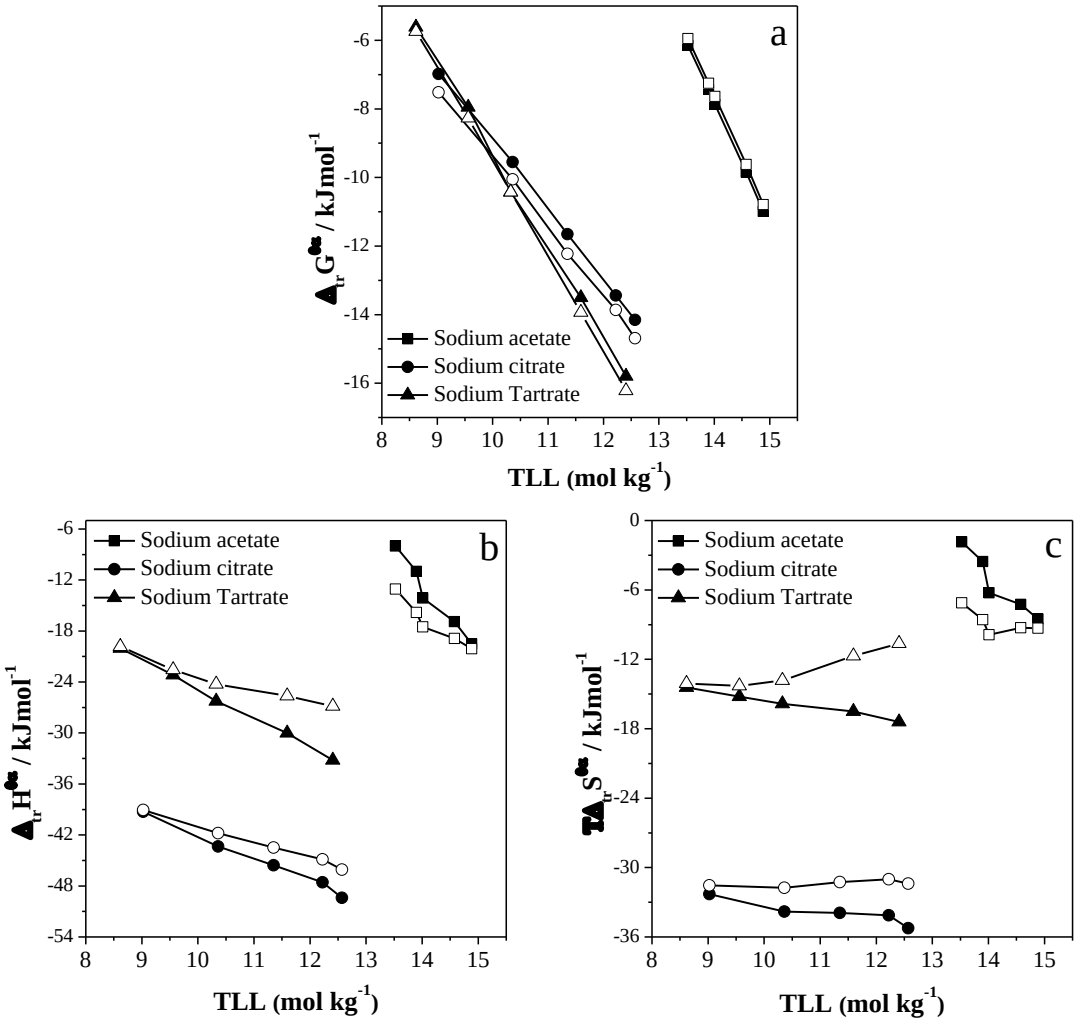

Figure 71. (a) $\Delta_{tr}G_{PhM}^{\theta,\infty}$ (b) $\Delta_{tr}H_{PhM}^{\theta,\infty}$ and (c) $T\Delta_{tr}S_{PhM}^{\theta,\infty}$ values of MV6B (closed symbols) and MVB (open symbols) as a function of the TLL of ATPS formed by (square symbol) AcetNa + PPO425 + H_2O, (round symbol) CitrNa + PPO425 + H_2O and (Triangular symbol) TartNa + PPO425 + H_2O ATPS at 298.15 K.

For both structures, the transference process occurs with $\Delta_{tr}G_{PhM}^{\theta,\infty}$ decrease in the ATPSs studied. Besides, these values become more negative with the increment of the TLL. Again, the difference in $\Delta_{tr}G_{PhM}^{\theta,\infty}$ values for both dyes structures is around the experimental error of the measurement, indicating that the charge does not contribute on the standard transference Gibbs free energy change for the ATPSs studied.

In contrast, the charge on the dye structure contribute in the enthalpy and entropy values depending of the anion and of the phases components concentration. The $\Delta_{tr}H_{PhM}^{\theta\infty}$ values show that the transference process for both structures is exothermic and the charge contribute to become this values more negatives in the ATPS formed by Tart or Citr. Suggesting that as the electrolyte concentration in the bottom phase increases, the break of interactions between the charged dye and the anions absorb less energy, while the new interactions between the anions release a greater amount of energy, making the values of $\Delta_{tr}H_{PhM}^{\theta\infty}$ more negative. This effect is more intense when the anion is Citr than Tart. In contrast, in Acet anion presence the absorption energy in the break of interactions PhM-Acet is greater than the release energy in the interaction Acet-Acet inducing to $\Delta_{tr}H_{PhM}^{\theta\infty}$ values less negatives.

The $T\Delta_{tr}S_{PhM}^{\theta,\infty}$ values exhibit a compensatory effect of entropy loss caused by the dye molecules transfer from a region with greater number of configurations for a region with smaller number of configurations. In addition, with the increase in the concentration of the components of the phases also increases the ionic pairs between the charged dye and the anions in the order Citr > Tart > Acet decreasing the water configurational entropy in both phases of ATPS.

4. Conclusion

The methyl groups transfer is more spontaneously and entropically directed in more hydrophilic systems. The phenyl group make more efficient and directed enthalpically the transference of PhM dyes in ATPS with less hydrophobicity degree. When the pseudopolication is formed by EO segment and cation Li^+ the transfer process of more hydrophobic molecules is entropically directed and more efficient than when formed by Na^+, but when the cation is or Mg^{2+} the -CH_3 and phenyl groups contribution

in the transfer process is less efficient and enthalpically directed. The charge on the dye molecule does not contribute in the partitioning process, but if in the specific intermolecular interactions modifying the entropy and enthalpy of the system. When the ATPS is formed by organic Acet anions, the transfer process becomes less efficient by decreasing the system enthalpy according to the methyl groups number in the dye structure increases. In contrast, when the ATPS is formed by Tart or Citr anions, the transfer process is more efficient when increase the methyl and phenyl groups decreasing the system enthalpy. The ATPSs studied allowed to determine the contribution of functional groups different on phenylmethane dyes in the process of partitioning, providing valuable information on the thermodynamic involved in the specific intermolecular interactions between solute and system components responsible for the process of species transfer in ATPS.

5. References

1. Kress, C.; Sadowski, G.; Brandenbusch, C., Solubilization of proteins in aqueous two-phase extraction through combinations of phase-formers and displacement agents. *Eur. J. Pharm. Biopharm.* **2017,** *112*, 38-44.

2. Mathiazakan, P.; Shing, S. Y.; Ying, S. S.; Kek, H. K.; Tang, M. S. Y.; Show, P. L.; Ooi, C. W.; Ling, T. C., Pilot-scale aqueous two-phase floatation for direct recovery of lipase derived from Burkholderia cepacia strain ST8. *Sep. Purif. Technol.* **2016,** *171*, 206-213.

3. Sant'Anna, V.; Correa, A. P. F.; da Motta, A. D.; Brandelli, A., Liquid-liquid extraction of antimicrobial peptide P34 by aqueous two-phase and micellar systems. *Prep. Biochem. Biotechnol.* **2016,** *46* (8), 838-843.

4. Lee, S. Y.; Khoiroh, I.; Ling, T. C.; Show, P. L., Aqueous Two-Phase Flotation for the Recovery of Biomolecules. *Sep. Purif. Rev.* **2016,** *45* (1), 81-92.

5. Zhang, Y. Q.; Sun, T. C.; Lu, T. Q.; Yan, C. H., Extraction and separation of tungsten (VI) from aqueous media with Triton X-100-ammonium sulfate-water aqueous two-phase system without any extractant. *J. Chromatogr. A* **2016,** *1474*, 40-46.

6. Salabat, A.; Abnosi, M. H.; Bahar, A. R., Amino acids partitioning in aqueous two-phase system of polypropylene glycol and magnesium sulfate. *J. Chromatogr. B* **2007,** *858* (1-2), 234-238.

7. Salabat, A.; Abnosi, M. H.; Motahari, A., Investigation of amino acid partitioning in aqueous two-phase systems containing polyethylene glycol and inorganic salts. *J. Chem. Eng. Data* **2008,** *53* (9), 2018-2021.

8. da Silva, N. R.; Ferreira, L. A.; Madeira, P. P.; Teixeira, J. A.; Uversky, V. N.; Zaslavsky, B. Y., Analysis of partitioning of organic compounds and proteins in aqueous polyethylene glycol-sodium sulfate aqueous two-phase systems in terms of solute-solvent interactions. *J. Chromatogr. A* **2015,** *1415*, 1-10.

9. da Silva, L. H. M.; da Silva, M. D. H.; Amin, J.; Martins, J. P.; Coimbra, J. S. D.; Minim, L. A., Hydrophobic effect on the partitioning of Fe(CN)(5)(NO) (2-) and Fe(CN)(6) (3-) anions in aqueous two-phase systems formed by triblock copolymers and phosphate salts. *Sep. Purif. Technol.* **2008,** *60* (1), 103-112.

10. de Alvarenga, J. M.; Fideles, R. A.; da Silva, M. V.; Murari, G. F.; Taylor, J. G.; de Lemos, L. R.; Rodrigues, G. D.; Mageste, A. B., Partition study of textile dye Remazol Yellow Gold RNL in aqueous two-phase systems. *Fluid Phase Equilibria* **2015,** *391*, 1-8.

11. de Oliveira, F. C.; Coimbra, J. S. D.; da Silva, L. H. M.; Rojas, E. E. G.; da Silva, M. D. H., Ovomucoid partitioning in aqueous two-phase systems. *Biochemical Engineering Journal* **2009,** *47* (1-3), 55-60.

12. Ebrahimi, T.; Shahriari, S., Extraction of Betanin Using Aqueous Two-Phase Systems. *Bull. Chem. Soc. Jpn.* **2016,** *89* (5), 565-572.

13. Hao, L. S.; Liu, M. N.; Xu, H. M.; Yang, N.; Nan, Y. Q.; Deng, Y. T., Partitioning of Dyes, Free Anthraquinones, and Tanshinones in Aqueous Two-Phase Systems of Cationic/Anionic Surfactants. *J. Dispersion Sci. Technol.* **2015,** *36* (7), 1047-1058.

14. Mageste, A. B.; de Lemos, L. R.; Ferreira, G. M. D.; da Silva, M. D. H.; da Silva, L. H. M.; Bonomo, R. C. F.; Minim, L. A., Aqueous two-phase systems: An efficient, environmentally safe and economically viable method for purification of natural dye carmine. *J. Chromatogr. A* **2009,** *1216* (45), 7623-7629.

15. Mageste, A. B.; Senra, T. D. A.; da Silva, M. C. H.; Bonomo, R. C. F.; da Silva, L. H. M., Thermodynamics and optimization of norbixin transfer processes in aqueous biphasic systems formed by polymers and organic salts. *Sep. Purif. Technol.* **2012,** *98*, 69-77.

16. Lacerda, V. G.; Mageste, A. B.; Santos, I. J. B.; da Silva, L. H. M.; da Silva, M. d. C. H., Separation of Cd and Ni from Ni–Cd batteries by an environmentally safe methodology employing aqueous two-phase systems. *Journal of Power Sources* **2009,** *193* (2), 908-913.

17. Di Nucci, H.; Nerli, B.; Pico, G., Comparison between the thermodynamic features of alpha 1-antitrypsin and human albumin partitioning in aqueous two-phase systems of polyethyleneglycol-dextran. *Biophys. Chem.* **2001,** *89* (2-3), 219-229.

18. Dreyer, S.; Salim, P.; Kragl, U., Driving forces of protein partitioning in an ionic liquid-based aqueous two-phase system. *Biochemical Engineering Journal* **2009,** *46* (2), 176-185.

19. Jimenez, Y. P.; Galleguillos, H. R.; Claros, M., Liquid-liquid partition of perchlorate ion in the aqueous two-phase system formed by NaNO3 + Poly(ethylene glycol) + H2O. *Fluid Phase Equilibria* **2016,** *421*, 93-103.

20. Chen, Y. H.; Deng, Y. C.; Meng, Y. S.; Zhang, S. M., Partitioning Equilibria and Thermodynamics of Gallium, Indium, and Thallium in Aqueous Two-Phase Systems. *J. Chem. Eng. Data* **2015,** *60* (5), 1464-1468.

21. Lu, Y. M.; Lu, W. J.; Wang, W.; Guo, Q. W.; Yang, Y. Z., Thermodynamic studies of partitioning behavior of cytochrome c in ionic liquid-based aqueous two-phase system. *Talanta* **2011,** *85* (3), 1621-1626.

22. Rengifo, A. F. C.; Ferreira, G. M. D.; Ferreira, G. M. D.; da Silva, M. C. F.; Rezende, J. D.; Pires, A. C. D.; da Silva, L. H. M., Driving forces for chymosin partitioning on the macromolecule-salt aqueous two phase system. *Food Bioprod. Process.* **2016,** *100*, 361-371.

23. Martins, J. P.; Carvalho, C. d. P.; Silva, L. H. M. d.; Coimbra, J. S. d. R.; Silva, M. d. C. H. d.; Rodrigues, G. D.; Minim, L. A., Liquid–Liquid Equilibria of an Aqueous Two-Phase System Containing Poly(ethylene) Glycol 1500 and Sulfate Salts at Different Temperatures. *Journal of Chemical & Engineering Data* **2008,** *53* (1), 238-241.

24. Huddleston, J. G.; Willauer, H. D.; Rogers, R. D., Phase Diagram Data for Several PEG + Salt Aqueous Biphasic Systems at 25 °C. *Journal of Chemical & Engineering Data* **2003,** *48* (5), 1230-1236.

25. Patricio, P. D.; Mageste, A. B.; de Lemos, L. R.; de Carvalho, R. M. M.; da Silva, L. H. M.; da Silva, M. C. H., Phase diagram and thermodynamic modeling of PEO plus organic salts + H2O and PPO + organic salts + H2O aqueous two-phase systems. *Fluid Phase Equilibria* **2011,** *305* (1), 1-8.

26. Ferreira, A. M.; Coutinho, J. A. P.; Fernandes, A. M.; Freire, M. G., Complete removal of textile dyes from aqueous media using ionic-liquid-based aqueous two-phase systems. *Sep. Purif. Technol.* **2014,** *128,* 58-66.

27. Andrews, B. A.; Asenjo, J. A., Protein partitioning equilibrium between the aqueous poly(ethylene glycol) and salt phases and the solid protein phase in poly(ethylene glycol)-salt two-phase systems. *Journal of Chromatography B: Biomedical Sciences and Applications* **1996,** *685* (1), 15-20.

28. de Barros, D. P. C.; Campos, S. R. R.; Madeira, P. P.; Azevedo, A. M.; Baptista, A. M.; Aires-Barros, M. R., Modeling the partitioning of amino acids in aqueous two phase systems. *J. Chromatogr. A* **2014,** *1329,* 52-60.

29. Silvério, S. C.; Rodríguez, O.; Teixeira, J. A.; Macedo, E. A., Gibbs free energy of transfer of a methylene group on {UCON+(sodium or potassium) phosphate salts} aqueous two-phase systems: Hydrophobicity effects. *The Journal of Chemical Thermodynamics* **2010,** *42* (8), 1063-1069.

30. Silverio, S. C.; Madeira, P. P.; Rodriguez, O.; Teixeira, J. A.; Macedo, E. A., Delta G(CH2) in PEG-salt and Ucon-salt aqueous two-phase systems. *J. Chem. Eng. Data* **2008,** *53* (7), 1622-1625.

31. Maia, F. M.; Rodríguez, O.; Macedo, E. A., Free Energy of Transfer of a Methylene Group in Biphasic Systems of Water and Ionic Liquids [C3mpip][NTf2], [C3mpyrr][NTf2], and [C4mpyrr][NTf2]. *Ind. Eng. Chem. Res.* **2012,** *51* (23), 8061-8068.

32. Silva, L. H. M. d.; Loh, W., Sistemas aquosos bifásicos: fundamentos e aplicações para partição/purificação de proteínas. *Química Nova* **2006**.

33. Haraguchi, L.; Mohamed, R.; Loh, W.; Pessôa Filho, P., Phase equilibrium and insulin partitioning in aqueous two-phase systems containing block copolymers and potassium phosphate. *Fluid Phase Equilibria* **2004,** *215* (1), 1-15.

34. da Silva, L. H. M.; Loh, W., Calorimetric investigation of the formation of aqueous two-phase systems in ternary mixtures of water, poly(ethylene oxide) and electrolytes (or dextran). *Journal of Physical Chemistry B* **2000,** *104* (43), 10069-10073.

Considerações finais:

Esta nova abordagem experimental permitiu descobrir que a transferência dos grupos metilo em SAB é mais eficiente e entropicamente dirigida em sistemas mais hidrofílicos. O número de grupos fenil na estrutura do corante de fenilmetano aumenta a hidrofobicidade da molécula tornando mais eficiente a transferência entalpicamente dirigida em ATPS com menor grau de hidrofobicidade. Quando a pseudopolication é formada por segmento EO e cátions Li^{+}, o processo de transferência dos corantes é entropicamente dirigido e mais eficiente do que quando e formado por Na^{+}ou mas ou Mg^{2+}. A carga na molécula do corante não contribui no potencial termodinâmico de partição, embora, trona-se fundamental nas interações intermoleculares específicas modificando a entropia e a entalpia do sistema. Quando o ATPS é formado por aníons orgânicos de Acet, o processo de transferência torna-se menos eficiente ao diminuir a entalpia do sistema conforme o número de grupos metilo na estrutura do corante aumenta. Em contraste, quando o ATPS é formado por aníons Tart ou Citr, o processo de transferência é mais eficiente ao aumentar os grupos metilo e fenilo aumentando a entalpia do sistema. Portanto, os ATPS estudados permitiram determinar a contribuição de diferentes grupos funcionais presentes na estrutura química dos corantes de fenilmetano no processo de partição, fornecendo informações valiosas sobre a termodinâmica envolvida nas interações intermoleculares responsáveis pelo processo de transferência de espécies em SAB.